Dissertation
submitted to the
Combined Faculties for the Natural Sciences and for Mathematics
of the Ruperto–Carola University of Heidelberg, Germany
for the degree of
Doctor of Natural Sciences

presented by

Diplom-Physicist:	Matthias Cuntz
born in:	Landau/Pfalz

Oral examination: 20$^{\text{th}}$ November 2002

A comprehensive global 3D model of $\delta^{18}O$ in atmospheric CO_2

Referees: Dr. Ingeborg Levin
Dr. Philippe Ciais

Zusammenfassung

Ein konsistentes globales 3D Modell des $\delta^{18}O$ im atmosphärischen CO_2

Ich habe ein konsistentes globales 3D Modell zur Simulation von $\delta^{18}O$ im atmosphärischen CO_2 entwickelt, mit dem Ziel, die gemessene $\delta^{18}O$–CO_2–Variation in der Atmosphäre zu verstehen. $\delta^{18}O$–CO_2 bietet die Möglichkeit, die CO_2–Bruttoflüsse der terrestrischen Biosphäre zu bestimmen. Modell-Oberflächenprozesse wurden ausführlich anhand experimenteller Daten validiert und das integrierte atmosphärische Meßsignal mit globalen Messungen verglichen. Die modellierten Oberflächenprozesse sind in allen außerhalb der hohen nördlichen Breiten realistisch; dort reichen die Beobachtungsdaten nicht aus, eine einheitliche Aussage zu treffen. Die Wasserisotope des Niederschlags werden sehr ähnlich zu den Messungen modelliert, jedoch ist das saisonale Bodenwassersignal zu stark gedämpft. Das Modell simuliert sehr genau den Jahresgang des atmosphärischen CO_2. Es zeigt jedoch einen um zwei Monate verfrühten Jahresgang im $\delta^{18}O$–CO_2. Diese Phasenverschiebung konnte mit derzeitigem Wissen über den $\delta^{18}O$–CO_2–Kreislauf nicht erklärt werden. Die Amplitude reagiert sehr empfindlich auf verschiedene Modellparametrisierungen, Standardwerte ergeben nur $^2/_3$ des beobachteten Jahresgangs. Aus den Modellrechnungen konnte ich folgern, daß die Hälfte des beobachteten Nord–Süd–Gradienten im $\delta^{18}O$–CO_2 durch die Kovarianz der $\delta^{18}O$–CO_2–Oberflächenflüsse mit atmosphärischem Transport erzeugt wird, die andere Hälfte resultiert aus unterschiedlichen $\delta^{18}O$–CO_2–Quellverteilungen in Nord– und Süd–Hemisphäre.

Abstract

A comprehensive global 3D model of $\delta^{18}O$ in atmospheric CO_2

I have built the first comprehensive global 3D model to simulate $\delta^{18}O$ in atmospheric CO_2. The aim is to disentangle this isotope signal which offers the potential to determine the CO_2 gross fluxes of the terrestrial biosphere. Model surface processes have been validated against regional experiments while the integrated atmospheric signal has been investigated comparing with global atmospheric observations. Modelled surface processes compare well with observed data over the whole latitude range except for high northern latitudes where the experimental data are very sparse. The water isotopes of rain are well reproduced but the soil signal is too attenuated in the model. The model further simulates very well the seasonal cycle of atmospheric CO_2. For $\delta^{18}O$–CO_2, it precedes the measured cycle by two month. This discrepancy could not be resolved with our current knowledge of $\delta^{18}O$–CO_2. The modelled amplitude is very sensitive to different parameterisations, standard values result in only $^2/_3$ of the observed amplitude. Concerning the meridional gradient in $\delta^{18}O$–CO_2, I could show that about one half of the signal comes from the covariance of $\delta^{18}O$–CO_2 sources with atmospheric transport and the other half from the imbalance of $\delta^{18}O$–CO_2 isofluxes between the northern and southern hemisphere.

Contents

Chapter 1

Introduction

"Life is woven out of air by light."

Jacob Moleschott,
1822–1893

1.1 Motivation

Putting all carbon taken up during one year by plants and micro–organisms on a freight train, would make up a train from Earth to the Moon and back. Plants cover almost the whole Earth surface either as terrestrial vegetation like trees, bushes, and grasses or as marine plants like algae. *Nomen est omen*, they are the "power plants" of our planet. They are taking up the energy from the sun and produce with its aid energy resources which can be used by other organisms. Terrestrial plants cover about one third of our planet and contribute about one half of the annual carbon turnover [*Prentice et al.*, 2001]. They take up carbon from the atmosphere as carbon dioxide (CO_2) and store it in sugars or amino acids resp. proteins. If these storage molecules are utilised to retrieve their inherent energy, most of the carbon is re–transformed to CO_2 and released back to the atmosphere. This forms an eternal cycle of carbon and the impetus of life on Earth.

When plants take up CO_2 from the atmosphere, they assimilate carbon; this process is thus called "assimilation". Plants use about half of the stored carbon to maintain their own system and to provide the energy for growth [e. g. *Ryan*, 1991]. For this, they use the energy stored in sugars and release carbon in the form of CO_2 to the atmosphere. Because of the similarity to the human expiratory process (where we release CO_2 as well), this is called "respiration". Not only plants respire CO_2, therefore the process of plants respiring CO_2 is specified as "autotrophic respiration". Only half of the assimilated carbon is finally used to build new plant material. After the death of this plant material (e. g. litter fall in autumn), it is re–used by organism to utilise the resources stored in the plant tissue, therewith composting it and releasing CO_2 to the atmosphere. This release is called "heterotrophic respiration".

Atmospheric CO_2 therefore is a composite of all kinds of CO_2 sources and sinks. However, only the net CO_2 flux i. e. the sum o f all sources and sinks can be deduced from atmospheric observations. For example, how much CO_2 is assimilated by plants

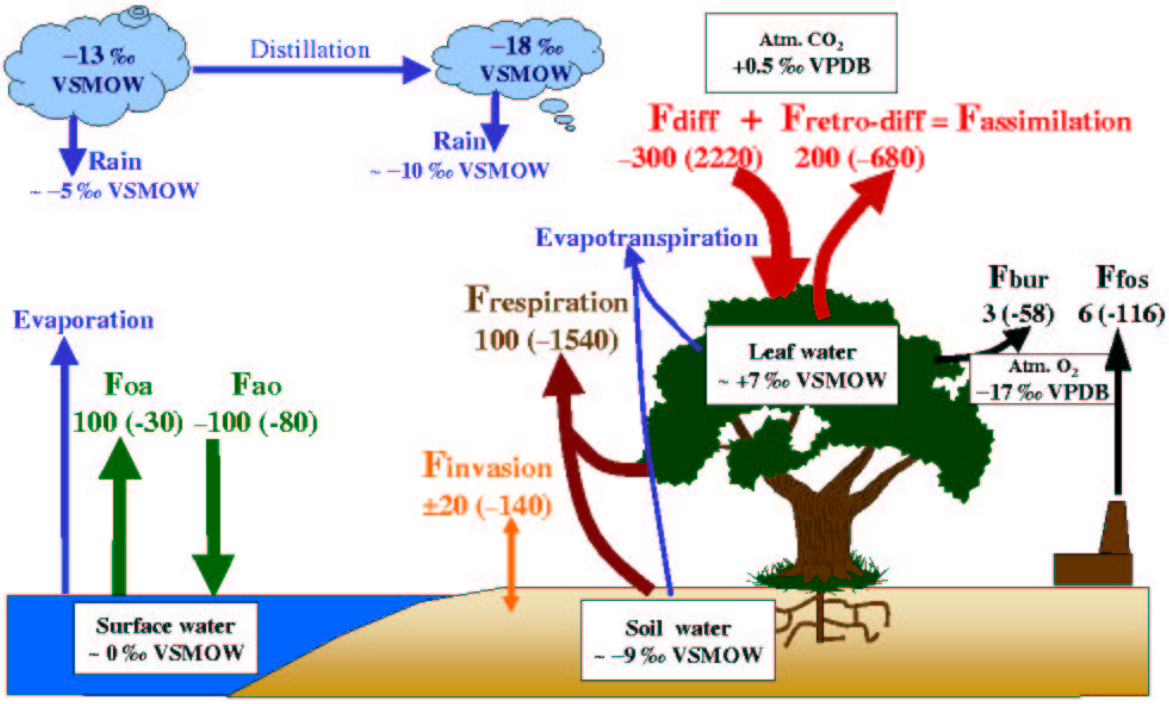

Figure 1.1: CO_2, $\delta^{18}O$–CO_2, and $\delta^{18}O$–H_2O cycles. Blue lines represent the water isotope cycle, other colours represent the CO_2 and $\delta^{18}O$–CO_2 cycles. Numbers with ‰–signs are the δ–values of the different reservoirs versus VSMOW for water and versus VPDB–CO_2 for CO_2. Numbers without ‰–signs are global annual carbon fluxes of CO_2 in PgC yr^{-1} and the number in parentheses are the correspondent $\delta^{18}O$–CO_2 isofluxes in PgC ‰ yr^{-1}. 'bur' stands for biomass burning and 'fos' for fossil fuel combustion. Positive fluxes are added to the atmosphere and negative fluxes are withdrawn from the atmosphere. As a rule of thumb, one can estimate that $\delta^{18}O$–CO_2 reported versus VPDB–CO_2 has the same δ–value (number) than the equilibrating water $\delta^{18}O$–H_2O reported versus VSMOW.

and, at the same time, how much CO_2 is respired by various respiration processes cannot be determined from concentration data alone. To separate different components of the net flux, a number of isotopomers[1] of CO_2 are used, depending on the component. For example, $^{13}CO_2$ is used to separate between marine and terrestrial biosphere fluxes [e. g. *Keeling et al.*, 1989], or $^{14}CO_2$ is used to separate the fossil fuel combustion contingent [e. g. *Levin et al.*, 1989]. $CO^{18}O$ offers the possibility to separate the different terrestrial biospheric gross fluxes, namely assimilation and respiration [e. g. *Farquhar et al.*, 1993; *Yakir and Wang*, 1996]. 1.1 % of all CO_2 molecules bear a ^{13}C atom inside. When CO_2 changes from one compartment to another, CO_2 molecules with a ^{12}C atom are more easily transfered than CO_2 molecules with a ^{13}C atom. For example, molecular diffusion transports "normal" CO_2 faster than $^{13}CO_2$ due to the different weights. This

[1]Isotopomers of CO_2 are all possible isotopic combinations of CO_2 (i. e. $^{12}C^{16}O^{16}O$, $^{13}C^{16}O^{16}O$, $^{12}C^{16}O^{18}O$, ...). I use 'C' and 'O' for the most abundant isotopes of carbon and oxygen, namely ^{12}C and ^{16}O.

so called fractionation can enrich (or deplete) $^{13}CO_2$ in a compartment, i. e. slightly more (or less) than 1.1 % of all CO_2 molecules are then $^{13}CO_2$ molecules. This is the primary mechanism why one can use $^{13}CO_2$ as a tracer to distinguish between CO_2 from different sources.

However, 0.4 % of all CO_2 molecules bear an ^{18}O isotope inside and also in the case of oxygen diffusion fractionation occurs. But $CO^{18}O$ has another particularity which makes it unique in its part. CO_2 in contact with water can exchange its oxygen isotope signature with those of the water pool. Because there are normally several orders of magnitude more water molecules associated with this process than CO_2 molecules, CO_2 takes over the isotopic signature of the water which barely changes itself. (This isotopic equilibration effect is temperature dependant, i. e. that the number of CO_2 molecules (per mole) which takes over the oxygen isotope signature of H_2O depends on temperature. The isotopic equilibration changes the ratio of $^{18}O/^{16}O$ atoms in one mole CO_2 significantly [*Brenninkmeijer et al.*, 1983].) This means that the ratio of ^{18}O to ^{16}O atoms in one mole CO_2 will be (almost) the same as the ratio of ^{18}O to ^{16}O atoms in one mole H_2O. One can say that CO_2 is isotopically "tagged" by or equilibrated with the water pool. CO_2 respired from soil (either heterotrophically respired CO_2 or autotrophically respired CO_2 leaving the plant via roots and entering the atmosphere through the soil) is therefore tagged by the isotopic composition of soil water. Statistically, a CO_2 molecule diffusing into plant leaves is fixed by photosynthesis with a probability of ⅓ whereas it diffuses back to the atmosphere with a probability of ⅔ [*Farquhar et al.*, 1993]. This means that only ⅓ of all CO_2 molecules entering the leaf are assimilated but all molecules are subject to fractionation and equilibration. This is depicted in Figure 1.1 where the CO_2 fluxes from and to different reservoirs with respect to the atmosphere are shown (numbers in petagrams of carbon per year, PgC $yr^{-1} = 10^{15}$ gC yr^{-1}). In parentheses are given the appendant $CO^{18}O$ fluxes, called isofluxes (in petagrams of carbon per mil per year[2], PgC ‰ yr^{-1}). The big red arrow represents the total CO_2 flux (-300 PgC yr^{-1}) which diffuses into the leaves, accompanied by a very big isoflux ($+2220$ PgC ‰ yr^{-1}). Both, flux and isoflux are opposed by back–diffused fluxes (200 PgC yr^{-1} resp. -680 PgC ‰ yr^{-1}). The isotopic exchange between CO_2 and water within leaves in presence of the enzyme carbonic anhydrase is so fast that back–diffused CO_2 re–entering the atmosphere is isotopically tagged by evaporating leaf water [*Farquhar et al.*, 1993]. Leaf water at the evaporating site is generally significantly enriched ($\sim+7$ ‰ VSMOW) with respect to soil moisture (~-9 ‰ VSMOW) [*Dongmann et al.*, 1974] and so is leaf CO_2 ($\sim+6$ ‰ VPDB–CO_2) with respect to soil respired CO_2 (~-7 ‰ VPDB–CO_2) [*Farquhar et al.*, 1993]. The higher leaf water is enriched the smaller is the retro–diffusive isoflux.[3] So, the higher leaf

[2] ‰ comes from the use of the δ–notation: $\delta = (R - R_{std})/R_{std} = R/R_{std} - 1$, with R as the $^{18}O/^{16}O$ ratio of the sample, R, resp. a standard material, R_{std}. All $\delta^{18}O$–CO_2 values are reported here relative to the Vienna Pee Dee Belemnite (VPDB–CO_2) standard with an isotope ratio of $R_{VPDB} = 2088.349077 \cdot 10^{-6}$ [*Allison et al.*, 1995]. All $\delta^{18}O$–H_2O values are reported here relative to the Vienna Standard Mean Ocean Water (VSMOW) with an absolute ratio of ^{18}O to ^{16}O atoms of $R_{VSMOW} = 2005.20 \cdot 10^{-6}$ [*Baertschi*, 1976]. With this standards, δ–values for both species lie normally around zero and vary only by a few ‰ around it. The $CO^{18}O$ δ–values are thence called $\delta^{18}O$–CO_2 and the $H_2^{18}O$ δ–values are called $\delta^{18}O$–H_2O throughout the thesis.

[3] $^3CO_2$ diffusing back in the atmosphere underlies the diffusion fractionation which depletes the outgoing CO_2 by about -7 ‰ relative to the CO_2 present in the stomate. Because of the presence of

water is enriched the greater is the (positive) influence of the (net) $CO^{18}O$ assimilation isoflux on atmospheric CO_2 ($F_{assimilation}$ in Figure 1.1).

Thus, with respect to ^{18}O, atmospheric $\delta^{18}O$–CO_2 has two distinct biospheric sources, the positive (net) $\delta^{18}O$–CO_2 assimilation isoflux ($F_{assimilation}$) and the negative $\delta^{18}O$–CO_2 respiration isoflux ($F_{respiration}$), that mix to the $\delta^{18}O$–CO_2 signal (δ_a) in the atmosphere (together with other minor isofluxes, also represented in Figure 1.1). The sources resp. isofluxes reflect thereby CO_2 fluxes, hydrological processes and temperature dependent fractionation factors. If one can constrain the atmospheric transport, the water isotopic composition in the different water pools, and other minor $CO^{18}O$ sources, deriving the CO_2 gross fluxes of the terrestrial biosphere, namely assimilation and respiration, reduces to the solution of two linear equations with two unknowns. This has already been done on a local scale [*Yakir and Wang*, 1996; *Langendörfer et al.*, 2002] and on the global scale [*Peylin*, 1999].

Yakir and Wang [1996] measured (among other things) the $\delta^{18}O$–H_2O signature of the water pools of a crop field and calculated the atmospheric transport from theoretical equations using micro–meteorological parameters. They could then solve the two linear equations for the biospheric gross fluxes of the crop field explicitly. *Langendörfer et al.* [2002] did also measure the $\delta^{18}O$–H_2O signature of the water pools of a forest but used measured ^{222}Radon activities as an atmospheric transport tracer (measuring also other parameters, most notably the atmospheric CO_2 mixing ratio and $\delta^{18}O$ in atmospheric CO_2). They could then calculate directly the CO_2 biospheric gross fluxes in the forest. These are the only two studies that I am aware of which ever used successfully $\delta^{18}O$–CO_2 to deduce the CO_2 gross fluxes on the local scale. Other studies failed because they could not determine atmospheric transport correctly [e. g. *Bowling et al.*, 1999].

The above explanations lead on the global scale to the conclusion that in order to understand the integrated atmospheric signal of $\delta^{18}O$ in CO_2 and/or deduce CO_2 biospheric gross fluxes from $\delta^{18}O$–CO_2, one must use a spatially explicit model of surface fluxes coupled to a 3D model of atmospheric transport including water isotopic composition. Few studies have attempted so far to model the distribution of $\delta^{18}O$ in atmospheric CO_2. The major conceptual difficulty lies in the requirement of a triad of models describing 1) the gross carbon fluxes, 2) the water isotope variability, and 3) the atmospheric transport. *Ciais et al.* [1997a, b] have put together those three components using output from different published models that were sampled as monthly averages. This approach gave a reasonably good agreement with atmospheric observations and provided useful a priori estimates to model gross fluxes with atmospheric inversion techniques [*Peylin*, 1999] (where inverse modelling solves explicitly the two linear equations on every point of the globe consistently). But there remains reservation for three reasons: First, there were inconsistencies among the different models used to construct $CO^{18}O$ fluxes which induced systematic errors that are impossible to estimate. Second, working with monthly mean fluxes does not allow to properly up–scale biogeochemical processes from the ecosystem level up to the quasi global scale. Third,

---

the enzyme carbonic anhydrase, CO_2 in the stomate is normally equilibrated with leaf water whereby leaf water is significantly enriched compared to soil water. So it depends on the enrichment of leaf water if the outgoing isoflux of $\delta^{18}O$–CO_2 is positive or negative, enriching or depleting the atmospheric CO_2. Generally, the net effect is negative and CO_2 originating from the back–diffusion flux depletes the atmospheric CO_2.

working with monthly fluxes neglects the existence of a strong diurnal cycle in the fluxes of photosynthesis and respiration that, unfortunately, covary with atmospheric transport in the boundary layer to generate mean gradients in CO_2 and in $\delta^{18}O$–CO_2.

The ratio of ^{18}O to ^{16}O in atmospheric CO_2 is determined, apart from atmospheric transport, by CO_2 fluxes and the water isotopic composition of water pools with which the source CO_2 interacts. In other words, $\delta^{18}O$–CO_2 depends on the water isotopic composition of its numerous sources, the atmosphere–biosphere exchange, and is transported in the atmosphere. Besides that, the water isotopic composition is determined by the hydrological cycle, and thus climate induced evaporation and condensation processes. The global distribution of atmospheric $\delta^{18}O$–CO_2 is hence an integrated signal over all these processes and their interactions. Model results are much more sensitive to the parameterisations of the coupled water and carbon cycles in an Earth System Model (ESM) than e. g. CO_2 or other isotope tracers. It can therefore act as an integrated measure of the overall model performance resp. the representation of all the different components and interactions in the ESM.

1.2 Outline of the Thesis

I have built a new, comprehensive global 3D model of $\delta^{18}O$ in atmospheric CO_2 where leaf and soil processes which determine the isotopic fluxes are encapsulated into a land surface carbon flux model that is consistently interfaced to a global atmospheric transport model. The new model is predominantly a feasibility study of the potential of $\delta^{18}O$ in atmospheric CO_2 to derive biospheric CO_2 gross fluxes. However, it exceeds several limitations present in earlier modelling studies which make it much more realistic than the former model approaches. My primary aim was to better understand $\delta^{18}O$ in atmospheric CO_2 and the model proofs to be a perfect tool for this task.

The model of $\delta^{18}O$ in atmospheric CO_2 is introduced in Chapter 2 and the models structure, its interdependencies, and parameterisations of the key processes are explained there. The models surface processes are compared to observations of various nature and on various scales in order to validate the calculated biospheric CO_2 fluxes and the isotopic composition of the different water pools. These fluxes and water pools constitute the main components that determine the $CO^{18}O$ fluxes which are emitted to or withdrawn from the atmosphere. The $CO^{18}O$ fluxes together with the CO_2 fluxes are the source functions that determine the $\delta^{18}O$–CO_2 concentrations in the atmosphere.

Chapter 3 focuses on the atmospheric signal of $\delta^{18}O$–CO_2. First, the seasonal cycle of CO_2 in the atmosphere is compared with observations. This is a required test of the realism of the CO_2 fluxes. Then, $\delta^{18}O$ in atmospheric CO_2 offers a unique integrated measure of the performances of the different modules (CO_2, transport, $\delta^{18}O$–CO_2, etc.) and their interactions. Here I investigate the seasonal cycle of $\delta^{18}O$–CO_2 and the north–south gradient of $\delta^{18}O$–CO_2. The sensitivity to different model formulations and inclusion or exclusion of different processes is studied for the seasonal cycle and the meridional gradient. But also the absolute $\delta^{18}O$–CO_2 value in the atmosphere can be calculated with the model for the first time. The model thereby follows closely the analytical solution for the $\delta^{18}O$–CO_2 global mean value. Also in this chapter, I point out the differences between the new, comprehensive model and former model

formulations. There are huge differences in the model behaviours that are mostly the results of interactions between different model components. Earlier model attempts did not include these interactions and I give in Chapter 3 new insight into the holistic nature of $\delta^{18}O$ in atmospheric CO_2.

Eurasia is the largest land mass in the northern hemisphere. Its role in the global carbon cycle is important but it is not known precisely. I examine the model behaviour over Eurasia in more detail in Chapter 4 looking especially on the East–West distribution of the CO_2 and $\delta^{18}O$–CO_2 source functions. Some peculiar results in Siberia are shown there which were only expected for far Eastern Siberia. I explain in this chapter how these results could be verified or contravened from future measurements.

Chapter 5 summarises the main findings of the three preceding chapters and emphasises model shortcomings that could be the reason of the ascertained model–data mismatch. I explain in the outlook how the model deficiencies can be treated and how the model can be applied further in carbon cycle research.

References

Allison, C. E., R. J. Francey, and H. A. Meijer, Recommandations for the reporting of stable isotope measurements of carbon and oxygen in CO_2 gas, in *References and Intercomparison Materials for Stable isotopes of Light Elements*, edited by IAEA-TECDOC-825, pp. 155–162, Int. At. Energy Agency, Vienna, 1995.

Baertschi, P., Absolute ^{18}O content of Standard Mean Ocean Water, *Earth Planet. Sci. Lett.*, *31*, 314–344, 1976.

Bowling, D. R., D. D. Baldocchi, and R. K. Monson, Partitioning net ecosystem exchange in a tennesse deciduous forest using stable isotopes of CO_2, Poster presentation, Ecological Society of America Annual Meeting, Spokane, WA, August 8–12, 1999.

Brenninkmeijer, C. A. M., P. Kraft, and W. G. Mook, Oxygen isotope fractionation between CO_2 and H_2O, *Isotope Geoscience*, *1*, 181–190, 1983.

Ciais, P., A. S. Denning, P. P. Tans, J. A. Berry, D. A. Randall, G. J. Collatz, P. J. Sellers, J. W. C. White, M. Trollier, H. A. J. Meijer, R. J. Francey, P. Monfray, and M. Heimann, A three dimensional synthesis study of $\delta^{18}O$ in atmospheric CO_2, part I: Surface fluxes, *J. Geophys. Res.*, *102*, 5 857–5 872, 1997a.

Ciais, P., P. P. Tans, A. S. Denning, R. J. Francey, M. Trollier, H. J. Meijer, J. W. C. White, J. A. Berry, D. A. Randall, J. J. G. Collatz, P. J. Sellers, P. Monfray, and M. Heimann, A three dimensional synthesis study of $\delta^{18}O$ in atmospheric CO_2, part II: Simulations with the TM2 transport model, *J. Geophys. Res.*, *102*, 5 873–5 883, 1997b.

Dongmann, G., H. W. Nürnberg, H. Förstel, and K. Wagner, On the enrichment of $H_2{}^{18}O$ in the leaves of transpiring plants, *Rad. and Environm. Biophys.*, *11*, 41–52, 1974.

Farquhar, G. D., J. Lloyd, J. A. Taylor, L. B. Flanagan, J. P. Syvertsen, K. T. Hubick, S. C. Wong, and J. R. Ehleringer, Vegetation effects on the isotope composition of oxygen in atmospheric CO_2, *Nature*, *363*, 439–443, 1993.

Keeling, C. D., R. B. Bacastow, A. F. Carter, S. C. Piper, T. P. Whorf, M. Heimann, W. G. Mook, and H. Roeloffzen, A three–dimensional model of atmospheric CO_2 transport based on observed winds, 1. Analysis on observational data, in *Aspects of Climate Variability in the Pacific and the Western Americas, Geophys. Monogr. Ser.*, edited by D. H. Peterson, vol. 55, pp. 165–236, AGU, Washington, D.C., 1989.

Langendörfer, U., M. Cuntz, P. Ciais, P. Peylin, T. Bariac, I. Milyukova, O. Kolle, T. Naegler, and I. Levin, Modelling of biospheric CO_2 gross fluxes via oxygen isotopes in a spruce forest canopy: a ^{222}Rn calibrated box model approach, *Tellus*, *54B*, 2002, in press.

Levin, I., J. Schuchard, B. Kromer, and K. O. Münnich, The continental European Suess effect, *Radiocarbon*, *31*, 431–440, 1989.

Peylin, P., The composition of ^{18}O in atmospheric CO_2: A new tracer to estimate global photosynthesis, Ph.D. thesis, L'Université Paris VI, Paris, 1999, in french.

Prentice, I. C., G. D. Farquhar, M. J. R. Fasham, M. L. Goulden, M. Heimann, V. J. Jaramillo, H. S. Kheshgi, C. Le Quéré, R. J. Scholes, and D. W. R. Wallace, The carbon cycle and atmospheric CO_2, in *Third Assessment Report of Climate Change*, edited by J. T. Houghton and D. Yihui, Report of the International Panel on Climate Change, chap. 3, pp. 38–71, Cambridge University Press, New York, 2001.

Ryan, M. G., Effects of climate change on plant respiration, *Ecol. Appl.*, *1*, 157–167, 1991.

Yakir, D., and X.-F. Wang, Fluxes of CO_2 and water between terrestrial vegetation and the atmosphere estimated from isotope measurements, *Nature*, *380*, 515–517, 1996.

Chapter 2

Validation of Surface Processes

2.1 Introduction

The atmospheric signal of CO_2 is an integrated measure of all processes adding CO_2 to and removing CO_2 from the atmosphere. Consequently, one can deduce only the net CO_2 flux from atmospheric measurements. Inversion studies of atmospheric CO_2 measurements make therefore only predictions of net CO_2 fluxes over different regions [e. g. *Gurney et al.*, 2002]. To separate the different components of the net flux, several tracers are used depending on the component. For example, ^{13}C is used to separate between ocean and terrestrial biosphere fluxes, or ^{14}C is used to separate the fossil fuel combustion contingent. ^{18}O offers the possibility to separate the different terrestrial biospheric gross fluxes, namely assimilation and respiration. This comes from the fact that CO_2 can exchange ^{18}O atoms with two isotopically distinct water pools, either with leaf water or with soil water. Statistically, a CO_2 molecule going into plant leaves is fixed by photosynthesis with a probability of $1/3$ whereas it diffuses back to the atmosphere with a probability of $2/3$. Nevertheless, the isotopic exchange between CO_2 and water within leaves in presence of the enzyme carbonic anhydrase is so fast that back–diffused CO_2 re–entering the atmosphere is isotopically "tagged" by evaporating leaf water. Leaf water at the evaporating site is generally significantly enriched with respect to soil moisture and so is leaf CO_2 with respect to soil respired CO_2. However, unlike for ^{13}C where the ocean, C4 plants, and C3 plants have distinct, narrowly defined signatures that are similar all over the globe, the ^{18}O isotopic labelling of CO_2 by photosynthesis and respiration varies in space and time reflecting hydrological processes and climate dependent fractionation factors. This means that in order to understand the integrated atmospheric signal of ^{18}O in CO_2, one must use a spatially explicit model of surface fluxes coupled to a 3D model of the atmospheric transport including water isotopic composition.

Few studies have attempted so far to model the distribution of ^{18}O in atmospheric CO_2. The major conceptual difficulty lies in the requirement of a triad of models describing 1) the gross carbon fluxes, 2) the water isotope variability, and 3) the atmospheric transport. *Ciais et al.* [1997a, b] have put together those three components using output from different published models that were sampled as monthly averages. This approach gave a reasonably good comparison with atmospheric observations and

provided useful a priori estimates to inverse modelling of the gross fluxes [*Peylin*, 1999], but it remains unsatisfactory for three reasons: First, there were inconsistencies among the different models that were used to construct $CO^{18}O$ fluxes inducing systematic errors that are impossible to estimate. Second, working with monthly mean fluxes does not allow to properly up–scale biogeochemical processes from the ecosystem level up to the quasi global atmospheric signal. Third, working with monthly fluxes neglects the existence of a strong daily cycle in the fluxes of photosynthesis and respiration that unfortunately covary with atmospheric transport in the boundary layer to generate mean gradients in CO_2 and in $\delta^{18}O$–CO_2.

In this chapter, I present a new, comprehensive model of ^{18}O in atmospheric CO_2 where leaf and soil processes that determine the isotopic fluxes are encapsulated into a land surface carbon flux model, that is consistently interfaced to a global atmospheric transport model. The CO_2 and $CO^{18}O$ flux model is described in section 2.2, and its results are compared against ground based, pointwise CO_2 flux measurements and isotopic data in section 2.3. Chapter 3 is devoted to the comparison between background measurements of CO_2 and $\delta^{18}O$–CO_2 in flask samples and the modelled $\delta^{18}O$–CO_2 values obtained by atmospheric transport acting on surface sources.

2.2 Model description

The model, herein named BETHY online or ECHAM/BETHY, integrates four parts that are shown in Figure 2.1 together with their interactions. ECHAM is thereby the Atmospheric General Circulation Model (AGCM) within which are embedded the calculations for the isotopic composition of different water pools (WFRAC) and the atmospheric tracer transport. BETHY is a biosphere model which is driven with variables from ECHAM and it releases its calculated CO_2 surface fluxes into the ECHAM atmosphere. OFRAC is the $CO^{18}O$ flux module which takes ECHAM and BETHY variables and the $\delta^{18}O$ value of CO_2 in the ECHAM atmosphere as input to calculate $CO^{18}O$ fluxes which are emitted in the atmosphere of ECHAM, too. I will further on describe the different parts of the model. I will introduce ECHAM and WFRAC only briefly because they are described in detail elsewhere [*Modellbetreuungsgruppe*, 1994; *Hoffmann et al.*, 1998]. An extensive description of BETHY can be found in *Knorr and Heimann* [2001a, b] but I will repeat the main aspects that influence the calculations of $CO^{18}O$ fluxes. OFRAC bases on the equations of *Ciais et al.* [1997a] which were adapted to calculate the $CO^{18}O$ fluxes online in an AGCM. I explain them in detail to elaborate on the differences between ECHAM/BETHY and earlier $\delta^{18}O$–CO_2 models.

ECHAM is a state of the art AGCM used in several studies [e. g. *Arpe et al.*, 1994; *Roeckner et al.*, 1992]. In this study, I used the T21 spectral truncation scheme which corresponds to a physical grid of 5.6°x5.6° (time step of 40 minutes). The model has 19 vertical layers from surface pressure up to a pressure level of 30 hPa and includes a tracer transport scheme. WFRAC is implemented in ECHAM calculating to each phase of "normal" water, H_2O, an isotopic counterpart, $H_2^{18}O$ and HDO. It showed its excellent capability to simulate recent and paleo water and snow isotope distributions in a variety of studies [e. g. *Hoffmann et al.*, 1998, 2000; *Werner et al.*, 2001].

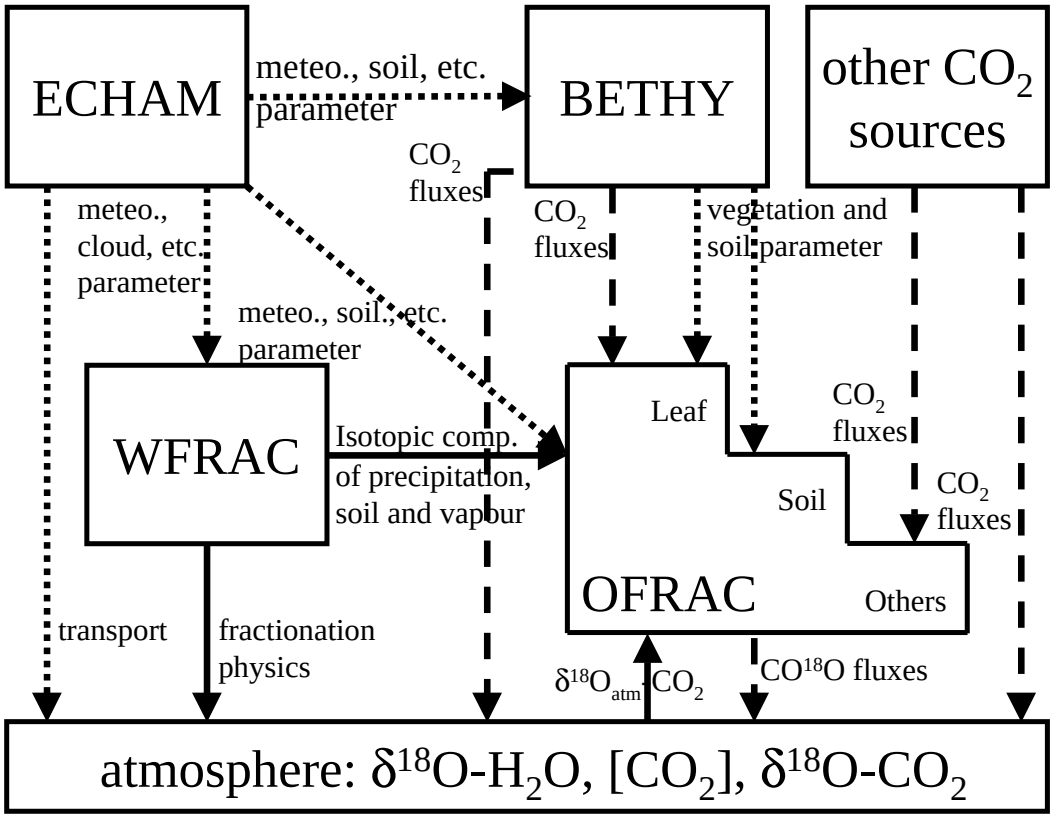

Figure 2.1: Interactions between the different parts of the model. ECHAM is the AGCM in which the water isotopes (WFRAC) and the tracer transport are included. BETHY is interfaced and the $CO^{18}O$ isotope module (OFRAC) is 'coupled' to ECHAM. Solid lines stand for isotopic processes, dashed lines for CO_2 and $CO^{18}O$ fluxes and dotted lines stand for physical and meteorological parameters, and for transport.

2.2.1 The CO_2 flux model BETHY

I interfaced a process–based model of terrestrial vegetation activity, the Biosphere Energy–Transfer Hydrology scheme (BETHY) to the AGCM ECHAM. It calculates CO_2 fluxes of the terrestrial biosphere together with further diagnostic variables of the biosphere like e. g. stomatal conductance and vegetation temperature. An extensive description of the BETHY offline model can be found in *Knorr* [2000] and *Knorr and Heimann* [2001a]. I interfaced BETHY rather than coupling it to ECHAM; this will be done in a future step. That means that BETHY online does not interfere in the AGCM ECHAM. BETHY online is forced by meteorological variables of ECHAM but ECHAM is not influenced by e. g. BETHY calculated stomatal conductance. BETHY uses its own land–surface scheme, too. Therefore in order to obtain realistic evapotranspiration rates, vegetation temperatures and, hence, realistic stomatal conductances from the ECHAM energy and water budgets, I recompute the latent and sensible heat fluxes from the canopy of BETHY (even if they are already computed by ECHAM but with its internal land surface scheme). Since plants constantly lose water through their stomatal pores while photosynthesing, water availability is related closely to carbon uptake.

The relationship between canopy net assimilation rate A_c (gross assimilation rate,

"GPP", minus leaf respiration, R_d), canopy conductance G_c (integral over stomatal conductances), and stomata–internal CO_2 mixing ratio c_i is:

$$A_c = G_c\,(c_a - c_i)\,\frac{p}{1.6 R_{gas} T_K} \tag{2.1}$$

where c_a is the mixing ratio of atmospheric CO_2, R_{gas} the universal gas constant, T_K air temperature in Kelvin, and p air pressure in Pascal. The photosynthesis part of the model computes absorption of photosynthetically active radiation (PAR) through the canopy with a two–flux scheme [*Sellers*, 1985] for three vertical layers of equal LAI, gross carbon uptake, and leaf respiration. Carbon uptake and leaf respiration are described with the so called Farquhar model for C3 [*Farquhar et al.*, 1980] and a similar model for C4 plants [*Collatz et al.*, 1992]. These are process–oriented models which require a rather large number of kinetic and structural parameters. Used plant functional types together with the assigned parameters are shown in Table 2.1. To describe the stomatal response to environmental factors, a semi–empirical approach is used with only one free parameter. Observations suggest that in the absence of water limitation, canopy conductance is determined by photosynthetic demand for CO_2 [*Schulze et al.*, 1994]. So a non–water–stressed canopy conductance, G_{c0}, is first computed at a standard non–water–stressed stomata–internal CO_2 mixing ratio, c_{i0} [*Jones*, 1983; *Knorr*, 1997]:

$$G_{c0} = \frac{A_{c0}}{c_a - c_{i0}} \frac{1.6 R T_K}{p} \tag{2.2}$$

where A_{c0} is the non–water–limited net leaf CO_2 uptake in µmole m^{-2} s^{-1}, so that G_{c0} is given in m/s. If there is a limitation of soil water to photosynthesis, stomate are supposed to close in response to air vapour pressure deficit, Δe [*Schulze et al.*, 1987; *Schulze*, 1986; *Turner*, 1986; *Fischer and Turner*, 1978]. I use the empirical formula [*Lindroth and Halldin*, 1986]:

$$G_c = G_{c0} \frac{1}{1 + b_e \Delta e}\,. \tag{2.3}$$

The factor b_e is assumed to change such that the transpiration through the stomata does not exceed the root supply rate, S [*Federer*, 1982]:

$$S = c_w \frac{W_s}{W_{s,max}} \tag{2.4}$$

where W_s is the soil water content adjusted to take soil freezing into account, $W_{s,max}$ the maximal root available soil water content and c_w an empirical parameter representing root density. I adopted a value of $c_w = 0.5$ mm/hour from a comparison with measured values of A_c and G_c for single days [*Knorr*, 1997] and a global sensitivity study on this parameter [*Knorr and Heimann*, 2001a].

Though, the computational and logical steps are: the BETHY online model calculates first A_c as A_{c0} from the Farquhar model using c_{i0}. The non–water–stressed canopy conductance, G_{c0}, is then computed from equation 2.2 (at $c_i = c_{i0}$). After determining G_c from equation 2.3, the Farquhar model is resolved with unknown c_i but with the additional constraint to satisfy equation 2.1.

Table 2.1: List of plant functional types used in the BETHY online model with assigned parameters: V_m: maximum carboxylation rate at 25 °C in µmole(CO_2) m^{-2} s^{-1}; J_m: maximum electron transport rate at 25 °C in µmole(CO_2) m^{-2} s^{-1} (C3) or k: CO_2 specificity at 25 °C in µmole(CO_2) m^{-2} s^{-1} (C4); h_V: height in m; C4: using C4 photosynthetic pathway instead of C3.

#	Plant Func. Types	V_m	J_m/k	h_V	C4
1	Trop. BL E trees	60	118	30.0	
2	Trop. BL D trees	90	179	15.0	
3	Temp. BL E trees	41	82	15.0	
4	Temp. BL D trees	35	70	15.0	
5	E coniferous trees	29	52	15.0	
6	D coniferous trees	53	95	15.0	
7	E shrubs	52	102	1.0	
8	D shrubs	160	266	1.0	
9	C3 short grass	42	80	0.3	
10	C3 long grass	42	80	2.0	
11	C4 short grass	8	140	0.3	x
12	C4 long grass	8	140	2.0	x
13	Tundra vegetation	20	37	0.3	
14	Swamp vegetation	20	37	0.3	
15	Arable crops	117	220	0.6	
16	Irrigated crops	123	227	0.6	
17	Tropical tree crops	60	106	2.0	
18	Citrus crops	60	106	2.0	
19	Temp. D tree crops	123	227	2.0	
20	Sugar cane	39	700	2.0	x
21	Maize	39	700	2.0	x
22	Rice	98	190	0.3	
23	Cotton	123	227	1.0	

Abbreviations: Trop.: tropical; Temp.: temperate; BL: broad–leaved; E: evergreen; D: deciduous

There are several descriptions of heterotrophic or soil respiration [*Raich and Potter*, 1995; *Lloyd and Taylor*, 1994; *Raich and Schlesinger*, 1992; *Meentemeyer*, 1978] that have in common that soil respiration follows approximately with temperature and that the micro–organism needs water to produce CO_2. I use the formulation of *Raich and Potter* [1995] with $Q_{10} = 1.5$ and 2 m air temperature, T_a, because this smaller value is more consistent with the observed seasonal cycle of atmospheric CO_2 [*Knorr and Heimann*, 1995] compared to the more 'traditional' value of $Q_{10} = 2.0$ [*Raich and Schlesinger*, 1992]. Furthermore, I include a proportional dependence on actual over

potential evapotranspiration, f_e [*Meentemeyer*, 1978]:

$$R_H = c_1 f_e Q_{10}^{T_a/10} \tag{2.5}$$

where

$$f_e = \frac{E_v}{E_{max}} \,. \tag{2.6}$$

E_v is the actual and E_{max} the maximum possible transpiration rate from soil and vegetation. The rate c_1 is renormalised such that the mean of R_H over 10 years equals the mean of NPP at every grid point; i. e. the terrestrial biosphere is supposed to be in equilibrium.

There is no phenology scheme inside the BETHY online version but it is taken as monthly input from the offline version of BETHY optimised with satellite derived fraction of photosynthetically active radiation absorbed by vegetation (FPAR) [*Knorr and Heimann*, 2001b].

2.2.2 Non–biospheric CO_2 fluxes

Ciais et al. [1997b] stated that one needs biomass burning and fossil fuel emissions to model a more realistic north–south gradient of δ^{18}O–CO_2. I introduce hence into the atmosphere non–biospheric CO_2 fluxes from linear interpolation between monthly mean input fields. First, I took the formulation of *Wanninkhof* [1992] to compute the air–sea gas exchange coefficient and the instantaneous ECHAM wind fields to calculate CO_2 ocean fluxes from the ocean ΔpCO_2 compilation of *Takahashi et al.* [1999]. Second, I include fossil fuel CO_2 emissions via the annual compilation of *Andres et al.* [1996] which I distributed on a monthly basis with coefficients given by *Marland et al.* [1998]. Further, I introduce biomass burning emissions into the atmosphere which includes forest and savanna burning (seasonal) and agricultural wastes and fuel wood burning (annually constant) [*Hao and Liu*, 1994]. All fluxes are scaled to values representative of the year 1990. Conceptually, re–growth after burning is not included in BETHY online and I have no closed carbon cycle, though. Because I look mainly at seasonal cycles and north–south gradients at the moment, it is not essential to close the carbon cycle. One can see below in equation 2.23 that the δ^{18}O–CO_2 cycle depends on gross biospheric fluxes which are at least one order of magnitude higher than the net biospheric fluxes and especially the fluxes missing to close the carbon cycle in the model.

2.2.3 The $CO^{18}O$ flux module OFRAC

The δ^{18}O isotopic signature of CO_2 is determined mainly by the isotopic equilibrium reaction:

$$\mathrm{COO} + \mathrm{H_2}^{18}\mathrm{O} \leftrightarrow \mathrm{CO}^{18}\mathrm{O} + \mathrm{H_2O} \,. \tag{2.7}$$

If this reaction occurs in nature, in most cases there are several orders of magnitude more water associated than CO_2. That means that the isotopic signature of CO_2 is fully determined by the isotopic signature of the equilibrating water which is barely changing itself. This equilibration process is temperature dependent and the fractionation follows

the relationship [*Brenninkmeijer et al.*, 1983]:

$$\epsilon_{eq}(T) = \left(\frac{17604}{T} - 17.93\right)/1000\,, \tag{2.8}$$

and

$$\alpha_{eq}(T) = 1 + \epsilon_{eq}(T) \tag{2.9}$$

is the fractionation factor. For example, the fractionation at 25 °C is: $\epsilon_{eq} = +41.11\,‰$ and $\mathrm{d}\epsilon_{eq}/\mathrm{d}T = -0.20\,‰\,^{\circ}\mathrm{C}^{-1}$, means higher temperatures lead to more depleted δ^{18}O–CO_2 values with constant δ^{18}O–H_2O. The isotope ratio of CO_2, R, equilibrated with water of composition R^W is hence: $R = \alpha_{eq}(T)\ R^W$.

Each flux of CO_2, F, is accompanied by a flux of $CO^{18}O$, ${}^{18}F$. If the flux exchanges CO_2 between two compartments or if there is a phase transition, a fractionation occurs (α can be higher, lower or equal to 1). For example, the complex phenomenon of diffusion out of the soil is accompanied by just one fractionation factor in the model. The $CO^{18}O$ flux is calculated therefore as:

$${}^{18}F = \alpha\ \alpha_{eq}(T)\, R^W F \tag{2.10}$$

where α represents the fractionation occurring at the transition from one compartment or phase into another.

Respiration

From the above follows directly the soil $CO^{18}O$ flux, ${}^{18}F_s$:

$${}^{18}F_s = \alpha_s R_s F_s = \alpha_s \alpha_{eq}(T_s)\, R_s^W F_s \tag{2.11}$$

where R_s^W is the isotopic ratio of the soil water pool that exchanges with CO_2 and is taken directly from the water isotope module, and F_s is the CO_2 flux from the soil to the atmosphere which comes from BETHY. Soil fractionation, $\epsilon_s = \alpha_s - 1$, is a sensitive parameter. *Ciais et al.* [1997a] used a value of $-5.0\,‰$ in order to prevent a secular trend in δ^{18}O–CO_2 of the atmosphere. *Peylin et al.* [1997] made a sensitivity study on this fractionation factor together with the fractionation associated with assimilation and found possible values also around $-5.0\,‰$ matching the seasonal amplitude at Point Barrow and the inter–hemispheric difference. However, in their model δ^{18}O of atmospheric CO_2, δ_a, was forced to $0\,‰$ vs. VPDB–CO_2 and they used the fractionation factors of soil and aboveground vegetation as free parameters to obtain zero trend in their recalculated δ_a values. The BETHY online isotope module calculates δ_a and $CO^{18}O$ fluxes depending on δ_a on every time step, and, therefore, δ_a stabilises globally (see eq. 2.23). That means that the fractionation factors can theoretically have any possible value and δ_a will have no trend after the asymptotic equilibrium value is reached. For ϵ_s, I take the recent value of *Miller et al.* [1999]: $\epsilon_s = -7.2\,‰$. *Miller et al.* give this value for the fractionation of CO_2 diffusion from soils when one takes the soil water isotopic composition at 15 cm depth. They included in this global estimate already the "invasion" effect that is explained below. I include the portion of the autotrophic respiration, R_A, which is not emitted via leaves, $R_a = R_A - R_d$, into F_s. Most of the CO_2 of the autotrophic respiration R_A is emitted by roots belowground (root respiration) and

thus underlies the same fractionation as the heterotrophic respiration. There is a small part of R_a which is emitted aboveground by stems and twigs. *Bariac et al.* [1994a, b] showed that there is almost no difference between the isotopic value of soil and plant organic water (except for leaves). Water isotopes in soil show a steep gradient in the top soil layer but the e–folding length to the constant, deep–soil value is only about 10 to 15 cm. *Bariac et al.* took the asymptotic value of $\delta^{18}O$–H_2O to compare with xylem water. Also, CO_2 in stems and twigs is expected to be in isotopic equilibrium with water. Thence, I include this flux in R_a so that F_s is the heterotrophic plus autotrophic without leaf respiration: $F_s = R_H + R_A - R_d$, which I call bio–respiration.

There is another flux at the air–soil interface which exists for $CO^{18}O$ and not for CO_2. The transport of CO_2 is a diffusional process and, therefore, the sum of two gross fluxes in and out of the soil. The flux into the soil is small due to the big mixing ratio difference of CO_2 in the soil and in the atmosphere. *Tans* [1998] wrote the net flux for $CO^{18}O$ as the sum of one flux leaving the soil, the above F_s, and a second flux of CO_2–molecules entering the soil with atmospheric isotope signature, equilibrating with soil water and leaving the soil with the signature of soil water. This second flux is called the "abiotic flux" [*Stern et al.*, 2001] or "invasion flux" and the effect is called "invasion" [*Tans*, 1998]. This means, CO_2 with the isotopic composition R_a entering the soil can equilibrate with soil water, R_s^W, and leaves the soil with the isotopic signature R_s. The invasion flux, ${}^{18}F_{inv}$, is then:

$$\begin{aligned} {}^{18}F_{inv} &= \sqrt{\Theta_a \kappa \Theta_w k_H D_{18} B}\; c_a \left(R_s - R_a\right) \\ &= F_{inv} \left(R_s - R_a\right) \end{aligned} \tag{2.12}$$

with

Θ_a	air–filled pore fraction of soil,
κ	tortuosity,
Θ_w	water–filled pore fraction,
k_H	CO_2 hydration rate in water,
D_{18}	free–air molecular diffusivity of $CO^{18}O$,
B	Bunsen solubility coefficient.

F_{inv} may be seen as a virtual CO_2 flux which is convenient for latter calculations.

Assimilation

CO_2 needs approximately 3 min at 10 °C for hydration in water. The average residence time of a CO_2 molecule in the stomata is about 0.02 s [*Ciais et al.*, 1997a]. But there is the enzyme carbonic anhydrase in leaves which catalyses and speeds up the reaction by a factor of 10^7 [*Stryer*, 1981]. This implies that every CO_2 molecule entering the stomata is hydrated. Then, the isotopic equilibrium reaction (eq. 2.7) can take place and CO_2 is in isotopic equilibrium with the water between the mesophyll cell wall and the chloroplast. There is a gradient between the CO_2 mixing ratio in the stomata, c_i, and in the chloroplast, c_c, during photosynthesis. There is no gradient if there is no photosynthetic activity. Leaf–scale measurements indicate that the average drawdown is of the order $(c_i - c_c)/c_a \approx 0.1 - 0.2$ [*Yakir and Sternberg*, 2000; *Lloyd*

and Farquhar, 1994]. But, the equilibration process occurs mainly at the chloroplast or cellular membrane (plasmalemma) where the average drawdown is approximately 0.1 [*Gillon and Yakir*, 2000a]. I denote the mixing ratio where the equilibrium reaction occurs as c_{cs} because it is likely to be the surface of the chloroplast [*Yakir*, 1998]. I take for c_{cs} the stomata–internal CO_2 mixing ratio c_i as a first guess and try to quantify the consequences of different equilibration places afterwards (see Chapter 3). Using c_{cs}, equation 2.1 becomes:

$$A = g_s\,(c_a - c_i) = g'_s\,(c_a - c_{cs}) \tag{2.13}$$

where g'_s is the sum of the (inverse) stomatal conductance and the conductance between the stomata and the plasmalemma (in this notation, g_s is the stomatal conductance for CO_2 in mole m^{-2} s^{-1} whereas G_c in equation 2.1 is the canopy conductance for water vapour in m s^{-1}). Assuming that the conductance is very similar for CO_2 and for $CO^{18}O$, the diffusion equation 2.13 for $CO^{18}O$ is:

$${}^{18}F_a = \alpha_d g'_s\,(R_a c_a - R_l c_{cs})\,\alpha_d g'_s\left(R_a c_a - \alpha_{eq}(T_v) R_l^W c_{cs}\right) \tag{2.14}$$

where ${}^{18}F_a$ is the flux of $CO^{18}O$ molecules into the leaves, α_d the kinetic fractionation factor for diffusion into the stomata ($\epsilon_d = -7.4\,‰$ [*Farquhar et al.*, 1993]), and R_l^W the isotopic composition of leaf water at the site of equilibration. Equation 2.13 shows that net assimilation is the sum of two opposing fluxes, in and out of the stomata. Rewriting the equation gives that the gross flux into the stomata is $Ac_a/(c_a - c_c)$ and the flux out of the stomata is $Ac_c/(c_a - c_c)$. This means that only about ½ to ⅓ $[(c_a - c_c)/c_a]$ of all CO_2 molecules entering the leaf will finally be assimilated. The isotopic composition of leaf water at the site of equilibration, R_l^W, is calculated with the Craig and Gordon steady state approximation [*Craig and Gordon*, 1965]:

$$R_{l-cg}^W = \alpha_{l-vap}^W \left(\frac{(1-h)\,R_i^W}{\alpha_k^W} + h R_{vap}^W\right) \tag{2.15}$$

with

h	air relative humidity,
α_{l-vap}^W	fractionation factor for $H_2{}^{18}O$ at the water–vapour phase transition,
α_k^W	combined kinetic fractionation factor for $H_2{}^{18}O$ for diffusion through the stomata and the leaf boundary layer,
R_{vap}^W	${}^{18}O/{}^{16}O$ ratio of water vapour in canopy air,
R_i^W	${}^{18}O/{}^{16}O$ ratio of xylem water, supplied to the leaf ≈ soil water.

The isotope ratios of vapour and soil water are calculated from the water isotope module on every time step. The relative humidity is an ECHAM diagnostic variable, and the canopy is approximated by the first ECHAM model layer. The fractionation of the water–vapour phase transition is calculated from *Majoube* [1971]. The kinetic fractionation, ϵ_k^W, is higher for molecular than for turbulent diffusion [*Merlivat and Jouzel*, 1979]. It depends also on plant physiology [*White*, 1983] and on wind speed [*Förstel et al.*, 1975]. I take a global value of $\epsilon_k^W = -26.0\,‰$ [*Farquhar et al.*, 1993] which itself results in an error. This error is diminished by the fact that α_k^W is weighted with the factor $(1-h)$ which is often close to 0. This is not true for dry areas but these are normally associated with low photosynthetic activity. The Craig

and Gordon steady state approximation is probably not 'reached' from leaf water at every time step. Measurements indicate a time lag between measured values and values calculated with the Craig and Gordon model [e. g. *Roche*, 1999]. To overcome this problem, one can use a transitory model whereby the leaf water value is a mixture of the Craig and Gordon calculation and the value one time step before [*Dongmann et al.*, 1974; *Förstel et al.*, 1975; *Bariac et al.*, 1994a, b]:

$$R_l^{W(t)} = R_{l-cg}^{W(t)} - \left(R_{l-cg}^{W(t)} - R_l^{W(t-1)}\right) \exp\left\{-\frac{1}{\tau\zeta}\Delta t\right\} \tag{2.16}$$

with

$R_l^{W(t)}$	leaf water isotopic composition at the site of evaporation at time t,
$R_l^{W(t-1)}$	leaf water isotopic composition at time step t−1,
$R_{l-cg}^{W(t)}$	Craig and Gordon steady state solution at time t,
τ	turnover time of leaf water: $\tau = V_l/E_v$,
	E_v is the transpiration rate,
	V_l is the leaf water volume,
ζ	$= (1-h)(\epsilon_{l-vap}^W + 1)(\epsilon_k^W + 1)$.

To estimate the exponential weighting factor, one needs the leaf water volume contributing to evapotranspiration, V_l, for which, to our knowledge, there are no estimates for different plant functional types in the literature. So I compared the steady state Craig and Gordon model and the transitional non–steady state model to laboratory measurements on Rajmah red kidney beans (*Phasedus vulgaris*) [*Roche*, 1999] and field measurements made during the EUROSIBERIAN CARBONFLUX (cf. Appendix) campaign in a 150 year old *Picea abies* (Norway Spruce) forest in Russia [*Langendörfer et al.*, 2002]. Both data showed a time lag of about two hours between Craig and Gordon and the transitory model and the transitory model compared much better with the measurements (results not shown here). Therefore, I assigned τ a fixed value of about three hours $(2/\ln 2)$ to account for non–steady state dynamic evolution of leaf water.

The enzyme carbonic anhydrase is distributed uniformly in the mesophyll cells and speeds up hydration of CO_2 in leaf water by a factor of 10^7 [*Stryer*, 1981]. This leads to the assumption that every CO_2 molecule once entered the stomatal cavity is almost instantaneously hydrated and soon isotopicly equilibrated with leaf water. CO_2 molecules which cannot be carboxylated in plants due to limitations like electron transport diffuse back in the atmosphere and carrying the leaf water isotopic composition into the atmosphere. Recent findings suggest that the carbonic anhydrase activity could be reduced so that not every CO_2 molecule which diffuses in the stomate becomes hydrated immediately but that one part of the CO_2 molecules can diffuse back in the atmosphere without being "tagged" by leaf water [*Gillon and Yakir*, 2000b, 2001]. This translates in equation 2.14 to a modified R_l. Be θ the degree of equilibration in %, i. e. if 80% of all CO_2 molecules entering the leaf become hydrated immediately, $\theta = 0.8$. θ percent of the CO_2 molecules will still get the isotopic signature of leaf water where the other $(1-\theta)$ percent will only be affected by diffusion fractionation, α_d. The modified R_l, named R_{l-ca}, will then be [*Gillon and Yakir*, 2000b]:

$$R_{l-ca} = \theta R_l + (1-\theta)\left\{1 + \left(1 - \frac{c_{cs}}{c_a}\right)\alpha_d\right\} R_a\,. \tag{2.17}$$

The $CO^{18}O$ flux is therefore equation 2.14 with R_l replaced by R_{l-ca}:

$$\begin{aligned} {}^{18}F_{a-ca} &= \alpha_d g'_s \left(R_a c_a - R_{l-ca} c_{cs}\right) \\ &= \alpha_d g'_s \left\{ R_a c_a - c_{cs} \left[\theta R_l + (1-\theta) \left\{ 1 + \left(1 - \frac{c_{cs}}{c_a} \right) \alpha_d \right\} R_a \right] \right\} \\ &= \alpha_d g'_s \left(R_a c_a - R_l c_{cs}\right) \\ &\quad -\alpha_d g'_s \left\{ (1-\theta)\, c_{cs} \left[\left\{ 1 + \left(1 - \frac{c_{cs}}{c_a} \right) \alpha_d \right\} R_a - R_l \right] \right\}. \end{aligned} \tag{2.18}$$

One can see that the second term in the difference is always posit iv (because the ratio of R_a will be only a few per mil lower than R_l but R_a is multiplied by a factor between 1 and 2). The first term in the summation is the $CO^{18}O$ flux with full carbonic anhydrase activity and it is normally positive. So the reduced carbonic anhydrase activity results in a reduced $CO^{18}O$ flux from the atmosphere into the leaf. The measurements of *Gillon and Yakir* [2001] indicate that carbonic anhydrase activity is more reduced in C4 plants than in C3 plants. C4 grasses for example can have a reduced carbonic anhydrase activity of down to $\theta = 0.4$ whereas C3 plants lie around $\theta = 0.9$ or higher. *Gillon and Yakir* estimate a global mean θ of 0.78 with their vegetation distribution and their value is quite similar to the global mean value of 0.8 with BETHY's vegetation distribution.

Ocean and anthropogenic emissions

The $CO^{18}O$ flux of the ocean is calculated as:

$$\begin{aligned} {}^{18}F_o &= -\alpha_w R_a F_{ao} + \alpha_w R_o F_{oa} \\ &= \alpha_w R_a F_o + \alpha_w \left(R_o - R_a\right) F_{oa} \end{aligned} \tag{2.19}$$

with

α_w	fractionation factor of CO_2 crossing the air–sea interface, including hydration,
R_a	$^{18}O/^{16}O$ ratio of CO_2 in air,
R_o	$^{18}O/^{16}O$ ratio of CO_2 equilibrated with ocean surface water,
F_{ao} and F_{oa}	CO_2 one way fluxes between atmosphere and ocean and vice versa,
F_o	net air–sea flux of CO_2 between atmosphere and ocean = $F_{oa} - F_{ao}$.

The fractionation is taken as $\epsilon_w = +0.8\,‰$ [*Vogel et al.*, 1970]. The equilibration process is calculated via equation 2.8 with the ECHAM driving climatological sea surface temperatures, and the $^{18}O/^{16}O$ of ocean surface water which is fitted to the empirical relationship:

$$\delta_0^W = a_1 + a_2 \cdot S \tag{2.20}$$

where S is the salinity in gram salt per kilogram water, and $a_1 = -16.75\,‰$ VSMOW and $a_2 = 0.5\,‰$ VSMOW are taken from *Ciais et al.* [1997a].

Fossil fuel emissions and biomass burning are assumed to be without fractionation, i. e. that the CO_2 emitted carries the signature of atmospheric oxygen, R_f:

$$ {}^{18}F_{fos} = R_f F_{fos} \tag{2.21}$$

$$ {}^{18}F_{bur} = R_f F_{bur} \tag{2.22}$$

with $\delta_f = (R_f / R_{VPDB} - 1) \cdot 1000 = -17\,‰$ VPDB–CO_2.

Global budget of δ^{18}O–CO_2

One can write down the global budget equation for the temporal evolution of δ^{18}O in atmospheric CO_2 (taking only the processes of *Ciais et al.* [1997a, b] for the moment):

$$\frac{d\delta_a}{dt} = \frac{1}{C_a M_a}\left[F_s\Delta_s + A\Delta_l + F_{ao}\Delta_o^{des} + F_o\Delta_o^{equ} + (F_{fos} + F_{bur})\,\Delta_f\right] \tag{2.23}$$

$$\begin{aligned}
\text{with}\quad \Delta_s &= \delta_s - \delta_a + \epsilon_s\,,\\
\Delta_l &= -\epsilon_l + \tfrac{c_{cs}}{c_a - c_{cs}}\,(\delta_l - \delta_a)\,,\\
\Delta_o^{equ} &= \epsilon_w\,,\\
\Delta_o^{des} &= \delta_o - \delta_a\,,\\
\Delta_f &= \delta_f - \delta_a\,.
\end{aligned}$$

M_a is the conversion factor between fluxes in GtC and mixing ratios in ppm ($M_a = 2.122\,\mathrm{GtC\,ppm^{-1}}$, i. e. that one needs about 2 GtC to change the atmospheric CO_2 mixing ratio by 1 ppm), Δ_l the discrimination of photosynthesis, and Δ_o^{equ} the equilibrium discrimination between ocean and atmosphere. The other Δs are no real discriminations. But I use the same symbol for simplicity and denominate them "discriminations" in quotation marks. Δ_s is therefore the "discrimination" associated to soil respired CO_2, Δ_o^{des} the tendency to equilibrate the difference between atmospheric and ocean dissolved CO_2, and Δ_f the "discrimination" of burning processes (simply the difference between the isotopic signatures of O_2 and CO_2). Analogous to plain CO_2, one calls the product of CO_2 flux and "discrimination" an isoflux. Like the change of CO_2 in the atmosphere is the sum of all CO_2 fluxes, the change of δ^{18}O is the sum of all isofluxes. One can rewrite equation 2.23 and finds a differential equation:

$$\frac{d\delta_a}{dt} = a - b\delta_a \tag{2.24}$$

which solution is an exponential evolution of atmospheric δ^{18}O–CO_2 with time:

$$\delta_a(t) = \frac{a}{b} - \frac{a}{b}\exp\{-bt\}\,. \tag{2.25}$$

The factor a is a combination of CO_2 fluxes and δ–values in the compartments, and b consist only of (per definition) positive CO_2 fluxes. Therefore, this is a stable differential equation, and the global δ^{18}O value stabilises at a/b when t becomes infinite:

$$a = F_s(\delta_s + \epsilon_s) + A(\epsilon_l + \frac{c_{cs}}{c_a - c_{cs}}\delta_l) + F_{ao}\delta_o + F_o\epsilon_w + (F_{fos} + F_{bur})\delta_f \tag{2.26}$$

$$b = F_s + \frac{c_{cs}}{c_a - c_{cs}}A + F_{ao} + F_{fos} + F_{bur}\,. \tag{2.27}$$

In contrast to earlier simulations of δ^{18}O in atmospheric CO_2, I must not adjust the fractionation factors to obtain a stable solution. I rather calculate δ_a on every time step and couple it to the $CO^{18}O$ surface fluxes, and hence δ_a will always stabilise if there is no trend in the CO_2 fluxes or the δ–values in the compartments, e. g. the water isotopic composition.

Including other processes in the calculation of δ^{18}O–CO_2 adds isofluxes in the global budget equation. Invasion for example adds the isoflux $F_{inv}\Delta_{inv}$ to equation 2.23 with

$\Delta_{inv} = \delta_s - \delta_a$, the "discrimination" of invasion. This adds consequently terms in the parentheses of equations 2.26 and 2.27 which adds $F_{inv}\delta_s$ to the parenthesis of a and F_{inv} to the parenthesis of b for the invasion effect. This changes the global mean value where δ_a stabilises with time, a/b. The effect of invasion now reduces the global mean δ_a. The proposed reduced activity of carbonic anhydrase changes leaf discrimination to:

$$\begin{aligned}\Delta_{l-ca} &= -\epsilon_l + \frac{c_{cs}}{c_a - c_{cs}} \left\{ \theta \left(\delta_l - \delta_a\right) + (1-\theta) \left(1 - \frac{c_{cs}}{c_a}\right) \epsilon_l \right\} \\ &= -\epsilon_l + \frac{c_{cs}}{c_a - c_{cs}} \left(\delta_l - \delta_a\right) \\ &\quad - \frac{c_{cs}}{c_a - c_{cs}} (1-\theta) \left\{ \delta_l - \delta_a - \left(1 - \frac{c_{cs}}{c_a}\right) \epsilon_l \right\} . \end{aligned} \tag{2.28}$$

The first two terms are leaf discrimination with full carbonic anhydrase activity, Δ_a, so that a reduced carbonic anhydrase activity normally reduces leaf discrimination and the global mean δ_a value will also stabilise at a lower value.

2.3 Results

In order to validate the model, I have to validate first the different modules: the biosphere model and associated CO_2 fluxes, the $CO^{18}O$ fluxes, the water isotope ratios, and the atmospheric transport. I focus in this chapter on the surface processes and try to compare the outcome of the model with other estimates and observations. I will validate only the terrestrial biosphere and exclude ocean fluxes, fossil fuel and biomass burning. I show in Chapter 3 that in order to simulate the seasonal cycle at almost all stations and to simulate the north–south gradient, ocean fluxes, fossil fuel, and biomass burning are not essential; contrary to the results of *Ciais et al.* [1997a, b]. For the north–south gradient, this comes mainly from the fact that in the model, the atmospheric $\delta^{18}O$–CO_2 mixing ratios influence the $\delta^{18}O$ fluxes which was not implemented in $\delta^{18}O$–CO_2 models before.

Fluxes and "Discriminations"

The sum of all CO_2 fluxes determines the temporal change of the CO_2 mixing ratio in the atmosphere; the sum of the isofluxes of $\delta^{18}O$–CO_2 determines the change of $\delta^{18}O$ in atmospheric CO_2, accordingly. The isoflux is thence the $CO^{18}O$ flux expressed in δ–units (in first order approximation). I calculate CO_2 fluxes and isofluxes directly in the model so the "discriminations" are an implication of both, namely the ratio of isoflux and CO_2 flux. The back calculated "discriminations" are consequently flux weighted "discriminations". Earlier $\delta^{18}O$–CO_2 models calculated CO_2 fluxes and "discriminations" separately and multiplied them to get isofluxes. These "discriminations" were thus not flux weighted. They tried to get around this problem using flux weighted variables to calculate their "discriminations" neglecting non–linearities in the calculations, mainly in the discrimination of assimilation. Inconsistencies among the different models, used to calculate isofluxes at last, added errors which were neither commensurable nor estimable. This problem is not present in the model where CO_2

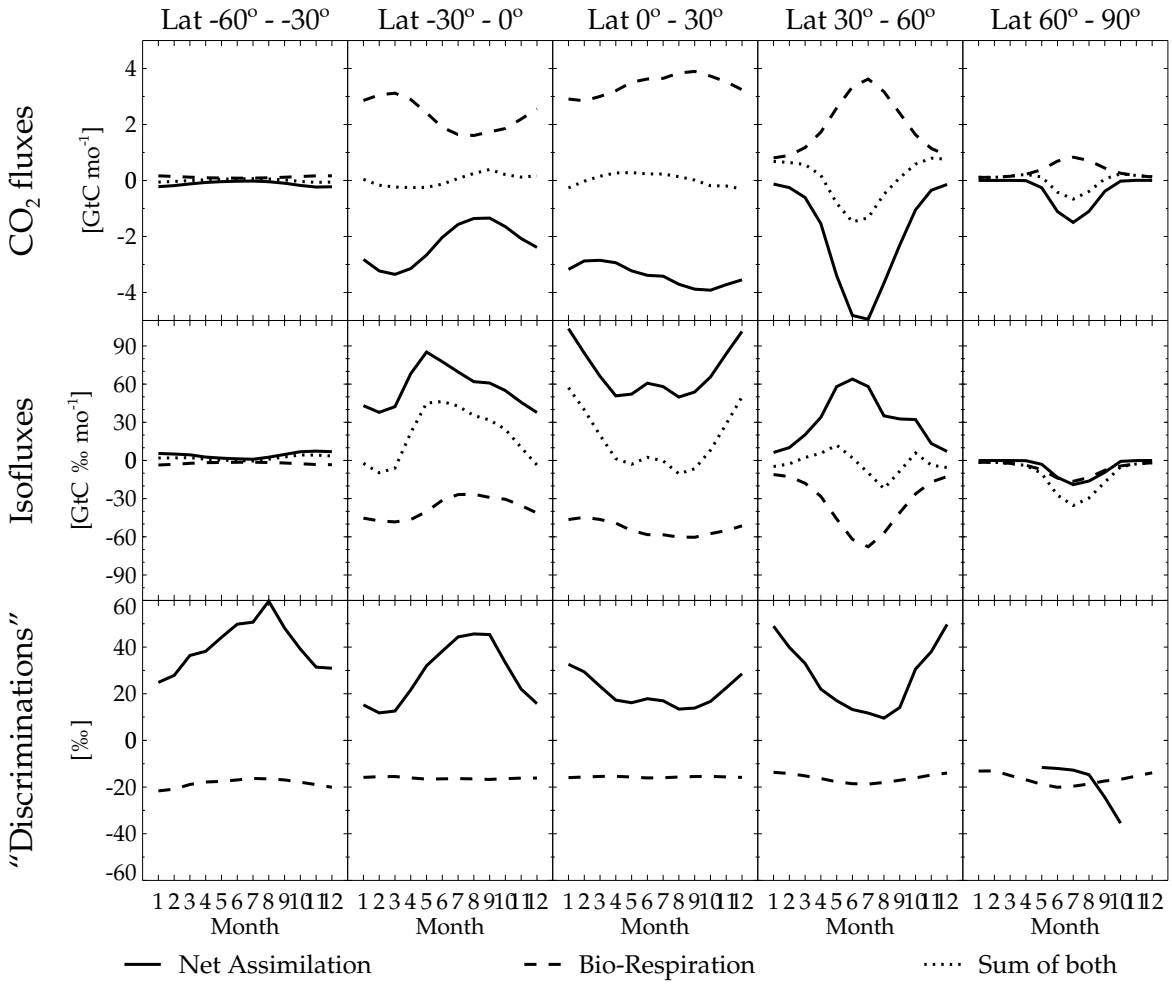

Figure 2.2: Seasonal cycle of CO_2 fluxes, isofluxes and therefrom resulting "discriminations" in 30° latitude bands calculated by ECHAM/BETHY. ("mo" is the abbreviation for month.)

fluxes and isofluxes are consistently calculated which leads to "discriminations" that can be compared to measurements. Unfortunately, measurements of "discriminations" of $\delta^{18}O$–CO_2 are difficult to achieve and therefore very sparce in the literature.

Figure 2.2 shows seasonal cycles of CO_2 fluxes, isofluxes, and resulting "discriminations" as 30° latitudinal means. CO_2 fluxes are given in GtC month^{-1} so one can see that the northern boreal zone (30 to 60 °N) is even more productive during the northern summer than the tropical zone during the southern summer. Poleward, net assimilation (and bio–respiration) decreases visibly. Contrary to assimilation, the northern boreal zone does not show the same maximum value in leaf isoflux as the tropical zone does. Comparing 30 to 60 °N with 0 to 30 °S shows that leaf discrimination diminishes similarly during the accordant summer with about 40 ‰ in winter and 20 ‰ in summer. But winter CO_2 assimilation is much higher in the southern latitude band which along with high discriminations leads to the peak in leaf isoflux in the southern winter. Leaf discrimination becomes negative in the high northern latitudes (missing values come

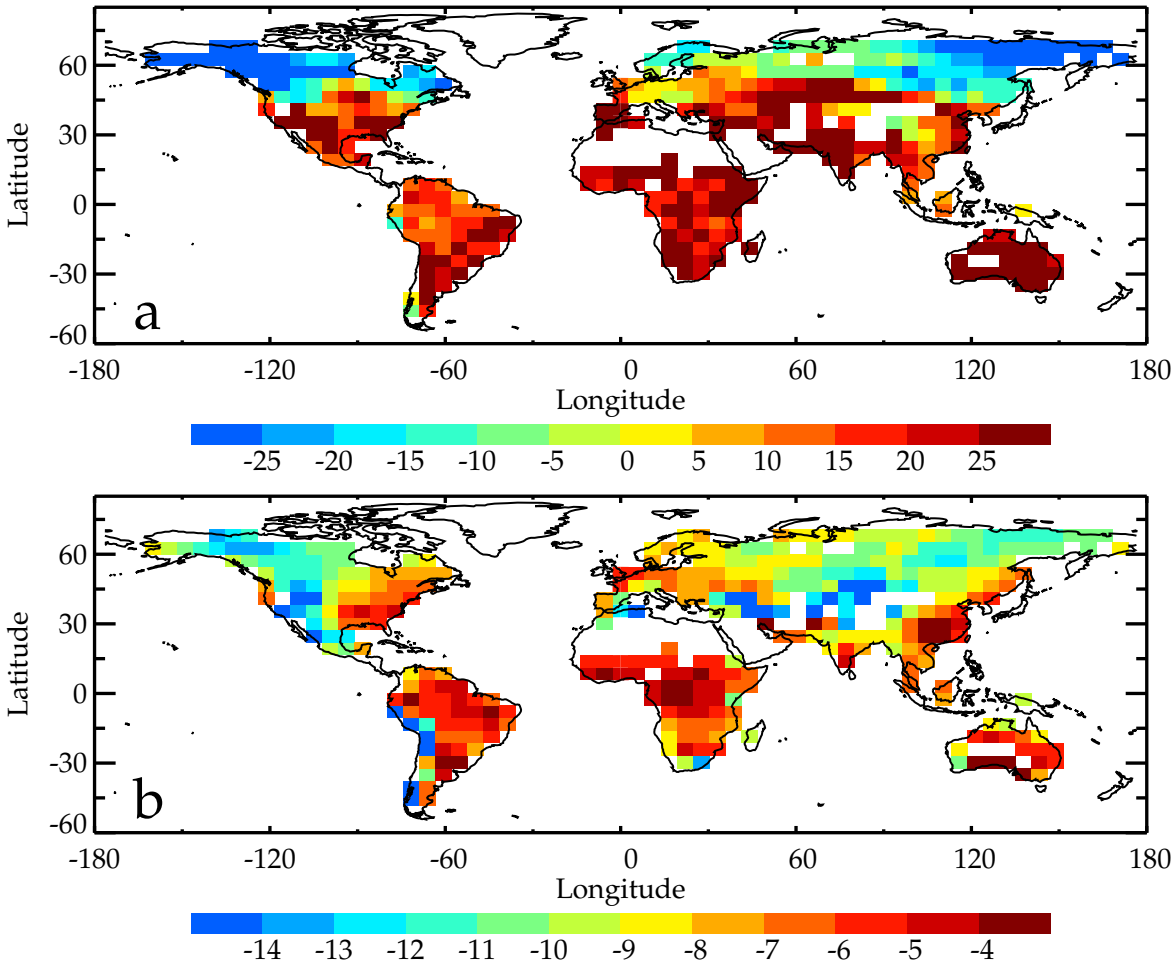

Figure 2.3: Annual mean leaf discrimination in ‰ (a), and annual mean isotopic composition of CO_2 in equilibrium with soil water in ‰ VPDB–CO_2 (b) calculated by ECHAM/BETHY.

from numerical instabilities at very low net assimilation when post–processing). I show in Chapter 4 that in Eurasia this is to 25 % due to the depletion of rain in the interior of the continent and to 75 % due to the increase of relative humidity from West to East Siberia which biases leaf water at the evaporating site to the isotopic composition of water vapour rather than to soil water. ECHAM temperatures are about 2 °C lower than those from ECMWF re–analysis in East–Siberia but very similar to ECMWF in Canada and Alaska [*Roeckner et al.*, 1996]. Lower temperature translates into higher relative humidities which in turn gives lower leaf water values and consequently lower leaf discriminations (2 °C lower temperature translates in about 10 ‰ lower leaf discrimination in the model). ECMWF re–analysis in East–Siberia are very arguable because the ECMWF re–analysis is model dependent too and not well constrained in Siberia due to low measurement coverage. I esteem that it is realistic that leaf discrimination becomes negative in Eastern–Siberia and it should be measurable as argued in Chapter 4. Negative photosynthetic discrminination is in fact directly implied by some concurrent vertical profiles of CO_2 and $\delta^{18}O$–CO_2 with and above the

convective boundary layer for central Siberia, even in mid–summer [*Lloyd et al.*, 2002a; *Styles et al.*, 2002a]. I show in Figure 2.3a the assimilation weighted annual mean leaf discrimination (in ‰) which can be compared to other estimates, e. g. to *Farquhar et al.* [1993]. One can see that leaf discrimination becomes negative already at around 45 °N in certain regions. On the other hand, Australia, Africa, and South America are very uniform in their mean discrimination (except for the Andes). The distribution pattern of leaf respiration is similar to the one estimated by *Farquhar et al.* [1993] but approximately a factor of 2 different. *Farquhar et al.* calculate a global mean leaf water isotopic composition of 4.4 ‰ VSMOW whereas the assimilation weighted leaf water isotopic composition is 6.3 ‰ VSMOW. They have a global mean stomata–internal CO_2 mixing ratio, c_i, of 235 ppm while I calculate a mean of 264 ppm. *Farquhar et al.* do not take c_i but the CO_2 mixing ratio at the chloroplast, c_c, which further reduces their enhancement factor $c_{cs}/(c_a - c_{cs})$ (where c_{cs} is either c_i or c_c) to about 1.3 in the global mean compared to about 3 in the model. Taking assimilation weighted leaf water isotopic composition is more realistic but whether c_{cs} is closer to c_i or c_c is still a matter of debate (see below).

Unlike leaf discrimination, soil "discrimination" is no real discrimination. Counter-intuitive to equation 2.23, leaf discrimination is independent of the atmospheric $\delta^{18}O$ level. One can see in equation 2.11 and equation 2.14 that the $CO^{18}O$ flux of respiration is independent of the isotope ratio in the atmosphere, R_a, but the $CO^{18}O$ flux of assimilation depends on it. What I call "discrimination" is the difference between the isotopic signature of the CO_2 flux of one process and the $\delta^{18}O$–CO_2 in the atmosphere. While the isotopic signature of the CO_2 flux depends not on the atmospheric $\delta^{18}O$ level, "discrimination" does. If the isotopic signature of the CO_2 flux depends on the atmospheric $\delta^{18}O$ level, it can cancel out in discrimination. If I include a new process in the calculation (e. g. computing with or without fossil fuel fluxes), the atmospheric $\delta^{18}O$ level will change, according to equations 2.23–2.27. This will change soil "discrimination" but the soil $CO^{18}O$ flux stays the same. The leaf $CO^{18}O$ flux instead will adapt to the new $\delta^{18}O$ level in the atmosphere: leaf $CO^{18}O$ flux will change but leaf discrimination will stay almost the same. I show therefore in Figure 2.3b the isotopic composition of CO_2 equilibrated with soil water in ‰ VPDB–CO_2 (and not soil "discrimination" in ‰). To derive soil "discrimination" from Figure 2.3b, one has to add soil fractionation during diffusion, ϵ_k taken as -7.2 ‰ [*Miller et al.*, 1999] in the model, and subtract the atmospheric $\delta^{18}O$–CO_2. ^{18}O isotopes in soil CO_2 are quite uniform inside continents and result in about -11 ‰ VPDB–CO_2 in the northern hemisphere and about -5 ‰ VPDB–CO_2 in the southern hemisphere. This result is very similar to *Ciais et al.* [1997a] which is surprising because *Ciais et al.* took rain isotopic composition and I take soil isotopic composition where the big seasonal cycle of isotopes in rain is very much attenuated. On top of that, the annual values are all flux weighted. I will show below that CO_2 leaving the soil in our model is isotopically almost constant during the year. The respiration weighted annual mean is therefore very similar to the not–respiration weighted annual mean. Because soil integrates the rain signal over long time periods, the annual mean of isotopes in rain water and soil water are very similar. Thus, I end up with an annual mean isotopic composition of CO_2 in equilibrium with soil water resembling very much the estimate of *Ciais et al.* [1997a].

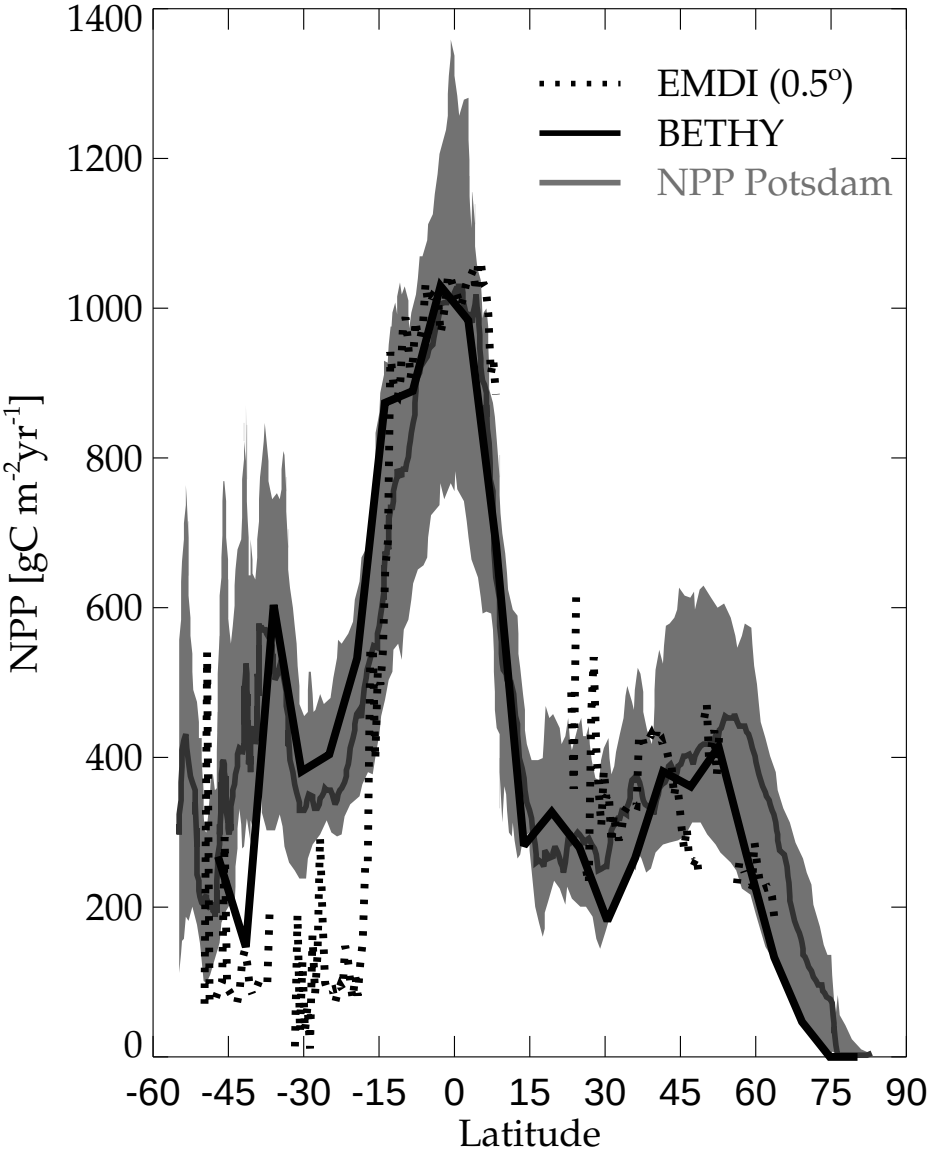

Figure 2.4: Comparison of Net Primary Productivity (NPP) of the EMDI measurement compilation (dotted line), the Potsdam NPP model intercomparison (grey solid line, plus area between 10^{th} and 90^{th} percentiles, grey) and BETHY online (black solid line) as latitudinal average.

Net Primary Productivity

The Potsdam NPP Model Intercomparison Project [*Kicklighter et al.*, 1999] compared 15 net primary productivity models. The shadowed area in Figure 2.4 shows the range between the 10^{th} and 90^{th} percentiles of the 15 models together with the median (solid grey line). Note that the y axis is in gC m^{-2} s^{-1}. The BETHY online model (solid black line) is very similar to the median of the 15 models and lies well in between the 10^{th} to 90^{th} percentile range. The most noteworthy difference is the lower productivity of ECHAM/BETHY at high latitudes. In the northern hemisphere above 60 °N,

ECHAM/BETHY is at the 10^{th} percentile level of the intercomparison and in the southern hemisphere between 40 and 45 °S, it falls even below the 10^{th} percentile level. I included in Figure 2.4 the gridded dataset compiled by the Ecosystem Model–Data Intercomparison (EMDI) project [*Olson et al.*, 2001] (details in the Appendix). In the southern extra tropics, the NPP measurements of EMDI are primarily from grassland. Grassland NPP measurements are often aboveground NPP measurements at one particular time and the value is converted to total NPP with a constant conversion factor. EMDI used a conversion factor of 2 to calculate total NPP from pointwise measured aboveground NPP. This factor seems to be too low for grasslands because grasses can lose lots of carbon to different processes which are hidden to single aboveground NPP measurements. So the aboveground part of grasses can be eaten by herbivores, destroyed by fires or die due to unfortunate environmental conditions and it can regrow afterwards and the belowground part of the grasses can lose carbon due to exudates or secretions of roots and transfer of carbon to mycorrhizae [*Long et al.*, 1989]. Anyway, the EMDI estimates are a factor of 4 lower than the model results. *Scurlock et al.* [2002] compared different methods of estimating NPP of grasslands and found differences of up to a factor of 3 in the NPP estimates of the different methods. So it is not certain that our model values are much too high but they should be taken with care. On the rest of the globe, the median of the 15 models and BETHY online compare well with the NPP estimations. Above 50 °N, the NPP data seems to support more closely the lower end of the Potsdam NPP models, and especially ECHAM/BETHY. But there are only few measurements in the data compilation above 50 °N, ending around 60 °N so that tundra vegetation is not represented which has potentially the same conversion problems as grasslands.

Net Ecosystem Exchange

I further try to compare the CO_2 flux part of the model with eddy flux measurements of Net Ecosystem Exchange (NEE). It is beyond doubt not very commensurate to compare the model with a grid length of about 500 km to measurements representative of an area of around 1 km^2. But nevertheless, it is a useful semi–quantitative information of the ECHAM/BETHY model performance. In addition, most NEE measurement sites are located in young re–growing forests which gives a bias to higher absolute NEE values. Also, the climate for the NEE calculations comes from ECHAM and is thus simulated and not the observed one at the stations. However, the phasing of NEE in the model should be comparable to the measurements and the amplitude should have the same order of magnitude. I took the compilation of eddy flux measurements in the context of FLUXNET [*Running et al.*, 1999] and added two forest sites in western and central Russia [*Milyukova et al.*, 2002; *Lloyd et al.*, 2002b; *Shibistova et al.*, 2002] (details in the Appendix). I chose only such stations for which I have the same ecosystem in the grid cell of the model (or surrounding grid cells) as at the measurement site. If the model has not the same ecosystem in the appropriate grid cell, I took an adjacent grid cell if possible, otherwise discarded the station. A list of all 20 stations used including BETHY's plant functional type number associated to it can be found in the Appendix in Table 2.2.

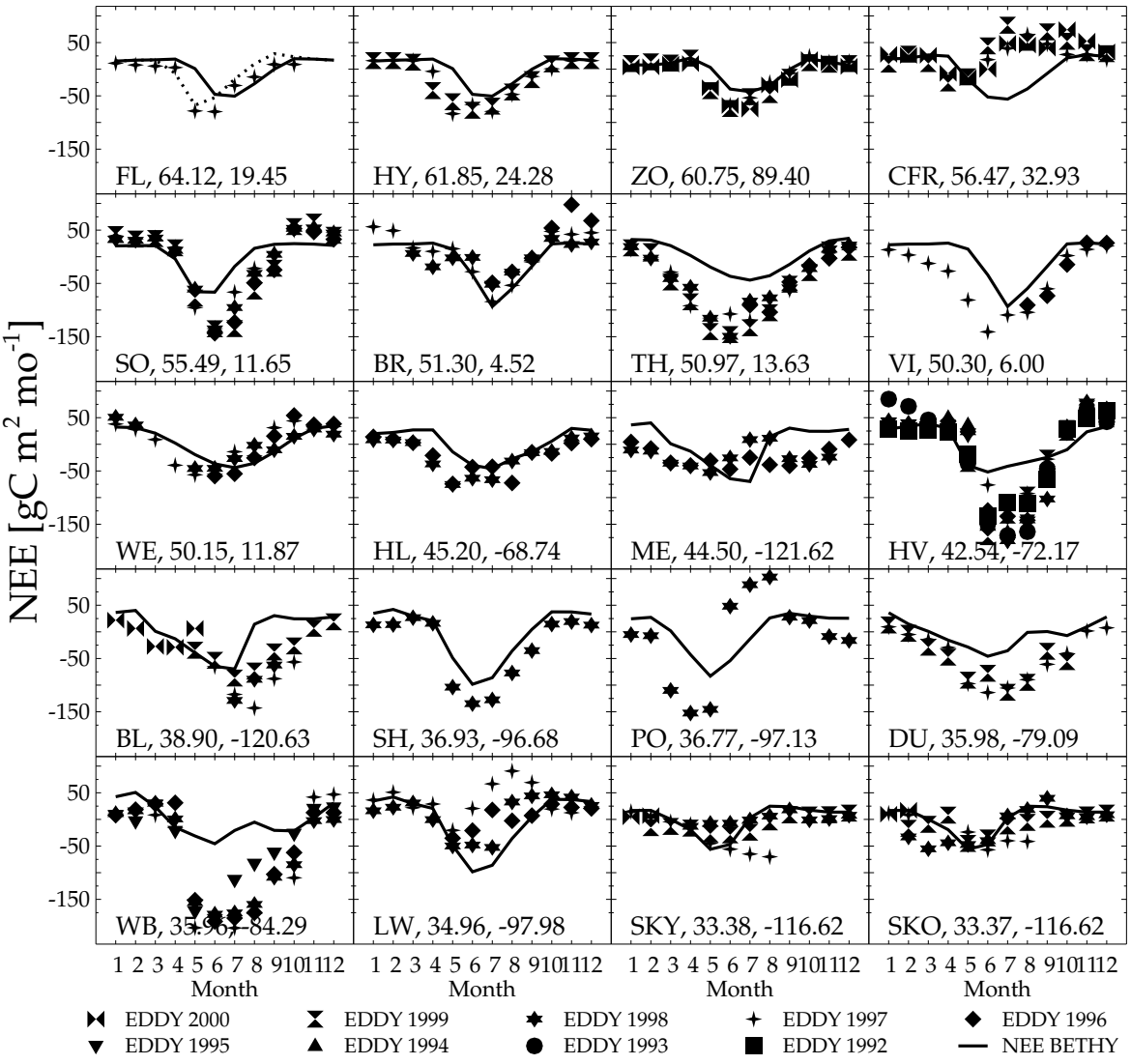

Figure 2.5: Net Ecosystem Exchange (NEE) at 20 different eddy flux sites (different symbols for each year) compared to mean ECHAM/BETHY (solid line). The values after the station abbreviation stand first for latitude and second for longitude of the site. The sites are in descending latitude order. The dotted line at Flakaliden is model NEE with assimilation shifted arbitrarily one month in advance.

Figure 2.5 shows the comparison between BETHY online monthly mean NEE fluxes and individual measurement years; the latter to demonstrate the big inter–annual variability of the measurements. ECHAM's meteorology instead represents a climatological mean state so there is no such inter–annual variability. I ranged the sites in latitudinal order so that one can easily see that all sites are above 30 °N and mainly in Europe and North America. ECHAM/BETHY seems to underestimate the NEE flux amplitude at half of the stations. Notably above 60 °N, ECHAM/BETHY is too low in amplitude which colludes with the low NPP predictions of ECHAM/BETHY at high northern latitudes (compared to the 15 NPP models, not compared to the EMDI NPP data

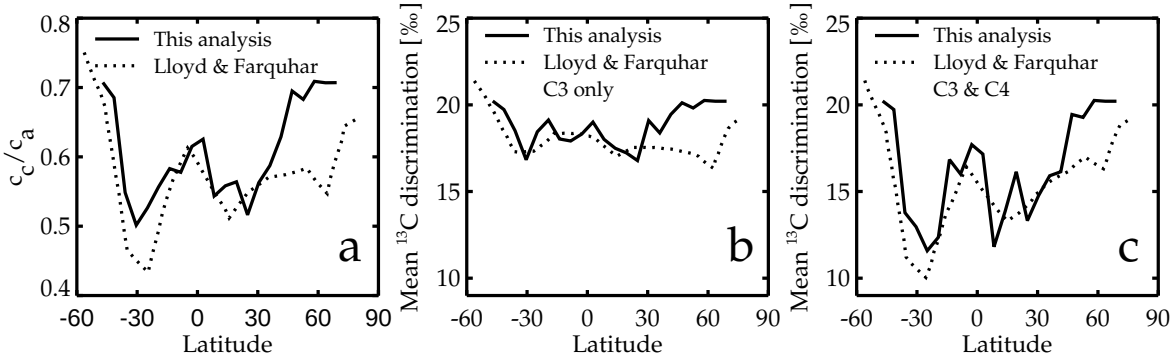

Figure 2.6: Latitudinal distribution of the stomata–internal CO_2 mixing ratio. The ratio of stomatal to atmospheric CO_2 mixing ratio is compared with *Lloyd and Farquhar* [1994] via c_c/c_a (a), ^{13}C photosynthetic discrimination of C3 assimilation (b) and C3 together with C4 assimilation (c).

compilation). The model over–predicts minimum NEE only at Central Forest Reserve (CFR) and Little Washita (LW) which both show a source of CO_2 in the measurements (which is not possible in the model because NEE is set to zero in the long term mean). The limit of the comparison can be seen at the stations Braschaat (BR), Tharandt (TH), Vielsalm (VI), and Weidenbrunnen (WE) which lie all in close vicinity. They occupy actually only two neighbouring grid cells in the model, so Braschaat and Vielsalm as well as Tharandt and Weidenbrunnen are compared to the same NEE flux of the model. But one can see that the compared stations show a different NEE amplitude of about a factor of 2. So ECHAM/BETHY simulates much better the lower NEE amplitude stations. In the latitude range above 50 °N, ECHAM/BETHY is always slightly out of phase. It shows its minimum NEE about one month too late. This behaviour can not be seen between 30 and 40 °N and the comparison is equivocal in between.

Stomata CO_2 Mixing Ratio

The CO_2 mixing ratio inside stomate is an important variable for leaf discrimination (see eq. 2.23). The factor $c_{cs}/(c_a - c_{cs})$ amplifies the difference between leaf water equilibrated CO_2 and atmospheric $\delta^{18}O$–CO_2. At an ambient CO_2 mixing ratio of 350 ppm and a stomatal CO_2 mixing ratio of 230 ppm, this factor is about 2. With further drawdown of c_{cs}, the factor diminishes as well, reaching 1 at 175 ppm. Even lower values of c_{cs}, e. g. at high assimilation rates, lead to a vanishing influence of leaf water on atmospheric $\delta^{18}O$–CO_2. I explained in section 2.2.3 that I take as a first guess the stomata–internal CO_2 mixing ratio c_i as an estimate of c_{cs}. The global assimilation weighted value of c_i is very high with 264 ppm. This leads to $c_{cs}/(c_a - c_{cs}) = 3$. This comes from the fact that I start from rather high non–water–limited c_i values which come from an overview of *Schulze et al.* [1994]. These literature survey of field measurements gives a c_{i0} of $0.87\,c_a$ for C3 plants which is much higher than laboratory measurements suggest: $\sim 0.7\,c_a$ [*Farquhar et al.*, 1989b; *Boyer et al.*, 1997]. I try to validate the c_i estimates indirectly via ^{13}C leaf discrimination. But ^{13}C fractionation by photosynthesis is determined by CO_2 mixing ratio in the chloroplast, c_c, rather

than in the stomata. *Lloyd and Farquhar* [1994] give a range of $0.16\,c_a$ to $0.2\,c_a$ for the difference between c_i and c_c at saturating photon irradiance. They use a value of $0.1\,c_a$ suggesting leaves operating on roughly 50 % of their maximum (light–saturated) photosynthetic capacity. *Yakir and Sternberg* [2000] recommend a value of $0.2\,c_a$ for an average drawdown on the chloroplast level. So I take midway between the different estimates and $c_i - c_c = 0.16\,c_a$.

In Figure 2.6a, the latitudinal distribution of c_c/c_a in ECHAM/BETHY is compared to the estimate of *Lloyd and Farquhar* [1994]. Both estimates are very similar but be aware that the global mean level of both curves depend on the above discussed drawdown from c_i to c_c. The difference in the southern hemisphere comes mainly from the different distribution of C4 plants in both approaches which can be seen also with Figure 2.6b and c. I calculated with c_c/c_a the ^{13}C leaf discrimination of C3 plants with the simple formula [*Farquhar et al.*, 1989a]:

$$\Delta_A^{13}C = a + (b - a)\frac{c_c}{c_a}\,. \tag{2.29}$$

$a = 4.4$ ‰ is thereby the kinetic fractionation of ^{13}C diffusion in air and b is the fractionation associated with carboxylation. There is a considerable amount of incertitude for the correct value of b. *Farquhar et al.* [1989a] found the best fit to measurements with $b = 27$ ‰ but taking c_i instead of c_c. *Lloyd and Farquhar* [1994] expanded the formula of *Farquhar et al.* by dividing the gradient between stomata and chloroplast in several steps. b is therefore a mixture of carboxylation of RUBISCO (RibUlose BISphosphate Carboxylase/Oxygenase) ($b_3 = 29$ ‰) and 5 to 10 % carboxylation of PEP (phospho*enol*pyrvate) carboxylase ($b_4 = -5.6$ ‰ at 25 °C). So they found a value of $b = 27$ ‰ but taking c_c. I follow their later conclusions and take $b = 27$ ‰ together with c_c for C3 plants, and I take a constant value of $a = 4.4$ ‰ for C4 plants. Taking only the simple formula (eq. 2.29) for calculating Δ^{13}C is of minor importance because the expansion of *Lloyd and Farquhar* results in only small changes in the latitudinal mean compared to the simple formula. Note that I follow the historical convention that fractionation and therefore discrimination in ^{13}C and ^{18}O have opposite signs. So the isoflux of δ^{13}C is $-\Delta_A^{13}$C times assimilation and the isoflux for δ^{18}O is $+\Delta_A^{18}$O times assimilation, i. e. a positive Δ_A^{13}C is comparable in its effect on the atmosphere to a negative Δ_A^{18}O. In Figure 2.6b is now plotted the latitudinal distribution of ^{13}C discrimination of C3 plants only and in Figure 2.6c of C3 and C4 plants together. The C3 distributions are extremely similar except for the high northern latitudes. Above 30 °N, the two estimates diverge. ECHAM/BETHY reaches its base, non–water–limited level of c_c/c_a of about 0.71 ($= 0.87 - 0.16$) (Fig 2.6a) whereas *Lloyd and Farquhar* do not reach such high values (they do in the southern extra tropics). *Lloyd and Farquhar* remarked the same phenomena in comparison to earlier estimates of *Farquhar et al.* [1993] that also diverged at high northern latitudes. The differences between BETHY online and the earlier investigation below 30 °N come mainly from the different distribution of C4 plants. In the used vegetation distribution, big parts of the African vegetation belt are covered by C4 long grasses which give the modelled minimum Δ_A^{13}C at 10 °N. C4 plant assimilation contributes to 21 % to global GPP at *Lloyd and Farquhar* [1994] whereas BETHY online calculates 18 %; only C4 long grasses (PFT 12, Table 2.1) count up to 12 %. This gives a mean discrimination of the terrestrial bio-

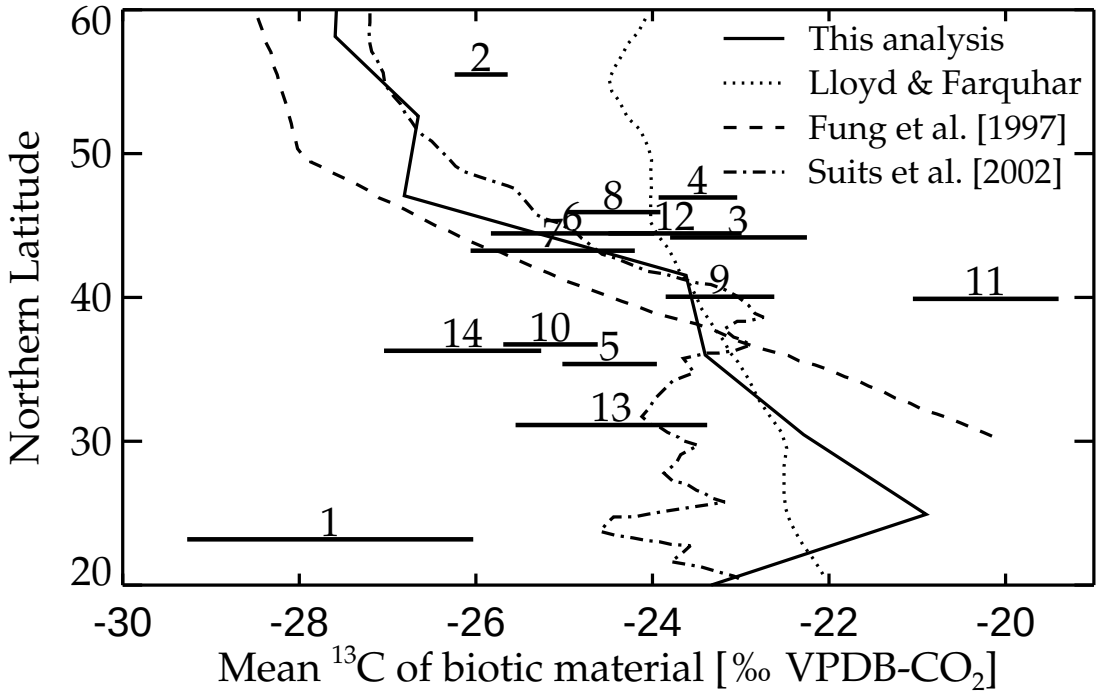

Figure 2.7: Latitudinal distribution of δ^{13}C source signature, δ_{bio}. Both studies of Figure 2.6 are compared to measurements of mean biotic ^{13}C of *Miller et al.* [2002]. The numbers correspond to continental sampling sites of NOAA/CMDL and are explained in Table 2.3 in the Appendix.

sphere of 16.1 ‰ VPDB–CO_2 in BETHY online compared to 14.8 ‰ VPDB–CO_2 in *Lloyd and Farquhar*. For C3 plants only, BETHY online gives 18.7 ‰ whereas *Lloyd and Farquhar* estimate 17.8 ‰ VPDB–CO_2. But the overall global mean discrimination deviates quite a lot from other investigations: 15.7 ‰ [*Fung et al.*, 1997], 18.0 ‰ [*Tans et al.*, 1993], 20.0 ‰ [*Quay et al.*, 1992], 17.6 ‰ [*Keeling et al.*, 1989]. Though, most studies were made only with C3 plants except *Fung et al.* and, therefore, they are not far from the C3 estimate.

Nevertheless, BETHY online (and *Lloyd and Farquhar* [1994]) deviates from measurements of δ^{13}C source signature, δ_{bio}, of *Miller et al.* [2002] (Figure 2.7 which are recalculated estimates of *Bakwin et al.* [1998]. (I plotted as well all model studies included in the comparison of *Miller et al.* [2002], namely *Lloyd and Farquhar* [1994], *Fung et al.* [1997], and *Suits et al.* [2002].) Due to the lack of e. g. a full carbon cycle (but also transported fossil fuel emissions and other factors), the terrestrial isotopic signature, δ_{bio}, is calculated here as:

$$\delta_{bio} = \frac{-7.9 - \Delta_A^{13}C}{1 + \Delta_A^{13}C/1000}\,, \tag{2.30}$$

i. e. with an atmospheric δ^{13}C value of -7.9 ‰ VPDB–CO_2 which is the annual northern hemispheric mean of *Bakwin et al.* [1998]. This formulation assumes that the respiration source has the same signature as assimilation which is not true due to the fossil fuel input (so called ^{13}C Suess effect). Equation 2.30 and the lack of a closed carbon

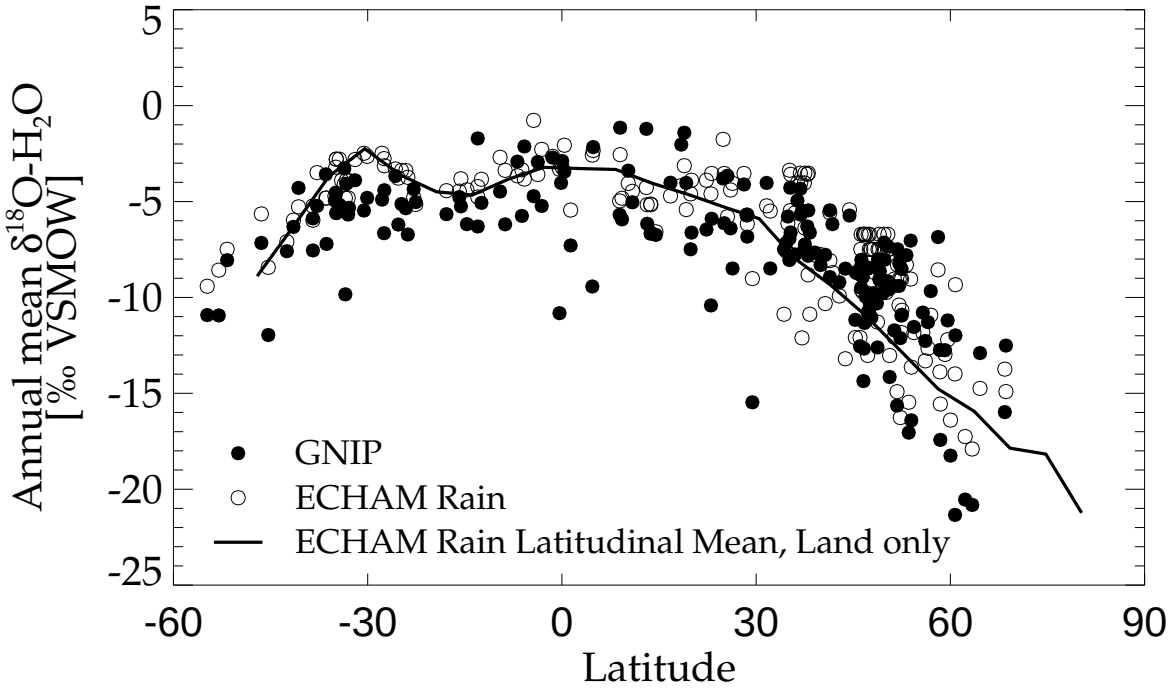

Figure 2.8: Annual mean values of the isotopic composition of rain from GNIP (closed circles) compared to the water isotope module (WFRAC) of ECHAM (open circles). The latitudinal mean of all land points (line) is given as an integrated comparison measure.

cycle in the model are shortcomings in the comparison but should not alter the qualitative statements. But I cannot stretch this comparison too much without having a full δ^{13}C–cycle included. ECHAM/BETHY shows slightly enriched values below 35 °N and lighter values in the high latitudes than the measurements (for the description of the numbers see the Appendix). *Miller et al.* [2002] and *Bakwin et al.* [1998] attributed the heavier values of *Lloyd and Farquhar* [1994] to the C4 distribution used by *Lloyd and Farquhar*. (*Bakwin et al.* used the same argument for *Fung et al.* [1997].) I have a different C4 distribution than *Lloyd and Farquhar* but one can see in Figure 2.6b and c that the ^{13}C discrimination of both models is very similar between 30 and 40 °N for C3 and C4 plants together but very different for C3 plants only. So the difference does not have to come only from C4 distribution alone. At high latitudes, I already remarked the small assimilation values of ECHAM/BETHY as well as the high c_c values.

Water Isotopes

Apart from the CO_2 fluxes and its interdependent variables, the isotopic composition of the water pools mainly determines δ^{18}O–CO_2. The water isotope module (WFRAC) was extensively tested and used so that I focus here on the north–south gradient which will in turn determine the latitudinal distribution of δ^{18}O–CO_2. I took stations of the Global Network of Isotopes in Precipitation (GNIP) of the International Atomic Energy Agency (IAEA) and the World Meteorological Organization (WMO) [*IAEA/WMO*,

2001] (details in the Appendix) and calculated the mean precipitation weighted annual average. In Figure 2.8 are shown the GNIP values (filled circles) together with the ECHAM annual means at the same stations (open circles). A standard deviation of around 10 ‰ pertains to the GNIP values. The solid line in Figure 2.8 is the latitudinal mean of ECHAM land grid points because most GNIP stations are on land and I am interested in the $CO^{18}O$ fluxes of the terrestrial biosphere. One can discern that ECHAM works very well at most stations not following the outliers in the measurements. I showed in Chapter 4 that ECHAM simulates equally well the east–west gradient in Eurasia, too. ECHAM follows nicely the dip at 15 °S resulting from the Intertropical Convergence Zone (ITCZ). However, it has a slight tendency to weakly overestimate the annual values.

Night time terrestrial source signature

The $CO^{18}O$ module (OFRAC) uses soil water isotopic composition not composition of rain to calculate soil $CO^{18}O$ fluxes. The soil acts as an integrator of rain, damping the sometimes big seasonal cycle of $\delta^{18}O$–H_2O. ECHAM uses a soil bucket model for water and erases almost totally the seasonal cycle changes. The soil bucket model has only one soil layer for water with no further discretisation. (ECHAM uses more than one soil layer for other variables like temperature.) I access this damping effect with CO_2 and $\delta^{18}O$–CO_2 measurements made in or above canopies. With the method developed by *Keeling* [1961], known as "Keeling plot", many studies tried to investigate the carbon isotope composition of CO_2 fluxes. One of the major assumptions of the Keeling plot is that the single source does not change during the time of investigation (neither should change the background mixing ratio). For $\delta^{13}C$, this can be well assumed during night but this is a priori not true for $\delta^{18}O$–CO_2 because temperature changes over the course of the night and therefore the equilibrium fractionation between water and CO_2 changes as well (eq. 2.8). There are other factors like the invasion effect which make a Keeling plot a priori not usable for $\delta^{18}O$. These factors give often a bent look to $\delta^{18}O$ Keeling plots. Anyway, one finds sometimes very 'good' Keeling plots, i. e. with high correlation coefficient and the measurements lying on a straight line. It is possible that this is due to compensating effects because the equilibration fraction tends to heavier values over the course of the night (with decreasing temperatures, eq. 2.8) and the invasion effect tends to lighter values due to increasing influence (with increasing CO_2 mixing ratios, eq. 2.12). But it should be very rare that both effects cancel each other out exactly. Though, these effects should rather be negligible in situations with 'good' Keeling plots. I inquired therefore the database of the Biosphere–Atmosphere Stable Isotope Network (BASIN) of the Global Change and Terrestrial Ecosystem core project (GCTE) Focus 1 [*Pataki et al.*, 2002] in which I found 2 470 data points of ecosystem CO_2 and $\delta^{18}O$–CO_2 measurements. I updated the measurements of French Guiana [*Nina Buchmann*, personal communication], added data of Australia, Brazil and Cameroon [*Jon Lloyd*, personal communication], and incorporated measurements of Russia [*Langendörfer et al.*, 2002; *Styles et al.*, 2002b] (details in the Appendix). Table 2.4 in the Appendix gives all sites and the associated BETHY plant functional type number of the measurements. I found 54 'good' ($r^2 > 0.7$) night time Keeling plots (using reduced major axis regression, also known as geometric mean regression). So I

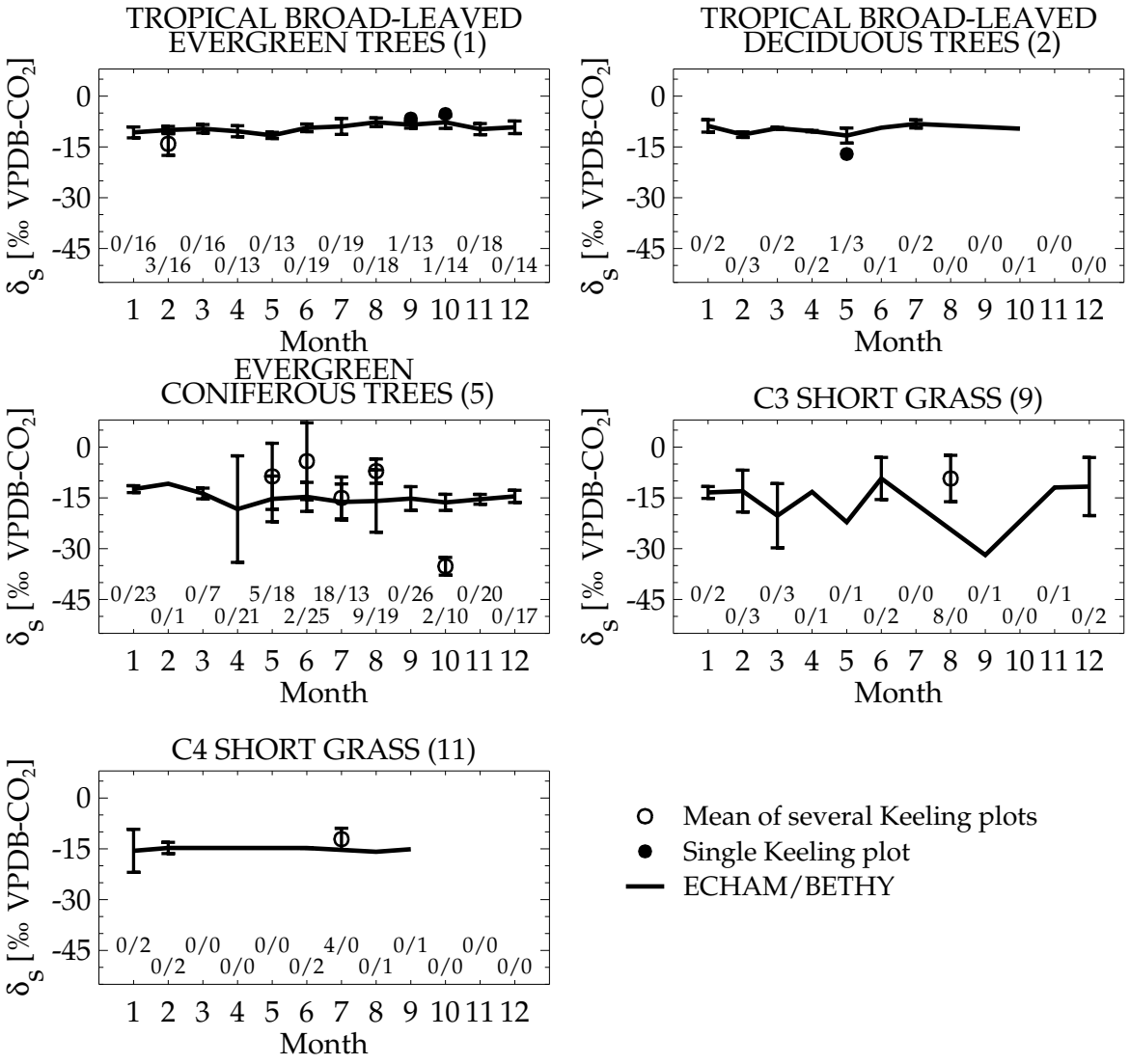

Figure 2.9: The isotopic signature of the night–time respiration $\delta^{18}O$–CO_2 source derived from "Keeling plots". Open circles are the mean of several, Keeling plot derived source signatures at the given BETHY plant functional type at one or several stations. The error bar is the standard deviation of the different source estimates. Closed circles instead signify a single Keeling plot. The errors of single Keeling plots are all in the order of the size of the circles and, therefore, no error bars are plotted to single Keeling plot values. The line connects the mean of the Keeling plot derived values in BETHY online. Here as well, an error bar is associated if more than one Keeling plot estimate exists. The numbers in each plot are first the number of measurement Keeling plots which entered the plotted value and second the number of model Keeling plots.

run our model (without invasion) for three consecutive days each month acquiring CO_2 and $\delta^{18}O$–CO_2 values each 40 minutes. I did then Keeling plots on all nights on each grid point and selected only Keeling plots with 'good' correlations ($r^2 > 0.9$). Taking the same coordinates as the measured Keeling plots (moving to adjacent grid cells if necessary) gave 503 individual source signature estimates in the model (out of 1110 for all stations, i. e. about half of the Keeling plots in the model were usable and the effect of source signature change negligible). I further grouped the stations to BETHY plant functional types and the result is shown in Figure 2.9. If there is more than one Keeling plot, their standard deviation is plotted as an error bar to the error weighted mean value. Except of C3 short grasses, stations which correspond to a given plant functional type are either single stations or lie all around the same latitude band. So ECHAM/BETHY looks quite uniform in each plant type with small error margins. The comparison is not very enlightening due to the lack of suitable measurements in which the discussed effects are not present. In summer, temperature drifts during night are important, and in winter, high CO_2 mixing ratios amplify the invasion effect so that no 'good' Keeling plot can be found. But what can clearly be seen in Figure 2.9 is that BETHY online shows almost no seasonal cycle in the isotopic source composition. The small seasonal cycle of the water isotopes in soil is totally cancelled out by the temperature difference between summer and winter. The sites of the BETHY plant functional types 5, 9, 11 lie almost all in the northern hemisphere (except Wagga Wagga in Australia). Here BETHY online shows lower values for the source isotopic composition during the summer month. Using no soil water model but a bucket model seems to be too crude to simulate well the influence of respiration on $\delta^{18}O$–CO_2 in canopies.

2.4 Discussion

There are two ominous results in the preceding section: the low assimilation values in high northern latitudes and the unchanging source signature of respired CO_2. I will further on subsume the above results and discuss these two points in general.

The results of the NPP comparison are somewhat contradictory (Figure 2.4). The BETHY online model lies only at the 10^{th} percentile of the 15 NPP models above 60 °N. On the other hand, the EMDI NPP compilation shows qualitatively the same behaviour as BETHY. NPP is defined as the total photosynthetic gain minus (respiratory) losses of vegetation (per unit ground area). Many earlier estimates of NPP ignored thereby the turnover and belowground processes, taking only aboveground NPP into account. Total NPP measurements are hard to fulfil because belowground processes are not easily accessible; e. g. fine root growth and death [*Long et al.*, 1989]. Different methods are thus used to estimate total NPP from measurements of e. g. aboveground NPP but most methods still neglect quite a number of processes. The EMDI project uses conversion factors from aboveground NPP to do its estimates. *Scurlock et al.* [2002] showed at least for grasslands that this method can lead to substantial errors. They state that current NPP estimates are clearly an underestimate of the *magnitude* of NPP. So the NPP compilation values are likely to be too small, to a different degree for different biomes. A recent atmospheric CO_2 data assimilation study points in the

same direction stating that a much higher NPP in high northern latitudes is needed to match the seasonal cycle of CO_2 [*Kaminski et al.*, 2002]. NPP derived by *Kaminski et al.* is even higher than the 90$^{\text{th}}$ percentile of the Potsdam intercomparison. But the results are very sensitive to e. g. the transport model used or the parameterisation of respiration. Though, the seasonal cycle of atmospheric CO_2 is derived from the net CO_2 fluxes and not from gross fluxes. I showed in Figure 2.5 that BETHY online underestimates NEE amplitudes at about half of the compared stations, notably above 60 °N. But the two most northern stations, Flakaliden in Sweden and Hyytiälä in Finland, are both installed in young re–growing forests so that I can not expect that BETHY online reproduces these rather high amplitudes. It is more vexatious that ECHAM/BETHY is not able to reproduce the right phase above 50 °N. NEE is the difference between respiration and assimilation that show their maximum at different times in the year (normally, respiration peaks later in the year than assimilation). Different NEE phasing can be due to over– or underestimation of one process (or both) or just the different phasing of one process. Taking Flakaliden as an example: shifting assimilation arbitrarily so that its minimum occurs one month earlier, results in the right phase and even the right amplitude in the model compared to the eddy measurements (dotted line in Figure 2.5). It is therefore not clear if the results of *Kaminski et al.* [2002] are transferable to the model, i. e. that I should increase the overall productivity beyond 60 °N.

Another item pointing in the direction that ECHAM/BETHY underestimates carbon fluxes in high northern latitudes is the high stomata–internal CO_2 mixing ratio modelled by BETHY. The estimates of *Lloyd and Farquhar* [1994] and the measurements of *Miller et al.* [2002] suggest lower c_i values above 45 °N. Lower c_i means normally higher assimilation which is also true in models but only if the model has no thresholds in the computation. BETHY calculates first a non–water–limited assimilation rate at a given c_i. This means that it takes carboxylation and electron transport limitation into account in this step. Then, it incorporates the water limitation of assimilation in the empirical formulation expressed in equation 2.3. The last step is to recalculate assimilation this time with fixed stomatal conductance from the water limitation step before, adjusting c_i compatibly. Therefore, c_i can not be higher than the non–water–limited c_i which is $0.87\,c_a$ for C3 plants and $0.67\,c_a$ for C4 plants in the model. This is much higher than laboratory measurements suggest (around $0.7\,c_a$ for C3 and $0.4\,c_a$ for C4 plants [*Boyer et al.*, 1997; *Farquhar et al.*, 1989b]) but comes from a literature survey of field measurements [*Schulze et al.*, 1994]. However, this plays mostly a role in non–water–limited cases. Reducing the non–water–limited c_i to laboratory values would bring *Lloyd and Farquhar* and ECHAM/BETHY together very closely. However, using the non–water–limited c_i of *Schulze et al.* [1994] or of *Farquhar et al.* [1989b] does not change assimilation a lot. It reduces assimilation only by about 5 % in the model. I point out in Chapter 3 that I take this c_i values to better model the seasonal cycle of atmospheric δ^{18}O–CO_2. I show as well in Chapter 3 that the seasonal cycle of CO_2 is rather large in the model at northern hemispheric stations which controverts the suspicion of small assimilation at high latitudes. Thereto, the mean δ_{bio} of the only station above 50 °N, Baltic Sea (2), points more in the direction of ECHAM/BETHY than in the direction of *Lloyd and Farquhar*, and BETHY online is very similar there to a recent modelling study of *Suits et al.* [2002].

So all the above points are ominous that BETHY online calculates too little assimilation in the northern hemisphere but it can not be ruled out from this bottom–up approach that BETHY online does actually calculate the right magnitude. It might rather be that the phasing of assimilation and/or respiration is not well represented.

A second intruding point in the validation of ECHAM/BETHY is the invariant signal of δ^{18}O–CO_2 of respiration over the course of the year. This comes from the attenuation effect to δ^{18}O–H_2O of the soil bucket model used in ECHAM. Depending on the depth, this behaviour is probably true for deep soil but not for the upper soil layers. *Miller et al.* [1999] proposed to take the water isotope value at around 15 cm depth to equilibrate with CO_2 and apply afterwards an effective kinetic fractionation of $-7.2\,‰$. *Riley et al.* [2002] showed that the approach of *Miller et al.* gives similar values as the analytical solution of *Tans* [1998] for most meteorological conditions. *Melayah et al.* [1996] measured (and modelled) the gradient in δ^{18}O–H_2O in the unsaturated soil layer of a clay loam soil (bare soil) over the course of three weeks. Surface water δ^{18}O changed during that time by about 10 ‰ (due to evaporation and rain) whereas water in 10 cm depth changed only by about 2 ‰ and did almost not change at all in 50 cm depth, even during the rain event. So there is definitely a more varying water isotopic composition in reality (at the place where CO_2 equilibrates with water) than the soil bucket model approximates but the variation is much attenuated compared to rain water. Still, the night time source signature comparison (Figure 2.9) suggests that BETHY online calculates CO_2 source signatures a few ‰ too low leading to lower soil "discrimination".

As I mentioned before, I take the high non–water–limited c_i values to better model the seasonal cycle of atmospheric δ^{18}O–CO_2. But the seasonal cycle of δ^{18}O depends strongly on the phasing of the isofluxes, like CO_2 depends on the phasing of the CO_2 fluxes. So taking high c_i values could be an overcompensation effect of the wrong soil "discrimination". So the model approach of *Riley et al.* [2002] seems promising to better include soil processes in δ^{18}O–CO_2 models.

2.5 Conclusions

ECHAM/BETHY showed its capability in simulating the different components necessary to properly estimate δ^{18}O in atmospheric CO_2. It is very similar in NPP to the median of 15 NPP models of all different kinds. In the northern hemisphere, it departs from the median and ends more at the lower estimates of the 15 models. A NPP data compilation supports more the smaller BETHY online NPP in this latitudes but the compilation is potentially biased to lower values. Maximum NEE appears too low as well at latitudes above 50 °N but data and model can easily be brought into agreement if one shifts assimilation or respiration by a few weeks. The high c_i values at high northern latitudes point in the same direction but this argument does not hold if one has thresholds introduced into its computation so that two interdependent variables decouple at the introduced threshold. Is it therefore not deducible with the current surface data if the northern hemispheric CO_2 fluxes are as low as BETHY online predicts or on the other extreme much higher as indicated by inversion techniques. The total rain isotopic composition is modelled very similar to the real values. ECHAM uses the simplest

formulation for soil water, namely a bucket; so there is only one soil water value and hence only one soil water isotope signature. Mixing new rain into the bucket does not change substantially the bucket isotopic value. The big seasonal change in the isotopic composition of rain is almost totally damped out in soil. Together with the temperature seasonal cycle, this leads to almost no variation in the isotopic composition of soil respired CO_2. So CO_2 fluxes, the stomata–internal CO_2 mixing ratio and the isotopic composition of soil water are the main determinant of atmospheric $\delta^{18}O$–CO_2. Chapter 3, I show that we need high c_i values to simulate the seasonal cycle of $\delta^{18}O$–CO_2. But the c_i estimates are most likely too high in the northern hemisphere. Diminishing c_i in the high northern latitudes would be very contra–productive for $\delta^{18}O$–CO_2 and would not change a lot in CO_2 fluxes. But the wrong signal of respired CO_2 could act as a compensation to the c_i effect.

The presented coupling of ECHAM/BETHY offers the possibility to study the relevant $\delta^{18}O$–CO_2 interactive processes in a global context much more realistic than any approach up to date. Simulating a daily cycle provides the capacity to study the complex timing of the different processes involved, in order to obtain $CO^{18}O$ fluxes. I demonstrated this capability in sampling the model to obtain night time "Keeling plots" on the 40 minute time step; a mandatory time resolution to compare the model with on site measurements. The interactive nature of ECHAM/BETHY along with its short calculation time step results in an altogether much more realistic analysis for $\delta^{18}O$–CO_2. I further explore the potential of ECHAM/BETHY in Chapter 3 in which I focus on the atmospheric signal.

Appendix: Data Sets

EMDI: The Ecosystem Model–Data Intercomparison project [*Olson et al.*, 2001] aims to compare model estimates of terrestrial carbon fluxes (NPP) to estimates from ground–based measurements and to improve the understanding of environmental controls on carbon allocation. It extended the work of the Global Primary Production Data Initiative (GPPDI) and compiled NPP estimates for 2 523 sites. I used the 3 855 so called Class C cells that represent NPP estimates for 0.5° grid cells for which inventory, modelling, or remote–sensing tools were used to scale up the point measurements. 17 grid cells were associated with two estimates for different biomes where I took the consistent biome with adjacent cells. So I ended up with 3838 0.5° grid cells mainly in Australia, China, the United States, Scandinavia, Senegal and South America.

FLUXNET: FLUXNET is a global network of micrometeorological tower sites that use eddy covariance methods to measure the exchanges of CO_2, water vapour, and energy between terrestrial ecosystems and the atmosphere [*Running et al.*, 1999]. It builds on regional networks of tower sites: Ameriflux (South and North America), CarboEurope/Euroflux (Europe), AsiaFlux (mainly East Asia), OzFlux (Australia and New Zealand), KoFLux (Korea and Thailand), and some independent tower sites. Only Ameriflux and Euroflux data is available through the Oak Ridge National Laboratory Distributed Active Archive Center (ORNL DAAC). The data is available in half–hourly, daily, weekly, monthly, and annual time intervals for each site and year. Selected gap–filling methods were used on both u* corrected data and data that had not been

Table 2.2: Stations used for NEE comparison with station abbreviations utilised in Figure 2.5. The last column is the number of BETHY's plant functional type (cf. Table 2.1).

ABB Site	Lat	Lon	#
BL Blodgett For., CA, US[a]	38.90	−120.63	5
BR Braschaat, BE[b]	51.30	4.52	4
DU Duke For., NC, US[c]	35.98	−79.09	5
FL Flakaliden, SE[d]	64.12	19.45	5
HL Howland For., ME, US[e]	45.20	−68.74	5
HV Harvard For., MA, US[f]	42.54	−72.17	4
HY Hyytiälä, FI[g]	61.85	24.28	5
LW Little Washita, OK, US[h]	34.96	−97.98	11
ME Metolius, OR, US[i]	44.50	−121.62	5
PO Ponca City, OK, US[j]	36.77	−97.13	15
SH Shidler, OK, US[j]	36.93	−96.68	11
SKO Sky Oaks, Old, CA, US[k]	33.37	−116.62	7
SKY Sky Oaks, Yng, CA, US[k]	33.38	−116.62	7
SO Soroe, DK[l]	55.49	11.65	9
TH Tharandt, DE[m]	50.97	13.63	5
CFR Centr. For. Res., RU[n]	56.47	32.93	5
VI Vielsalm, BE[o]	50.30	6.00	4
WB Walker Branch, TN, US[p]	35.96	−84.29	4
WE Weidenbrunnen, DE[q]	50.15	11.87	5
ZO Zotino, RU[r]	60.75	89.40	5

[a] *Goldstein et al.* [2000], [b] *Janssens et al.* [2001], [c] *Lai et al.* [2002], [d] *Lindroth et al.* [1998], [e] *Hollinger et al.* [1999], [f] *Barford et al.* [2001], [g] *Markkanen et al.* [2001], [h] *Meyers* [2001], [i] *Law et al.* [2001]; *Anthoni et al.* [1999], [j] *Burba and Verma* [2001], [k] *Oechel et al.* [1998], [l] *Pilegaard et al.* [2001], [m] *Bernhofer et al.* [2002]; *Grünwald and Bernhofer* [2000], [n] *Milyukova et al.* [2002], [o] *Aubinet et al.* [2001], [p] *Baldocchi et al.* [2001], [q] *Bernhofer et al.* [2002], [r] *Lloyd et al.* [2002b]; *Shibistova et al.* [2002]

corrected for u* (u* correction = correction for underestimation of carbon fluxes due to stable atmospheric stratification). The original eddy data were processed using four methods developed by *Falge et al.* [2001a, b]. The "Look–up table" method with u* corrected NEE algorithm is recommended to be the most robust method for most sites. The data for Hyytiälä in Finland was updated by Tanja Suni [*personal communication*] because of problems in winter fluxes.

EUROSIBERIAN CARBONFLUX: I added two eddy flux measurement forest sites in Russia from the EUROSIBERIAN CARBONFLUX project [*Milyukova et al.*, 2002; *Lloyd et al.*, 2002b; *Shibistova et al.*, 2002]. The EUROSIBERIAN CARBONFLUX project includes a combination of surface flux measurements by means of the eddy covariance technique at selected stations together with atmospheric observations

Table 2.3: Continental station sites with correspondent numbers used in Figure 2.7 to compare with ECHAM/BETHY's δ_{bio}.

#	Code	Site	Lat	Lon
1	ASK	Assekrem, DZ	23.18	5.42
2	BAL	Baltic Sea, PL	55.50	16.67
3	BSC	Black Sea, RO	44.17	28.68
4	HUN	Hegyhatsal, HU	46.95	16.65
5	ITN	North Carolina, US	35.37	-77.39
6	KZD	Plateau Assy, KZ	44.45	77.57
7	KZM	Sary Taukam, KZ	43.25	77.88
8	LEF	Wisconsin, US	45.93	-90.27
9	NWR	Colorado, US	40.05	-105.58
10	TAP	Tae–anh Penin., KR	36.73	126.13
11	UTA	Utah, US	39.90	-113.72
12	UUM	Ulaan Uum, MN	44.45	111.10
13	WIS	Negev Desert, IL	31.13	34.88
14	WLG	Mt. Waliguan, CN	36.29	100.90

from aircraft of the CO_2 mixing ratio, and other atmospheric tracers linked to the carbon cycle (carbon isotopes, N_2O, SF_6, O_2/N_2, CH_4) [*Schulze et al.*, 2002]. The eddy measurements are provided as half–hourly, u* corrected NEE estimates from which I calculated the monthly means.

Table 2.2 provides the coordinates of all 20 stations together with the number of BETHY's plant functional type (cf. Table 2.1) and the abbreviations used in Figure 2.5.
NOAA/CMDL: The numbers in Figure 2.7 correspond to continental sampling sites of the NOAA/CMDL Cooperative Air Sampling Network. I took the same numbers for each stations as *Miller et al.* [2002] and the correspondent station names are given in Table 2.3.
GNIP: The Global Network of Isotopes in Precipitation (GNIP) of the International Atomic Energy Agency (IAEA) and the World Meteorological Organization (WMO) [*IAEA/WMO*, 2001] have been surveying the content of hydrogen and oxygen isotopes in precipitation since 1961. More than 550 meteorological stations in 93 countries have been collecting monthly precipitation samples for GNIP, i. e. they have been collecting monthly composite total rainfall, for tritium, deuterium and ^{18}O analysis. I filtered out 186 station records with sufficient data and calculated the precipitation weighted annual mean $\delta^{18}O$–H_2O.
BASIN etc.: The Biosphere–Atmosphere Stable Isotope Network (BASIN) is an activity of the Global Change and Terrestrial Ecosystem core project (GCTE) Focus 1 which aims to improve the understanding of carbon cycle processes at the ecosystem, regional, and global scales [*Pataki et al.*, 2002]. It assembles a collection of CO_2 and stable isotope measurements mainly in Europe, and North and South America. CO_2 and $\delta^{13}C$ is measured at all sites of the BASIN database but $\delta^{18}O$–CO_2 measurements are rather scarce. So I found 25 sites in the database with valid $\delta^{18}O$ measurements but

Table 2.4: Stations used for source signature comparison of respired CO_2 in Figure 2.9. The last column is the number of BETHY's plant functional type (cf. Table 2.1).

Site	Lat	Lon	#
Boreas, Pine, CA	55.93	−98.62	5
Boreas, Spruce, CA	55.91	−98.51	5
Cascade, WA, US	47.32	−121.58	5
Cascade Head, OR, US	44.48	−124.10	5
Brasilia, BR	−10.57	−47.58	2
Corvallis, OR, US	44.62	−123.20	5
Konza Prairie, KS, US	39.08	−96.58	11
Lethbridge, CA	49.90	−112.60	9
Logan, UT, US	41.90	−111.82	15
Manaus, For., BR	−2.59	−60.11	1
Manaus, Pasture, BR	−2.59	−60.11	12
Mbalmayo, CM	3.51	11.50	1
Metolius, OR, US	44.48	−121.62	5
Ottawa, CA	45.32	−75.67	5
Paracou, GF	5.03	−53.00	1
Red Butte Canyon, UT, US	40.78	−111.77	4
Rondonia, For., BR	−10.08	−61.93	1
Rondonia, Pasture, BR	−10.76	−61.36	1
Santarem, For. km 64, BR	−2.86	−54.96	1
Santarem, For. km 83, BR	−3.02	−54.97	1
Santarem, Pasture, BR	−3.02	−54.96	12
Sisters, OR, US	44.25	−121.23	5
Central For. Reserve, RU	56.47	32.93	5
Wagga Wagga, AU	−35.12	147.37	9
Wind River, 500 yr, WA, US	45.82	−121.95	5
Wind River, 40 yr, WA, US	45.82	−121.95	5
Wind River, 20 yr, WA, US	45.82	−121.95	5
Zotino, RU	60.75	89.40	5

for two sites, I did not find the appropriate ecosystem in the model. This gave 2 470 data points with CO_2 and $\delta^{18}O$–CO_2 out of the BASIN database. I updated the record of Paracou in French Guiana by 42 measurements made by Nina Buchmann [*personal communication*]. On top of this, I added 93 CO_2 and $\delta^{18}O$–CO_2 measurements made by Jon Lloyd and colleagues [*personal communication*] in Wagga Wagga, Australia, Brasilia, Brazil [*Miranda et al.*, 1996] and Mbalmayo, Cameroon. I added as well 192 data points in Russia from the EUROSIBERIAN CARBONFLUX project described above [*Langendörfer et al.*, 2002; *Styles et al.*, 2002b]. Table 2.4 gives the station, its coordinates, and the number of BETHY's plant functional type. Together, this gives 2 797 single measurements of CO_2 and $\delta^{18}O$–CO_2 in which I found 54 night time events where the data was appropriate for Keeling plots.

References

Andres, R. J., G. Marland, I. Fung, and E. Matthews, A 1 x 1 distribution of carbon dioxide emissions from fossil fuel consumption and cement manufacture, 1950–1990, *Global Biogeoch. Cycl.*, *10*, 419–429, 1996.

Anthoni, P. M., B. E. Law, and M. H. Unsworth, Carbon and water vapor exchange of an open–conopied ponderosa pine ecosystem, *Agricultural and Forest Meteorology*, *95*, 151–168, 1999.

Arpe, K., L. Bengtsson, L. Dümenil, and E. Roeckner, The hydrological cycle in the ECHAM3 simulations of the atmospheric circulation, in *Global Precipitation and Climate Change*, edited by M. Desbois and F. Desalmand, pp. 361–377, Springer–Verlag, New York, 1994.

Aubinet, M., B. Chermanne, M. Vandenhaute, B. Longdoz, M. Yernaux, and E. Laitat, Long term carbon dioxide exchange above a mixed forest in the belgian ardennes, *Agricultural and Forest Meteorology*, *108*, 293–315, 2001.

Bakwin, P. S., P. P. Tans, J. W. C. White, and R. J. Andres, Determination of the isotopic $^{13}C/^{12}C$ discrimination by terrestrial biology from a global network of observations, *Global Biogeoch. Cycl.*, *12*, 555–562, 1998.

Baldocchi, D., E. Falge, and K. Wilson, A spectral analysis of biosphere–atmosphere trace gas flux densities and meteorological variables across hour to multi–year time scales, *Agricultural and Forest Meteorology*, *107*, 1–27, 2001.

Barford, C. C., S. C. Wofsy, M. L. Goulden, J. W. Munger, E. H. Pyle, S. P. Urbanski, L. Hutyra, S. R. Saleska, D. Fitzjarrald, and K. Moore, Factors controlling long– and short–term sequestration of atmospheric CO_2 in a mid–latitude forest, *Science*, *294*, 1 688–1 691, 2001.

Bariac, T., J. Gonzalez-Dunia, N. Katerji, O. Béthenod, J. M. Bertolini, and A. Mariotti, Variabilité spatialle de la composition isotopique de l'eau (^{18}O, ^{2}H) dans le continuum sol–plante–atmosphère : 2. approche en conditions naturelles, *Chemical Geology (Isotope Geoscience Section)*, *115*, 317–333, 1994a.

Bariac, T., J. Gonzalez-Dunia, D. Tessier, and A. Mariotti, Variabilité spatialle de la composition isotopique de l'eau (^{18}O, ^{2}H) au sein des organes des plantes aériennes : 1. approche en conditions controlées, *Chemical Geology (Isotope Geoscience Section)*, *15*, 307–315, 1994b.

Bernhofer, C., M. Aubinet, R. Clement, A. Grelle, T. Grünwald, A. Ibrom, P. Jarvis, C. Rebmann, E.-D. Schulze, and J. D. Tenhunen, Spruce forests (norway and sitka spruce, including douglas fir): Carbon and water fluxes and balances, ecological and ecophysiological determinants, in *Biospheric exchanges of carbon, water, and energy of European forests*, edited by R. Valentini et al., Ecological Studies, Springer Verlag, Berlin, Heidelberg, 2002, in press.

Boyer, J. S., S. C. Wong, and G. D. Farquhar, CO_2 and water vapor exchange across leaf cuticle (epidermis) at various water potentials, *Plant Physiol.*, *114*, 185–191, 1997.

Brenninkmeijer, C. A. M., P. Kraft, and W. G. Mook, Oxygen isotope fractionation between CO_2 and H_2O, *Isotope Geoscience*, *1*, 181–190, 1983.

Burba, G. G., and S. B. Verma, Prairie growth, PAR albedo and seasonal distribution of energy fluxes, *Agricultural and Forest Meteorology*, *107*, 227–240, 2001.

Ciais, P., A. S. Denning, P. P. Tans, J. A. Berry, D. A. Randall, G. J. Collatz, P. J. Sellers, J. W. C. White, M. Trollier, H. A. J. Meijer, R. J. Francey, P. Monfray, and M. Heimann, A three dimensional synthesis study of δ^{18}O in atmospheric CO_2, part I: Surface fluxes, *J. Geophys. Res.*, *102*, 5 857–5 872, 1997a.

Ciais, P., P. P. Tans, A. S. Denning, R. J. Francey, M. Trollier, H. J. Meijer, J. W. C. White, J. A. Berry, D. A. Randall, J. J. G. Collatz, P. J. Sellers, P. Monfray, and M. Heimann, A three dimensional synthesis study of δ^{18}O in atmospheric CO_2, part II: Simulations with the TM2 transport model, *J. Geophys. Res.*, *102*, 5 873–5 883, 1997b.

Collatz, G. J., M. Ribas-Carbo, and J. A. Berry, Coupled photosynthesis–stomatal conductance model for leaves of C_4 plants, *Aust. J. Plant Physiol*, *19*, 519–538, 1992.

Craig, H., and L. I. Gordon, *Deuterium and oxygen–18 variations in the Ocean and the Marine Atmosphere*, Cons. Naz. delle Ric., Lab. di Geol. Nucl., Tries, Italy, 1965.

Dongmann, G., H. W. Nürnberg, H. Förstel, and K. Wagner, On the enrichment of $H_2{}^{18}O$ in the leaves of transpiring plants, *Rad. and Environm. Biophys.*, *11*, 41–52, 1974.

Falge, E., D. Baldocchi, R. J. Olson, P. Anthoni, M. Aubinet, C. Bernhofer, G. Burba, R. Ceulemans, R. Clement, H. Dolman, A. Granier, P. Gross, T. Grünwald, D. Hollinger, N.-O. Jensen, G. Katul, P. Keronen, A. Kowalski, C. T. Lai, B. E. Law, T. Meyers, J. Moncrieff, E. Moors, J. W. Munger, K. Pilegaard, Ü. Rannik, C. Rebmann, A. Suyker, J. Tenhunen, K. Tu, S. Verma, T. Vesala, K. Wilson, and S. Wofsy, Gap filling strategies for defensible annual sums of net ecosystem exchange, *Agricultural Forest and Meteorology*, *107*, 43–69, 2001a.

Falge, E., D. Baldocchi, R. J. Olson, P. Anthoni, M. Aubinet, C. Bernhofer, G. Burba, R. Ceulemans, R. Clement, H. Dolman, A. Granier, P. Gross, T. Grünwald, D. Hollinger, N.-O. Jensen, G. Katul, P. Keronen, A. Kowalski, C. T. Lai, B. E. Law, T. Meyers, J. Moncrieff, E. Moors, J. W. Munger, K. Pilegaard, Ü. Rannik, C. Rebmann, A. Suyker, J. Tenhunen, K. Tu, S. Verma, T. Vesala, K. Wilson, and S. Wofsy, Gap filling strategies for longterm energy flux data sets, *Agricultural Forest and Meteorology*, *107*, 71–77, 2001b.

Farquhar, G. D., S. von Caemmener, and J. A. Berry, A biochemical model of photosynthesis CO_2 fixation in leaves of C_3 species, *Planta*, *149*, 78–90, 1980.

Farquhar, G. D., J. R. Ehleringer, and K. T. Hubick, Carbon isotope discrimination and photosynthesis, *Annu. Rev. Plant Physiol. Plant Mol. Biol.*, *40*, 503–537, 1989a.

Farquhar, G. D., K. T. Hubick, A. G. Condon, and R. A. Richards, Carbon isotope fractionation and plant water–use efficiency, in *Stable Isotopes in Ecological Research*, edited by P. W. Rundel, Springer–Verlag, New York, 1989b.

Farquhar, G. D., J. Lloyd, J. A. Taylor, L. B. Flanagan, J. P. Syvertsen, K. T. Hubick, S. C. Wong, and J. R. Ehleringer, Vegetation effects on the isotope composition of oxygen in atmospheric CO_2, *Nature*, *363*, 439–443, 1993.

Federer, C. A., Transpirational supply and demand: plant, soil, and atmospheric effects evaluated by simulation, *Water Resour. Res.*, *18*, 355–362, 1982.

Fischer, R. A., and N. C. Turner, Plant productivity in the arid and semiarid zones, *Ann. Rev. Plant Physiol.*, *29*, 277–317, 1978.

Förstel, H., A. Putral, G. Schleser, and H. Leith, The world pattern of oxygen–18 in rain water and its importance in understanding the biogeochemical oxygen cycle, in *Isotope Ratios as Pollutant Source and Behavier Indicators*, pp. 323–344, Int. At. Energy Agency, Vienna, 1975.

Fung, I., C. B. Field, J. A. Berry, M. V. Thompson, J. T. Randerson, C. M. Malmstroem, P. M. Vitousek, G. J. Collatz, P. J. Sellers, D. A. Randall, A. S. Denning, F. Badeck, and J. John, Carbon 13 exchanges between the atmosphere and biosphere, *Global Biogeoch. Cycl.*, *11*, 507–533, 1997.

Gillon, J., and D. Yakir, Internal conductance to CO_2 diffusion and $C^{18}OO$ discrimination in C_3 leaves, *Plant Physiology*, *123*, 201–213, 2000a.

Gillon, J., and D. Yakir, Naturally low carbonic anhydrase activity in C_4 and C_3 plants limits discrimination against $C^{18}OO$ during photosynthesis, *Plant, Cell and Environment*, *23*, 903–915, 2000b.

Gillon, J., and D. Yakir, Influence of carbonic anhydrase activity in terrestrial vegetation on the ^{18}O content of atmospheric CO_2, *Science*, *291*, 2 584–2 587, 2001.

Goldstein, A. H., N. E. Hultman, J. M. Fracheboud, M. R. Bauer, J. A. Panek, M. Xu, Y. Qi, A. B. Guenther, and W. Baugh, Effects of climate variability on the carbon dioxide, water, and sensible heat fluxes above a ponderosa pine plantation in the sierra nevada (CA), *Agricultural and Forest Meteorology*, *101*, 113–129, 2000.

Grünwald, T., and C. Bernhofer, Data gap filling with regression modelling, in *Forest ecosystem modelling, upscaling and remote sensing*, edited by R. J. M. Ceulemans, F. Veroustrate, V. Gond, and J. B. H. F. Van Rensbergern, pp. 61–67, SPB Academic Publishing bv, The Haque, The Netherlands, 2000.

Gurney, K. R., R. M. Law, A. S. Denning, P. J. Rayner, D. Baker, P. Bousquet, L. Bruhwiler, Y. H. Chen, P. Ciais, S. Fan, I. Y. Fung, M. Gloor, M. Heimann, K. Higuchi, J. John, T. Maki, S. Maksyutov, K. Masarie, P. Peylin, M. Prather, B. C. Pak, J. Randerson, J. Sarmiento, S. Taguchi, T. Takahashi, and C. W. Yuen, Towards robust regional estimates of annual mean CO_2 sources and sinks, *Nature*, *415*, 626–630, 2002.

Hao, W. M., and M.-H. Liu, Spatial and temporal distribution of tropical biomass burning, *Global Biogeoch. Cycl.*, *8*, 495–503, 1994.

Hoffmann, G., M. Werner, and M. Heimann, Water isotopes module of the ECHAM atmospheric general circulation model: A study on timescales from days to several years, *J. Geophys. Res.*, *103*, 16 871–16 896, 1998.

Hoffmann, G., V. Masson, and J. Jouzel, Stable water isotopes in atmospheric general circulation models, *Hydrological Processes*, *14*, 1 385–1 406, 2000.

Hollinger, D. Y., S. M. Goltz, E. A. Davidson, J. T. Lee, K. Tu, and H. T. Valentine, Seasonal patterns and environmental control of carbon dioxide and water vapour exchange in an ecotonal boreal forest, *Global Change Biology*, *5*, 891–902, 1999.

IAEA/WMO, Global network of isotopes in precipitation, The GNIP Database. Accessible at: http://isohis.iaea.org, 2001.

Janssens, I. A., A. S. Kowalski, and R. Ceulemans, Intercomparison of forest floor CO_2 efflux estimates by eddy correlation and a chamber–based empirical model, *Agricultural and Forest Meteorology*, *106*, 61–69, 2001.

Jones, H. G., *Plants and Microclimate*, Cambridge University Press, Cambridge, UK, 1983.

Kaminski, T., W. Knorr, M. Heimann, and P. J. Rayner, Assimilating atmospheric data into a terrestrial biosphere model: A case study of the seasonal cycle, *J. Geophys. Res.*, p. submitted, 2002.

Keeling, C. D., The concentration and isotopic abundances of carbone dioxide in rural and marine air, *Geochim. Cosmochim. Acta*, pp. 277–298, 1961.

Keeling, C. D., R. B. Bacastow, A. F. Carter, S. C. Piper, T. P. Whorf, M. Heimann, W. G. Mook, and H. Roeloffzen, A three–dimensional model of atmospheric CO_2 transport based on observed winds, 1. Analysis on observational data, in *Aspects of Climate Variability in the Pacific and the Western Americas, Geophys. Monogr. Ser.*, edited by D. H. Peterson, vol. 55, pp. 165–236, AGU, Washington, D.C., 1989.

Kicklighter, D. W., A. Bondeau, A. L. Schloss, J. Kaduk, A. D. McGuire, and T. P. of the Potsdam NPP Model Intercomparison, Comparing global models of terrestrial net primary productivity (npp): global pattern and differentiation by major biomes, *Global Change Biology*, *5 (Suppl. 1)*, 16–24, 1999.

Knorr, W., Satellite remote sensing and modelling of the global CO_2 exchange of land vegetation: a synthesis study, Ph.D. thesis, Max–Planck Institute for Meteorologie, Hamburg, 1997, in german.

Knorr, W., Annual and interannual CO_2 exchange of the terrestrial biosphere: process–based simulations and uncertainties, *Global Ecology and Biogeography*, *9*, 225–252, 2000.

Knorr, W., and M. Heimann, Impact of drought stress and other factors on seasonal land biosphere CO_2 exchange studied through an atmospheris tracer transport model, *Tellus*, *47B*, 471–489, 1995.

Knorr, W., and M. Heimann, Uncertainties in global terrestrial biosphere modeling: 1. a comprehensive sensitivity analysis with a new photosynthesis and energy balance scheme, *Global Biogeoch. Cycl.*, *1*, 207–225, 2001a.

Knorr, W., and M. Heimann, Uncertainties in global terrestrial biosphere modeling: Part ii: Global constraints for a process–based vegetation model, *Global Biogeoch. Cycl.*, *1*, 227–246, 2001b.

Lai, C. T., G. Katul, J. Butnor, D. Ellsworth, and R. Oren, Modelling night–time ecosystem respiration by a constrained source optimization method, *Global Change Biology*, *8*, 124–141, 2002.

Langendörfer, U., M. Cuntz, P. Ciais, P. Peylin, T. Bariac, I. Milyukova, O. Kolle, T. Naegler, and I. Levin, Modelling of biospheric CO_2 gross fluxes via oxygen isotopes in a spruce forest canopy: a ^{222}Rn calibrated box model approach, *Tellus*, *54B*, 2002, in press.

Law, B. E., P. Thornton, J. Irvine, S. Van Tuyl, and P. M. Anthoni, Carbon storage and fluxes in ponderosa pine forests at different developmental stages, *Global Change Biology*, *7*, 755–777, 2001.

Lindroth, A., and S. Halldin, Numerical analysis of pine forest evaporation and surface resistance, *Agriculture and Forest Meteorology*, *38*, 59–79, 1986.

Lindroth, A., A. Grelle, and A. S. Moren, Long–term measurements of boreal forest carbon balance reveal large temperature sensitivity, *Global Change Biology*, *4*, 443–450, 1998.

Lloyd, J., and G. D. Farquhar, ^{13}C discrimination during CO_2 assimilation by the terrestrial biosphere, *Oecologia*, *99*, 201–215, 1994.

Lloyd, J., and J. A. Taylor, On the temperature dependance of soil respiration, *Functional Ecology*, *8*, 315–323, 1994.

Lloyd, J., R. L. Langenfelds, R. J. Francey, M. Gloor, N. M. Tschebakova, D. Zolotukhine, W. A. Brand, R. A. Werner, A. Jordan, C. A. Allison, V. Zrazhewske, O. Shibistova, and E.-D. Schulze, A trace gas climatology above Zotino, central Siberia, *Tellus*, *54B*, 2002a, in press.

Lloyd, J., O. Shibistova, D. Zolothukhine, O. Kolle, A. Arneth, J. Styles, N. M. Tchebakova, and E.-D. Schulze, Seasonal and annual variations in the photosynthetic productivity and carbon balance of a central Siberian pine forest, *Tellus*, *54B*, 2002b, in press.

Long, S. P., E. G. Moya, S. K. Imbamba, A. Kamnalrut, M. T. F. Piedade, J. M. O. Scurlock, Y. K. Shen, and D. O. Hall, Primary productivity of natural grass ecosystems of the tropics: a reappraisal, *Plant and Soil*, *115*, 155–166, 1989.

Majoube, M., Fractionnement en oxygene–18 et en deuterium entre l'eau et sa vapeur, *Journal de Chimie et Physique*, *58*, 1 423–1 436, 1971.

Markkanen, T., Ü. Rannik, P. Keronen, T. Suni, and T. Vesala, Eddy covariance fluxes over a boreal scots pine forest, *Boreal Environment Research*, *6*, 65–78, 2001.

Marland, G., R. J. Andres, T. A. Boden, C. Johnston, and A. Brenkert, Global, regional and national CO_2 emission estimates from fossil fuel burning, cement production and gas flaring: 1751–1996 (revised March 1999), *Data Report ORNL NDP–030*, Carbon Dioxide Inf. Anal. Cent., Oak Ridge Natl. Lab., Oak Ridge, Tenn., 1998.

Meentemeyer, V., Macroclimate and lignin control of litter decomposition rates, *Ecology*, *59*, 465–472, 1978.

Melayah, A., L. Bruckler, and T. Bariac, Modeling the transport of water stable isotopes in unsaturated soils under natural conditions. 2. comparison with field experiments, *Water Resources Research*, *32*, 2 055–2 065, 1996.

Merlivat, L., and J. Jouzel, Global climatic interpretation of the deuterium–oxygen 18 relationship for precipitation, *Journal of Geophysical Research*, *84*, 5 029–5 033, 1979.

Meyers, T. P., A comparison of summertime water and CO_2 fluxes over rangeland for well watered and drought conditions, *Agricultural and Forest Meteorolog*, *106*, 205–214, 2001.

Miller, J. B., D. Yakir, J. W. C. White, and P. P. Tans, Measurement of $^{18}O/^{16}O$ in the soil–atmosphere CO_2 flux, *Global Biogeoch. Cycl.*, *13*, 761–774, 1999.

Miller, J. B., P. P. Tans, J. W. C. White, T. J. Conway, and B. W. Vaughn, The atmospheric signal of terrestrial carbon isotopic discrimination and its implication for partitioning carbon fluxes, *Tellus*, 2002, in press.

Milyukova, I. M., O. E. Kolle, A. B. Varlagin, N. N. Vygodskaya, E.-D. Schulze, and J. Lloyd, Carbon balance of a southern taiga spruce stand in european russia, *Tellus*, *54B*, 2002, in press.

Miranda, A. C., H. S. Miranda, J. Lloyd, J. Grace, R. J. Francey, P. Riggan, and J. Brass, Fluxes of carbon dioxide and water vapour over cerrado vegetation in Central Brazil. An analysis using eddy correlation and stable isotope techniques, *Plant, Cell and Environment*, *20*, 315–328, 1996.

Modellbetreuungsgruppe, The ECHAM3 atmospheric general circulation model, *Tech. Rep. 6*, Deutsches Klimarechenzentrum, Hamburg, 1994.

Oechel, W. C., G. L. Vourlitis, S. J. Hastings, R. P. Ault, and P. Bryant, The effects of water table manipulation and elevated temperature on the net CO_2 flux of wet sedge tundra ecosystems, *Global Change Biology*, *4*, 77–90, 1998.

Olson, R. J., J. M. O. Scurlock, S. D. Prince, D. L. Zheng, and K. R. J. (eds.), NPP multi–biome: NPP and driver data for ecosystem model–data intercomparison, Available on–line [http://www.daac.ornl.gov/] from the Oak Ridge National Laboratory Distributed Active Archive Center, Oak Ridge, Tennessee, U.S.A., 2001.

Pataki, D. E., J. R. Ehleringer, L. B. Flanagan, D. Yakir, D. R. Bowling, C. Still, N. Buchmann, J. Kaplan, and J. A. Berry, The application and interpretation of keeling plots in terrestrial carbon cycle research, *Global Biogeoch. Cycl.*, 2002, in press.

Peylin, P., The composition of ^{18}O in atmospheric CO_2: A new tracer to estimate global photosynthesis, Ph.D. thesis, L'Université Paris VI, Paris, 1999, in french.

Peylin, P., P. Ciais, P. P. Tans, K. Six, J. A. Berry, and A. S. Denning, ^{18}O in atmospheric CO_2 simulated by a 3–D transport model: A sensitivity study to vegetation and soil fractionation factors, *Phys. and Chem. of the Earth*, *21*, 463–469, 1997.

Pilegaard, K., P. Hummelshoj, N. O. Jensen, and Z. Chen, Two years of continuous CO_2 eddy–flux measurements over a danish beech forest, *Agricultural and Forest Meteorology*, *107*, 29–41, 2001.

Quay, P. D., B. Tilbrook, and C. S. Wong, Oceanic uptake of fossil fuel CO_2 : Carbon–13 evidence, *Science*, *256*, 74–79, 1992.

Raich, J. W., and C. S. Potter, Global patterns of carbon dioxide emissions from soils, *Global Biogeoch. Cycl.*, *9*, 23–36, 1995.

Raich, J. W., and W. H. Schlesinger, The global carbon dioxide flux in soil respiration and its relationship to vegetation and climate, *Tellus*, *44B*, 81–99, 1992.

Riley, W. J., C. J. Still, M. S. Torn, and J. A. Berry, A mechanistic model of $H_2^{18}O$ and $C^{18}OO$ fluxes between ecosystems and the atmosphere: Model description and sensitivity analyses, *Global Biogeoch. Cycl.*, 2002, in press.

Roche, C., Interactions biosphere–atmosphere aux echelles locales et composition isotopique (^{13}C, ^{18}O) du CO_2 atmospherique : application a la foret landaise, Ph.D. thesis, Université Paris VI, Pierre et Marie Curie, 1999, in french.

Roeckner, E., K. Arpe, L. Bengtsson, S. Brinkop, L. Dümenil, M. Esch, E. Kirk, F. Lunkeit, M. Ponater, B. Rockel, R. Sausen, U. Schlese, S. Schubert, and M. Windelband, Simulation of the present–day climate with the ECHAM model: impact of model physics and resolution, *Tech. Rep. 93*, Max–Planck Institut für Meteorologie, Hamburg, 1992.

Roeckner, E., K. Arpe, L. Bengtsson, M. Christoph, M. Clausen, L. Dümenil, M. Esch, M. Giorgetta, U. Schlese, and U. Schulzweida, The atmospheric general circulation model ECHAM–4: Model description and simulation of present–day climate, *Tech. Rep. 218*, Max–Planck Institut für Meteorologie, Hamburg, 1996.

Running, S. W., D. D. Baldocchi, D. P. Turner, S. T. Gower, P. S. Bakwin, and K. A. Hibbard, A global terrestrial monitoring network intergrating tower fluxes, flask sampling, ecosystem modeling and EOS satellite data, *Remote Sensing of Environment*, *70*, 108–127, 1999, fLUXNET data available on–line [http://www.daac.ornl.gov/] from the Oak Ridge National Laboratory Distributed Active Archive Center, Oak Ridge, Tennessee, U.S.A.

Schulze, E.-D., Carbon dioxide and water exchange in response to drought in the atmosphere and in the soil, *Ann. Rev. Plant Physiol.*, *13*, 127–141, 1986.

Schulze, E.-D., N. C. Turner, T. Gollan, and K. A. Shakel, Stomatal response to air humidity and to soil drought, in *Stomatal Function*, edited by E. Zeiger, G. Farquhar, and I. Cowan, pp. 311–321, Stanford University Press, Stanford, USA, 1987.

Schulze, E.-D., F. M. Kelliher, C. Lloyd, and R. Leuning, Relationships among maximum stomatal conductance, ecosystem surface conductance, carbon assimilation rate, and plant nitrogen nutrition: a global ecology scaling exercise, *Ann. Rev. Ecol. Syst.*, *25*, 629–660, 1994.

Schulze, E.-D., N. N. Vygodskaya, N. Tschebakova, C. I. Czimczik, D. Kozlov, J. Lloyd, D. Mollicone, E. Myachkova, K. Sidorov, A. Varlagin, and C. Wirth, The eurosiberian transect: An introduction to the experimental region, *Tellus*, *54B*, 2002, in press.

Scurlock, J. M. O., K. Johnson, and R. J. Olson, Estimating net primary productivity from grassland biomass dynamics measurements, *Global Change Biology*, *8*, 736–753, 2002.

Sellers, P. J., Canopy reflectance, photosynthesis, and transpiration, *Int. J. Remote Sensing*, *6*, 1 335–1 372, 1985.

Shibistova, O., J. Lloyd, G. Zrazhewskaya, A. Arneth, O. Kolle, N. Astrakhantceva, I. Shijneva, A. Knohl, and J. Schmerler, Ecosystem respiration budget for a pinus sylvestris stand in central Siberia, *Tellus*, *54B*, 2002, in press.

Stern, L. A., R. Amundson, and W. T. Baisden, Influence of soils on oxygen isotope ratio of atmospheric CO_2, *Global Biogeoch. Cycl.*, *15*, 753–760, 2001.

Stryer, L., *Biochemistry*, W. H. Freeman and Co, San Francisco, 1981.

Styles, J. M., J. Lloyd, D. Zolotukhin, K. A. Lawton, N. M. Tschebakova, R. J. Francey, A. A. Arneth, D. Salamakho, O. Kolle, and E.-D. Schulze, Estimates of regional surface CO_2 exchange and carbon and oxygen isotope discrimination during photosynthesis from concentration profiles in the atmospheric boundary layer, *Tellus*, *54B*, 2002a, in press.

Styles, J. M., M. R. Raupach, G. D. Farquhar, O. E. Kolle, K. A. Lawton, W. A. Brand, R. A. Werner, A. Jordan, E.-D. Schulze, O. Shibistova, and J. Lloyd, Soil and canopy CO_2, $^{1}3CO_2$, H_2O and sensible heat flux partitions in a forest canopy inferred from concentration measurements, *Tellus*, *54B*, 2002b, in press.

Suits, N. S., A. S. Denning, J. A. Berry, C. J. Still, J. Kaduk, and J. Randerson, Seasonal and spatial variations in carbon isotopic ratios of plant biomass, terrestrial CO_2 fluxes and atmospheric CO_2, *Global Biogeoch. Cycl.*, 2002, in review.

Takahashi, T., R. H. Wanninkhof, R. A. Feely, R. F. Weiss, D. W. Chipman, N. Bates, J. Olafsson, C. Sabine, and S. C. Sutherland, Net sea–air CO_2 flux over the global oceans: An improved estimate based on the sea–air pCO_2 difference, in *2nd International Symposium, CO_2 in the Oceans, extended abstracts*, Center Global Env. Res., Tsukuba, Japan, 1999.

Tans, P. P., Oxygen isotopic equilibrium between carbon dioxide and water in soils, *Tellus*, *50B*, 163–178, 1998, with Erratum, *Tellus, 50B*, 400, 1998.

Tans, P. P., J. A. Berry, and R. F. Keeling, Oceanic ^{13}C data: a new window on CO_2 uptake by the oceans, *Global Biogeoch. Cycl.*, *7*, 353–368, 1993.

Turner, N. C., Adaptation to water deficits: a changing perspective, *Aust. J. Plant Physiol.*, *13*, 338–342, 1986.

Vogel, J. C., P. M. Grootes, and W. G. Mook, Isotopic fractionation between gaseous and dissolved carbon dioxide, *Z. Phys.*, *230*, 225–238, 1970.

Wanninkhof, R., Relationship between wind speed and gas exchange over the ocean, *J. Geophys. Res.*, *97*, 7 373–7 382, 1992.

Werner, M., M. Heimann, and G. Hoffmann, Isotopic composition and origin of polar precipitation in present and glacial climate simulations, *Tellus*, *53B*, 53–71, 2001.

White, J. W. C., The climatic significance of D/H ratios in white pine in the Northeastern United States, Ph.D. thesis, Columbia University, New York, 1983.

Yakir, D., Oxygen–18 of leaf water: a crossroad for plant–associated isotopic signals, in *Stable isotopes: integration of biological, ecological and geochemical processes*, edited by H. Griffiths, chap. 10, pp. 147–168, βIOS Scientific Publisher Limited, Oxford, UK, 1998.

Yakir, D., and L. S. L. Sternberg, The use of stable isotopes to study ecosystem gas exchange, *Oecologia*, *123*, 297–311, 2000.

Chapter 3

Mapping the Atmospheric Signal

3.1 Introduction

The emission of human induced CO_2 mostly in the northern hemisphere causes the atmospheric CO_2 mixing ratio to increase with time and imprints a strong north–south gradient on the CO_2 mixing ratio. Anthropogenic emissions of CO_2 are of the same order of magnitude as natural net CO_2 fluxes of the biosphere everywhere on the globe. Therefore, the north–south gradient in CO_2 mixing ratio is to a large extent due to anthropogenic emissions. This is different for the $\delta^{18}O$ isotopic composition of atmospheric CO_2. The fluxes for the isotopic CO_2 signal are called isofluxes and are a convolution of CO_2 fluxes and the difference between the isotopic ratio of these fluxes and the atmospheric isotope ratio. The latter difference is called "discrimination" so that the isoflux is the CO_2 flux times "discrimination". This means that for the isotopic composition of atmospheric CO_2 the importance of each CO_2 flux can be attenuated or amplified by "discrimination". *Peylin* [1999] showed that the global $\delta^{18}O$–CO_2 isoflux of anthropogenic emissions is comparable to the global net (or total) $\delta^{18}O$–CO_2 isoflux of the biosphere but that it can differ by more than an order of magnitude in certain regions, notably north of 50 °N and in the southern tropics. It is hence mainly the biosphere which defines the spatial distribution of $\delta^{18}O$–CO_2. (The gradient reflects in part the underlying gradient of the isotopic value of the soil water which is communicated, with modification, to the atmosphere only in the presence of fluxes with the terrestrial biosphere.) Because of the small seasonal variance of the fossil fuel emissions, the seasonal cycle of $\delta^{18}O$–CO_2 is also determined mostly by the biospheric CO_2 gross fluxes, i. e. assimilation and respiration which in contrast to fossil fuel combustion show big seasonal variations. To understand the atmospheric signal of $\delta^{18}O$–CO_2, it is therefore essential to understand the biospheric CO_2 fluxes and their associated "discriminations". On the other hand, one can learn about the biospheric CO_2 fluxes by examining the atmospheric $\delta^{18}O$–CO_2 signal.

I have developed a comprehensive global 3D model of $\delta^{18}O$ in atmospheric CO_2 which is described in detail in Chapter 2. In the present chapter, I focus on the modelled spatiotemporal distribution of atmospheric $\delta^{18}O$–CO_2. I examine the mean seasonal cycle of CO_2 and $\delta^{18}O$–CO_2 at atmospheric stations and the gradient between the Arctic and Antarctica of $\delta^{18}O$–CO_2. I investigate subsequently the sensitivity of the model to different parameters, processes, and parameterisations.

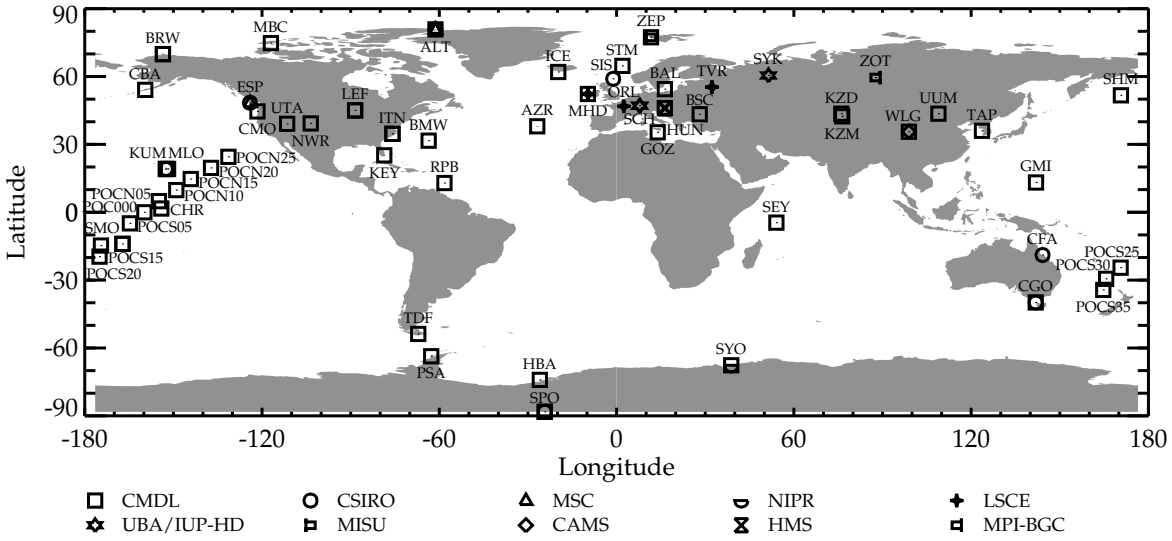

Figure 3.1: Global distribution of the 59 atmospheric measurement stations used in this study. Different symbols denote different laboratories that measure CO_2 (and $\delta^{18}O$–CO_2).

3.2 Data and Model

3.2.1 Data Sets Used

The GLOBALVIEW–CO_2 database consist presently of 165 stations at 118 locations with measurements of 22 different institutions [*GLOBALVIEW-CO_2*, 2002]. The stations are distributed world–wide with a strong bias towards coastal or marine environments. Some stations are still influenced by close–by terrestrial sources and sinks but the majority select air measurements from the marine boundary layer (MBL) and are referred to as marine background stations. Which stations are considered to be MBL sites can be found in the GLOBALVIEW–CO_2 documentation. I added five non–MBL stations to GLOBALVIEW–CO_2 comprising four new aircraft sites in Eurasia [*Levin et al.*, 2002a] plus one discrete sampling record at Schauinsland, Germany (SCH) [*Schmidt et al.*, 2001]. A characteristic of MBL stations is that discrete and (quasi–)continuous measurements are very close in the monthly or annual mean. Non–MBL stations show quite large deviations between means of continuous and discrete samples even if one applies filter methods to catch mostly large scale representative continental air. Figure 3.1 shows the distribution of 59 stations that I used here for the comparison because I have $\delta^{18}O$–CO_2 data at these stations as well. Figure 3.2 presents seasonal cycles at 45 measurement sites (out of 59 stations in Figure 3.1) for which I have sufficient data to calculate seasonal cycles of $\delta^{18}O$–CO_2 (continuous measurements are open and discrete measurements are closed symbols; the lines are model results and are explained in the result section). One number after the station abbreviation represents the number of model grid cells or vertical layers by which I shifted the model in order to take into account different sampling and filtering methods applied to the measurements [cf. *Ramonet and Monfray*, 1996]. For example MHD1 means that I took

one grid cell further to the west than the actual Mace Head coordinate to sample the model. The 4 aircraft sites have the name affix '030' that is the GLOBALVIEW–CO_2 affix for aircraft measurements made in 3000 m height, e. g. SYK030 for aircraft measurements over Syktyvkar, Russia in 3000 m a.s.l. One can see the difference between MBL and non–MBL stations at e. g. the two stations Point Barrow (BRW), MBL, and Schauinsland (SCH), non–MBL, where continuous and discrete sampling procedures are installed. Whereas Point Barrow shows almost no difference between continuous and discrete sampling, Schauinsland shows a reduced peak–to–peak amplitude of 1/3 in the continuous record. The continuous record at Schauinsland is filtered for night–time values and with wind speed thresholds [*Schmidt et al.*, 1996] whereas the flasks are filled during morning and may to some extent be influenced by local sources and sinks. Schauinsland is a mountain station situated 1205 m above the Rhein valley. I do not take the ground level on Schauinsland, in the model at about 360 m, but the fourth vertical layer at about 1300 m. The model box is therefore far from local sources and sinks so that it is more comparable with the continuous measurements there. This is important to keep in mind when comparing δ^{18}O–CO_2 monthly means of non–MBL flask records with model monthly means whereby the model was not sampled or filtered in the same way as the measurements.

I merged further δ^{18}O–CO_2 data at the 59 stations of Figure 3.1 where δ^{18}O–CO_2 is measured on atmospheric flask samples. This includes 50 sites, named CMDL/ INSTAAR, where the flasks were collected from the NOAA Carbon Cycle Group at the Climate Monitoring and Diagnostics Laboratory (CMDL) and measured afterwards from the Stable Isotope Laboratory of the Institute for Artic and Alpine Research (INSTAAR) at the University of Colorado. At most stations, air was not dried in the NOAA Global Air Sampling Network before 1998/1999. *Trolier et al.* [1996] found out that δ^{18}O–CO_2 measured at flasks collected at more humid sampling sites are most likely contaminated by exchange with water condensed on the flask wall [*Gemery et al.*, 1996]. CMDL records from higher latitude sites appear credible for δ^{18}O in atmospheric CO_2. Therefore, I discarded all non–dried flasks between 35 °S and 35 °N but kept the non–dried flasks on all other latitudes.

I added to the CMDL stations seven stations with samples collected for and measured by the Division of Atmospheric Research at the Commonwealth Scientific and Industrial Research Organisation (CSIRO). The samples are all dried prior to filling so that the above problem does not apply to CSIRO data. CSIRO established a link to the VPDB–CO_2 scale in 1987 [*Francey and Goodman*, 1988], however with a change of mass spectrometer in 1991, the calibration of δ^{18}O–CO_2 was propagated under the assumption of similar instrument responses. A new assignment onto the VPDB–CO_2 calibration scale was introduced in 1999 (CG99) that recognised much greater susceptibility of the new mass spectrometer to "cross contamination" and thus removed a relative bias of around 0.8 ‰ in data obtained using the new mass spectrometer. Full details, including a minor revision of the CG99 assignment, are in preparation for publication. CMDL and CSIRO measurements at the same stations differ now by this offset [*Masarie et al.*, 2001]. It is very likely that the CMDL values are wrong by this offset due to erroneous standard material preparation. I shifted thus all CMDL values by 0.8 ‰ to merge the two independent data sets. I focus in this chapter on seasonal cycles and on the north–south gradient of δ^{18}O in atmospheric CO_2. The mean seasonal

cycle is not altered by the offset but the absolute annual mean values do, determining the north–south gradient change. But, both laboratories have among others a sampling site on South Pole, Antarctica, so that I can refer all annual means relative to the South Pole annual mean value of its sampling network and the merged data set should give an internally consistent relative north–south gradient. Taking South Pole is somewhat arbitrary but the South Pole station is far from sources and sinks of CO_2 and $\delta^{18}O$–CO_2 and therefore reasonable as a reference point.

As for CO_2, I added four $\delta^{18}O$–CO_2 flask aircraft sites in Eurasia [*Levin et al.*, 2002a] plus the $\delta^{18}O$–CO_2 flask record at Schauinsland [*Schmidt et al.*, 2001]. Measurements of samples from these sites were made at the Institut für Umweltphysik, University of Heidelberg (IUP–HD), Laboratoire des Sciences du Climat et de l'Environnement (LSCE), Max–Planck Institut für Biogeochemie (MPI-BGC), and CSIRO. Because all five stations are non–MBL stations, they are only used here for comparison of the seasonal cycles so that systematic offsets between different labs [*Levin et al.*, 2002b] play no role in this context. These stations were already used to analyse the East–West distribution of CO_2 and $\delta^{18}O$–CO_2 over Eurasia [*Levin et al.*, 2002a; *Cuntz et al.*, 2002] whereby systematic offsets may contribute to the statements made in these publications.

The new combined data set of $\delta^{18}O$–CO_2 shows slightly reduced seasonal amplitudes only at equatorial stations compared to a former data compilation [*Peylin et al.*, 1999] whereas it is rather similar at the rest of the globe. An Arctic–to–Antarctic difference of $\delta^{18}O$–CO_2 of about 1.7 ‰ was already recognised in the first CSIRO data compilation in 1987 [*Francey and Tans*, 1987] and confirmed later by CMDL/INSTAAR measurements [*Ciais et al.*, 1997b; *Peylin et al.*, 1999]. But the new combined data set exhibits a north–south gradient of 2.0 ‰ with very little interannual variability. I am confident that this is a robust feature of $\delta^{18}O$–CO_2 and will not change in future data acquisition.

3.2.2 Model Runs

The model ECHAM/BETHY is described in detail in Chapter 2. It is possible to run the model with or without the diverse processes described in Chapter 2. The $CO^{18}O$ fluxes are calculated interactively with the $\delta^{18}O$ value of the atmosphere and, therefore, $\delta^{18}O$ will attain a different mean atmospheric level depending on the processes included in the particular model run. This can be seen from the global budget equation for $\delta^{18}O$–CO_2 which I repeat here from Chapter 2:

$$\frac{d\delta_a}{dt} = \frac{1}{C_a M_a}\left[F_s\Delta_s + A\Delta_l + F_{ao}\Delta_o^{des} + F_o\Delta_o^{equ} + (F_{fos} + F_{bur})\,\Delta_f\right] \qquad (3.1)$$

$$\begin{aligned}
\text{with}\quad \Delta_s &= \delta_s - \delta_a + \epsilon_s \\
\Delta_l &= -\epsilon_l + \tfrac{c_{cs}}{c_a - c_{cs}}\,(\delta_l - \delta_a) \\
\Delta_o^{equ} &= \epsilon_w \\
\Delta_o^{des} &= \delta_o - \delta_a \\
\Delta_f &= \delta_f - \delta_a \quad .
\end{aligned}$$

M_a is the conversion factor between fluxes in GtC and mixing ratios in ppm, Δ_l the discrimination of photosynthesis, Δ_o^{equ} the equilibrium discrimination between ocean and atmosphere, Δ_s the "discrimination" associated to soil respired CO_2, Δ_o^{des}

Table 3.1: Global annual CO_2 fluxes (in GtC yr^{-1}), assimilation weighted annual mean CO_2 mixing ratios (in ppm), assimilation weighted annual mean δ values (in ‰ VPDB–CO_2), and ϵ–constants (in ‰) calculated and used in ECHAM/BETHY.

Variable	Value	Variable	Value
A	97.3	δ_l	6.3
F_s	98.0	δ_s	−6.9
F_{ao}	99.4	δ_o	1.2
F_o	2.6	δ_f	−17.0
F_{fos}	5.8	ϵ_l	−7.4
F_{bur}	3.1	ϵ_s	−7.2
c_a	353	ϵ_w	0.8
c_{cs}	264		

the tendency to equilibrate the difference between atmospheric and ocean dissolved CO_2, and Δ_f the "discrimination" of burning processes. The product of CO_2 flux and "discrimination" is called isoflux. Writing the global budget equation in a short form gives:

$$\frac{d\delta_a}{dt} = a - b\delta_a \,, \tag{3.2}$$

with

$$\begin{aligned} a &= \frac{1}{C_a M_a}\left[F_s(\delta_s+\epsilon_s) + A(\epsilon_l + \frac{c_{cs}}{c_a - c_{cs}}\delta_l) + F_{ao}\delta_o + F_o\epsilon_w + (F_{fos}+F_{bur})\delta_f\right] \\ b &= \frac{1}{C_a M_a}\left[F_s + \frac{c_{cs}}{c_a - c_{cs}}A + F_{ao} + F_{fos} + F_{bur}\right] . \end{aligned} \tag{3.3}$$

The solution of this differential equation is:

$$\delta_a(t) = \frac{a}{b} - \frac{a}{b}\exp\{-bt\} \,. \tag{3.4}$$

So the global δ_a will stabilise at a/b when t becomes much larger than b^{-1}. Including or excluding a process in a model run is like setting the appendant CO_2 flux to zero and a/b will change accordingly.

The model stabilises around a global δ^{18}O–CO_2 value of 2.3 ‰ VPDB–CO_2 including all processes and e. g. around 3.0 ‰ VPDB–CO_2 taking only assimilation and respiration into account. The data, based on the CSIRO assignment onto the VPDB–CO_2 scale, indicate a global MBL surface mean of 0.5 ‰ VPDB–CO_2 (with a South Pole value of 1.1 ‰ VPDB–CO_2). In the model, the global mean value depends on what processes are included. For example, taking "invasion" into account, mentioned in Chapter 2, there is the extra term $F_{inv}\Delta_{inv}$ in the global budget equation (eq. 3.1) with $\Delta_{inv} = (\delta_s - \delta_a)$, the discrimination of invasion. This adds $F_{inv}\delta_s$ to the parenthesis of a and F_{inv} to the parenthesis of b (eq. 3.2 & 3.3). The model calculates 18.6 GtC yr^{-1} CO_2 invasion flux that would reduce the global mean to 1.9 ‰ VPDB–CO_2.

When I start the model from one particular global uniform value in the atmosphere, b^{-1} denotes the e–folding time of the stabilisation. The e–folding differs between 1.3 and 1.9 years depending on the processes included and it needs at least 3 e–folding times to establish a stable annual mean north–south gradient. So I initialise the model with 0 ‰ VPDB–CO_2 everywhere and let the model run for 15 years. I then take the mean of the last 5 years for the analyses. The model is not sensitive to the initial value but the stabilisation process is always determined by b. The standard model run includes the same processes as included by *Ciais et al.* [1997a, b], namely assimilation, respiration, ocean exchange, fossil fuel combustion, and biomass burning. Individual process contributions to the atmospheric δ^{18}O–CO_2 signal are calculated as so called δ–anomalies, δ^{i*} [*Heimann and Keeling*, 1989]:

$$\begin{aligned} \delta^{i*} &= \frac{c^i \left(\delta^i - \delta^{bg}\right)}{\sum_i c^i} \\ &= \frac{c^i \left(\delta^i - \delta^{bg}\right)}{c_a} \end{aligned} \tag{3.5}$$

where c^i is the contribution of process i to the overall CO_2 concentration, δ^i the δ value of this contribution, and δ^{bg} is an atmospheric "background" δ_a which I take as 0 ‰ VPDB–CO_2. The sum of all δ^{i*} gives $\delta_a - \delta^{bg}$. They are hence additive whereas the individual δ^i are not (compare *Peylin et al.* [1997] who used δ^{i*} versus *Ciais et al.* [1997b] who used δ^i).

3.3 Results and Discussion

The δ^{18}O value of atmospheric CO_2 depends on the CO_2 fluxes and the "discriminations" of the involved processes. It is therefore essential to model properly atmospheric CO_2 values. If the model compares badly to the measurements at a specific station, I cannot expect to reproduce δ^{18}O–CO_2 at that station. If I do not compare well in CO_2 but in δ^{18}O–CO_2 it is possible that the "discriminations" are incorrect. But if one process is important for CO_2, it can be unimportant for δ^{18}O–CO_2. So if this process produces a bad seasonal cycle in CO_2 but is unimportant in δ^{18}O–CO_2, it is still possible to simulate a realistic seasonal cycle in δ^{18}O. Hence in the seasonal cycle comparison (Fig. 3.2 and 3.3), all processes that have an amplitude greater than 30 % of the modelled total amplitude are included.

3.3.1 CO_2 Seasonal Cycle

I show in Figure 3.2 mean seasonal cycles of atmospheric CO_2 at the 45 selected stations, alphabetically sorted by their GLOBALVIEW–CO_2 abbreviation. Measured monthly means are plotted as symbols whereby each institution has its particular symbol. Filled symbols represent flask and open symbols represent continuous measurements. The solid bold lines are the model results of the standard run with all processes included (ECHAM/BETHY). As mentioned before, I included thin lines for the contribution of individual processes to the total seasonal cycle if the amplitude of

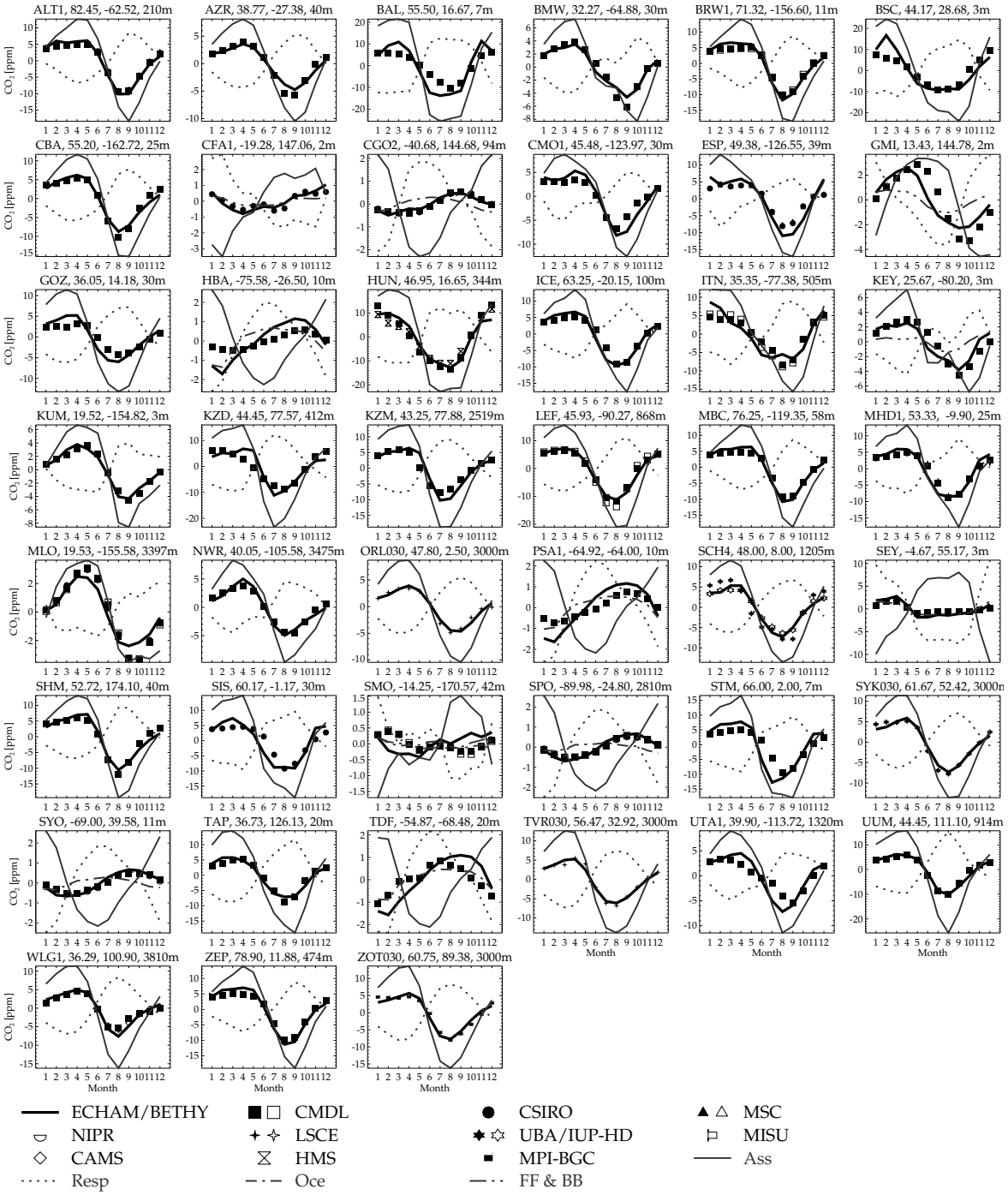

Figure 3.2: Mean seasonal cycle of CO_2 at atmosphere observatories. Filled symbols are flask measurements of different laboratories, open symbols denote (quasi–) continuous measurements, the solid thick line is the ECHAM/BETHY standard run and thin lines show the contribution of each process. Individual processes are only plotted if their peak–to–peak amplitude exceeds 30 % of the total model amplitude. Ass signifies assimilation, Resp respiration, Oce the ocean contribution, and fossil fuel combustion and biomass burning are combined in FF & BB. Note that every station has its individual CO_2 scale.

the individual process contribution is more than 30 % of the total amplitude. The thin lines represent the respective processes: assimilation (Ass, thin solid line), respiration (Resp, thin dotted line), ocean (Oce, thin dash dot line), and fossil fuel and biomass burning (FF & BB, thin dash triple dot line). The seasonal cycle is mostly determined by assimilation and respiration so that another process becomes important only at 11 out of 45 stations. ECHAM/BETHY performs very well at most stations with 10 evident exceptions, namely Baltic Sea (BAL), Black Sea (BSC), Mariana Islands, Guam (GMI), Halley Station, Antarctica (HBA), Mauna Loa, Hawaii (MLO), Palmer Station, Antarctica (PSA), Tutuila, American Samoa (SMO), Norway Shipboard (STM), Tierra Del Fuego, Argentina (TDF), and Wendover, Utah (UTA). The Baltic and the Mediterranean Sea are no open seas in the ECHAM T21 spectral truncation but are closed basins. The parameterisations of climate surface processes over the Baltic and Mediterranean grid points behave therefore similar to land with a reduced roughness length. The nearby continental signal is transported very fast over the two basins so that BAL and GOZ are influenced too much by adjacent terrestrial biosphere fluxes in the model. The Black Sea does not exists at all in the T21 truncation so that the sea–land circulation system is not represented, too. But BSC station is located at the west coast of the Black Sea and is probably influenced by sea and land breezes. Tutuila (SMO) lays almost directly on the equator in the pacific ocean. The South Pacific Convergence Zone (SPCZ) passes over SMO only once per year in the model so that it misses the peculiar form of the seasonal cycle at SMO. The same phenomenon but with the Intertropical Convergence Zone (ITCZ) is present in ECHAM at Christmas Island (not shown here because the available data is not appropriate for a reasonable seasonal cycle of $\delta^{18}O$–CO_2 there). But this seems to be a problem of ECHAM only in the Pacific Ocean because ECHAM/BETHY is capable to catch the peculiar seasonal cycle of Mahe Island, Seychelles (SEY) in the Indic ocean and at Ascension Island in the Atlantic Ocean (not shown here because I have no $\delta^{18}O$–CO_2 measurements there), the seasonal cycles of both are also mainly determined by the ITCZ. Mariana Islands (GMI) shows a too low amplitude and Wendover (UTA) shows a too high amplitude in the model and both show a phase shift of about one month compared to the data. I showed in Chapter 2 that it is possible that this behaviour comes from a wrong timing between assimilation and respiration. Shifting the respiration CO_2 contribution in the output of the model does indeed lead to a much better agreement between model and measurements at GMI and UTA. Halley Station (HBA), Palmer Station (PSA), and Tierra Del Fuego (TDF) lie all around the Antarctic circus polar current and are strongly influenced by the ocean CO_2 net flux. ECHAM4 has up to 6 m s^{-1} stronger winds in the southern ocean during summer compared to re–analyses of the European Centre of Medium–range Weather Forecast (ECMWF) [*Roeckner et al.*, 1996] which results in a high CO_2 ocean sink in the vicinity of Antarctica. Comparing Cape Grim (CGO) and South Pole (SPO) with the interjacent stations shows that the peak–to–peak amplitude of the mean seasonal cycle is very similar at CGO and SPO but doubled in between. This portends notedly to an ocean effect at the Antarctic coast stations. Mauna Loa (MLO) and Cape Kumukahi (KUM) are two stations on Hawaii. MLO station is situated in 3397 m on the northern flank of Mauna Loa volcano. KUM is a ground station on the eastern most projection of the island of Hawaii. The peak–to–peak amplitude at MLO is only about 60 % of the KUM amplitude and its phase lags behind for about

one month. ECHAM/BETHY catches well the seasonal cycle at KUM but is too weak at MLO. It was recognised before that the vertical advection in ECHAM is too strong for tracers [*Timmreck et al.*, 1999] but that convection is quite realistically reproduced [*Mahowald et al.*, 1995]. So it depends on the relative strength of vertical advection to convection around sources to simulate well high altitude stations and some could be represented wrong by ECHAM/BETHY. This could be the reason why the Norwegian Shipboard (STM) station is out of phase by one month and too big in amplitude. I showed in Chapter 2 that the maximum in Net Ecosystem Exchange (NEE) occurs in June/July in Europe but most northern hemispheric atmospheric stations show their minimum in atmospheric CO_2 in August/September. This time–lag comes from the atmospheric transport which accounts for about one month [*Ciais et al.*, 2001]. But the model shows an immediate response to NEE fluxes in atmospheric CO_2 at STM showing its atmospheric minimum already in July.

3.3.2 δ^{18}O–CO_2 Seasonal Cycle

ECHAM/BETHY proofs to simulate well the seasonal cycle of CO_2 at most stations. I show further the seasonal cycle of $\delta^{18}O$ in atmospheric CO_2 at the same 45 stations in Figure 3.3. I plotted as well all processes that amplitude is at least 30 % of the total model amplitude. The seasonal cycle in δ^{18}O–CO_2 is almost completely determined by assimilation and respiration. There are only two stations where another process has a noticeable influence. These are the influence of the ocean at Halley Station, Antarctica (HBA) and the contribution of fossil fuel combustion at Mahe Island, Seychelles (SEY). SEY receives northern hemispheric air during northern spring, summer, and autumn and southern hemispheric air during winter. This leads to a different contribution of fossil fuel combustion in winter against the rest of the year and leads to a transport at SEY. The model shows the correct amplitude at high northern hemispheric stations but a two months phase shift, e. g. at Alert (ALT), Barrow (BRW), or Mace Head (MHD). There δ^{18}O–CO_2 has its minimum in October whereas the model shows its minimum in August as for CO_2. This time lag is present at almost all stations. It was also present in earlier δ^{18}O–CO_2 models like that of *Peylin et al.* [1999] not as pronounced in the high northern and southern latitudes but with the same strength elsewhere. The model fails to catch the amplitude of the seasonal cycle outside the high northern latitudes where it calculates about ⅔ of the measured amplitude. *Peylin et al.* concluded that respiration is the dominant process controlling the seasonal cycle and that assimilation acts like a correction to the respiration dominated seasonal cycle. As explained in Chapter 2, I calculate CO_2 fluxes and isofluxes directly in the model so the "discriminations" are an implication of both, namely the ratio of isoflux to CO_2 flux. Leaf discrimination is therefore assimilation weighted, making it bigger and strengthening its influence. Assimilation has the same influence on δ^{18}O–CO_2 as respiration has in the model so that the parameterisations of assimilation processes become more important in the model compared to offline models like those of *Ciais et al.* [1997a, b] and *Peylin et al.* [1997, 1999]. For example, changing only the non–water–limited stomatal CO_2 mixing ratio, c_{i0}, from one parameter set found in the literature to another parameter set found equally in the literature as explained in Chapter 2, does almost not change assimilation but alters the amplitude of δ^{18}O–CO_2 at high northern hemispheric sta-

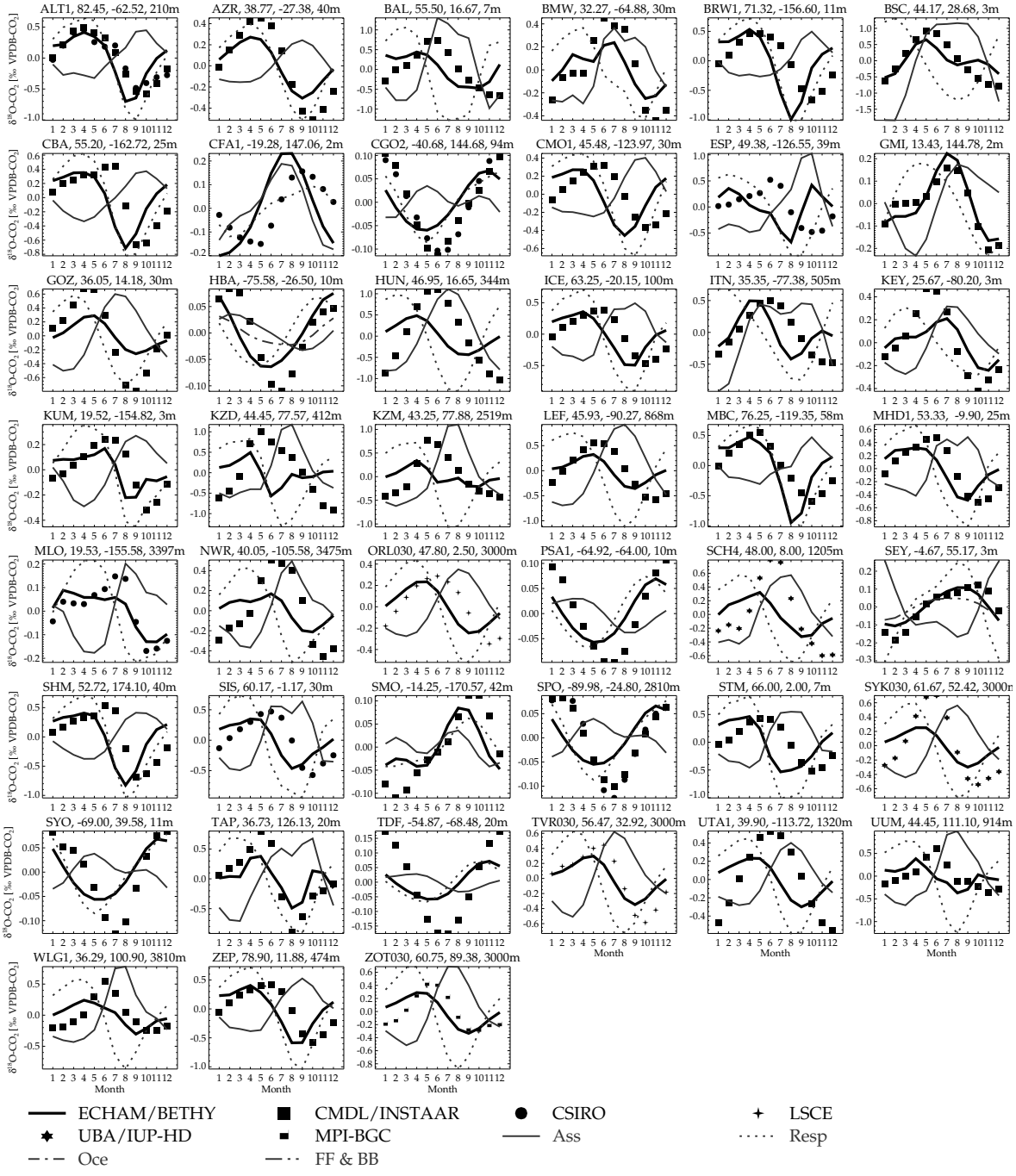

Figure 3.3: Mean seasonal cycle of δ^{18}O–CO_2 at atmosphere observatories. Symbol and line definitions are the same as in Figure 3.2. Note that every station has its individual δ^{18}O–CO_2 scale.

tions by a factor of 2 due to the factor $c_{cs}/(c_a - c_{cs})$ in leaf discrimination (s. eq. 3.1 and Chapter 2). I have chosen the higher c_{i0} because they are derived from a literature survey of field measurements [*Schulze et al.*, 1994, and Chapter 2] rather then from laboratory measurements [*Farquhar et al.*, 1989; *Boyer et al.*, 1997, and Chapter 2]. The c_{i0} values are most important at high northern latitudes where water–limitation is less frequent and plants are limited by other factors than water. Note that south hemispheric stations outside the tropics show generally very small seasonal cycles, reduced by a factor of 10 compared to northern hemispheric stations [compare South Pole (SPO) with a peak–to–peak amplitude of 0.15 ‰ to Alert (ALT) with an amplitude of ca. 1 ‰]. They are therefore hard to measure and one can see at SPO the differences in the data between CMDL/INSTAAR and CSIRO. Anyway, the model shows only $^2/_3$ of the amplitude outside high latitudes but it is clearly possible to find a reasonable parameter set which fits the amplitude at the stations. For the time being, I stayed with the parameters of *Ciais et al.* and *Peylin et al.* for comparison but fixed a value of $\epsilon_s = -7.2$ ‰ [*Miller et al.*, 1999] whereas this was a fit parameter in the earlier models in order to have no atmospheric trend.

There are a few phenomena in the CO_2 and $\delta^{18}O$–CO_2 data which are interesting to notice:

- One expects a time lag between the phasing of the production function (CO_2 fluxes and isofluxes) and the phasing of the seasonal cycle of the atmospheric concentrations because the trace gases have to be transported from the site of production to the stations. Northern hemispheric NEE measurements, shown in Chapter 2, exhibit their minimum NEE in June/July and northern hemispheric CO_2 measurements in the atmosphere show their minimum in August/September (e. g. BRW, ICE, SIS, SYK, and ZOT). So there is a 1 to 2 month time lag between NEE and the atmospheric CO_2 measurements. The transport can be simplified in horizontal and vertical transport and one can state that the horizontal transport is the main responsible for the time lag at atmospheric background stations (or MBL stations) and that vertical transport is responsible for the time lag at altitude stations. ECHAM/BETHY reproduces this time shift at ground stations and at altitude stations in CO_2. $\delta^{18}O$–CO_2 measurements in the northern hemisphere show their minimum shifted by two months compared to CO_2. ECHAM/BETHY does not capture this time shift but shows the CO_2 and $\delta^{18}O$–CO_2 minimum at the same time at ground stations, but it shows a shift by one month at altitude stations. Well known examples for the time lag between ground and altitude are the CO_2 measurements at Kumukahi (KUM) and Mauna Loa (MLO). It is interesting to recognise that KUM and MLO are exceptions of the above rule for $\delta^{18}O$–CO_2. The measurements at KUM and MLO show a one month time lag for CO_2 but have their $\delta^{18}O$–CO_2 minimum exactly the same time.
- At some continental stations, $\delta^{18}O$–CO_2 lags even more behind CO_2: 3 months at e. g. SCH, 4 months at BSC, and 5 months at KZM. ECHAM/BETHY does not follow these special signals but is very homogenous in its response at the atmospheric stations, i. e. it shows the $\delta^{18}O$–CO_2 minimum the same time as CO_2 at ground stations and 1 month shifted at altitude stations.
- $\delta^{18}O$–CO_2 in the southern hemisphere shows very small seasonal cycles with peak–to–peak amplitudes of about 0.2 ‰. A ‘good’ pair–to–pair difference be-

tween flasks filled simultaneously is about 0.05 ‰. If flasks are stored for a long time (e. g. at South Pole), CO_2 has time to exchange isotopically with residing water. But this depends on the remaining water in the flasks and the temperatures during storage and transport. So CSIRO applies a drift correction of 0.1 ‰ yr^{-1} which is an empirical value and afflicted with a large error. So the combined uncertainty per flask measurement is of the same order as the seasonal cycle amplitude. But δ^{18}O–CO_2 in the southern extra–tropics is very similar at all stations (CGO, HBA, PSA, SPO, and SYO). I checked the data in order to circumvent an artefact due to the fit function used but I am confident that the presented seasonal cycles are real and no artefact present. So, the measurements and ECHAM/BETHY are both homogenous in the southern hemisphere where the model precedes the data by one to two months and shows only ⅔ of the measured amplitude.

I examine the seasonal cycle of ECHAM/BETHY further in section 3.3.4 where I explore the behaviour of ECHAM/BETHY due to modified parameters, changed parameterisations, and the inclusion or exclusion of different processes.

3.3.3 North–south Gradient and Rectifier Effect

The biosphere is set to equilibrium for CO_2 over a ten year model run. This means that I have no annual mean net CO_2 flux from the biosphere. The according δ^{18}O gross fluxes, called isofluxes, are the convolution of CO_2 fluxes and "discriminations". If the annual mean leaf discrimination is not equal soil "discrimination", the total biospheric isoflux is not zero. Considering only the biosphere for the moment, if this is true in the model, the atmospheric δ value will change according to equation 3.1. But changing δ_a will alter leaf and soil "discrimination". δ_a will finally stabilise at a certain value (a/b, s. eq. 3.1–3.3) and the annual mean leaf and soil "discriminations" stay constant and equal each other in their absolute value (with the opposite sign). Making a run with only biospheric fluxes stabilises δ_a at about 3 ‰ VPDB–CO_2 with isofluxes of ±1650 GtC ‰ yr^{-1}, for assimilation and respiration respectively, which is equivalent to "discriminations" of about ±16.8 ‰. But leaf and soil isoflux are not equal in every grid cell unlike CO_2 (s. Chapter 2) because equation 3.1 is only valid for the total globe. On one grid cell, there is also transport from adjacent grid cells which change the atmospheric δ^{18}O–CO_2. Leaf isoflux is about the same in the northern and southern hemisphere, adding up to 825 GtC ‰ yr^{-1} per hemisphere in the biosphere only run. This is due to varying reasons: northern hemispheric net assimilation accounts for 57.3 GtC yr^{-1} and southern hemispheric net assimilation for 40 GtC yr^{-1} leading to a leaf discrimination of 14.4 ‰ and 20.6 ‰, respectively. Soil isoflux does not apportion equally between the two hemispheres: −985 GtC ‰ yr^{-1} in the northern hemisphere and −665 GtC ‰ yr^{-1} in the southern hemisphere, yielding similar soil "discriminations" of −17.1 ‰ and −16.4 ‰ on the northern and southern hemisphere at each case. So there is an imbalance in the total isoflux between the northern and southern hemisphere. The southern hemisphere emits an isoflux of +160 GtC ‰ yr^{-1} which is balanced in the northern hemisphere by a total isoflux of −160 GtC ‰ yr^{-1}. Hence, there is a gradient in isoflux, means δ^{18}O–CO_2 flux, and this gradient is mirrored in the atmospheric δ^{18}O–CO_2 values.

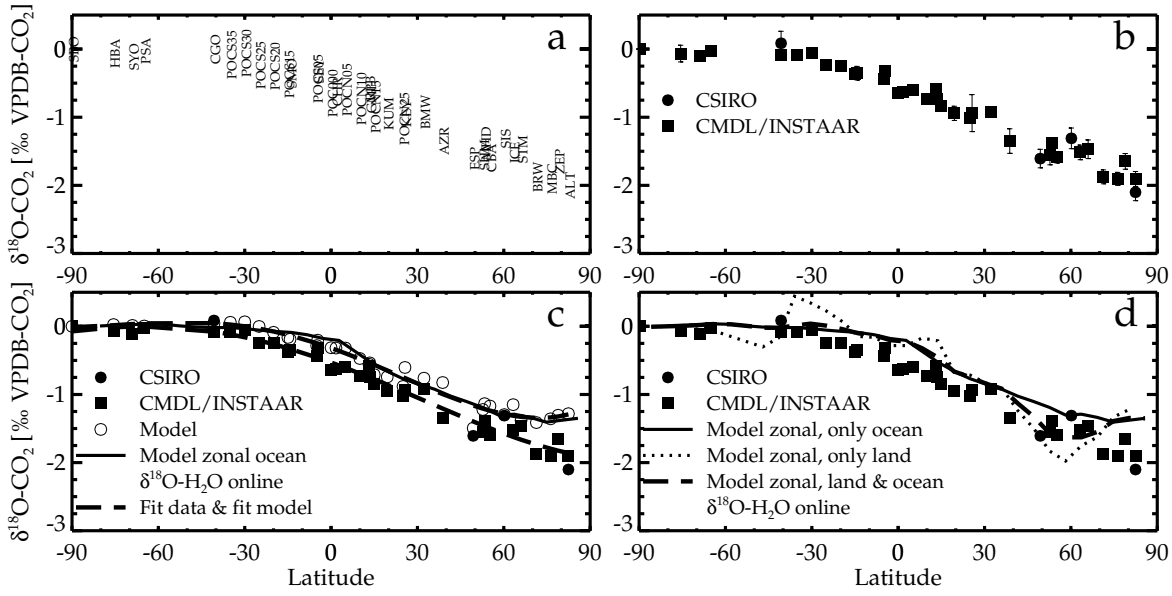

Figure 3.4: Meridional gradient of δ^{18}O–CO_2 relative to South Pole. a) shows the station abbreviations of MBL stations centred over its mean value relative to South Pole, b) the same data but symbolised for each individual laboratory with error bars signifying the standard deviation of inter–annual variations at the station relative to South Pole, c) the data as in b) but with ECHAM/BETHY results at the station coordinates as open circles together with least square fits of 4 polynomials through data and through model values (dashed lines) as well as the latitudinal mean of the lowest model layer of ocean grid cells (solid line), d) the same symbols as in c) but with the latitudinal mean of ocean grid cells (solid line), land grid cells (dotted line) and all grid cells (dashed line).

I show in Figure 3.4 the meridional gradient of δ^{18}O in atmospheric CO_2. I added to the 45 stations of the seasonal cycle analysis 11 ship stations between 35 °S and 35 °N (POCS35 to POCN35), Christmas Island (CHR), Ragged Point, Barbados (RPB), and Gobabeb, Namibia (NMB) where either the record length or the data density were not sufficient to calculate a seasonal cycle. But the absolute atmospheric level should not be corrupted because I did a rigorous data selection, trying to avoid all kinds of contamination. I excluded then all non–MBL stations to see a non–biased long–range atmospheric signal (it rests only stations from CMDL/INSTAAR and CSIRO). Non–MBL station data is filtered in most cases so that the excluded stations would not represent the latitudinal variation but a signal in–between the ocean north–south gradient and the true meridional gradient. To simplify single plots, I show in Figure 3.4a the station abbreviations centred over its mean value and in Figure 3.4b the values as symbols together with one standard deviation between different years which shows the inter–annual variation of the local station relative to South Pole. I calculated the annual mean only if the full year was covered so that there are some stations with only one annual mean value and no error bar is associated with it. If the two laboratories measure on a particular station, the station abbreviation is centred over the mean of

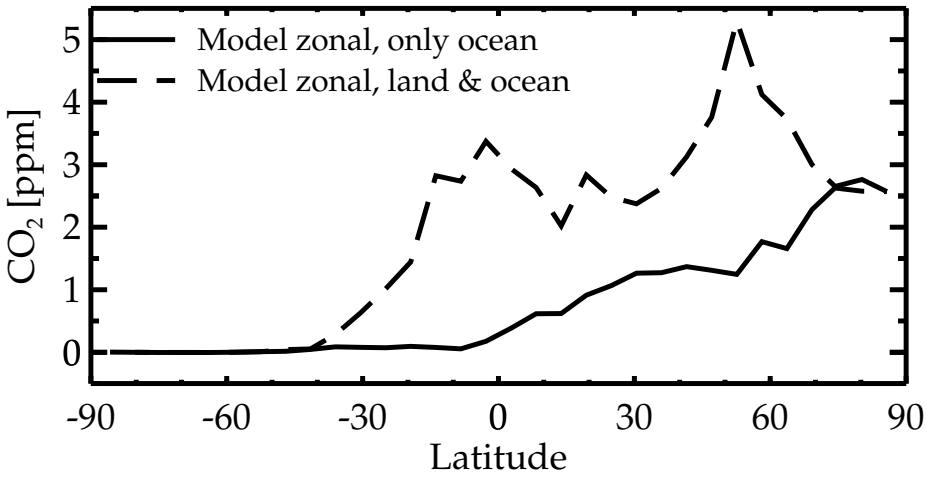

Figure 3.5: Meridional gradient of ground level CO_2 relative to South Pole in ECHAM/BETHY. The solid line is the latitudinal mean of atmospheric CO_2 over ocean grid cells and the dashed line of all grid cells (land and ocean).

both laboratories. I included in Figure 3.4c the model predictions of ECHAM/BETHY at the actual stations (open circles) together with the zonal mean of the lowest model layer over ocean grid cells (solid line). This is what I think that the data actually represents. To demonstrate this, I did a least square fit of a polynomial function to the measurements and to the model values at the stations (dashed lines). The χ^2 of the least square fits did not change significantly if I used more than 4 polynomials, so the dashed lines are fits with 4 polynomials. One can see for the model values that the least square fit deviates only at the tropics from the latitudinal mean of ocean grid cells and is otherwise nearly identical to it. A cubic fit, often used to represent measurements of CO_2 [e. g. *Denning et al.*, 1995], had much higher χ^2 values and did not represent the measurements very well. I plotted further in Figure 3.4d the latitudinal means of all grid cells (dashed line), only ocean grid cells (solid line), and only land grid cells (dotted line). The conventionally used latitudinal mean of all grid cells to represent the north–south gradient is very similar to the only ocean grid cells latitudinal mean but shows a local minimum at around 60 °N. This is no consequence of sources and sinks alone but also of the rectifier effect. The rectifier effect comes from the covariance of surface exchange fluxes with meridional transport and vertical mixing [*Denning et al.*, 1996b] and is treated below. Contrary to CO_2, the $\delta^{18}O$–CO_2 budget is not closed on every grid cell and I have a negative total isoflux in the northern hemisphere which tends to bias over land. I see the same phenomena in CO_2 (Figure 3.5) where the biosphere is in equilibrium. The rectifier effect causes a north minus south difference of 2.5 ppm which is even bigger than the estimate of *Denning et al.* [1995]. Taking a plain latitudinal mean over all grid points ends at the same Arctic–to–Antarctic difference of 2.5 ppm but shows two local maxima, one around 0 and one around 55–60 °N, reaching values of 5 ppm (Figure 3.5). The same behaviour can be seen in the TRANSCOM project phase 1 [*Law et al.*, 1996] where models with a high rectifier effect show all maxima

around 60 °N and a drop in mixing ratio afterwards. This true latitudinal signal is not represented in the actual station distribution of GLOBALVIEW–CO_2 and I think one should use only ocean grid points to compare measurements with model latitudinal means and eventually deduce carbon sources and sinks [e. g. *Law et al.*, 1996]. *Tans et al.* [1990] and *Denning et al.* [1995] bypassed this problem by using a fit through modelled station values. Figure 3.4c shows that both approaches are very similar whereas the latitudinal mean over ocean grid cells is easier to calculate, independent of the used fit procedure (e. g. cubic or higher polynomials, error–weighting, etc.), and independent of a wrong station representation in the model (e. g. data selection, smoothed model orographie, etc.) [cf. *Ramonet and Monfray*, 1996].

The model shows a strong covariance between vertical and horizontal transport and surface fluxes called rectifier effect in a generic manner. I show in Figure 3.6 these effect for the biospheric fluxes of CO_2 and $\delta^{18}O$ in CO_2. The biosphere is thereby in equilibrium so that there is no net CO_2 flux in the annual mean per grid point. As explained earlier, this yields a zero annual net flux for $\delta^{18}O$–CO_2 only in the global mean and not on every grid point. The annual mean $\delta^{18}O$–CO_2 distribution mirrors the imbalance of these fluxes as well as the covariance between flux and transport. The vertical transport during daytime in the growing season is vigorous and the Net Ecosystem Exchange (NEE) is negative, means a sink. This results in only a small negative gradient in CO_2 mixing ratio between the surface and the Planetary Boundary Layer (PBL). Vertical transport is almost suppressed during nighttime and NEE is positive, means a source. This yields a strong mixing ratio gradient between the surface and the PBL. Taking the daily (monthly) mean in one height leads to a shift in CO_2 mixing ratio that is positive at the ground and negative in the higher PBL, i. e. that one averages higher values at the ground and lower values at mid– PBL. This effect is normally called Diurnal Rectifier Effect (DRE) [*Stephens et al.*, 1999]. The DRE is very strong in summer but significantly lower during winter. The same phenomena happens on seasonal time scales as well: transport patterns in summer and winter are different, e. g. higher wind speeds inside the continents during winter lead to a faster dilution of concentration differences. This covary with the seasonal pattern of NEE which is negative during summer and positive during autumn/winter and can lead to lower annual mean surface values [*Ciais et al.*, 2000; *Taylor*, 1998]. This second effect is normally called Seasonal Rectifier Effect (SRE). Both rectifier effects are superimposed in nature and in the model whereby the DRE makes about 80 % of the signal over land; only 25 % of the signal over ocean are attributed to it [*Denning et al.*, 1996b]. I call the total effect further the Combined Rectifier Effect (CRE). I subtracted from all atmospheric values the trend at South Pole as a reference to make Figure 3.6 directly comparable with Figure 3.4. One can see the north–south gradient of Figure 3.4 in plate p of Figure 3.6. Over Ocean, the annual mean $\delta^{18}O$–CO_2 varies between about 0.5 ‰ VPDB–CO_2 to about -2 ‰ VPDB–CO_2. Between 45 °N and 60 °N over ocean, $\delta^{18}O$–CO_2 is about constant and measures around -1.5 ‰ VPDB–CO_2. Over land in the same latitude band, $\delta^{18}O$–CO_2 is lower down to -2.5 ‰ so that a latitudinal mean would show lower values for land and ocean points together versus only ocean points. This is the minimum in the $\delta^{18}O$–CO_2 north–south gradient of all grid points in Figure 3.4d and present in earlier $\delta^{18}O$–CO_2 modelling studies [*Ciais et al.*, 1997b; *Peylin et al.*, 1999]. One can only loom the CO_2 interhemispheric gradient of Figure 3.5 in plate g for

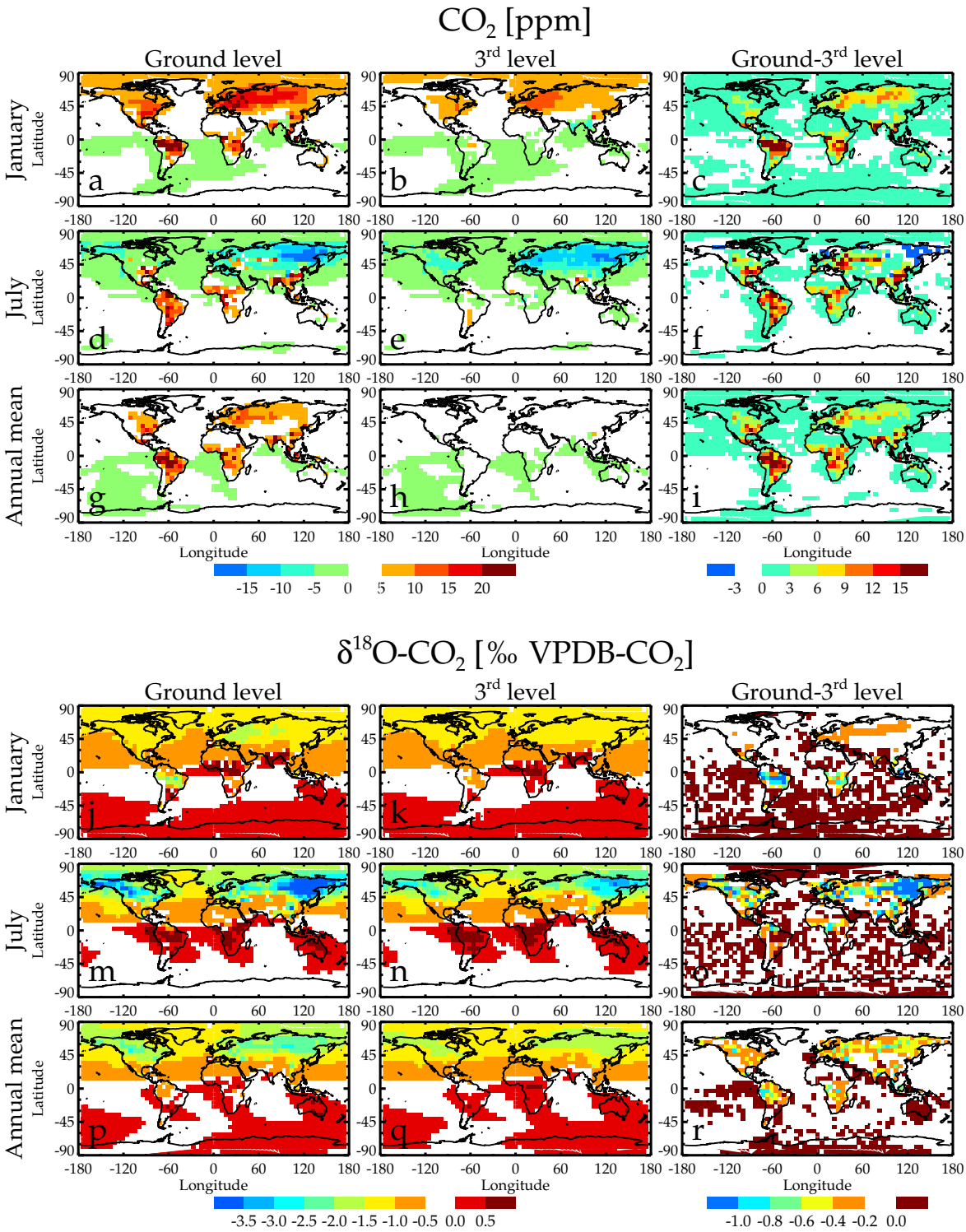

Figure 3.6: Rectifier effect of the biospheric fluxes in ECHAM/BETHY for CO_2 and $\delta^{18}O$–CO_2. The first column is the ground level (around 30 m), the second column the third model level (around 800 m), and the third column is the difference between ground and third level. Note that the colour bar in the third column differs from the combined colour bar for column one and two. I subtracted the trend at South Pole from each grid point as a reference.

only ocean grid points because it is lower than the steps of the colour scale but one can easily spot the local maximum of CO_2 in the northern boreal zone which leads to the characteristic maximum at 60 °N of the latitudinal mean CO_2 mixing ratio of all grid cells. The third model level lies in the middle of the PBL (ca. 800 m) in summer but outside of the PBL in winter and during night (most times). ECHAM/BETHY shows an accumulation of CO_2 at the ground level with respect to the third level (third column in Figure 3.4a–i) over the continents most of the time. The difference between ground and third level gets negative only in eastern Siberia and in Alaska in July (plate f). The very low daily cycle of fluxes in this regions covary with a meridional transport which is stronger than the vertical transport, i. e. that the SRE outweighs the DRE in this regions. The Amazon region shows generally the biggest CO_2 rectification gradients yielding superelevations of up to 20 ppm in the annual mean (plate i). Convection is very strong in the tropics and together with high CO_2 fluxes, this leads to the strong rectifier signal. But East–Europe, West–Siberia, and South–East–Asia show as well very high gradients between ground and 800 m in July which attain values of up to 30 ppm (plate f) comparable with rectification gradients in the Amazon (plate c). It is nevertheless surprising that CO_2 over Eurasia shows almost everywhere lower values than over the ocean in July (plate d). The CRE is uncovered there only in the difference to the 800 m level (plate f). $\delta^{18}O$–CO_2 shows conceptually a similar picture with accumulation over the continents and a quite uniform meridional distribution over the oceans. High CO_2 mixing ratio differences come along with high negative $\delta^{18}O$–CO_2 differences. This is not true for the Amazon region in July. $\delta^{18}O$–CO_2 fluxes are not in equilibrium over each grid point, respectively over one hemisphere, so that one can see the positive anomalies of $\delta^{18}O$–CO_2 over the southern hemispheric continents in July, notably in the Amazon (plate m&n) and always negative values of $\delta^{18}O$–CO_2 over the continents of the northern hemisphere above 30 °N. The negative difference of CO_2 between ground and third level over eastern Siberia and Alaska in July (plate d–f) is accompanied by very big differences in $\delta^{18}O$–CO_2 (plate m–o). This comes from negative leaf discrimination in this region in the model (s. Chapter 2 and 4). An already negative rectifier response in CO_2 is amplified by negative leaf discrimination. This affects the annual mean difference so that $\delta^{18}O$–CO_2 at the ground is more negative than at 800 m over the whole Eurasian and the North–American continents (plate r) whereas CO_2 shows superelevations only in East–Europe, West–Siberia, and at the American East Coast (plate i)

3.3.4 Sensitivity Studies

The standard run includes assimilation, respiration, ocean fluxes, fossil fuel combustion and biomass burning. These are the same processes that *Ciais et al.* [1997a, b] included in their model study. They claimed that first of all assimilation and respiration are responsible for the seasonal cycle of $\delta^{18}O$–CO_2 but that one needs fossil fuel combustion input and the biomass burning process to simulate a realistic north–south gradient. I performed several sensitivity runs that are summarised in this section, notably I included or excluded diverse processes, and added new processes that were explained in Chapter 2, changed the globally fixed fractionations, and changed the formulation of some processes. I show in the plots only a selection of these sensitivity runs because

Table 3.2: Names and contents of sensitivity runs. Ass stands for assimilation, Resp for respiration, Oce for the ocean exchange, FF for fossil fuel combustion, BB for biomass burning, Inv for the invasion effect, Carb. Anhy. for reduced carbonic anhydrase activity, c_a vari. for variable atmospheric CO_2 mixing ratios in assimilation calculation, and $\delta^{18}O$ rain for monthly mean rain and vapour isotope input instead of $\delta^{18}O$–H_2O online calculation.

Name	Ass	Resp	Oce	FF	BB	Inv	Carb. Anhy.	c_a vari.	$\delta^{18}O$ rain
AR	X	X							
AROCE	X	X	X						
ARFF	X	X		X					
ARBB	X	X			X				
ARINV	X	X				X			
ARCA	X	X					X		
ARCaVar	X	X						X	
ARMM	X	X							X
STD	X	X	X	X	X				
STDMM	X	X	X	X	X				X

$\delta^{18}O$–CO_2 in ECHAM/BETHY is almost exclusively determined by assimilation and respiration, as one can remark in this section.

I label in Table 3.2 only the sensitivity studies which are discussed in the text in detail and show which processes are included in the runs. For example, AR stands then for the run which includes only assimilation and respiration and STD abbreviates the standard run.

North–south gradient

ECHAM uses a soil bucket model for water as explained in Chapter 2. So there is only one soil water content and one soil water $\delta^{18}O$–H_2O. This simplification yields soil $\delta^{18}O$–H_2O values which do not change significantly during the course of the year. $\delta^{18}O$ in CO_2 leaving the soil has thence almost the same value all year long in the model even if there is a major change in $\delta^{18}O$–H_2O of incoming rain. In reality, $\delta^{18}O$–H_2O at the soil surface changes considerably when it rains but this is attenuated in deeper soil so that $\delta^{18}O$–H_2O of very deep soil does not change markedly [e. g. *Melayah et al.*, 1996]. The prevailing opinion is that $\delta^{18}O$ of CO_2 leaving the soil is in isotopic equilibrium with soil water at about 15 cm depth [*Riley et al.*, 2002; *Miller et al.*, 1999]. $\delta^{18}O$–H_2O at 15 cm depth does not follow the whole stroke of $\delta^{18}O$–H_2O of incoming rain but is also notedly attenuated there. Former $\delta^{18}O$ in atmospheric CO_2 models used monthly rain and its isotope values as an approximation for the "correct" δ–value of equilibrating soil water [e. g. *Peylin et al.*, 1999]. $\delta^{18}O$–H_2O in 15 cm depth will lie between the two extremes, rain and soil bucket respectively, most of the time but can reach much higher values during longer drought periods. But these periods are also marked by reduced CO_2 production in soil and by roots due to the limitation of water. I conducted thus a

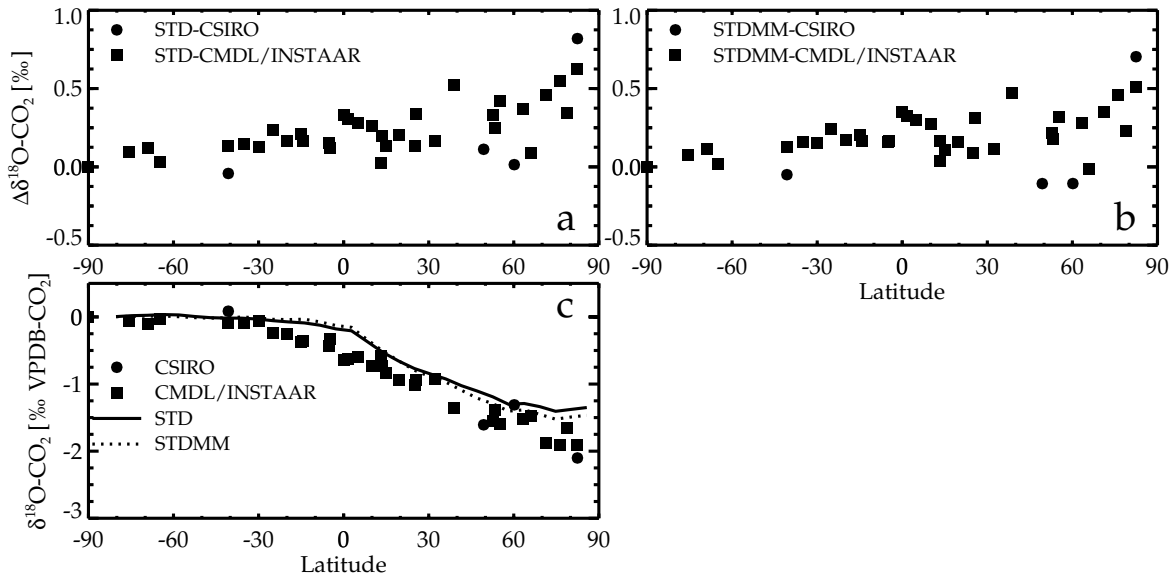

Figure 3.7: Meridional gradient of δ^{18}O–CO_2 relative to South Pole. a) shows the difference between the model values at particular stations and the measurements at this stations b) the same as a) but with a model run where the water isotopes are introduced as monthly mean rain and vapour isotope values, and c) data and latitudinal mean over ocean grid cells of the standard run and the run with monthly mean water isotope input of b).

sensitivity experiment where δ^{18}O–CO_2 fluxes of the standard run (STD) do not depend on the online calculated δ^{18}O–H_2O values but are rather prescribed to monthly means of δ^{18}O–H_2O rain of the standard model run (STDMM). I treat this sensitivity run in detail because it shows one of the largest influences on the north–south gradient of all sensitivity runs (s. Figure 3.8). Because even this sensitivity run has a relatively minor influence to the overall north–south gradient of δ^{18}O–CO_2, I do not display detailed plots of the other sensitivity studies but rather explain the outcome in words. Figure 3.7 shows the results of the STDMM run for the north–south gradient. Figure 3.7a shows the differences of the model standard run, STD (with δ^{18}O–CO_2 calculated online on every time step), and the measurements at the stations. Figure 3.7b opposes the difference of the STDMM model run and the measurements. Figure 3.7c shows then the latitudinal mean over ocean grid cells of both runs (the solid line is STD and the dotted line is STDMM). Rain isotope input did not change greatly the north–south gradient in δ^{18}O–CO_2. The spread in the differences between model and measurements is not reduced and the latitudinal mean over ocean grid cells does change only marginally.

Former model studies of δ^{18}O in atmospheric CO_2 described the influence of different processes on the north–south gradient as well. I show in Figure 3.8a the contribution of each individual process to the latitudinal mean of δ^{18}O–CO_2 of the standard run. The figure suggests that if one removes one process, the total signal is also reduced by this process. But this is not true in the online model because adding or removing a process feedbacks on the global δ^{18}O–CO_2 level in the atmosphere, therefore changes "discriminations" and thus the contributions of all other processes to the atmospheric

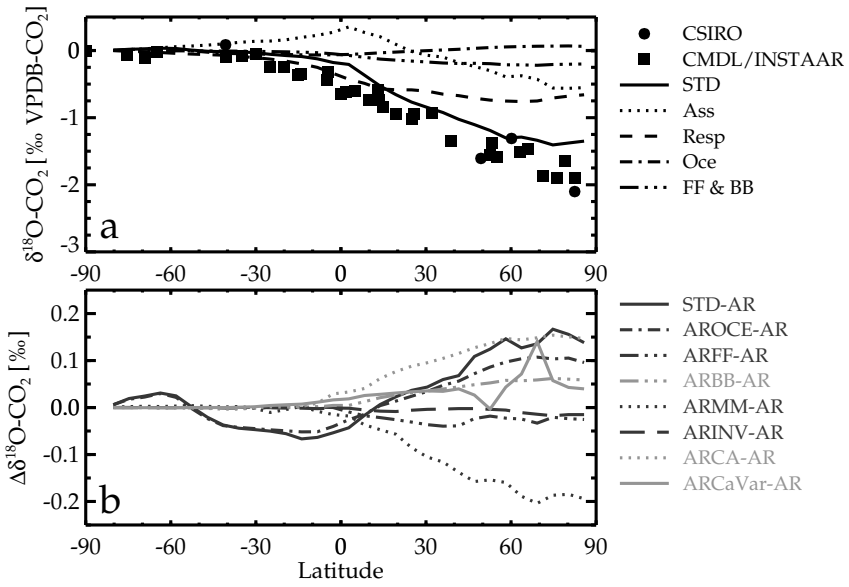

Figure 3.8: Contribution of different processes to the north–south gradient in δ^{18}O–CO_2. a) The total north–south gradient split up in the contributions of individual processes. The δ–anomalies are additive and sum up to the total signal so that adding up the different contributions at every latitude gives the total signal (solid line). b) The total signal of different runs including only certain processes minus the north–south gradient of a run with only assimilation and respiration included. Ass stands for assimilation, Resp for respiration, Oce for the ocean contribution, FF for the fossil fuel signal, BB for biomass burning, Inv for the invasion effect, Carb. Anhy. for the change due to reduced carbonic anhydrase activity, and variable c_a for a run where assimilation depends on the instantaneous CO_2 mixing ratio in the lowest model layer.

signal. This can be studied in Figure 3.8b and Figure 3.9 where I plotted the results of several sensitivity runs. For example, adding up assimilation and respiration in Figure 3.8a gives a δ^{18}O–CO_2 value at the North Pole of $-1.2\,‰$ (relative to South Pole). The total δ^{18}O–CO_2 value at the North Pole of the standard run is about $-1.35\,‰$ but the Arctic–to–Antarctic difference goes down to $-1.5\,‰$ in the AR run. One can see in Figure 3.8b that all three extra processes of the standard run together reduce the north–south gradient by only about $0.15\,‰$ (solid line). The strongest influence have the ARMM (dotted black line) and CA runs (dotted grey line). (Note that Figure 3.7c represents the STDMM run and Figure 3.9e the ARMM run.) As explained in Chapter 2, the enzyme carbonic anhydrase, distributed in the mesophyll cells, speeds up the hydration of CO_2 by a factor 10^7 [*Stryer*, 1981]. CO_2 molecules entering the stomata are hence immediately hydrated even if they can not be taken up by RUBISCO due to limitations of e. g. electron transport (cf. Chapter 2). If CO_2 molecules are not assimilated by the plant, they diffuse back in the stomata and subsequently into the canopy. But once CO_2 molecules were hydrated in leaf water, they have most probably isotopically equilibrated with it and the back–diffused CO_2 molecules carry the leaf water isotopic signature in the atmosphere. If the activity of carbonic anhydrase is reduced, not all CO_2 molecules entering the stomata are hydrated before they diffuse back into

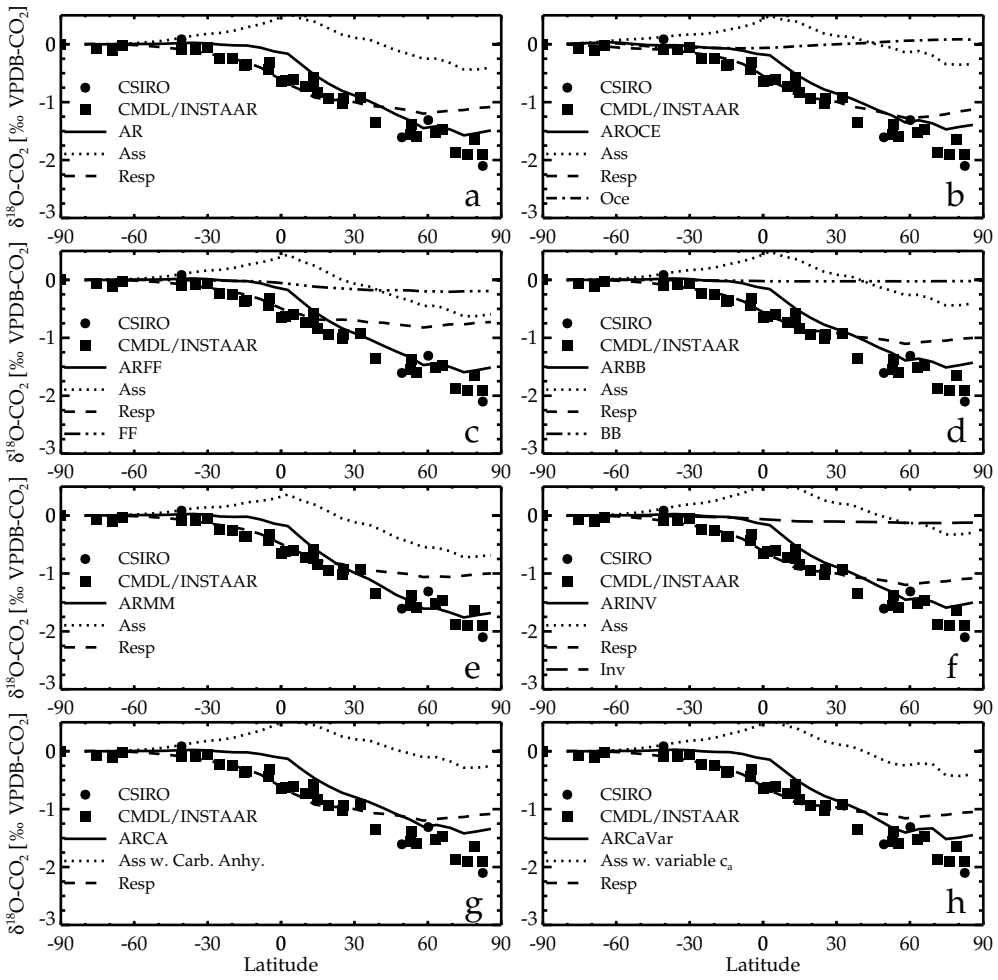

Figure 3.9: North–south gradient of all runs in Figure 3.8b split up in their individual processes. a) is the run with only assimilation and respiration which total δ^{18}O–CO_2 signal was subtracted in Figure 3.8b from the total δ^{18}O–CO_2 north–south gradient of the different runs.

the canopy [*Gillon and Yakir*, 2001]. This reduces leaf discrimination by only 1 ‰ in the global mean in the model and reduces hence the influence of assimilation on δ^{18}O of atmospheric CO_2. Lower stomata–internal CO_2 mixing ratios increase the effect of reduced carbonic anhydrase activity. I have high stomata–internal CO_2 mixing ratios (at least at high northern latitudes, see Chapter 2) so that *Gillon and Yakir* [2001] estimate a greater global reduction of leaf discrimination of 2–3 ‰. However, this effect is of the same order of magnitude as the ARMM run and likewise its influence on the meridional gradient is negligible.

To demonstrate the change of leaf discrimination and soil "discrimination" due to different processes in more detail, I plot in Figure 3.9a the meridional gradient of δ^{18}O–CO_2 of the AR run together with the individual contributions of assimilation and respiration. Figure 3.9b–h show then the results of sensitivity runs whereon each another process is added to assimilation and respiration, namely the ocean fluxes, fossil fuel combustion, biomass burning, the isotopic water source as monthly mean input

fields of rain water isotopes, the invasion effect, the reduced carbonic anhydrase activity, and varying CO_2 concentrations in air, c_a. (Normally, c_a is fixed to 353 ppm in the calculation of assimilation in ECHAM/BETHY but not in the $CO^{18}O$ flux calculations.) Comparing Figure 3.9a with Figure 3.9c shows the change in the model behaviour due to fossil fuel combustion input. One can see in Figure 3.8b that the total meridional mean changes only little but Figures 3.9a&c show that the contributions of assimilation and respiration change considerably. Fossil fuel combustion adds about $-0.2\,‰$ to the total signal, assimilation changed also about $-0.2\,‰$ compared to AR run but this is almost totally compensated by the change in the respiration contribution by around $+0.35\,‰$. Monthly mean rain isotope input strengthens the influence of assimilation and weakens the respiration contribution (Figure 3.9e) whereas reduced carbonic anhydrase acts the other way round (Figure 3.9g), weakens assimilation influence and consequently strengthens respiration (δ_a is reduced due to reduced leaf discrimination what in turn reinforces soil "discrimination"). Figures 3.8b&3.9f show that the "invasion effect" (explained in Chapter 2) does not change markedly the meridional gradient neither. I changed in further runs the fractionations, ϵ, applied to the different processes (as explained in Chapter 2) but the interactively calculated "discriminations" changed accordingly like demonstrated in Figure 3.9 so that I ended up always with a very similar picture (results not shown here). I did also exchange the global fractionations with parameterisations depending on climate and/or biospheric variables [e. g. *Ball*, 1987; *Farquhar and Lloyd*, 1993; *Roden and Ehleringer*, 1999; *White*, 1983] but the effect on the meridional gradient were again negligible (results not shown here). In summary, assimilation and respiration are the determining factors of the meridional gradient and because of interactively calculated "discriminations", none of the proposed other processes helps to improve the modelling of the north–south gradient.

Seasonal cycle

The seasonal variations of the isofluxes alters the influence of individual processes with time. The seasonal cycle can well be influenced by changes to model formulations even if the meridional gradient is not. I explain in this section the influence of different sensitivity tests on the seasonal cycle but do not plot the results because all performed sensitivity studies changed mainly the amplitude of the seasonal cycle and non changed the phase significantly. I diagnose the seasonal amplitude of $\delta^{18}O$–CO_2 as somewhat arbitrary and must resolve the phase mismatch between model and measurements first before I can find a feasible set of parameters for the amplitude.

The ARMM and STDMM runs were explained in detail in the previous section. The water isotopic composition distribution is reflected in the north–south gradient mainly as respiration weighted annual mean. But, the ARMM and STDMM runs differ from their 'parent' runs, with $\delta^{18}O$–H_2O calculated online, stronger in the seasonal cycle than in the annual mean of $\delta^{18}O$–H_2O. Unfortunately, the phasing of the rain water isotopes coincides with the phase of the CO_2 fluxes in the model so that the ARMM and STDMM runs did not change significantly the seasonal cycle of $\delta^{18}O$–CO_2 (results not shown here). The evidence of reduced carbonic anhydrase activity leads to a different pattern in atmospheric $\delta^{18}O$–CO_2. Carbonic anhydrase activity in C3 plants is

less reduced than in C4 plants and I tested that this effect can change substantially the seasonal cycle at some stations due to a modified influence of assimilation on the total signal but it does not improve the phase mismatch between model and measurements. Other processes with no great seasonal variation, like fossil fuel combustion, had predictablely almost no influence on the seasonal cycle of δ^{18}O–CO_2. But some seasonal processes missing in the model might influence δ^{18}O–CO_2. I tested that such example cannot be the "invasion effect".

It is very possible that the parameterisations used, comparable to *Ciais et al.* [1997a, b], are not sufficient to describe the seasonal cycle of δ^{18}O–CO_2. Exchanging for example the global fractionations, ϵ, with parameterisations that depend on climate and/or biospheric variables (s. previous section for citations) did change the amplitude and therewith the phase of the seasonal cycle of δ^{18}O–CO_2. These parameterisations changed the amplitude sometimes significantly but the phase did not much ameliorate. Sensitivity studies with different sets of global fractionation values showed the same behaviour. Reducing for example the kinetic fractionation of δ^{18}O–CO_2 leaving the soil thereby diminishes the influence of respiration on δ^{18}O–CO_2. Changing the fractionation in a reasonable range can amplify or divide the amplitude of the seasonal cycle by almost a factor of 1.5. But still, the phase would not change greatly by this.

None of the tested processes and parameterisations did resolve the mismatch between the model and the observations, neither in the north–south gradient nor in the seasonal cycle. Though I have changed biosphere "discriminations" a good deal but did not change greatly the phasing of the seasonal cycle in the model. I think therefore that either an important process is missing in the model or the biosphere CO_2 gross fluxes are erroneous. The latter is quite the contrary to what indicates the very good CO_2 seasonal cycle comparison but a good comparison in CO_2 can be found with quite different flux patterns [*Kaminski et al.*, 2001]. The weakest point in the model is the formulation of the heterotrophic respiration because it is described with only a very simple formulation. First tests with modified formulations of heterotrophic respiration resulted in a convergence of model and observations in δ^{18}O–CO_2 but the model deviated from the observations in CO_2. This effect can be seen in the simulation of *Peylin et al.* [1999] who used monthly biosphere fluxes from the SIB2 [*Denning et al.*, 1996a, b] model to compute δ^{18}O–CO_2. SIB2 shows the same phase in assimilation as BETHY but respiration has its maximum 1 to 2 month later north of 30 °N (because SIB2 uses soil temperature for the calculation of heterotrophic respiration [*Denning et al.*, 1996a] whereas I use air temperature [s. Chapter 2] which shows its maximum about one month earlier then soil temperature). The simulation of *Peylin et al.* show δ^{18}O–CO_2 seasonal cycles closer to the measurements than mine in high northern latitudes but their simulated CO_2 seasonal cycle shows hence a phase shift to the observations. SIB2 and BETHY are very similar in the phase of respiration outside high northern latitudes so that consequently the simulations of *Peylin et al.* show the same phase lag as ECHAM/BETHY in δ^{18}O–CO_2 whereas the CO_2 seasonal cycles match the phase of the observed cycle in both models.

3.4 Summary and Concluding Remarks

I have built a comprehensive global 3D model of $\delta^{18}O$ in atmospheric CO_2. The model simulates very well the seasonal cycle of CO_2 at atmosphere observatories but still at 25 % of the stations ECHAM/BETHY fails to follow closely the seasonal cycle of CO_2 due to model deficiencies, mainly to deficiencies in the AGCM ECHAM rather than in the biospheric part BETHY. ECHAM/BETHY shows a seasonal cycle of $\delta^{18}O$ in atmospheric CO_2 very similar to the cycle in CO_2, i. e. that CO_2 and $\delta^{18}O$–CO_2 show their minimum and maximum at the same time. The modelled seasonal cycle of $\delta^{18}O$–CO_2 precedes the measurements by two months on almost all stations. All sensitivity studies performed with ECHAM/BETHY did not resolve this model shortcoming although impact the amplitude. Whereas the seasonal amplitude of $\delta^{18}O$–CO_2 changes with different parameters or parameterisations up to a factor of 3, there is no significant effect on the phase. I think that it is always possible to find a reasonable set of parameters that fits the seasonal amplitude at most stations but consider it as a futile exercise as long as the question of the phase mismatch is not solved.

The biosphere is set to equilibrium in the model, i. e. there is no annual mean net biosphere flux from any land point in the model. The annual mean net $\delta^{18}O$–CO_2 isoflux is zero only in the global mean but imbalanced on every grid point. This yields a northern hemispheric isoflux of -160 GtC ‰ yr^{-1} which is balanced in the southern hemisphere by $+160$ GtC ‰ yr^{-1}. A first order two box model such as that used in TRANSCOM phase 1 [*Law et al.*, 1996] relates concentration differences, c_-, with source strength differences, S_-:

$$c_- = \frac{\tau}{2} S_- \tag{3.6}$$

where τ is the interhemispheric exchange time. The range in τ in the models of TRANSCOM Phase 1 was roughly between 1 and 2 years (I did no experiment to determine τ in ECHAM). The source strength difference between northern and southern hemispheric $\delta^{18}O$–CO_2 isofluxes yields therewith a concentration difference of -0.25 to -0.45 ‰ whereas the model shows a difference of about -0.6 ‰ in the lowest model layer over the ocean. The excess in the model comes from the rectifier effect, i. e. the covariance between the diurnal and seasonal cycle of $\delta^{18}O$–CO_2 with transport. It has a much stronger impact on the north–south gradient than any other process evokes in the model apart from assimilation and respiration.

All sensitivity studies did not change the gradient of $\delta^{18}O$–CO_2 between Arctic and Antarctica by more than 10 % neither did they change the phase of the modelled seasonal cycle of $\delta^{18}O$–CO_2 significantly. I recognise three mechanisms which could be responsible for the mismatch:

1. *The imbalance in net $\delta^{18}O$–CO_2 isoflux*
   A mean τ of 1.5 years (assuming that the rectifier effect is correctly represented) implies that the imbalance should be greater by a factor of ca. 1.5, means $S_- =$ 480 GtC ‰ yr^{-1}. This can be achieved by several reasons and Figure 3.9e shows that a more varying rain isotope source points in the right direction. But also a change in CO_2 fluxes can lead to another imbalance in the net $\delta^{18}O$–CO_2 isoflux. I discussed in Chapter 2 that ECHAM/BETHY feature low CO_2 fluxes at high northern latitudes. Increasing assimilation and therewith respiration in high

northern latitudes yields a greater imbalance in δ^{18}O–CO_2 net isoflux. I discussed as well in Chapter 2 that the accompanying stomata–internal CO_2 mixing ratios, c_i, of ECHAM/BETHY are higher than other estimates. But reduced c_i (at high northern latitudes) would lead to a reduced imbalance between northern and southern hemisphere in the δ^{18}O–CO_2 net isoflux which departs the model further from the observations.

2. *The rectifier effect*
   The covariance between the diurnal and seasonal cycle of δ^{18}O–CO_2 with transport is already very strong in the model and achieves a meridional gradient in CO_2 which is higher than all models in TRANSCOM Phase 1 except for the CSIRO model which is comparable to ECHAM/BETHY [*Law et al.*, 1996]. To bring modelled and observed north–south gradient in δ^{18}O–CO_2 closer together, the rectifier effect has to be even stronger as it already is in the model.
3. *The stratosphere–troposphere exchange (STE)*
   Gamo et al. [1989] reported for the first time δ^{18}O–CO_2 values in the stratosphere that were enriched by 2 to 3 ‰ compared to tropospheric values. This is probably due to the isotopic exchange of CO_2 with ozone in the stratosphere [*Thiemens*, 1999] that is known to be highly enriched in ^{18}O [e. g. *Mauersberger*, 1981]. The exchange between troposphere and stratosphere has a strong seasonal cycle, is much bigger in the northern hemisphere than in the southern hemisphere, and has a maximum exchange in spring [*Zahn et al.*, 1999, 2000, and references therein]. Intrusion into the stratosphere passes mainly in the tropics whereas stratospheric air penetrates the troposphere in the extra–tropics contributing to a north–south gradient in δ^{18}O–CO_2 [*Peylin et al.*, 1997] and possibly to the seasonal cycle at tropospheric stations. Having 19 model levels, the representation of the stratosphere is very coarse in ECHAM so that STE exchange is not realistic [*Timmreck et al.*, 1999; *Kjellström et al.*, 2000]. I could therefore not include this process in the model and it is possible that the seasonal exchange of the STE changes the δ^{18}O–CO_2. However, the isotope enrichment of CO_2 in the lower stratosphere compared to the upper troposphere is only around 2 ‰. The box model of *Hesshaimer* [1997] estimates a gross STE CO_2 flux of 200 GtC yr^{-1} that yields an isoflux of about 200 GtC ‰ yr^{-1} which is of the order of magnitude than other processes like e. g. fossil fuel combustion. Though, the only δ^{18}O–CO_2 modelling study that includes the stratospheric enrichment [*Peylin et al.*, 1997] adapted a $C^{18}O$ flux in the upper troposphere in order to match the measured profiles in δ^{18}O–CO_2 of *Gamo et al.* [1989] returning an isoflux of 200 GtC ‰ yr^{-1}. It is possible that the stratospheric enrichment plays its role in the δ^{18}O–CO_2 cycle but it is likely that the Arctic–to–Antarctic difference does not change importantly but behaves similar to the other sensitivity runs due to the interactive nature of the calculations. But the STE is highest in spring and more pronounced in the extra–tropics. This could transport enriched δ^{18}O–CO_2 to tropospheric stations mainly in spring which could shift the maximum of the seasonal cycle and consequently the minimum, too.

The atmospheric transport and the biospheric δ^{18}O–CO_2 fluxes determine almost completely the seasonal cycle and the north–south gradient of δ^{18}O in atmospheric CO_2. This underlines the high potential of δ^{18}O in atmospheric CO_2 to decipher the bio-

spheric CO_2 gross fluxes, eventually. If one controls the atmospheric transport, the atmospheric signal of $\delta^{18}O$–CO_2 can thus be used to deduce CO_2 gross fluxes. Inversion techniques with global atmospheric transport models attempt this on a global scale [*Peylin*, 1999]. On a local scale, investigators handle the atmospheric transports either with transport tracers like ^{222}Radon [*Langendörfer et al.*, 2002] or with theoretical calculations [*Yakir and Wang*, 1996]. But until now, no global study has been able to resolve the discrepancy between modelled and measured seasonal cycles of $\delta^{18}O$–CO_2.

References

Ball, J. T., Calculations related to gas exchange, in *Stomatal Function*, edited by E. Zeiger, G. D. Farquhar, and I. R. Cowan, pp. 445–476, Stanford University Press, Stanford, CA, 1987.

Boyer, J. S., S. C. Wong, and G. D. Farquhar, CO_2 and water vapor exchange across leaf cuticle (epidermis) at various water potentials, *Plant Physiol.*, *114*, 185–191, 1997.

Ciais, P., A. S. Denning, P. P. Tans, J. A. Berry, D. A. Randall, G. J. Collatz, P. J. Sellers, J. W. C. White, M. Trollier, H. A. J. Meijer, R. J. Francey, P. Monfray, and M. Heimann, A three dimensional synthesis study of $\delta^{18}O$ in atmospheric CO_2, part I: Surface fluxes, *J. Geophys. Res.*, *102*, 5 857–5 872, 1997a.

Ciais, P., P. P. Tans, A. S. Denning, R. J. Francey, M. Trollier, H. J. Meijer, J. W. C. White, J. A. Berry, D. A. Randall, J. J. G. Collatz, P. J. Sellers, P. Monfray, and M. Heimann, A three dimensional synthesis study of $\delta^{18}O$ in atmospheric CO_2, part II: Simulations with the TM2 transport model, *J. Geophys. Res.*, *102*, 5 873–5 883, 1997b.

Ciais, P., P. Peylin, and P. Bousquet, Regional biospheric carbon fluxes as inferred from atmospheric CO_2 measurements, *Ecol. Appl.*, *10*, 1 574–1 589, 2000.

Ciais, P., R. J. Francey, P. S. Bakwin, K. A. Masarie, and P. P. Tans, Atmospheric CO_2 and tracers measurements to monitor the carbon cycle and its future evolution, in *Sixth International Carbon Dioxide Conference: extended abstracts*, pp. 1–4, Organizing Committee of the 6$^{\text{th}}$ Conference, Sendai, Japan, 2001.

Cuntz, M., P. Ciais, and G. Hoffmann, Modelling the continental effect of oxygen isotopes over Eurasia, *Tellus*, *54B*, 2002, in press.

Denning, A. S., I. Y. Fung, and D. A. Randall, Latitudinal gradient of atmospheric CO_2 due to seasonal exchange with land biota, *Nature*, *376*, 240–243, 1995.

Denning, A. S., G. J. Collatz, C. Zhang, D. A. Randall, J. A. Berry, P. J. Sellers, G. D. Colello, and D. A. Dazlich, Simulations of terrestrial carbon metabolism and atmospheric CO_2 in a general circulation model, part 1: Surface carbon fluxes, *Tellus*, *48B*, 521–542, 1996a.

Denning, A. S., D. A. Randall, G. J. Collatz, and P. J. Sellers, Simulations of terrestrial carbon metabolism and atmospheric CO_2 in a general circulation model, part 2: Simulated CO_2 concentrations, *Tellus*, *48B*, 543–567, 1996b.

Farquhar, G. D., and J. Lloyd, Carbon and oxygen isotope effects in the exchange of carbon dioxide between terrestrial plants and the atmosphere, in *Stable Isotopes and Plant Carbon–Water Relations*, edited by J. R. Ehleringer, A. E. Hall, and G. D. Farquhar, pp. 47–70, Academic Press, New York, 1993.

Farquhar, G. D., K. T. Hubick, A. G. Condon, and R. A. Richards, Carbon isotope fractionation and plant water–use efficiency, in *Stable Isotopes in Ecological Research*, edited by P. W. Rundel, Springer–Verlag, New York, 1989.

Francey, R. J., and H. S. Goodman, The DAR stable isotope reference scale for CO_2, in *Baseline Atmospheric Program (Australia) 1986*, edited by B. W. Forgan and P. J. Fraser, pp. 40–46, Department of Administrative Services, Bureau of Meteorology in cooperation with CSIRO Division of Atmospheric Research, 1988.

Francey, R. J., and P. P. Tans, Latitudinal variation in oxygen–18 of atmospheric CO_2, *Nature*, *327*, 495–497, 1987.

Gamo, T., M. Tsutsumi, H. Sakai, T. Nakazawa, M. Tanaka, H. Honda, H. Kubo, and T. Itoh, Carbon and oxygen isotope ratios of carbon dioxide of a stratospheric profile over japan, *Tellus*, *41B*, 127–133, 1989.

Gemery, P. A., M. Trolier, and J. W. C. White, Oxygen isotopic exchange between carbon dioxide and water following atmospheric sampling using glass flasks, *J. Geophys. Res.*, *101*, 14 415–14 420, 1996.

Gillon, J., and D. Yakir, Influence of carbonic anhydrase activity in terrestrial vegetation on the ^{18}O content of atmospheric CO_2, *Science*, *291*, 2 584–2 587, 2001.

GLOBALVIEW-CO_2, Cooperative atmospheric data integration project — carbon dioxide, CD–ROM, NOAA CMDL, Boulder, Colorado [Also available on Internet via anonymous FTP to ftp.cmdl.noaa.gov, Path: ccg/co2/GLOBALVIEW], 2002.

Heimann, M., and C. D. Keeling, A three–dimentional model of atmospheric CO_2 transport based on observed winds: 2. model description and simulated tracer experiments, in *Aspects of climate variability in the Pacific and the Western Americas, Geophysical monograph 55*, edited by P. D. H., pp. 237–275, AGU, 1989.

Hesshaimer, V., Tracing the global carbon cycle with bomb radiocarbon, Ph.D. thesis, Universiät Heidelberg, 1997.

Kaminski, T., M. Heimann, P. Peylin, P. Bousquet, and P. Ciais, Inverse modeling of atmospheric carbon dioxide fluxes, *Science*, *294*, 259, 2001.

Kjellström, E., J. Feichter, and G. Hoffmann, Transport of SF_6 and $^{14}CO_2$ in the atmospheric general circulation model ECHAM4, *Tellus*, *52B*, 1–18, 2000.

Langendörfer, U., M. Cuntz, P. Ciais, P. Peylin, T. Bariac, I. Milyukova, O. Kolle, T. Naegler, and I. Levin, Modelling of biospheric CO_2 gross fluxes via oxygen isotopes in a spruce forest canopy: a ^{222}Rn calibrated box model approach, *Tellus*, *54B*, 2002, in press.

Law, R. M., P. J. Rayner, A. S. Denning, D. Erickson, I. Y. Fung, M. Heimann, S. C. Piper, M. Ramonet, S. Taguchi, J. A. Taylor, C. M. Trudinger, and I. G. Watterson, Variations in modeled atmospheric transport of carbone dioxide and the consequences for CO_2 inversion, *Global Biogeoch. Cycl.*, *4*, 1996, 783–796.

Levin, I., P. Ciais, R. Langenfelds, M. Schmidt, M. Ramonet, K. Sidorov, N. Tchebakova, M. Gloor, M. Heimann, E.-D. Schulze, N. N. Vygodskaya, O. Shibistova, and J. Lloyd, Three years of trace gas observations over the eurosiberian domain derived from aircraft sampling — a concerted action, *Tellus*, *54B*, 2002a, in press.

Levin, I., U. Langendörfer, M. Schmidt, C.Facklam, M. Ramonet, C. Bourg, V. Kazan, P. Ciais, R. L. Langenfelds, C. E. Allison, R. J. Francey, A. Jordan, W. A. Brand, R. E. M. Neubert, H. A. J. Meijer, and K. Holmén, Eurosiberian carbonflux — CO_2 intercomparison, in *Report of the eleventh WMO/IAEA meeting of experts on carbon dioxide concentration and related tracer measurement techniques, Tokyo, 25.–28. Sep. 2001*, edited by S. Toru, chap. 3.8, pp. 35–50, World Meteorological Organisation, 2002b, in press.

Mahowald, N. M., P. J. Rasch, and R. G. Prinn, Cumulus parameterizations in chemical transport models, *J. Geophys. Res.*, *100*, 26 173–26 189, 1995.

Masarie, K. A., R. L. Langenfelds, C. E. Allison, T. J. Conway, E. J. Dlugokencky, R. J. Francey, P. C. Novelli, L. P. Steele, P. P. Tans, B. Vaughn, and J. W. C. White, NOAA/CSIRO flask air intercomparison experiment: A strategy for directly assesing consistency among atmospheric measurements made by independent laboratories, *J. Geophys. Res.*, *106*, 20 445–20 464, 2001.

Mauersberger, K., Measurements of heavy ozone in the stratosphere, *Geophysical Research Letters*, *8*, 935–937, 1981.

Melayah, A., L. Bruckler, and T. Bariac, Modeling the transport of water stable isotopes in unsaturated soils under natural conditions. 2. comparison with field experiments, *Water Resources Research*, *32*, 2 055–2 065, 1996.

Miller, J. B., D. Yakir, J. W. C. White, and P. P. Tans, Measurement of $^{18}O/^{16}O$ in the soil–atmosphere CO_2 flux, *Global Biogeoch. Cycl.*, *13*, 761–774, 1999.

Peylin, P., The composition of ^{18}O in atmospheric CO_2: A new tracer to estimate global photosynthesis, Ph.D. thesis, L'Université Paris VI, Paris, 1999, in french.

Peylin, P., P. Ciais, P. P. Tans, K. Six, J. A. Berry, and A. S. Denning, ^{18}O in atmospheric CO_2 simulated by a 3–D transport model: A sensitivity study to vegetation and soil fractionation factors, *Phys. and Chem. of the Earth*, *21*, 463–469, 1997.

Peylin, P., P. Ciais, A. S. Denning, P. P. Tans, J. A. Berry, and W. C. White, A three–dimensional study of $\delta^{18}O$ in atmospheric CO_2: contributin of different land ecosystems, *Tellus*, *51B*, 642–667, 1999.

Ramonet, M., and P. Monfray, CO_2 baseline concept in 3–D atmospheric transport models, *Tellus*, *48*, 502–520, 1996.

Riley, W. J., C. J. Still, M. S. Torn, and J. A. Berry, A mechanistic model of $H_2^{18}O$ and $C^{18}OO$ fluxes between ecosystems and the atmosphere: Model description and sensitivity analyses, *Global Biogeoch. Cycl.*, 2002, in press.

Roden, J. S., and J. R. Ehleringer, Observations of hydrogen and oxygen isotopes in leaf water confirm the Craig–Gordon model under wide–ranging environmental conditions, *Plant Physiology*, *120*, 1 165–1 173, 1999.

Roeckner, E., K. Arpe, L. Bengtsson, M. Christoph, M. Clausen, L. Dümenil, M. Esch, M. Giorgetta, U. Schlese, and U. Schulzweida, The atmospheric general circulation model ECHAM–4: Model description and simulation of present–day climate, *Tech. Rep. 218*, Max–Planck Institut für Meteorologie, Hamburg, 1996.

Schmidt, M., R. Graul, H. Sartorius, and I. Levin, Carbon dioxide and methane in continental europe: a climatology, and ^{222}Radon-based emission estimates, *Tellus*, *48B*, 457–473, 1996.

Schmidt, M., R. Neubert, C. Facklam, R. Heinz, R.Weller, and I. Levin, Variability of CO_2 and its stable isotopes at Schauinsland (Germany) and Neumayer (Antarctica), in *Sixth International Carbon Dioxide Conference: extended abstracts*, pp. 116–119, Organizing Committee of the 6$^{\text{th}}$ Conference, Sendai, Japan, 2001.

Schulze, E.-D., F. M. Kelliher, C. Lloyd, and R. Leuning, Relationships among maximum stomatal conductance, ecosystem surface conductance, carbon assimilation rate, and plant nitrogen nutrition: a global ecology scaling exercise, *Ann. Rev. Ecol. Syst.*, *25*, 629–660, 1994.

Stephens, B. B., S. C. Wofsy, R. F. Keeling, P. P. Tans, and M. J. Potosnak, The CO_2 budget and rectification airborne study: Strategies for measuring rectifiers and regional fluxes, in *Inverse Methods in Global Biogeochemical Cycles*, edited by P. Kasibhatla et al., vol. 114 of *Geophysical Monograph Series*, pp. 311–324, American Geophysical Union, Washington D. C., 1999.

Stryer, L., *Biochemistry*, W. H. Freeman and Co, San Francisco, 1981.

Tans, P. P., I. Y. Fung, and T. Takahashi, Observational constraints on the global atmospheric carbon dioxide budget, *Science*, *247*, 1 431–1 438, 1990.

Taylor, J. A., Atmospheric mixing and the CO_2 seasonal cycle, *Geophysical Research Letters*, *25*, 4 173–4 176, 1998.

Thiemens, M. H., Mass–independent isotope effects in planetary atmospheres and the early solar system, *Science*, *283*, 341–345, 1999.

Timmreck, C., H.-F. Graf, and J. Feichter, Simulation of Mt. Pinatubo volcanic aerosol with the Hamburg climate model ECHAM4, *Theor. Appl. Climatol.*, *62*, 85–108, 1999.

Trolier, M., J. W. C. White, P. P. Tans, K. A. Massarie, and P. A. Gemery, Monitoring the isotopic composition of atmospheric CO_2: Measurements from the NOAA global air sampling network, *J. Geophys. Res.*, *101*, 25 897–25 916, 1996.

White, J. W. C., The climatic significance of D/H ratios in white pine in the Northeastern United States, Ph.D. thesis, Columbia University, New York, 1983.

Yakir, D., and X.-F. Wang, Fluxes of CO_2 and water between terrestrial vegetation and the atmosphere estimated from isotope measurements, *Nature*, *380*, 515–517, 1996.

Zahn, A., R. Neubert, M. Maiss, and U. Platt, Fate of long–lived trace species near the northern hemispheric tropopause: Carbon dioxide, methane, ozone, and sulfur hexafluoride, *J. Geophys. Res.*, *104*, 13 923–13 942, 1999.

Zahn, A., R. Neubert, and U. Platt, Fate of long–lived trace species near the northern hemispheric tropopause: 2. isotopic composition of carbon dioxide ($^{13}CO_2$, $^{14}CO_2$, and $C^{18}O^{16}O$), *J. Geophys. Res.*, *105*, 6 719–6 735, 2000.

Chapter 4

Modelling the continental effect of oxygen isotopes over Eurasia

4.1 Introduction

Our current knowledge does not yet allow to balance the global budget of carbon dioxide within better than ±30% [*Prentice et al.*, 2001]. The momentary consensus is that there is a terrestrial carbon sink in the northern hemisphere. But the contribution of different geographic locations as well as biomes is not yet clear. For example, it is a matter of debate how this sink is distributed between North America and Eurasia but even further if the North American continent and Eurasia are sources or sinks for CO_2. Using inversion techniques with current models do not provide an unequivocal distribution of CO_2 sources and sinks [e. g. *Bousquet et al.*, 2000; *Rayner et al.*, 1999; *Fan et al.*, 1998; *Ciais et al.*, 1995a, b]. Given the existing distribution of CO_2 stations, this problem is mathematically under–constrained and needs therefore further and independent constraints.

Though, we aim to better quantify the biospheric CO_2 fluxes. In the last few years, $\delta^{18}O$ in atmospheric CO_2 got the intention to tackle this problem. Observations of the oxygen isotopic composition of CO_2 have the capability to distinguish between carbon gross fluxes of the terrestrial biosphere, namely assimilation and respiration. Because of the isotopic exchange of CO_2 with water [*Mills and Urey*, 1940], CO_2 exchanged by the biospheric fluxes carries the isotopic signature of different water pools. These pools are the leaf water and the soil moisture, respectively. $\delta^{18}O$ of atmospheric CO_2 is, therefore, primarily a convolution of CO_2 gross fluxes and water isotope signatures. In constraining the isotopic signature of the water pools, interacting with carbon dioxide, we can estimate separately the gross CO_2 biosphere fluxes.

The global ^{18}O signature of H_2O in the unsaturated soil layer is about $-10\,‰$ on average (vs. VSMOW, see below). However, the geographical distribution of the water isotopes is mainly controlled by the rainout of air masses transported to the interior of the continents. This mechanism produces extremely strong continental gradients of the isotopic composition of precipitation and of the corresponding soil water and makes a detailed modelling of the above mentioned rain out mechanism necessary. Subsequently when water evaporates, lighter molecules are preferentially evaporated leaving a heavier

water pool. For example, water at the evaporating site of leaves is enriched by about 10–20 ‰ (vs. soil water). Net assimilation [which is the Gross Primary Productivity (GPP) minus leaf respiration and equals about 0.85 GPP] and net ecosystem respiration fluxes are around 100 $GtC\,yr^{-1}$ [*Schimel et al.*, 1996] whereas net exchange between biosphere and atmosphere (NBP) is only 0–2 $GtC\,yr^{-1}$, globally. That means that the resulting $\delta^{18}O$–CO_2 signal is the result of (mainly) two huge opposing fluxes that I name hereafter "isofluxes", even more pronounced than for CO_2 [*Ciais et al.*, 1997a; *Farquhar et al.*, 1993]. From the convolution originates that a small change of the CO_2 gross fluxes leads to a big change in the isofluxes. The biospheric gross fluxes should, therefore, be deducible [*Peylin*, 1999].

Eurasia is the largest land mass in the northern hemisphere. Its role in the global carbon cycle is important but is not known precisely. In addition to CO_2 fluxes, there is a special depletion in rainfall, and subsequent water pools in the biosphere, in the interior of Eurasia [*Dansgaard*, 1964], which could lead to peculiar effects in $\delta^{18}O$. Namely, one might expect leaf water $\delta^{18}O$–H_2O to be more negative than the atmosphere over most of the continental land mass, yielding photosynthesis to diminish $\delta^{18}O$ in atmospheric CO_2 rather than increasing it as usually expected.

I have built a consistent global model of $\delta^{18}O$ in atmospheric CO_2 which calculates at each time step the water isotopic composition of the different water pools (in leaves, in soils, and in the atmosphere), the CO_2 and $CO^{18}O$ fluxes from and into the atmosphere, and in fine the atmospheric CO_2 concentrations together with its $\delta^{18}O$–CO_2 value, including transport. Though, I built a tool to investigate the CO_2 cycle together with the $\delta^{18}O$ cycles in CO_2 and water, because the exchange of CO_2 and water is fully coupled in the model. Here, I am going to investigate the distribution of CO_2 with $\delta^{18}O$ over the interior of Eurasia. I compare the model results with literature data and measurement made within the European Project EUROSIBERIAN CARBONFLUX.

4.2 Experimental and Model Set–up

4.2.1 The Model

The model combines the Atmospheric General Circulation Model (AGCM) ECHAM, including transport of inert tracers and the water isotope cycle, the biosphere model BETHY and a newly build ^{18}O–CO_2 flux module (see Fig. 4.1). ECHAM is the general circulation model of the Max–Planck Institut für Meteorologie (MPI–MET) in Hamburg, a state of the art global climate model used in several studies [e. g. *Arpe et al.*, 1994; *Roeckner et al.*, 1992] (for a full model description see *Modellbetreuungsgruppe* [1994]). In this study, I use the spectral model ECHAM in the T21 resolution corresponding to a physical grid of 5.6°x5.6° (time step of 40 minutes). The model has 19 vertical layers from surface pressure up to a pressure level of 30 hPa. It includes an inert tracer transport scheme which transports the tracer identical to the water vapour with the semi–Lagrangian advection scheme according to *Rasch and Williamson* [1990].

The water isotope module (WFRAC) was implemented in cycle 3 of ECHAM by *Hoffmann et al.* [1998] and later built into cycle 4 by *Werner* [2000]. Herein, the water isotopes are treated exactly in parallel to models moisture. However, at each phase

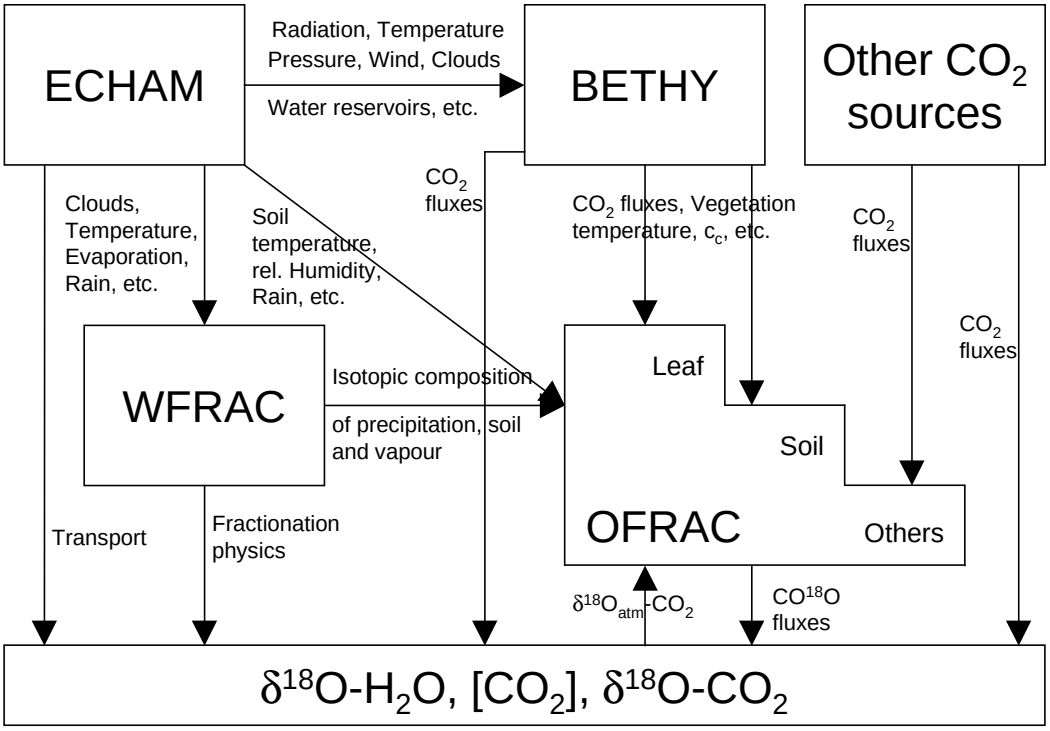

Figure 4.1: Information flow of the coupled model. ECHAM is the atmospheric general circulation model [*Modellbetreuungsgruppe*, 1994]; BETHY is the biosphere model [*Knorr and Heimann*, 2001a, b]; other CO_2 sources are monthly input fields, for example ocean fluxes; WFRAC is the water isotope module [*Werner*, 2000]; OFRAC is the newly build CO_2 isotopomer flux module; and $\delta^{18}O$ etc. stands for the transported CO_2 and $\delta^{18}O$ concentrations in the atmosphere.

transition a temperature dependent fractionation [*Majoube*, 1971] is applied to the water isotopes continuously depleting the vapour phase compared to the liquid or solid phase.

I interfaced the process–based model of terrestrial vegetation activity, BETHY, to the AGCM ECHAM. It calculates at each time step of the AGCM, CO_2 fluxes of the terrestrial biosphere together with further diagnostic variables like e. g. stomatal conductance and vegetation temperature. The BETHY online model uses a conservative vegetation distribution map [*Wilson and Henderson-Sellers*, 1985] adjusted to include C4 vegetation [*Knorr and Heimann*, 2001a]. In order to obtain realistic evapotranspiration rates, vegetation temperatures and, therefore, realistic stomatal conductances from the ECHAM energy and water budgets, I recompute the latent and sensible heat fluxes from the canopy. Since plants constantly lose water through their stomatal pores while photosynthesising, water availability is related closely to carbon uptake. A detailed description of the original model can be found in *Knorr and Heimann* [2001a, b]. To interface BETHY to ECHAM, I mainly removed the BETHY–internal weather generator and soil model. These variables are taken directly from ECHAM. Deficiencies due to interfacing and not coupling BETHY to ECHAM and other points are discussed in Chapter 2 and 3.

The ^{18}O–CO_2 flux module (OFRAC) follows the overall picture of *Farquhar et al.* [1993] and *Ciais et al.* [1997a]. The main difference between the approaches used in *Farquhar et al.* [1993], *Ciais et al.* [1997a, b], and *Peylin et al.* [1999] and my model is the more credible estimation of the ^{18}O–CO_2 fluxes. I use a time step more adapted to physiological processes and compute the ^{18}O–CO_2 fluxes interactively in dependence of the synchronous $CO^{18}O$ concentration in the atmosphere. Each time step, i. e. each 40 minutes, BETHY computes assimilation and respiration CO_2 fluxes. The ^{18}O–CO_2 flux module OFRAC computes for every CO_2 flux a corresponding $CO^{18}O$ flux, namely to assimilation, respiration, ocean, fossil fuel and biomass burning. The corresponding $CO^{18}O$ fluxes are the product of the CO_2 fluxes with the isotope ratio of the CO_2 dissolved in water and the fractionation occurring at the transition from one compartment to the other [see e. g. *Ciais et al.*, 1997a]. $CO^{18}O$ is then transported together with CO_2 by the AGCM ECHAM as inert tracer. It thus permits to calculate $\delta^{18}O$ in atmospheric CO_2 each time step and $\delta^{18}O$–CO_2 can feedback semi–implicitly on the $CO^{18}O$ fluxes.

4.2.2 The Experimental data

In the EUROSIBERIAN CARBONFLUX project are four different aircraft measurement sites for CO_2 concentrations together with $\delta^{18}O$–CO_2 values outside the atmospheric boundary layer (ABL): Orléans, France (47°55' N, 1°54' E), Tver, Russia (56°28' N, 32°56' E), Syktyvkar, Russia (61°40' N, 50°45' E) and Zotino, Russia (60°45' N, 89°24' E) [*Levin et al.*, 2002]. In Tver and Zotino, there are also eddy–covariance flux towers installed measuring Net Ecosystem Exchange (NEE) [*Milyukova et al.*, 2002; *Lloyd et al.*, 2002b]. I include three other sites for NEE from the EUROFLUX network further west to have a meridional coverage: Sarrebourg, France (48°40' N, 7°05' E) [*Granier*, 2002], Flakaliden, Sweden (64°14' N, 19°46' E) [*Lindroth*, 2002], and Hyytiälä, Finland (64°51' N, 24°17' E) [*Vesala*, 2002, and Suni, T. personal communication].

I also compare the modelled isotopic signature in precipitation to stations of the Global Network for Isotopes in Precipitation (GNIP) of the International Atomic Energy Agency (IAEA), Vienna, Austria [*IAEA/WMO*, 2001]. The GNIP–database incorporates more than 100000 measurements of the three isotopes Deuterium, Tritium and ^{18}O–H_2O in precipitation and gives monthly mean values for the measurement period. The GNIP stations are not identical to the above locations of CO_2 measurements so I selected GNIP stations nearby. These are namely Thonon–les–Bains, France (46°13' N, 6°16' E), St. Petersburg, Russia (59°34' N, 30°10' E), Kirov, Russia (58°23' N, 49°22' E), and Enisejsk, Russia (58°16' N, 92°05' E).

All $\delta^{18}O$–H_2O values of water reported here are relative to the standard Vienna SMOW (VSMOW) [*Baertschi*, 1976] and $\delta^{18}O$–CO_2 relative to Vienna Pee Dee belemnite (VPDB–CO_2) [*Allison et al.*, 1995].

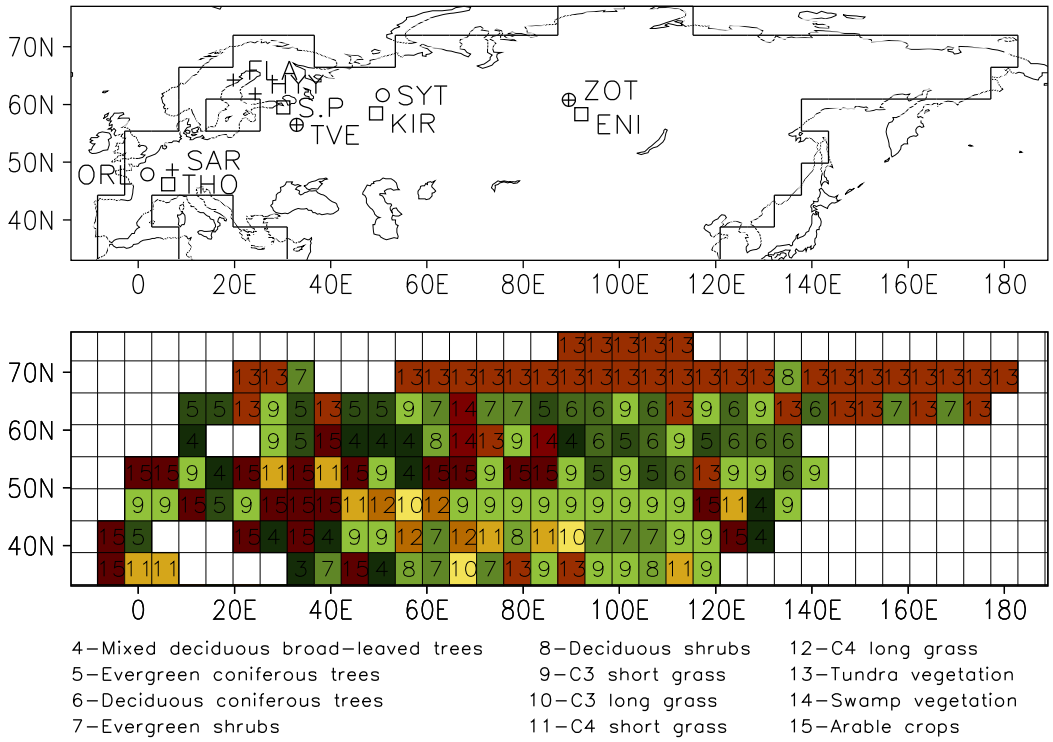

Figure 4.2: Two different representations of the investigation area. In the upper plate are indicated the measurement stations of water isotopes (squares), CO_2 fluxes (cross) and atmospheric CO_2 with isotopes (circles) (ORL=Orléans, THO=Thonon–les–Bains, SAR=Sarrebourg, FLA=Flakaliden, HYY=Hyytiälä, S.P=St. Petersburg, TVE=Tver, SYT=Syktyvkar, KIR=Kirov, ZOT=Zotino, and ENI=Enisejsk). In the lower plate: The boxes are the grids of the model and the colours with numbers stand for each used vegetation class (4 to 15 of 23 overall in the model).

4.3 Results and Discussion

Figure 4.2 shows the investigation area together with the locations of the measurement stations. However, I used only the area between 40 °N and 70 °N for the calculation of the longitudinal gradients. But keep in mind that the model is run globally, so it fully accounts for lateral input/output of H_2O, CO_2 and isotopes to/from the Eurasian domain in this study. In the upper plate is also indicated the border of the land masses in the model. Combining the upper with the lower panel gives a clear picture of the used model resolution. In the bottom plate, I show the vegetation distribution which is used in BETHY. There is mostly tundra vegetation in North–Siberia and a mixture of evergreen and deciduous conifers over temperate and boreal Eurasia as well as in East–Siberia. The southern part is dominated by grasses (C3 and C4) and crops. It is apparent in the vegetation distribution that, apart from the longitudinal gradient in climate due to continentality, a gradient in latitude exists which also plays a role for $\delta^{18}O$–CO_2.

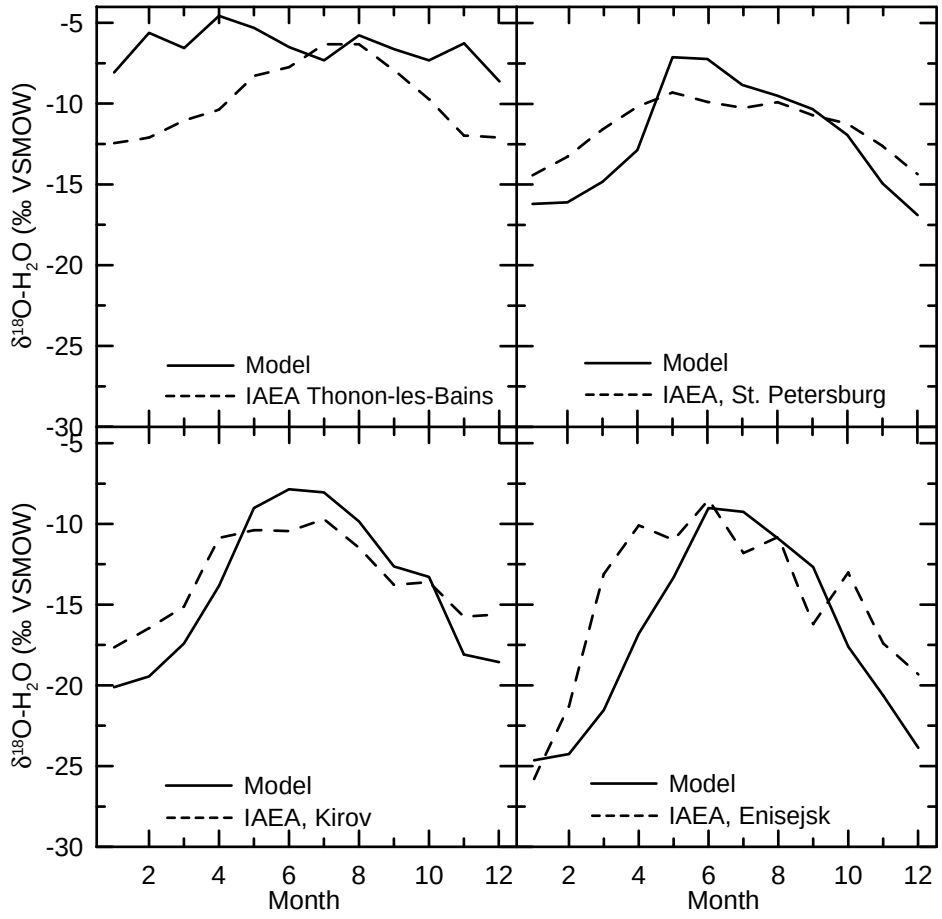

Figure 4.3: Comparison of modelled and measured water isotopic composition of precipitation at four selected IAEA stations.

The δ^{18}O signal in CO_2 is mainly the convolution of the water isotopic composition with the CO_2 fluxes. Hence, both parts of the convolution have to be validated. I compare first the water isotopes with measurements from the GNIP database and next CO_2 net fluxes with measurements of eddy–flux towers. I will then compare the seasonal cycle of CO_2 and δ^{18}O–CO_2 in the free troposphere, namely at ca. 3000 m a.s.l.

4.3.1 Water isotopes

On a global scale, a detailed comparison of the water isotope module of ECHAM with global observations of the IAEA observations gave an excellent agreement of the spatial and temporal patterns of the simulated and observed isotope fields [*Hoffmann et al.*, 1998]. To illustrate this, I show here some typical results of the monthly δ^{18}O–H_2O in precipitation over Eurasia (Fig. 4.3). Note that all IAEA stations in Russia are actually closed now, so the presented data includes no recent water isotopic composition. Nevertheless, there is no obvious trend in time in the water isotopic composition, so I can use the older data for isotopes in precipitation as an isotope climatology. In Figure 4.4, one can clearly see the continental impoverishment in rainfall isotope data at the four

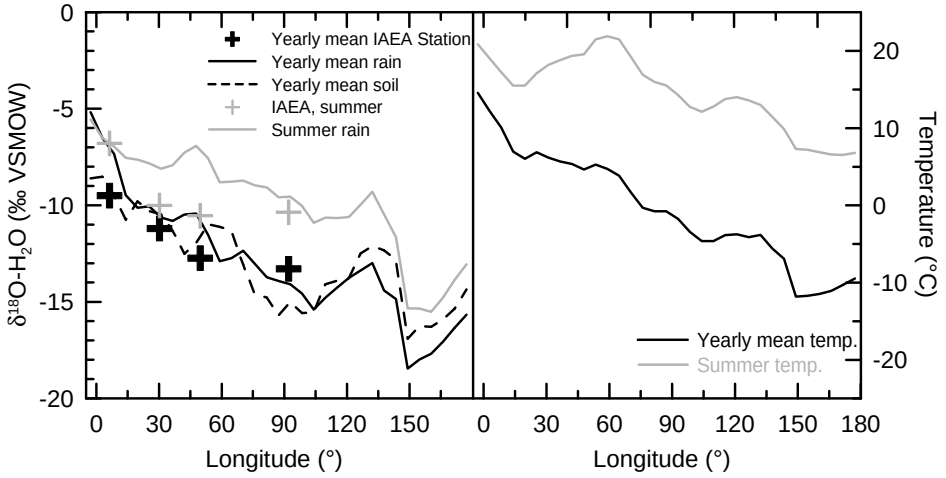

Figure 4.4: Longitudinal gradient of water isotopes and temperature over Eurasia of yearly and summer means. It is shown the modelled meridional summer and yearly mean rain and soil water in comparison to the four IAEA stations of Figure 4.3. The summer composition of soil water is not shown because it is very similar to the yearly mean. The model output is processed similarly as the station data but the monthly means of the model are already rainfall weighted means.

selected IAEA stations distributed along the eastward transport trajectory of water vapour over Eurasia. The continental gradient and its origin (the rainout mechanism) is already described in the first review of the IAEA network [*Dansgaard*, 1964]. One can also see that the isotopic composition of the soil water is close to rain water in the model. The difference originates mainly from different infiltration and runoff of winter and summer precipitation [*Hoffmann et al.*, 1998]. Figure 4.3 illustrates the increasing continentality which is also linked to an increasing seasonal amplitude, not only in temperature but also in water isotopes (up to 120 °E approximately). A larger seasonal amplitude of δ^{18}O–H_2O in precipitation is consistently observed (and simulated by ECHAM) in higher latitudes compared to lower latitudes and in the interior of the continents compared to regions under a marine influence. The increasing seasonality of the water isotopes, moving continent inwards, lowers mainly the winter values (summer: about -8 to -10 ‰ both in St. Petersburg and in Enisejsk; winter: -16 ‰ in St. Petersburg and -24 ‰ in Enisejsk). As a consequence, the spatial gradient of the water isotopes, strongly expressed in the annual mean and even more in winter time, is comparatively weaker during plants growing season in late spring and summer.

4.3.2 Net Ecosystem Exchange

Figure 4.5 shows the comparison of the measured Net Ecosystem Exchange (NEE) on eddy–flux towers with the modelled fluxes of BETHY. It should be raised a caution flag on such a comparison because NEE measurements are representative of a very short area (¡1 km^2) compared to the model grid. It is however a useful semi–quantitative information of the BETHY model performance. Included is the modelled

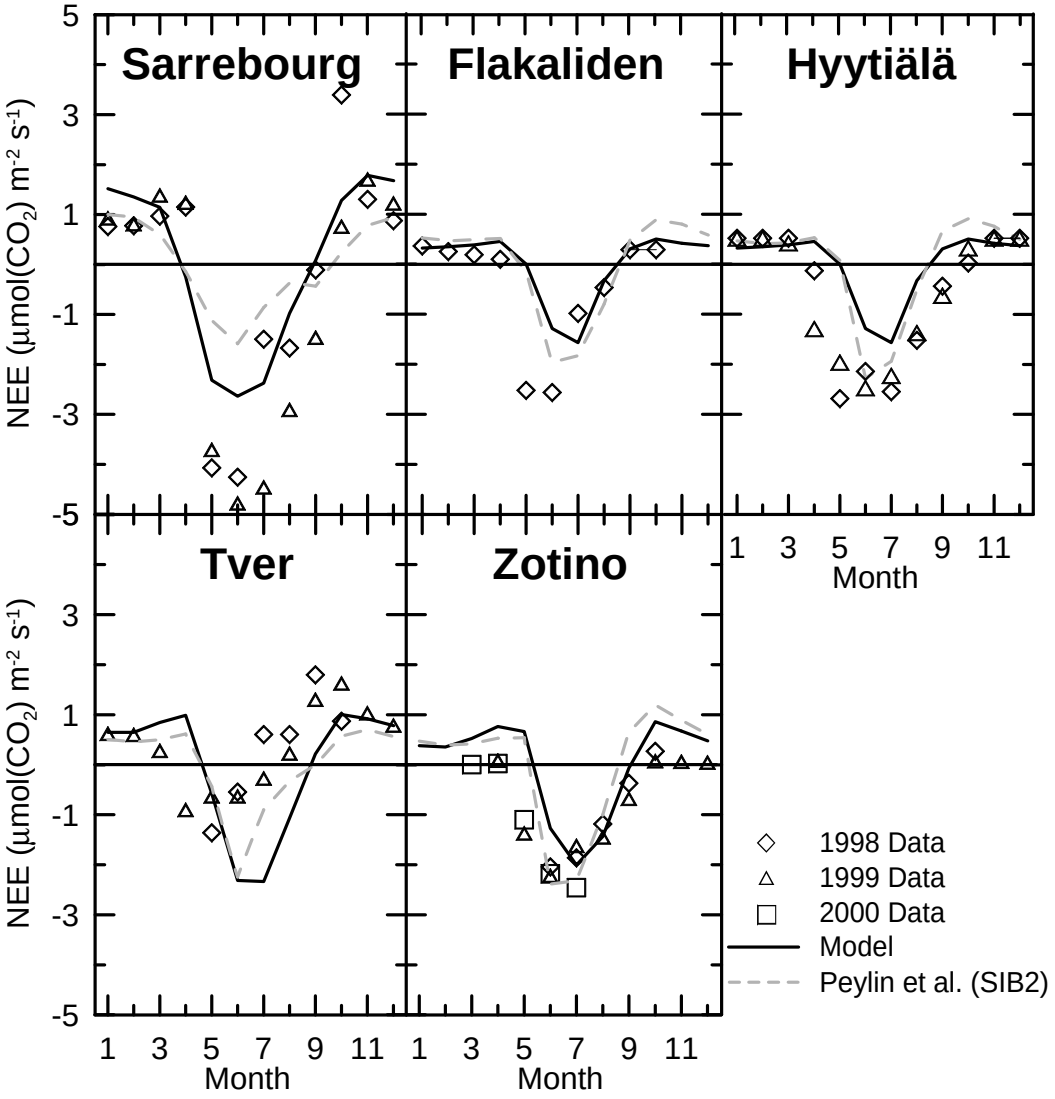

Figure 4.5: Net ecosystem exchange (NEE) modelled and measured with eddy–flux towers in Sarrebourg, Flakaliden, Hyytiälä, Tver, and Zotino.

NEE (at monthly time steps) of *Peylin et al.* [1999] which comes from SIB2 [*Sellers et al.*, 1996b, a], for comparison. BETHY's net fluxes are too small in amplitude but they are realistic for the phase of NEE at almost all flux tower sites. The same is true for the fluxes of SIB2 but with a slightly larger, though, more realistic amplitude. BETHY has a larger net flux amplitude only at the most western station Sarrebourg. Flakaliden is the northern most station which shows a very sharp decrease of NEE in May at the time probably when the temperature in Flakaliden passes the threshold temperature for assimilation for the dominant species *picea abies*, there. This behaviour is captured by BETHY but not as pronounced as in the measurements. There is no such abrupt behaviour in Hyytiälä whereas the model still shows a sudden beginning of assimilation. (Hyytiälä falls in the same grid box as Flakaliden in the model.) In Tver, both models are very comparable but BETHY reproduces better the large posi-

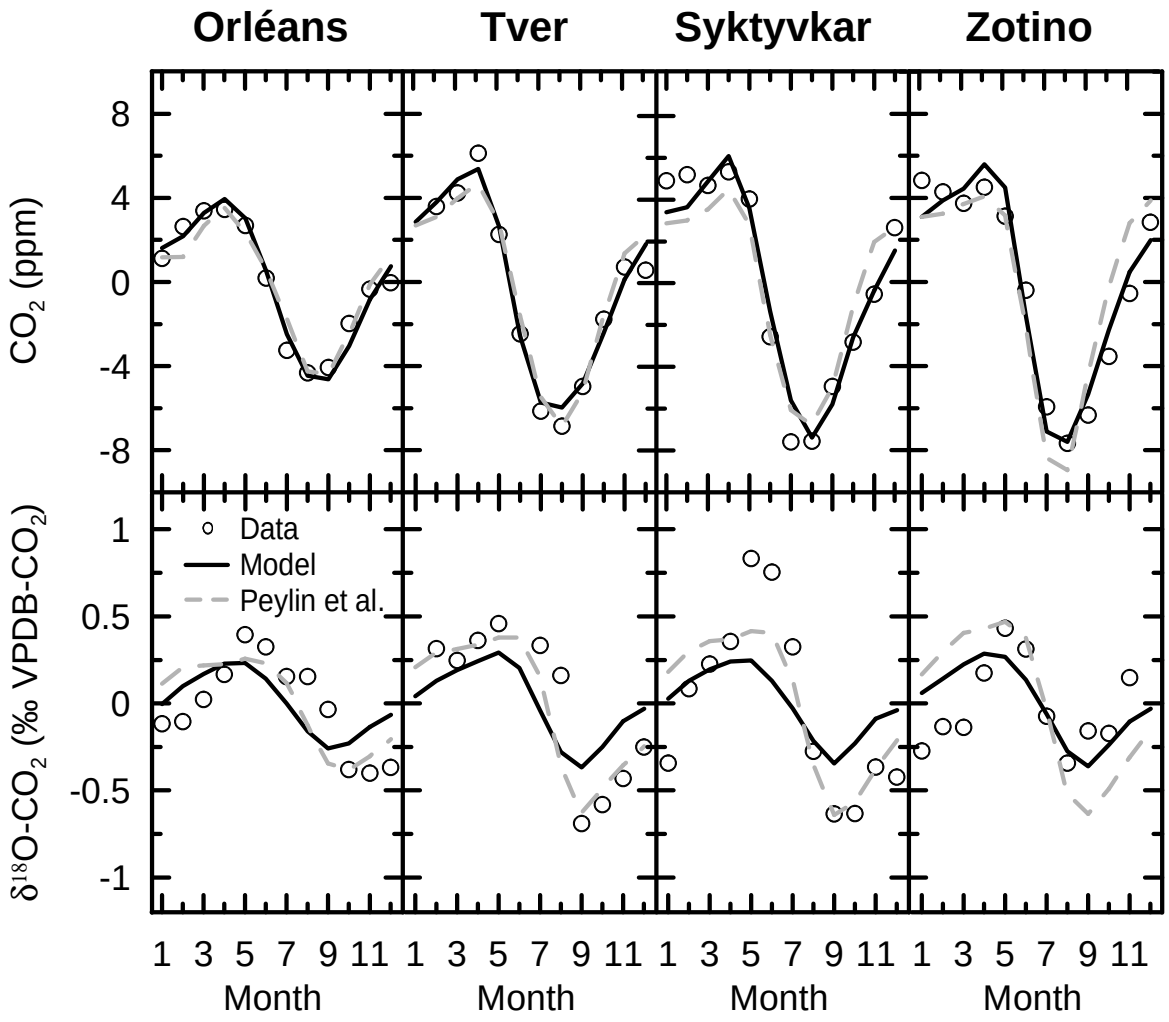

Figure 4.6: Measured and modelled mean seasonal cycle of CO_2 and $\delta^{18}O$–CO_2 at Orléans, Tver, Syktyvkar, and Zotino in 3000 m a.s.l. Note that the data of Tver is not at 3000 m but a mean seasonal cycle extracted from flights above the atmospheric boundary layer (ABL).

tive flux to the atmosphere at the end of the growing season. Both models predict too much respiration in Zotino at the end of the year but SIB2 simulates well the minimum value in June. Remind that NEE is actually the sum of two opposing fluxes, of assimilation and ecosystem respiration, where the maximum of assimilation ranges from 3 mmole(CO_2) $m^{-2}\,s^{-1}$ in Flakaliden to 7.5 mmole(CO_2) $m^{-2}\,s^{-1}$ in Tver. The amplitude and the phase of NEE are very sensitive to the phasing of the two fluxes, especially in regions with a contrasted seasonal climate. Contrary, the western part of Eurasia, with a mild climate, and hence not as pronounced seasonal variations as in the interior, is much more insensitive to the respective phasing of assimilation and respiration.

4.3.3 Seasonal cycle of atmospheric measurements

CO_2 and the $CO^{18}O$ fluxes emitted into the atmosphere are transported via advection, convection and turbulent diffusion. There is no known fractionation associated with these processes, so CO_2 and $CO^{18}O$ are transported as passive tracers. I have not closed the carbon cycle budget globally in the model so I can not strictly compare the absolute values. One flux omitted in the model is deforestation but there is probably only a small seasonality associated with it. So I can still compare the simulated seasonal cycle, both of CO_2 and $\delta^{18}O$–CO_2 with the observations. The upper panel of Figure 4.6 shows the mean seasonal cycle of CO_2 in 3000 m a.s.l. as measured (circles) [*Levin et al.*, 2002] and modelled by ECHAM/BETHY (solid line) and [*Peylin et al.*, 1999] (dashed line). The atmospheric CO_2 concentrations of *Peylin et al.* are the monthly SIB2 fluxes transported in the TM2 atmospheric transport model [*Heimann*, 1995]. The seasonal cycle of CO_2 is well reproduced by both models. The amplitude of the data and both models are almost the same. Nevertheless at Syktyvkar and Zotino ECHAM/BETHY seems to produce slightly more realistic amplitudes than *Peylin et al.* thus seems to capture better the seasonal cycle of CO_2 even if its not significant. The lower panel of Figure 4.6 shows the mean seasonal cycle in $\delta^{18}O$–CO_2 with measurements discussed in [*Levin et al.*, 2002]. The $CO^{18}O$ fluxes of *Peylin et al.* are the synthesis of the SIB2–CO_2 fluxes with the GISS water isotopes [*Jouzel et al.*, 1987] on a monthly mean basis and the transport of TM2. Both models follow the phase of the cycle, but *Peylin et al.* have a higher amplitude. One can clearly see that the amplitude in the CO_2 seasonal cycle remains roughly constant when going into the interior of the continent, from Tver to Zotino. Only Orléans is much lower which reflects its maritime influence. In contrast to that, the amplitude of $\delta^{18}O$–CO_2 increases from Orléans to Syktyvkar and then decreases in Zotino again. This behaviour is not well understood [*Levin et al.*, 2002]. There are several possible explanations: 1. There are different transport patterns west and east of the Ural, i. e. west of the Ural is more influenced by the Azores high and the Icelandic low and east of the Ural is mostly influenced by the Siberian high (winter) and low (summer) [*Aizen et al.*, 2001]. Zotino is therefore more influenced by northern latitudes [*Levin et al.*, 2002]; 2. The free troposphere is much more influenced by ABL air west of the Ural than east of it but measurements [*Lloyd et al.*, 2002a; *Ramonet et al.*, 2002] and simulations with regional scale models [*Chevillard et al.*, 2002; *Kjellström et al.*, 2002] indicate the contrary; 3. There is a positive gradient of CO_2 gross (not necessarily net fluxes, cf. CO_2 seasonal cycle) and hence $\delta^{18}O$–CO_2 fluxes from the Atlantic to the Ural and a negative gradient from the Ural to the Pacific; 4. There is no gradient of the CO_2 gross fluxes but there is one in discrimination. Unfortunately, the model does not fully resolve the Ural mountains in its influence on weather regimes because it has a smoothed orography and a rather coarse resolution.

Even if I can not compare the absolute values with the measurements, the longitudinal gradient between Orléans and Zotino should be comparable, anyway. In Table 4.1 are listed the differences in ECHAM/BETHY and in the data of the mean and amplitudes of CO_2 and $\delta^{18}O$–CO_2 between Tver, Syktyvkar, Zotino and Orléans. Table 4.1 indicates that there is practically no difference in the amplitude of the seasonal cycle of CO_2 between the three stations in Russia but the offset between the means differs a lot. *Levin et al.* [2002] argued that this offset is not significant because the differ-

Table 4.1: Comparison of absolute modelled and measured concentrations relative to Orléans[a].

	Model			Data		
	TVE−ORL	SYT−ORL	ZOT−ORL	TVE−ORL	SYT−ORL	ZOT−ORL
Mean CO_2 [ppm]	1.1	0.6	0.3	−1.1±2.4	3.1±1.9	1.2±2.1
Ampl. CO_2 [ppm]	2.8	4.9	4.6	5.3±2.4	5.1±1.9	4.7±2.1
	(1.3)	(1.6)	(1.5)	(1.7±0.7)	(1.7±0.7)	(1.6±0.6)
Mean $\delta^{18}O$ [‰]	−0.2	−0.2	−0.3	−0.8±0.3	−0.8±0.4	−0.5±0.4
Ampl. $\delta^{18}O$ [‰]	0.2	0.1	0.2	0.4±0.3	0.7±0.4	0.0±0.4
	(1.3)	(1.2)	(1.3)	(1.4±0.9)	(1.8±1.1)	(1.0±0.7)

[a]ORL=Orléans, TVE=Tver, SYT=Syktyvkar, ZOT=Zotino. Mean is the difference of total averages and Ampl. is the difference in Amplitude of the mean seasonal cycles. The values in parentheses are the ratio of the amplitude of the mean seasonal cycle to the amplitude at Orléans.

ences occur not over the whole measurement period and even disappear by the end of 2000. From $\delta^{13}C$ measurements in CO_2, the authors suggested that there is a big interannual variability in the net fluxes. In contrary, the mean in $\delta^{18}O$–CO_2 remains almost constant between Tver and Syktyvkar and decreases via Zotino whereas the amplitude increases from Orléans over Tver to Syktyvkar and decreases approaching Zotino, where it reaches the size of Orléans again. The model does not capture the behaviour of the data but produces $\delta^{18}O$–CO_2 fields rather uniform in size and amplitude over whole Russia and $\delta^{18}O$–CO_2 does not change significantly over the continent at 3000 m.

4.3.4 Diurnal rectification gradient

An interesting phenomenon in the carbon cycle, although it hinders an accurate inversion of fluxes, is the covariation between surface fluxes and vertical or horizontal transport, called rectifier effect in a generic manner. I further investigate here the diurnal rectifier effect [*Stephens et al.*, 1999]. During daytime in the growing season, the vertical transport is vigorous and NEE is negative (sink), resulting in a small negative gradient in CO_2 concentrations between the surface and the ABL. During night–time, vertical transport is almost suppressed and NEE is positive (source) inducing a large CO_2 accumulation near the ground in the shallow nocturnal boundary layer. If one measures only near the ground, the mean concentration in time is shifted to higher values while the mean mid–ABL concentration is shifted to lower CO_2 values. Inverse modelling efforts, taking monthly or yearly mean concentrations, have to take into account this spatial gradient induced by the "diurnal rectifier effect" (DRE). Current inverse models take mostly stations on the ocean where the DRE is not very large if the continental influence can be neglected [*Denning et al.*, 1996]. But stations nearby or inside Eurasia like Shemya Islands (Aleutians) or Ulaan Uum (Mongolia) could be strongly influenced by the DRE, which magnitude and extent is yet poorly known. There are even inverse models now which invert CO_2 and $\delta^{18}O$ in atmospheric CO_2

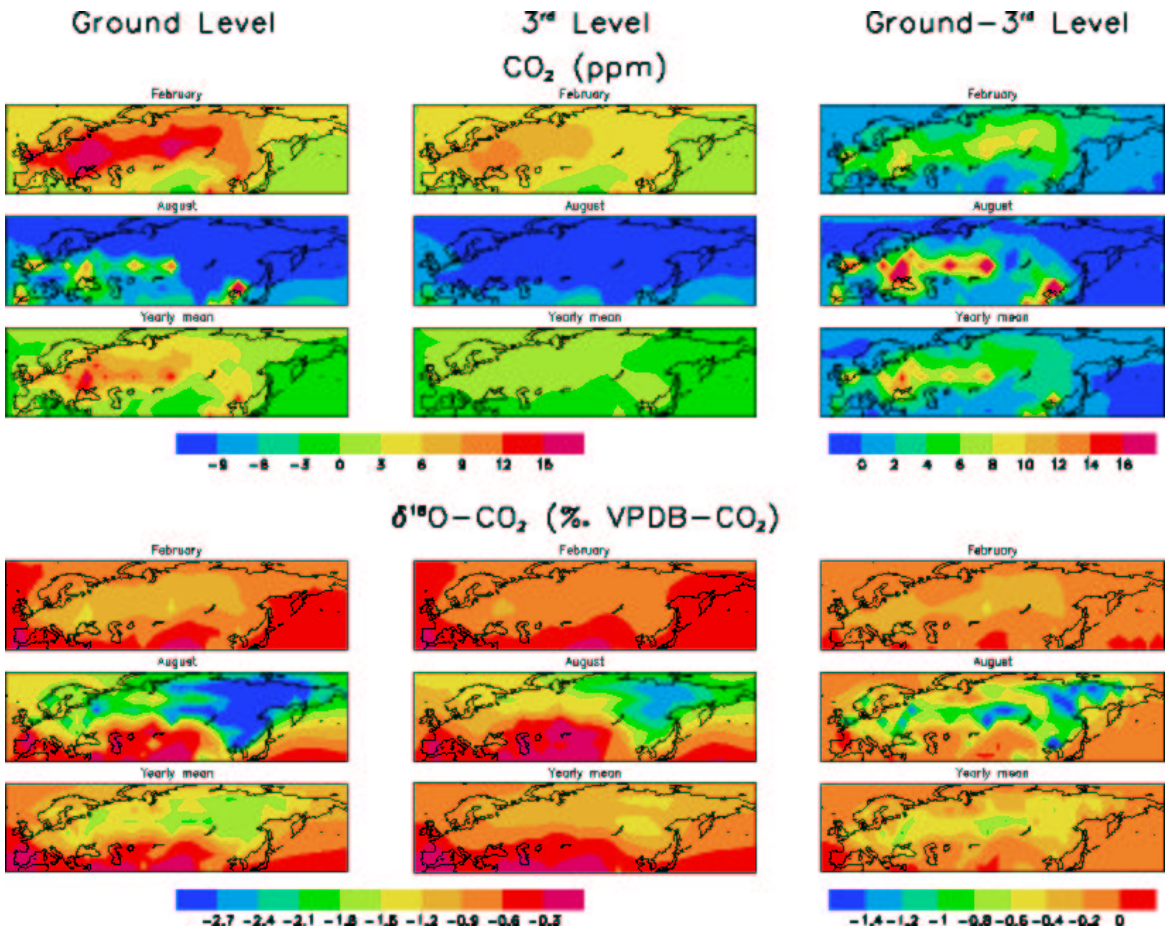

Figure 4.7: Rectification gradients of CO_2 and $\delta^{18}O$–CO_2 at ground (first column) and third (second column) level of the model, approximately 30 resp. 800 m above ground. The third column is the difference between the first and second column. In the third column, the colour bar differs from the one used in columns one and three. I suppressed longitude and latitude labelling to make the plot intelligible. Longitude ranges from 15 °W to 170 W° (−15° to 190°) and Latitude ranges from 35 to 75 °N. I subtracted the global mean concentration from each grid point as a reference. This gives negative values everywhere in $\delta^{18}O$–CO_2 over Eurasia because of the simulated strong north–south gradient.

where the DRE is ignored [*Peylin*, 1999]. The DRE effect is very strong in summer but of minor influence in winter. Additionally to the DRE, there are also different transport patterns between summer and winter, vertically and horizontally which also covary with the seasonal pattern of NEE. This effect can lead to another generation of mean spatial concentration gradients [e. g. *Denning et al.*, 1995] and is referred here as "seasonal rectifier effect" (SRE). Covariations with vertical transports induce normally an enhancement of the measured concentrations near the ground [*Stephens et al.*, 1999] whereas horizontal transport can lead to an abasement [*Ciais et al.*, 2000; *Taylor*, 1998]. The sign of this SRE can be negative or positive depending on the transport patterns and or the regions considered. Our model shows both rectifier effects which are not

distinguishable in a normal simulation. To simplify matters, I will call the overall effect also diurnal rectifier effect because DRE makes approximately 80% of the total rectifier effect over land [*Denning et al.*, 1996]. Figure 4.7 illustrates the DRE in ECHAM/ BETHY. I show the simulated fields for February, August and the yearly mean CO_2 and $\delta^{18}O$–CO_2 in the first (ca. 30 m above ground) and third level (ca. 800 m above ground) of the model. The third level lies in the middle of the ABL in summertime but in night– and winter–time outside of it. I also excluded the concentrations of fossil fuel and biomass burning of CO_2 and $\delta^{18}O$–CO_2 in Figure 4.7 in order to examine only the rectification gradients induced by covariations of biospheric fluxes and transport. The model shows an accumulation of CO_2 at the ground level with respect to 800 m over the continent on a monthly average basis. This accumulation ranges from 1 ppm over Eastern–Siberia in winter up to 30 ppm over some regions over Western–Russia in summer and to 40 ppm over South–East–Asia. The wintertime CO_2 accumulation is not very pronounced over Eurasia but it reaches a maximum of 10 ppm in South–Siberia. Otherwise, it is quite uniform between 2 and 6 ppm in the rest of the investigation area. In summer, there is a vast area between 40 and 60 °N and 30 and 90 °E where the monthly mean concentrations at the ground are more than 6 to 30 ppm higher compared to 800 m. West of it, the DRE seems to be again quite uniform around 3 ppm and east of it, the DRE falls even beyond 0. In summer, the 800 m level lies most of the time in the CBL during day and indicates, though, the net effect of daytime NEE with reduced CO_2 concentrations. Though, $\delta^{18}O$ in atmospheric CO_2 shows a similar pattern in winter as CO_2 does. It shows a small accumulation of negative $\delta^{18}O$–CO_2 (of the respired CO_2) in Europe and Western–Siberia near the ground with values around -0.3 ‰ compared to 800 m. In contrast to Western–Siberia, I see almost no difference between ground and third level in $\delta^{18}O$–CO_2 in winter in Eastern–Siberia. During summer, there is a drawdown in $\delta^{18}O$–CO_2 between 800 m and the surface of more than -0.4 ‰ over the whole domain reaching values of -1.5 ‰ around St. Petersburg and around Jakutsk in Eastern–Siberia. This pattern mirrors the DRE of CO_2 in Europe and West–Siberia but it is different over Eastern–Siberia. This surprising signal over Eastern–Siberia comes from negative ^{18}O leaf discrimination east of approximately 90 °E (see below and Fig. 4.9c). Already at Zotino, the DRE signal for $\delta^{18}O$–CO_2 differs from the one of CO_2. I plotted in Figure 4.8 vertical profiles up to an altitude of approximately 4500 m in February and August. I subtracted at each station the value of the tropopause model level (ca. 12 km) from the model values. Contrasting Orléans and Zotino in August, one can see that a comparable vertical profile in CO_2 (ca. 5 ppm), reflecting DRE, leads to a very different profile in $\delta^{18}O$–CO_2. This comes from the fact that leaf discrimination at Zotino is around zero during the growing season in the model, so that the signal of $\delta^{18}O$–CO_2 is determined mostly by the soil isoflux then (see below and Fig. 4.9c). One can also notice that the magnitude of the accumulation as well as the difference between ground and 800 m changes between the stations and reflects thus the specific isoflux sign at each measurement station. Current inverse modelling efforts include very rarely the diurnal cycle so they include only the seasonal covariations between fluxes and transport. Thus, for example, the prediction that assimilation in Siberia must be increased in current biosphere models [*Peylin*, 1999] could be an artefact. On the other hand, choosing a site where leaf discrimination is zero in summer and measuring vertical profiles would make it possible to quantify the diurnal

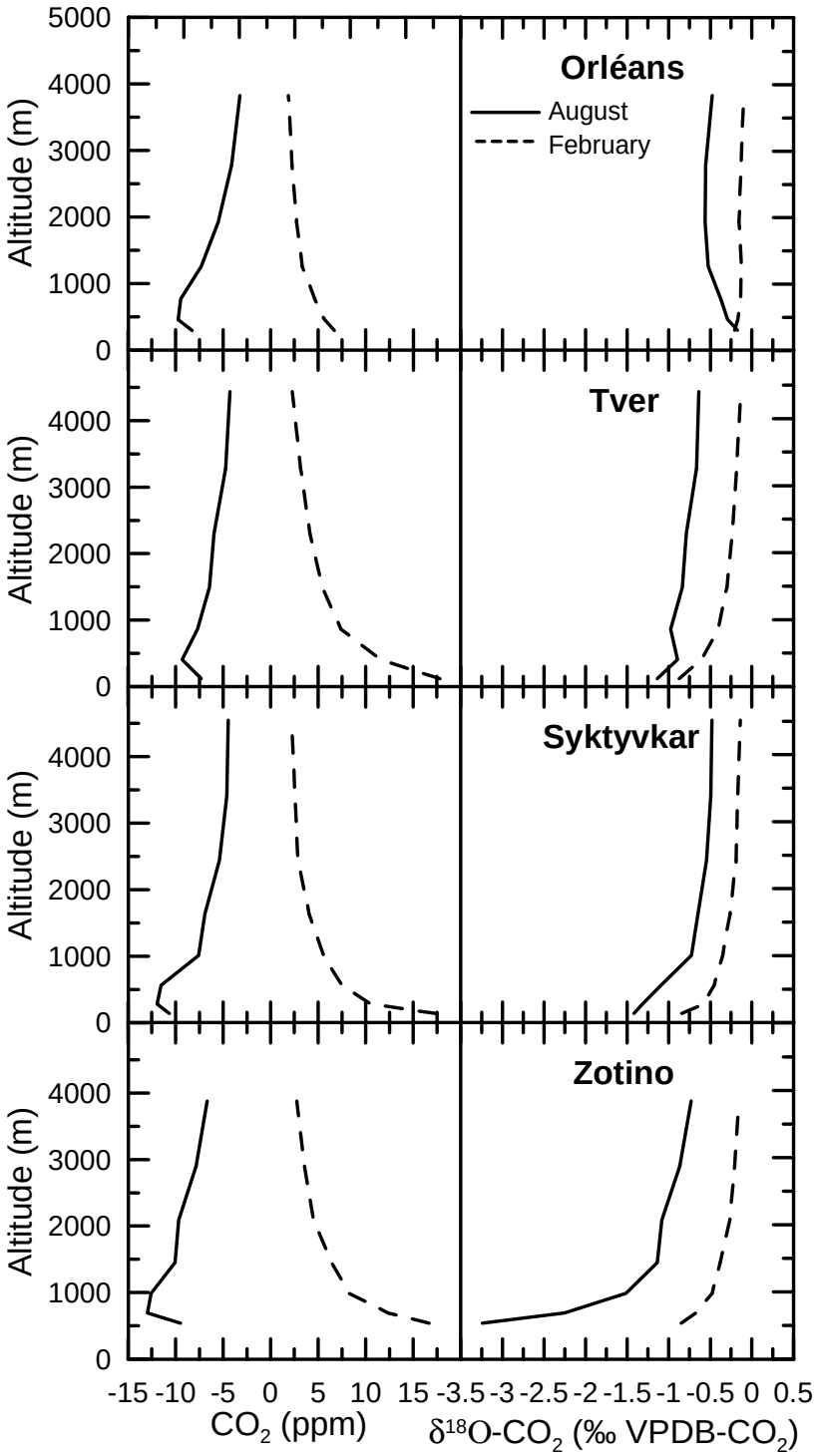

Figure 4.8: Simulated monthly mean vertical profiles of CO_2 and $\delta^{18}O$–CO_2 from ground to about 4500 m at Orléans, Tver, Syktyvkar, and Zotino in August and February, computed from 40 min varying NEE, $\delta^{18}O$–CO_2 fluxes and atmospheric transport.

variation in vertical transport alone, supposing one knows, respectively measures, soil "discrimination" (s. below). This suggests that δ^{18}O–CO_2 could be used under these conditions to validate atmospheric transport models to reduce the uncertainties implied by the existence of DRE.

4.3.5 Relating the simulated and observed longitudinal gradients to controlling climate variables

Writing the global balance equation for δ^{18}O in atmospheric CO_2 (regarding only the biospheric activity) leads to:

$$M_a \frac{d\delta_a}{dt} = F_R \Delta_R + A \Delta_A \tag{4.1}$$

with

$$\Delta_R = \delta_s - \delta_a + \epsilon_s \tag{4.2}$$

$$\Delta_A = -\epsilon_l + \frac{c_c}{c_a - c_c} (\delta_l - \delta_a) \ . \tag{4.3}$$

M_a is the number of moles CO_2 in the atmosphere, δ_a is δ^{18}O of atmospheric CO_2, A the net assimilation (assimilation minus leaf respiration), Δ_A the discrimination of assimilation (called leaf discrimination, too), F_R the total biospheric respiration minus leaf respiration (heterotrophic plus autotrophic minus leaf respiration), called net ecosystem respiration, Δ_R the difference between soil respired δ^{18}O–CO_2 and atmospheric δ^{18}O–CO_2 (I call it soil "discrimination" even if it is not a real discrimination), ϵ_l the diffusion fractionation of CO_2 entering and leaving the stomata, c_c the CO_2 concentration at the surface of the chloroplasts, c_a the CO_2 concentration of the atmosphere (precisely the canopy), δ_l the δ^{18}O of CO_2 dissolved and isotopicly equilibrated with leaf water, δ_a the δ^{18}O of atmospheric CO_2, δ_s the δ^{18}O of CO_2 dissolved and equilibrated with soil water, and ϵ_s the fractionation during diffusion of CO_2 out of the soil. The product of A and Δ_A is called the isoflux of assimilation or leaf isoflux and F_R times Δ_R is called the isoflux of respiration or soil isoflux. *Peylin et al.* [1999] calculated separately the assimilation and respiration fluxes and Δ of assimilation and respiration, both on a monthly mean basis. They transported the product of flux times Δ in TM2.

Having demonstrated that the model reproduces well the water isotopic composition, the CO_2 fluxes as well as the atmospheric CO_2 concentrations, one can still argue that the amplitude of the seasonal cycle of δ^{18}O–CO_2 is not well represented in our model (see Fig. 4.6). Nevertheless, it is interesting to know what causes discrimination to be negative in the model in East–Siberia. Additionally, none of the existing global models is capable to reproduce δ^{18}O in atmospheric CO_2 globally in phase and amplitude up to now.

I show in Figure 4.9 the meridional gradient of the CO_2 fluxes and isofluxes calculated by the ECHAM/BETHY model. The upper panel (Fig. 4.9a) shows the annual net assimilation (see above) given in GtC yr^{-1} per longitude band. The black line is the result of the model again in comparison to *Peylin et al.* (grey line). Three major points

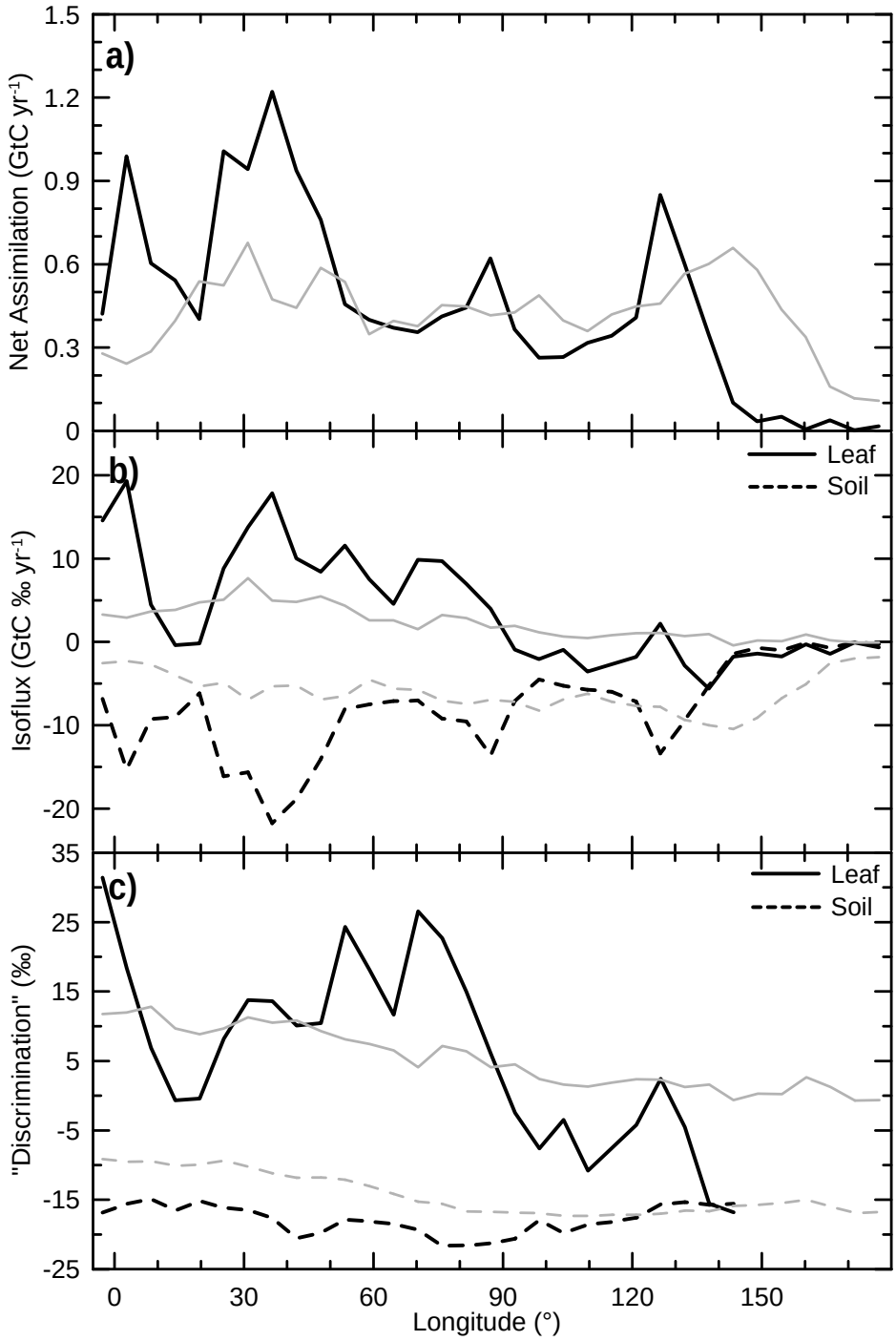

Figure 4.9: Yearly mean net carbon assimilation (GPP–Leaf respiration), isofluxes and their "discriminations" depending of longitude over Eurasia (top to bottom). Note that NEE is set to zero over each grid cell for a ten years run in BETHY and each year in SIB2 so that the ecosystem respiration equals net assimilation. BETHY is in black and *Peylin et al.* [1999] in grey. (For the definition of isoflux and "discrimination" see the text.)

in Figure 4.9a are the two maxima in Europe and the difference between BETHY and SIB2 east of 120 °E. The first maxima (5 °E) in assimilation represents western Europe up to South Scandinavia, Central Europe, and the Mediterranean Balkan area, from north to south. There, it is a very temperate climate in ECHAM which is favourable for assimilation. The second large maxima in assimilation around 40 °E comes from the presence of arable crops around the black sea and in Western–Russia (Fig. 4.2). The last maxima of assimilation in BETHY at around 130 °E corresponds to the great agricultural plains in Northern–China. East of 20 °E, SIB2 shows practically no gradient in assimilation and SIB2 shows larger photosynthesis rates than BETHY in the far North–East Siberian tundra. Both flux models show almost identical total net assimilation for the complete Eurasian domain (north of 40 °N), namely 14.5 GtC yr^{-1}, and discarding the peaks in BETHY, both models are roughly similar. The middle panel (Fig. 4.9b) shows patterns of isofluxes for photosynthesis (straight line) and respiration (dashed line). The lower panel (Fig. 4.9c) shows Δ, the "discrimination", both of photosynthesis (straight line) and respiration (dashed line). Δ in the model is the division of the isoflux by its CO_2 flux and it is therefore a flux weighted Δ, where the weighting accounts for temporal variability in fluxes each 40 min. My Δ thus reflect exactly what is "seen" by the atmosphere. In contrast, *Peylin et al.* calculated first monthly Δ and the CO_2 fluxes separately, from which they deduced the isofluxes afterwards. *Peylin et al.* took only relative humidity and the CO_2 concentration at the surface of the chloroplasts assimilation weighted in the calculation of leaf water isotopic composition whereas all other variables are taken as monthly averages. They predict a small decrease of the leaf isoflux and a decrease in the soil isoflux from west to east inside Eurasia (ca. 5 GtC ‰ yr^{-1}). ECHAM/BETHY shows noticeably different fields, decreasing in assimilation from about 20 GtC ‰ yr^{-1} to small negative values. Though, the total isoflux (sum of leaf and soil isoflux) of the biosphere is yet quite similar for both models over Eurasia. It is remarkable that leaf discrimination (Fig. 4.9c) in ECHAM/BETHY gets negative after 90 °E (the missing values after 150 °E come from the fact that one divides the isoflux by a very small CO_2 flux which leads to numerical instability and is therefore discarded). Between 50 and 90 °E, the difference between ECHAM/BETHY and *Peylin et al.* comes certainly from the different assimilation weighting procedure. Both models are using the so–called Farquhar–formulation [*Farquhar et al.*, 1980] for assimilation. If the assimilation between 50 and 90 °E is fairly similar in both studies (Fig. 4.9a), the determining parameters like temperature and humidity should be quite similar as well. But already with temperature, one can see that it will make a big difference in e.g. the equilibration of CO_2 with water (-0.4 ‰ per degree increase) if one considers explicitly a diurnal cycle or not. Though, we try to understand what determines the continentality gradient in Figure 4.9c. The leaf discrimination is determined by the isotopic composition of CO_2 equilibrated with leaf water at the evaporating site, δ_l, the atmospheric $\delta^{18}O$–CO_2 value, and the factor $c_c/(c_a - c_c)$ which is the amplification of leaf fractionation due to back–diffusion (eq. 4.3). The leaf water at the evaporating site is calculated from the Craig–and–Gordon formulation:

$$\delta_l^w = \epsilon_l^w + \delta_s^w - \epsilon_k + h\,(\delta_{vap} - \delta_s^w + \epsilon_k)\ . \tag{4.4}$$

ϵ_l^w is the fractionation of the liquid–vapour phase transition (according to [*Majoube*, 1971]), δ_s^w the source water isotopic composition, ϵ_k the kinetic fractionation factor

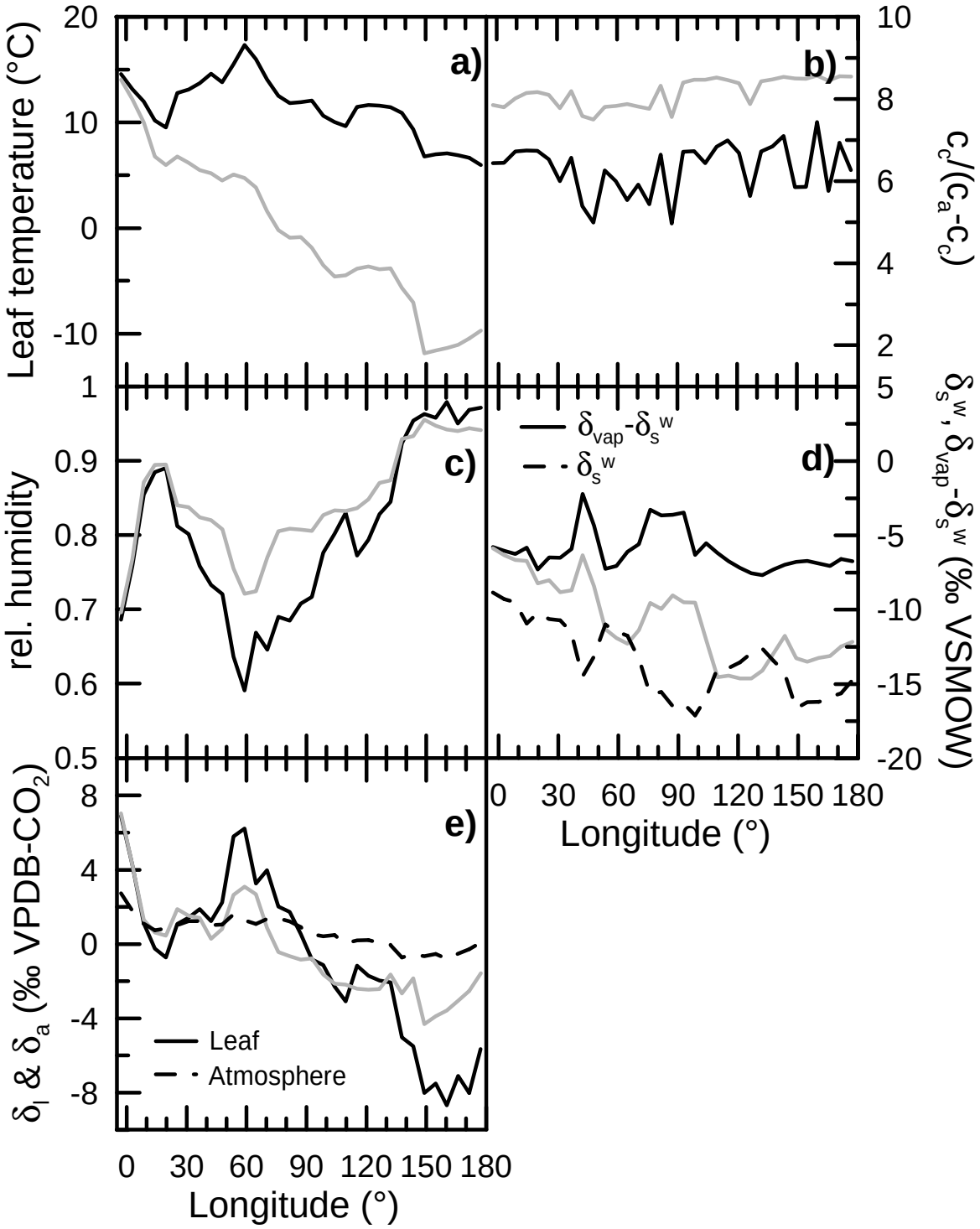

Figure 4.10: Variables which determine the δ^{18}O–CO_2 discrimination of assimilation. Black lines are assimilation weighted values and grey lines are not assimilation weighted (see text for the difference between assimilation weighted or not).

(taken constant), h the relative humidity, and δ_{vap} the isotopic composition of water vapour. CO_2 equilibrated with this leaf water is then:

$$\delta_l = \epsilon_l^w + \epsilon_{eq}\,, \tag{4.5}$$

where ϵ_{eq} is the equilibrium fractionation calculated after *Brenninkmeijer et al.* [1983].

In Figure 4.10 are plotted the variables which determine the "discriminations" and hence the isofluxes. I plotted both, the assimilation weighted (black lines) and the plain variables (grey lines). (Assimilation weighted variables are multiplied with the assimilation flux at each time step and the yearly sum of these products is then divided by the yearly sum of assimilation. They give therefore more realistic mean values.) One can divide Northern–Eurasia into two parts: the western part from the Atlantic to the Ural (Europe) and the eastern part from the Ural to the Pacific (Siberia), say from 0 to 60 °E and from 60 to 180 °E. I observe in Figure 4.10 an increase in leaf temperature (Fig. 4.10a) and thus in δ^{18}O–CO_2 (Fig. 4.10e) equilibrated with leaf water (at the evaporating site) in Europe and a decrease in Siberia. The converse picture is true for relative humidity (Fig. 4.10c) in the canopy. δ^{18}O–H_2O of ground water (Fig. 4.10d) decreases by about -5 ‰ over the whole continent whereas δ^{18}O–H_2O vapour minus ground water stays constant despite some fluctuations (Fig. 4.10d). This leads to an overall decrease in leaf δ^{18}O–H_2O across Siberia of around -20 ‰ between the Ural and the Pacific. In this signal, -5 ‰ comes from the decrease in source isotope composition and almost -15 ‰ comes from the increase in relative humidity. The temperature controlled equilibration of CO_2 with water isotopes opposes this big drop. But the assimilation weighted leaf temperature (Fig. 4.10a) decreases only by 10 °C across Siberia, so it lowers the gradient in δ_l only by about -2 ‰ (Fig. 4.10e). Since the model shows no east minus west gradient in the atmospheric δ^{18}O–CO_2 (Fig. 4.10e), the decrease of δ_l over Siberia is amplified by $c_c/(c_a - c_c)$ (Fig. 4.10b) and leads to the strong east–west gradient of leaf discrimination of about -40 ‰ (Fig. 4.9c).

4.4 Conclusions

I constructed a model of biospheric CO_2 exchange interfaced to an AGCM which is fit with a calculation of the isotopic composition of water as well. I implemented a new module to calculate in a fully consistent manner with climate, the cycling of ^{18}O–H_2O in the surface water pools (soil, leaves) and the pertaining δ^{18}O–CO_2 fluxes exchanged with the overlaying atmosphere. I studied the space and time distribution of water oxygen isotopes, CO_2 biospheric fluxes, atmospheric CO_2 and δ^{18}O in atmospheric CO_2, δ^{18}O–CO_2 fluxes, the isotopic discrimination of assimilation, and the isotopic "discrimination" of respiration with respect to CO_2 across Northern–Eurasia. It is shown that the water isotopic composition is simulated well and shows a realistic meridional negative gradient going from west to east. This gradient is much smaller for summer than for winter, so the relevant gradient in water isotopic composition is only about -5 ‰. The NEE flux that I simulate appears too small in amplitude at the selected flux tower sites, but the comparison can be only semi–quantitative. The seasonal cycle at 3000 m a.s.l. of δ^{18}O in atmospheric CO_2 offers a unique integrated measure of the performances of the different modules (NEE, transport, δ^{18}O–CO_2, etc.,

and their interactions). The atmospheric seasonal cycle is modelled very well for CO_2 but the amplitude of $\delta^{18}O$–CO_2 is underestimated, although the model reproduces the right phase.

I found that the diurnal rectifier effect, implied by covariations of biotic fluxes with vertical transport in the ABL, is very pronounced over Eurasia and different between CO_2 and $\delta^{18}O$–CO_2. This comes mostly from the fact that leaf discriminations becomes zero or negative even in the yearly mean east of 90 °E, due to the continentality.

Together with the isofluxes of $\delta^{18}O$–CO_2, I demonstrated that there is a big gradient in leaf discrimination from west to east over Eurasia, and leaf discrimination can even become negative in the most continental area of Eastern–Siberia. I interpret this signal on one hand from the water isotope gradient but mostly from the gradient in relative humidity that lowers the evaporating leaf water $\delta^{18}O$–H_2O and, therefore, the leaf discrimination.

References

Aizen, E. M., V. B. Aizen, J. M. Melack, T. Nakamura, and T. Ohta, Precipitation and atmospheric circulation patterns at mid–latitudes of asia, *Int. J. Climatol.*, *21*, 535–556, 2001.

Allison, C. E., R. J. Francey, and H. A. Meijer, Recommandations for the reporting of stable isotope measurements of carbon and oxygen in CO_2 gas, in *References and Intercomparison Materials for Stable isotopes of Light Elements*, edited by IAEA-TECDOC-825, pp. 155–162, Int. At. Energy Agency, Vienna, 1995.

Arpe, K., L. Bengtsson, L. Dümenil, and E. Roeckner, The hydrological cycle in the ECHAM3 simulations of the atmospheric circulation, in *Global Precipitation and Climate Change*, edited by M. Desbois and F. Desalmand, pp. 361–377, Springer–Verlag, New York, 1994.

Baertschi, P., Absolute ^{18}O content of Standard Mean Ocean Water, *Earth Planet. Sci. Lett.*, *31*, 314–344, 1976.

Bousquet, P., P. Peylin, P. Ciais, C. L. Quéré, F. P., and P. P. Tans, Regional changes in carbon dioxide fluxes of land and oceans since 1980, *Science*, *290*, 1 342–1 346, 2000.

Brenninkmeijer, C. A. M., P. Kraft, and W. G. Mook, Oxygen isotope fractionation between CO_2 and H_2O, *Isotope Geoscience*, *1*, 181–190, 1983.

Chevillard, A., U. Karstens, P. Ciais, S. Lafont, and M. Heimann, Simulation of atmospheric CO_2 over Europe and Siberia using the regional scale model REMO, *Tellus*, *54B*, 2002, in press.

Ciais, P., P. P. Tans, M. Trolier, J. W. White, and R. J. Francey, A large northern hemisphere terrestrial CO_2 sink indicated by the $^{13}C/^{12}C$ ratio of atmospheric CO_2, *Science*, *269*, 1 098–1 102, 1995a.

Ciais, P., P. P. Tans, W. C. White, M. Trolier, R. J. Francey, J. A. Berry, D. R. Randall, P. J. Sellers, F. G. Collatz, and D. S. Schimel, Partitioning of ocean and land uptake of CO_2 as inferred by $\delta^{13}C$ measurements from the NOAA climate monitoring and diagnostics laboratory global air sampling, *J. Geophys. Res.*, *100*, 5 051–5 070, 1995b.

Ciais, P., A. S. Denning, P. P. Tans, J. A. Berry, D. A. Randall, G. J. Collatz, P. J. Sellers, J. W. C. White, M. Trollier, H. A. J. Meijer, R. J. Francey, P. Monfray, and M. Heimann, A three dimensional synthesis study of $\delta^{18}O$ in atmospheric CO_2, part I: Surface fluxes, *J. Geophys. Res.*, *102*, 5 857–5 872, 1997a.

Ciais, P., P. P. Tans, A. S. Denning, R. J. Francey, M. Trollier, H. J. Meijer, J. W. C. White, J. A. Berry, D. A. Randall, J. J. G. Collatz, P. J. Sellers, P. Monfray, and M. Heimann, A three dimensional synthesis study of $\delta^{18}O$ in atmospheric CO_2, part II: Simulations with the TM2 transport model, *J. Geophys. Res.*, *102*, 5 873–5 883, 1997b.

Ciais, P., P. Peylin, and P. Bousquet, Regional biospheric carbon fluxes as inferred from atmospheric CO_2 measurements, *Ecol. Appl.*, *10*, 1 574–1 589, 2000.

Dansgaard, W., Stable isotopes in precipitation, *Tellus*, *16*, 436–468, 1964.

Denning, A. S., I. Y. Fung, and D. A. Randall, Latitudinal gradient of atmospheric CO_2 due to seasonal exchange with land biota, *Nature*, *376*, 240–243, 1995.

Denning, A. S., D. A. Randall, G. J. Collatz, and P. J. Sellers, Simulations of terrestrial carbon metabolism and atmospheric CO_2 in a general circulation model, part 2: Simulated CO_2 concentrations, *Tellus*, *48B*, 543–567, 1996.

Fan, S., M. Gloor, J. Mahlman, J. Pacala, J. Sarmiento, T. Takahashi, and P. Tans, Atmospheric and oceanic CO_2 data and models imply a large terrestrial carbon sink in North America, *Science*, *282*, 442–446, 1998.

Farquhar, G. D., S. von Caemmener, and J. A. Berry, A biochemical model of photosynthesis CO_2 fixation in leaves of C_3 species, *Planta*, *149*, 78–90, 1980.

Farquhar, G. D., J. Lloyd, J. A. Taylor, L. B. Flanagan, J. P. Syvertsen, K. T. Hubick, S. C. Wong, and J. R. Ehleringer, Vegetation effects on the isotope composition of oxygen in atmospheric CO_2, *Nature*, *363*, 439–443, 1993.

Granier, A., Sarrebourg, France, the Euroflux data set 2000, in *Carbon, Water and Energy exchanges of European forests*, edited by R. Valentini et al., Ecological Studies, Springer Verlag, Heidelberg, 2002, in press.

Heimann, M., The global atmospheric tracer model TM2, *Tech. Rep. 10*, Deutsches Klimarechenzentrum, Hamburg, 1995.

Hoffmann, G., M. Werner, and M. Heimann, Water isotopes module of the ECHAM atmospheric general circulation model: A study on timescales from days to several years, *J. Geophys. Res.*, *103*, 16 871–16 896, 1998.

IAEA/WMO, Global network of isotopes in precipitation, The GNIP Database. Accessible at: http://isohis.iaea.org, 2001.

Jouzel, J., G. L. Russell, R. J. Suozzo, R. D. Koster, J. W. C. White, and W. S. Broecker, Simulations of the HDO and $H_2^{18}O$ atmospheric cycles using the NASA/GISS general circulation model: The seasonal cycle for present–day conditions, *J. Geophys. Res.*, *92*, 14 739–14 760, 1987.

Kjellström, E., K. Holmén, K. Eneroth, and M. Engardt, Summertime siberian CO_2 simulations with the regional transport model MATCH: A feasibility study of carbon uptake calculations from EUROSIB data, *Tellus*, *54B*, 2002, in press.

Knorr, W., and M. Heimann, Uncertainties in global terrestrial biosphere modeling: 1. a comprehensive sensitivity analysis with a new photosynthesis and energy balance scheme, *Global Biogeoch. Cycl.*, *1*, 207–225, 2001a.

Knorr, W., and M. Heimann, Uncertainties in global terrestrial biosphere modeling: Part ii: Global constraints for a process–based vegetation model, *Global Biogeoch. Cycl.*, *1*, 227–246, 2001b.

Levin, I., P. Ciais, R. Langenfelds, M. Schmidt, M. Ramonet, K. Sidorov, N. Tchebakova, M. Gloor, M. Heimann, E.-D. Schulze, N. N. Vygodskaya, O. Shibistova, and J. Lloyd, Three years of trace gas observations over the eurosiberian domain derived from aircraft sampling — a concerted action, *Tellus*, *54B*, 2002, in press.

Lindroth, A., Flakaliden, Sweden, the Euroflux data set 2000, in *Carbon, Water and Energy exchanges of European forests*, edited by R. Valentini et al., Ecological Studies, Springer Verlag, Heidelberg, 2002, in press.

Lloyd, J., R. L. Langenfelds, R. J. Francey, M. Gloor, N. M. Tschebakova, D. Zolotukhine, W. A. Brand, R. A. Werner, A. Jordan, C. A. Allison, V. Zrazhewske, O. Shibistova, and E.-D. Schulze, A trace gas climatology above Zotino, central Siberia, *Tellus*, *54B*, 2002a, in press.

Lloyd, J., O. Shibistova, D. Zolothukhine, O. Kolle, A. Arneth, J. Styles, N. M. Tchebakova, and E.-D. Schulze, Seasonal and annual variations in the photosynthetic productivity and carbon balance of a central Siberian pine forest, *Tellus*, *54B*, 2002b, in press.

Majoube, M., Fractionnement en oxygene–18 et en deuterium entre l'eau et sa vapeur, *Journal de Chimie et Physique*, *58*, 1 423–1 436, 1971.

Mills, G. A., and H. C. Urey, The kinetics of isotopic exchange between carbon dioxide, bicarbonate ion, carbonate ion and water, *J. Am. Chem. Soc.*, *62*, 1 019–1 026, 1940.

Milyukova, I. M., O. E. Kolle, A. B. Varlagin, N. N. Vygodskaya, E.-D. Schulze, and J. Lloyd, Carbon balance of a southern taiga spruce stand in european russia, *Tellus*, *54B*, 2002, in press.

Modellbetreuungsgruppe, The ECHAM3 atmospheric general circulation model, *Tech. Rep. 6*, Deutsches Klimarechenzentrum, Hamburg, 1994.

Peylin, P., The composition of ^{18}O in atmospheric CO_2: A new tracer to estimate global photosynthesis, Ph.D. thesis, L'Université Paris VI, Paris, 1999, in french.

Peylin, P., P. Ciais, A. S. Denning, P. P. Tans, J. A. Berry, and W. C. White, A three–dimensional study of $\delta^{18}O$ in atmospheric CO_2: contributin of different land ecosystems, *Tellus*, *51B*, 642–667, 1999.

Prentice, I. C., G. D. Farquhar, M. J. R. Fasham, M. L. Goulden, M. Heimann, V. J. Jaramillo, H. S. Kheshgi, C. Le Quéré, R. J. Scholes, and D. W. R. Wallace, The carbon cycle and atmospheric CO_2, in *Third Assessment Report of Climate Change*, edited by J. T. Houghton and D. Yihui, Report of the International Panel on Climate Change, chap. 3, pp. 38–71, Cambridge University Press, New York, 2001.

Ramonet, M., P. Ciais, I. Nepomniachii, K. Sidorov, J. Lloyd, R. Neubert, D. Picard, V. Kazan, S. Biraud, O. Kolle, and D. S. E, 3 years of aircraft CO_2 and isotope measurements over Fyodorovskoye in European Russia, *Tellus*, *54B*, 2002, in press.

Rasch, P. J., and D. L. Williamson, Computational aspects of moisture transport in global models of the atmosphere, *Q. J. R. Meteorol. Soc.*, *116*, 1 071–1 090, 1990.

Rayner, P. J., I. G. Enting, R. J. Francey, and R. Langenfelds, Reconstructing the recent carbon cycle from atmospheric CO_2, ^{13}C and O_2/N_2 observations, *Tellus*, *51B*, 213–232, 1999.

Roeckner, E., K. Arpe, L. Bengtsson, S. Brinkop, L. Dümenil, M. Esch, E. Kirk, F. Lunkeit, M. Ponater, B. Rockel, R. Sausen, U. Schlese, S. Schubert, and M. Windelband, Simulation of the present–day climate with the ECHAM model: impact of model physics and resolution, *Tech. Rep. 93*, Max–Planck Institut für Meteorologie, Hamburg, 1992.

Schimel, D., D. Alves, I. Enting, M. Heimann, F. Joos, D. Raynaud, T. Wigley, M. Prather, R. Derwent, D. Ehhalt, P. Fraser, E. Sanhueza, X. Zhou, P. Jonas, R. Charlson, H. Rohde, S. Sadasivan, K. P. Shine, Y. Fouquart, V. Ramaswamy, S. Solomon, J. Srinivasan, D. Albritton, I. Isaken, M. Lal, and D. Wuebbles, 2. radiative forcing of climate change, in *Climate Change 95, The Science of Climate Change*, edited by J. Houghton, L. M. Filho, B. Callander, N. Harris, A. Kattenberg, and K. Maskell, pp. 65–131, Intergovt. Panel on Clim. Change, Cambridge, England, 1996.

Sellers, P. J., S. O. Los, C. J. Tucker, C. O. Justice, D. A. Dazlich, G. J. Collatz, and D. A. Randall, A revised land surface parameterization (SiB2) for atmospheric GCM: Part II the generation of global fields of terrestrial biospherical parameters from satellite data, *J. Climate*, *9*, 706–737, 1996a.

Sellers, P. J., D. A. Randall, G. J. Collatz, J. A. Berry, C. B. Field, D. A. Dazlich, C. Zhang, and G. D. Collelo, A revised land surface parameterization (SiB2) for atmospheric GCM: Part I model formulation, *JOC*, *9*, 676–705, 1996b.

Stephens, B. B., S. C. Wofsy, R. F. Keeling, P. P. Tans, and M. J. Potosnak, The CO_2 budget and rectification airborne study: Strategies for measuring rectifiers and regional fluxes, in *Inverse Methods in Global Biogeochemical Cycles*, edited by P. Kasibhatla et al., vol. 114 of *Geophysical Monograph Series*, pp. 311–324, American Geophysical Union, Washington D. C., 1999.

Taylor, J. A., Atmospheric mixing and the CO_2 seasonal cycle, *Geophysical Research Letters*, *25*, 4 173–4 176, 1998.

Vesala, T., Hyytiälä, Finland, the Euroflux data set 2000, in *Carbon, Water and Energy exchanges of European forests*, edited by R. Valentini et al., Ecological Studies, Springer Verlag, Heidelberg, 2002, in press.

Werner, M., Räumliche und zeitliche variabilität von wasserisotopen im polaren niederschlag, Ph.D. thesis, Universiät Hamburg, 2000, in german.

Wilson, M. F., and A. Henderson-Sellers, A global archive of land cover and soils data for use in general circulation models, *J. Climate*, *5*, 119–143, 1985.

Chapter 5

Summary and Outlook

5.1 Summary

In the three preceding chapters, I have described, tested, and applied the model of $\delta^{18}O$ in atmospheric CO_2 that I developed during my doctorate. The model serves different purposes: First, it is a test of $\delta^{18}O$–CO_2, a supposedly promising tracer to decipher CO_2 gross fluxes of the terrestrial biosphere. Second, it serves as a tool to test our integrated understanding of the Earth system with its interactions. Third, it builds a basis for multi–tracer modelling which allows to constrain various aspects of the carbon cycle at the same time.

The global comprehensive 3D model of $\delta^{18}O$ in atmospheric CO_2 integrates the Atmospheric General Circulation Model (AGCM) ECHAM, including the water isotope cycle and tracer transport, the biosphere model BETHY, and a newly build $\delta^{18}O$–CO_2 flux module. $\delta^{18}O$–CO_2 surface isofluxes are a convolution of biospheric CO_2 fluxes (marine and terrestrial) and the water isotopic composition. $\delta^{18}O$–CO_2 is then transported in the atmosphere where the measured signal of $\delta^{18}O$ in atmospheric CO_2 is an integrated measure of all these processes and their interactions. The new comprehensive model is different from earlier model approaches due to its consistent calculation of the water isotopic composition of the different water pools (in leaves, soils, and in the atmosphere), the CO_2 and $\delta^{18}O$–CO_2 fluxes from and to the atmosphere, and the atmospheric transport in the same model framework and with the same time step. It implies inherently a diurnal cycle in all processes by acting on a 40 minute time step and thus takes into account the covariance between the different processes involved. The $\delta^{18}O$–CO_2 isofluxes depend thereby on the atmospheric $\delta^{18}O$–CO_2 value which causes the model to behave differently than earlier models attempts. With the new model, for the first time the absolute $\delta^{18}O$–CO_2 concentration in the atmosphere can be calculated reducing the number of free parameters. It overcomes therewith inconsistencies of other $\delta^{18}O$–CO_2 models and constitutes a proper up–scaling of biogeochemical processes from the ecosystem level to the quasi global atmospheric signal.

I have tested the model's surface processes against a variety of other model estimates and observations and it exhibits a very robust, conservative behaviour lying mostly in–between the range of different estimates respectively observations. However, there are four precarious model behaviours, three derived from the biosphere model BETHY and the fourth from the water isotope module:

1. *The model does not follow closely the measured phase of Net Ecosystem Exchange (NEE) (s. Chapter 2.3).* Measurements and model have very different catchment areas for NEE so that a comparison of the amplitudes of measured and modelled NEE has to be handled with care. But the model should display the same seasonal phasing as the measurements. ECHAM/BETHY deviates from the measured phase at about half of the compared stations. Unfortunately, it does not systematically precede or lag the observations. But as I have pointed out in Chapter 2.4, a different timing of e. g. respiration can bring model and observations closer together.
2. *The model shows low assimilation at high northern latitudes (s. Chapter 2.3).* There are contradictory opinions in the literature how well biosphere models represent assimilation in high northern latitudes. Atmospheric measurements usually indicate that existing biosphere models underestimate assimilation there [e. g. *Kaminski et al.*, 2002; *Peylin*, 1999] whereas ground based measurements indicate more an overestimation of NEE in high northern latitudes [*Jon Lloyd*, personal communication]. ECHAM/BETHY shows low assimilation in the northern extra–tropics being on the lower end of other model estimates. A data compilation of Net Primary Production (NPP) measurements seems to support my model results of low assimilation at high northern latitudes. In addition, ECHAM/BETHY compares very well with the observed seasonal cycle in atmospheric CO_2 at high northern latitudes showing rather a slight overestimation of the CO_2 seasonal amplitude than an underestimation (s. Chapter 3.3.1).
3. *The stomata–internal CO_2 mixing ratios, c_i, at high northern latitudes are greater than previous estimates (s. Chapter 2.3).* But a recent revision of atmospheric $\delta^{13}C$ measurements together with a new model study of $\delta^{13}C$ seem to support the high ECHAM/BETHY values.
4. *The seasonal cycle of the $\delta^{18}O$–CO_2 signature leaving the soil is suppressed (s. Chapter 2.3).* ECHAM's soil single bucket model integrates the sometimes large seasonal cycle of incoming rain $\delta^{18}O$–H_2O. This single bucket value shows almost no change during the year so that CO_2 leaving the soil bears the same $\delta^{18}O$ value all year long. This contradicts the common perception of the $\delta^{18}O$–CO_2 soil isoflux but unfortunately the present data of canopy $\delta^{18}O$–CO_2 measurements is not suitable to definitely pinpoint the model deficiency. Nevertheless, it is very likely that the soil bucket model is too simplistic to describe the $\delta^{18}O$–CO_2 soil isoflux.

Points 1, 2, and 3 could not be solved with the present data available in the literature. Points 4 is a real model deficiency but Chapter 3.3.4 illustrates that its influence on $\delta^{18}O$–CO_2 is small.

The integral performances of the model has been tested against measurements of atmospheric CO_2 and $\delta^{18}O$–CO_2. The atmosphere integrates all sources and sinks of CO_2 and $\delta^{18}O$–CO_2. The measured atmospheric signal of CO_2 combines thereby mainly the net biospheric fluxes and transport, while $\delta^{18}O$–CO_2 adds the water respectively water isotope cycle. ECHAM/BETHY compares very well with atmospheric CO_2 measurements but it shows big differences in $\delta^{18}O$–CO_2 (s. Chapter 3.3). The obvious conclusion would be that the water isotope cycle in ECHAM/BETHY is erroneous. But quite the contrary can be stated: it reproduces measurements of $\delta^{18}O$–H_2O in rain very well. The isotopic signal of $\delta^{18}O$–H_2O is communicated to $\delta^{18}O$–CO_2 in the atmosphere only via liquid water pools in the presence of CO_2 fluxes so that small

shortcomings in the CO_2 fluxes, that are not deducible with the CO_2 signal alone, are multiplied with the water isotopic composition and may have large consequences for atmospheric $\delta^{18}O$–CO_2. The atmospheric signal of $\delta^{18}O$–CO_2 measures therefore not only the CO_2 sources, the water isotopic composition and the transport but also the interplay between these different processes. In the standard model parameterisation, the amplitude of the modelled seasonal cycle is only $^2/_3$ of the observed amplitude, the phase of the seasonal cycle precedes the observed phase by two month, and the meridional gradient is slightly too small in the model compared to observations. The seasonal amplitude is thereby seen as somehow arbitrary in the model because it is sensitive to model formulations whereas the phase of the seasonal cycle and the north–south gradient did not change largely in all sensitivity studies (s. Chapter 3.3.4). Notably new processes like the invasion effect or the reduced carbonic anhydrase activity were not included in earlier model studies of $\delta^{18}O$–CO_2 and proposed in the literature as possible explanations of the model–data mismatch. But none of the new processes did resolve the discrepancies between ECHAM/BETHY and the observed $\delta^{18}O$ in atmospheric CO_2, neither in the seasonal cycle nor in the north–south gradient.

I have studied the model in more detail over Eurasia, the largest land mass in the northern hemisphere. The role of Eurasia in the global carbon cycle is certainly important but is not known precisely. In the context of the EUROSIBERIAN CARBONFLUX project, a concerted attempt was made recently to investigate the carbon cycle in Eurasia. In this regard, I have analysed the behaviour of ECHAM/BETHY over the Eurasian continent and could thereby profit from the EUROSIBERIAN CARBONFLUX measurements. Whereas I have focused in Chapter 2 and 3 on the analysis of the meridional gradient, Chapter 4 was dedicated to the East–West distribution of the CO_2 and $\delta^{18}O$–CO_2 source functions. *Farquhar et al.* [1993] already pointed out peculiar negative leaf discrimination in their model at the eastern projection of Siberia. I have found also negative leaf discrimination over a vast area east of 90 °E which widens the scope of *Farquhar et al.*'s findings. There is also an evident East–West gradient in leaf discrimination whereof 75 % could be attributed in my model to the increase in relative humidity from the Ural mountains to the Pacific coast and only 25 % to the depletion of rain water isotopes further East in Siberia. Therewith I could disprove the common misinterpretation of the annual mean rain water isotopic composition as the main determine of the East–West gradient in leaf discrimination but show indeed that it is only summer rain isotopic composition which is relevant to the effective annual mean leaf discrimination. To prove the model findings, I have finally proposed an observation strategy in measuring vertical profiles of CO_2 and $\delta^{18}O$–CO_2 over Eurasia.

5.2 Outlook

None of the existing models of $\delta^{18}O$ in atmospheric CO_2 is capable to simulate correctly the spatiotemporal distribution of atmospheric $\delta^{18}O$–CO_2. There are five reasons that I can figure out which are either incorrectly described in the models or have the potential to strongly influence the model results:

1. The formulation of heterotrophic respiration is very coarse in present–day biosphere models. It consists mainly of one formula and follows closely temperature [*Lloyd and Taylor*, 1994; *Raich and Potter*, 1995]. But heterotrophic respiration can well be influenced by other processes than temperature such as nitrogen content in the soil [*Mattson*, 1995]. There exists an imbalance in recent biosphere models between the rather complex formulation of assimilation and the very basic description of respiration. I have pointed out in Chapter 2.4 that a different formulation of respiration can yield much better results.
2. The soil bucket model of ECHAM attenuates too much the seasonal cycle of δ^{18}O–H_2O in soil water of the unsaturated soil zone. Soil CO_2 efflux exhibits therefore almost the same δ^{18}O–CO_2 value all year long. This is clearly a model shortcoming but it does not strongly influence the model results (s. Chapter 3.3.4). Nevertheless, the performed sensitivity analysis used rain isotope input fields that coincided in their seasonal phasing with the seasonal phasing of assimilation in the model so that no strong sensitivity could be observed. To exclude the possibility of an artefact due to the synchronous seasonal cycles, the formulation of soil respired δ^{18}O–CO_2 should be ameliorated following stronger meteorological conditions. Just recently, *Riley et al.* [2002] published a formulation that overcomes computational problems in calculating a soil δ^{18}O–H_2O profile and where a more realistic formulation of the δ^{18}O–CO_2 soil isoflux is possible.
3. ECHAM/BETHY uses a conservative vegetation distribution map [*Wilson and Henderson-Sellers*, 1985] adjusted to include C4 vegetation [*Knorr*, 2000]. The vegetation distribution of *Wilson and Henderson-Sellers* is assembled on a 0.5° grid and is then transfered to the ECHAM 5.6° grid [*Knorr*, 1997]. Different transfer functions are possibly resulting in different vegetation distributions and therefore different CO_2 fluxes. Though, the CO_2 fluxes are comparable between different vegetation distributions but as explained earlier, these differences can be amplified by the water isotopic composition.
4. *Hoffmann et al.* [1998] showed that different horizontal model resolutions in ECHAM produce slightly different water isotopic compositions in the divers water pools. *Timmreck et al.* [1999] showed that a higher vertical resolution can overcome problems in the vertical advection formulation in ECHAM. Until now, I have stayed with the lowest horizontal and vertical resolution of ECHAM due to limited computer resources.
5. The isotopic exchange of highly enriched ozone with CO_2 in the stratosphere could not be included in the model because the stratosphere–troposphere exchange (STE) is possibly wrong in ECHAM by up to 75 % [*Timmreck et al.*, 1999; *Kjellström et al.*, 2000]. The isoflux appertaining to the STE is about four times higher than the isoflux resulting from fossil fuel combustion so that the STE can markedly change the model behaviour in δ^{18}O–CO_2. A higher vertical resolution shows a much more realistic STE and the STE accompanying isoflux could be included in the higher resolution model.

The model developed here allows for the first time to calculate the absolute $\delta^{18}O$–CO_2 concentration in the atmosphere. Former model studies had to tune their model to show no trend in atmospheric $\delta^{18}O$–CO_2 [*Ciais et al.*, 1997] and could therefore not calculate the absolute atmospheric $\delta^{18}O$–CO_2 value. The interactive formulation of the $\delta^{18}O$–CO_2 fluxes in my model allows to overcome this tuning and it is therefore possible to examine e. g. interannual variations in $\delta^{18}O$–CO_2. It is an open question, to which extent climate, water isotopic composition, and CO_2 flux variabilities determine the interannual variations in $\delta^{18}O$–CO_2, present in the observations.

The model builds a solid basis to include easily other tracers than CO_2 and $\delta^{18}O$–CO_2 like the O_2/N_2–ratio, $\delta^{18}O$–O_2, $\delta^{17}O$–O_2, or $\delta^{17}O$–CO_2. All these tracers allow to constrain different aspects of the global carbon cycle, namely the O_2/N_2–ratio constrains ocean CO_2 fluxes, $\delta^{18}O$–O_2 constrains the combined ocean and terrestrial productivity [*Keeling and Najjar*, 1993], $\delta^{17}O$–CO_2 constrains the STE [*Thiemens*, 1999], and $\delta^{17}O$–O_2 constrains STE together with terrestrial biosphere production [*Luz et al.*, 1999] i. e. CO_2 gross fluxes. Including all these tracers would narrow down the quite substantial error ranges on the CO_2 fluxes of the global carbon cycle.

Atmospheric transport inversions deduce surface fluxes from atmospheric measurements in changing the surface fluxes such that they would exhibit an almost perfect fit with observations transported in the specific transport model. But these inversion techniques are not only based on the consistency of modelled concentrations with measurements but they rely also on different prior assumptions regarding the unknown surface fluxes [*Kaminski et al.*, 2001]. The better the a priori estimates are the lower are the associated errors in the derived fluxes. Inversions in global carbon cycle sciences are mostly done with CO_2 mixing ratios deducing CO_2 net fluxes of the ocean and the terrestrial biosphere. But recently multi–tracer inversions started to be explored to reduce the degrees of freedom in the inversions [*Peylin*, 1999; *Rayner et al.*, 1999]. The results are still contradictory because the a priori isotope informations were not sufficient to reduce the degrees of freedom. Better estimates of the surface isofluxes are needed to determine eventually the terrestrial CO_2 gross fluxes from $\delta^{18}O$ in atmospheric CO_2.

References

Ciais, P., A. S. Denning, P. P. Tans, J. A. Berry, D. A. Randall, G. J. Collatz, P. J. Sellers, J. W. C. White, M. Trollier, H. A. J. Meijer, R. J. Francey, P. Monfray, and M. Heimann, A three dimensional synthesis study of $\delta^{18}O$ in atmospheric CO_2, part I: Surface fluxes, *J. Geophys. Res.*, *102*, 5 857–5 872, 1997.

Farquhar, G. D., J. Lloyd, J. A. Taylor, L. B. Flanagan, J. P. Syvertsen, K. T. Hubick, S. C. Wong, and J. R. Ehleringer, Vegetation effects on the isotope composition of oxygen in atmospheric CO_2, *Nature*, *363*, 439–443, 1993.

Hoffmann, G., M. Werner, and M. Heimann, Water isotopes module of the ECHAM atmospheric general circulation model: A study on timescales from days to several years, *J. Geophys. Res.*, *103*, 16 871–16 896, 1998.

Kaminski, T., M. Heimann, P. Peylin, P. Bousquet, and P. Ciais, Inverse modeling of atmospheric carbon dioxide fluxes, *Science*, *294*, 259, 2001.

Kaminski, T., W. Knorr, M. Heimann, and P. J. Rayner, Assimilating atmospheric data into a terrestrial biosphere model: A case study of the seasonal cycle, *J. Geophys. Res.*, p. submitted, 2002.

Keeling, R. F., and R. P. Najjar, What atmospheric oxygen measurements can tell us about the global carbon cycle, *Global Biogeoch. Cycl.*, *7*, 37–67, 1993.

Kjellström, E., J. Feichter, and G. Hoffmann, Transport of SF_6 and $^{14}CO_2$ in the atmospheric general circulation model ECHAM4, *Tellus*, *52B*, 1–18, 2000.

Knorr, W., Satellite remote sensing and modelling of the global CO_2 exchange of land vegetation: a synthesis study, Ph.D. thesis, Max–Planck Institute for Meteorologie, Hamburg, 1997, in german.

Knorr, W., Annual and interannual CO_2 exchange of the terrestrial biosphere: process–based simulations and uncertainties, *Global Ecology and Biogeography*, *9*, 225–252, 2000.

Lloyd, J., and J. A. Taylor, On the temperature dependance of soil respiration, *Functional Ecology*, *8*, 315–323, 1994.

Luz, B., E. Barkan, M. L. Bender, M. H. Thiemens, and K. A. Boering, Triple–isotope composition of atmospheric oxygen as a tracer of biosphere productivity, *Nature*, *400*, 547–550, 1999.

Mattson, K. G., CO_2 efflux from coniferous forest soils: comparison of measurement methods and effects of added nitrogen, in *Soils and Global Change*, edited by R. Lal, J. Kimble, E. Levine, and B. A. Stewart, pp. 329–342, CRC Press, Inc., Boca Raton, Florida, 1995.

Peylin, P., The composition of ^{18}O in atmospheric CO_2: A new tracer to estimate global photosynthesis, Ph.D. thesis, L'Université Paris VI, Paris, 1999, in french.

Raich, J. W., and C. S. Potter, Global patterns of carbon dioxide emissions from soils, *Global Biogeoch. Cycl.*, *9*, 23–36, 1995.

Rayner, P. J., I. G. Enting, R. J. Francey, and R. Langenfelds, Reconstructing the recent carbon cycle from atmospheric CO_2, ^{13}C and O_2/N_2 observations, *Tellus*, *51B*, 213–232, 1999.

Riley, W. J., C. J. Still, M. S. Torn, and J. A. Berry, A mechanistic model of $H_2^{18}O$ and $C^{18}OO$ fluxes between ecosystems and the atmosphere: Model description and sensitivity analyses, *Global Biogeoch. Cycl.*, 2002, in press.

Thiemens, M. H., Mass–independent isotope effects in planetary atmospheres and the early solar system, *Science*, *283*, 341–345, 1999.

Timmreck, C., H.-F. Graf, and J. Feichter, Simulation of Mt. Pinatubo volcanic aerosol with the Hamburg climate model ECHAM4, *Theor. Appl. Climatol.*, *62*, 85–108, 1999.

Wilson, M. F., and A. Henderson-Sellers, A global archive of land cover and soils data for use in general circulation models, *J. Climate*, *5*, 119–143, 1985.

List of Figures

List of Tables

Bibliography

Aizen, E. M., V. B. Aizen, J. M. Melack, T. Nakamura, and T. Ohta, Precipitation and atmospheric circulation patterns at mid–latitudes of asia, *Int. J. Climatol.*, *21*, 535–556, 2001.

Allison, C. E., R. J. Francey, and H. A. Meijer, Recommandations for the reporting of stable isotope measurements of carbon and oxygen in CO_2 gas, in *References and Intercomparison Materials for Stable isotopes of Light Elements*, edited by IAEA-TECDOC-825, pp. 155–162, Int. At. Energy Agency, Vienna, 1995.

Andres, R. J., G. Marland, I. Fung, and E. Matthews, A 1 x 1 distribution of carbon dioxide emissions from fossil fuel consumption and cement manufacture, 1950–1990, *Global Biogeoch. Cycl.*, *10*, 419–429, 1996.

Anthoni, P. M., B. E. Law, and M. H. Unsworth, Carbon and water vapor exchange of an open–conopied ponderosa pine ecosystem, *Agricultural and Forest Meteorology*, *95*, 151–168, 1999.

Arpe, K., L. Bengtsson, L. Dümenil, and E. Roeckner, The hydrological cycle in the ECHAM3 simulations of the atmospheric circulation, in *Global Precipitation and Climate Change*, edited by M. Desbois and F. Desalmand, pp. 361–377, Springer–Verlag, New York, 1994.

Aubinet, M., B. Chermanne, M. Vandenhaute, B. Longdoz, M. Yernaux, and E. Laitat, Long term carbon dioxide exchange above a mixed forest in the belgian ardennes, *Agricultural and Forest Meteorology*, *108*, 293–315, 2001.

Baertschi, P., Absolute ^{18}O content of Standard Mean Ocean Water, *Earth Planet. Sci. Lett.*, *31*, 314–344, 1976.

Bakwin, P. S., P. P. Tans, J. W. C. White, and R. J. Andres, Determination of the isotopic $^{13}C/^{12}C$ discrimination by terrestrial biology from a global network of observations, *Global Biogeoch. Cycl.*, *12*, 555–562, 1998.

Baldocchi, D., E. Falge, and K. Wilson, A spectral analysis of biosphere–atmosphere trace gas flux densities and meteorological variables across hour to multi–year time scales, *Agricultural and Forest Meteorology*, *107*, 1–27, 2001.

Ball, J. T., Calculations related to gas exchange, in *Stomatal Function*, edited by E. Zeiger, G. D. Farquhar, and I. R. Cowan, pp. 445–476, Stanford University Press, Stanford, CA, 1987.

Barford, C. C., S. C. Wofsy, M. L. Goulden, J. W. Munger, E. H. Pyle, S. P. Urbanski, L. Hutyra, S. R. Saleska, D. Fitzjarrald, and K. Moore, Factors controlling long– and short–term sequestration of atmospheric CO_2 in a mid–latitude forest, *Science*, *294*, 1 688–1 691, 2001.

Bariac, T., J. Gonzalez-Dunia, N. Katerji, O. Béthenod, J. M. Bertolini, and A. Mariotti, Variabilité spatialle de la composition isotopique de l'eau (^{18}O, ^{2}H) dans le continuum sol–plante–atmosphère : 2. approche en conditions naturelles, *Chemical Geology (Isotope Geoscience Section)*, *115*, 317–333, 1994a.

Bariac, T., J. Gonzalez-Dunia, D. Tessier, and A. Mariotti, Variabilité spatialle de la composition isotopique de l'eau (^{18}O, ^{2}H) au sein des organes des plantes aériennes : 1. approche en conditions controlées, *Chemical Geology (Isotope Geoscience Section)*, *15*, 307–315, 1994b.

Bernhofer, C., M. Aubinet, R. Clement, A. Grelle, T. Grünwald, A. Ibrom, P. Jarvis, C. Rebmann, E.-D. Schulze, and J. D. Tenhunen, Spruce forests (norway and sitka spruce, including douglas fir): Carbon and water fluxes and balances, ecological and ecophysiological determinants, in *Biospheric exchanges of carbon, water, and energy of European forests*, edited by R. Valentini et al., Ecological Studies, Springer Verlag, Berlin, Heidelberg, 2002, in press.

Bousquet, P., P. Peylin, P. Ciais, C. L. Quéré, F. P., and P. P. Tans, Regional changes in carbon dioxide fluxes of land and oceans since 1980, *Science*, *290*, 1 342–1 346, 2000.

Bowling, D. R., D. D. Baldocchi, and R. K. Monson, Partitioning net ecosystem exchange in a tennesse deciduous forest using stable isotopes of CO_2, Poster presentation, Ecological Society of America Annual Meeting, Spokane, WA, August 8–12, 1999.

Boyer, J. S., S. C. Wong, and G. D. Farquhar, CO_2 and water vapor exchange across leaf cuticle (epidermis) at various water potentials, *Plant Physiol.*, *114*, 185–191, 1997.

Brenninkmeijer, C. A. M., P. Kraft, and W. G. Mook, Oxygen isotope fractionation between CO_2 and H_2O, *Isotope Geoscience*, *1*, 181–190, 1983.

Burba, G. G., and S. B. Verma, Prairie growth, PAR albedo and seasonal distribution of energy fluxes, *Agricultural and Forest Meteorology*, *107*, 227–240, 2001.

Chevillard, A., U. Karstens, P. Ciais, S. Lafont, and M. Heimann, Simulation of atmospheric CO_2 over Europe and Siberia using the regional scale model REMO, *Tellus*, *54B*, 2002, in press.

Ciais, P., P. P. Tans, M. Trolier, J. W. White, and R. J. Francey, A large northern hemisphere terrestrial CO_2 sink indicated by the $^{13}C/^{12}C$ ratio of atmospheric CO_2, *Science*, *269*, 1 098–1 102, 1995a.

Ciais, P., P. P. Tans, W. C. White, M. Trolier, R. J. Francey, J. A. Berry, D. R. Randall, P. J. Sellers, F. G. Collatz, and D. S. Schimel, Partitioning of ocean and land uptake of CO_2 as inferred by $\delta^{13}C$ measurements from the NOAA climate monitoring and diagnostics laboratory global air sampling, *J. Geophys. Res.*, *100*, 5 051–5 070, 1995b.

Ciais, P., A. S. Denning, P. P. Tans, J. A. Berry, D. A. Randall, G. J. Collatz, P. J. Sellers, J. W. C. White, M. Trollier, H. A. J. Meijer, R. J. Francey, P. Monfray, and M. Heimann, A three dimensional synthesis study of $\delta^{18}O$ in atmospheric CO_2, part I: Surface fluxes, *J. Geophys. Res.*, *102*, 5 857–5 872, 1997a.

Ciais, P., P. P. Tans, A. S. Denning, R. J. Francey, M. Trollier, H. J. Meijer, J. W. C. White, J. A. Berry, D. A. Randall, J. J. G. Collatz, P. J. Sellers, P. Monfray, and M. Heimann, A three dimensional synthesis study of $\delta^{18}O$ in atmospheric CO_2, part II: Simulations with the TM2 transport model, *J. Geophys. Res.*, *102*, 5 873–5 883, 1997b.

Ciais, P., P. Peylin, and P. Bousquet, Regional biospheric carbon fluxes as inferred from atmospheric CO_2 measurements, *Ecol. Appl.*, *10*, 1 574–1 589, 2000.

Ciais, P., R. J. Francey, P. S. Bakwin, K. A. Masarie, and P. P. Tans, Atmospheric CO_2 and tracers measurements to monitor the carbon cycle and its future evolution, in *Sixth International Carbon Dioxide Conference: extended abstracts*, pp. 1–4, Organizing Committee of the 6^{th} Conference, Sendai, Japan, 2001.

Collatz, G. J., M. Ribas-Carbo, and J. A. Berry, Coupled photosynthesis–stomatal conductance model for leaves of C_4 plants, *Aust. J. Plant Physiol*, *19*, 519–538, 1992.

Craig, H., and L. I. Gordon, *Deuterium and oxygen–18 variations in the Ocean and the Marine Atmosphere*, Cons. Naz. delle Ric., Lab. di Geol. Nucl., Tries, Italy, 1965.

Cuntz, M., P. Ciais, and G. Hoffmann, Modelling the continental effect of oxygen isotopes over Eurasia, *Tellus*, *54B*, 2002, in press.

Dansgaard, W., Stable isotopes in precipitation, *Tellus*, *16*, 436–468, 1964.

Denning, A. S., I. Y. Fung, and D. A. Randall, Latitudinal gradient of atmospheric CO_2 due to seasonal exchange with land biota, *Nature*, *376*, 240–243, 1995.

Denning, A. S., G. J. Collatz, C. Zhang, D. A. Randall, J. A. Berry, P. J. Sellers, G. D. Colello, and D. A. Dazlich, Simulations of terrestrial carbon metabolism and atmospheric CO_2 in a general circulation model, part 1: Surface carbon fluxes, *Tellus*, *48B*, 521–542, 1996a.

Denning, A. S., D. A. Randall, G. J. Collatz, and P. J. Sellers, Simulations of terrestrial carbon metabolism and atmospheric CO_2 in a general circulation model, part 2: Simulated CO_2 concentrations, *Tellus*, *48B*, 543–567, 1996b.

Dongmann, G., H. W. Nürnberg, H. Förstel, and K. Wagner, On the enrichment of $H_2{}^{18}O$ in the leaves of transpiring plants, *Rad. and Environm. Biophys.*, *11*, 41–52, 1974.

Falge, E., D. Baldocchi, R. J. Olson, P. Anthoni, M. Aubinet, C. Bernhofer, G. Burba, R. Ceulemans, R. Clement, H. Dolman, A. Granier, P. Gross, T. Grünwald, D. Hollinger, N.-O. Jensen, G. Katul, P. Keronen, A. Kowalski, C. T. Lai, B. E. Law, T. Meyers, J. Moncrieff, E. Moors, J. W. Munger, K. Pilegaard, Ü. Rannik, C. Rebmann, A. Suyker, J. Tenhunen, K. Tu, S. Verma, T. Vesala, K. Wilson, and S. Wofsy, Gap filling strategies for defensible annual sums of net ecosystem exchange, *Agricultural Forest and Meteorology*, *107*, 43–69, 2001a.

Falge, E., D. Baldocchi, R. J. Olson, P. Anthoni, M. Aubinet, C. Bernhofer, G. Burba, R. Ceulemans, R. Clement, H. Dolman, A. Granier, P. Gross, T. Grünwald, D. Hollinger, N.-O. Jensen, G. Katul, P. Keronen, A. Kowalski, C. T. Lai, B. E. Law, T. Meyers, J. Moncrieff, E. Moors, J. W. Munger, K. Pilegaard, Ü. Rannik, C. Rebmann, A. Suyker, J. Tenhunen, K. Tu, S. Verma, T. Vesala, K. Wilson, and S. Wofsy, Gap filling strategies for longterm energy flux data sets, *Agricultural Forest and Meteorology*, *107*, 71–77, 2001b.

Fan, S., M. Gloor, J. Mahlman, J. Pacala, J. Sarmiento, T. Takahashi, and P. Tans, Atmospheric and oceanic CO_2 data and models imply a large terrestrial carbon sink in North America, *Science*, *282*, 442–446, 1998.

Farquhar, G. D., and J. Lloyd, Carbon and oxygen isotope effects in the exchange of carbon dioxide between terrestrial plants and the atmosphere, in *Stable Isotopes and Plant Carbon–Water Relations*, edited by J. R. Ehleringer, A. E. Hall, and G. D. Farquhar, pp. 47–70, Academic Press, New York, 1993.

Farquhar, G. D., S. von Caemmener, and J. A. Berry, A biochemical model of photosynthesis CO_2 fixation in leaves of C_3 species, *Planta*, *149*, 78–90, 1980.

Farquhar, G. D., J. R. Ehleringer, and K. T. Hubick, Carbon isotope discrimination and photosynthesis, *Annu. Rev. Plant Physiol. Plant Mol. Biol.*, *40*, 503–537, 1989a.

Farquhar, G. D., K. T. Hubick, A. G. Condon, and R. A. Richards, Carbon isotope fractionation and plant water–use efficiency, in *Stable Isotopes in Ecological Research*, edited by P. W. Rundel, Springer–Verlag, New York, 1989b.

Farquhar, G. D., J. Lloyd, J. A. Taylor, L. B. Flanagan, J. P. Syvertsen, K. T. Hubick, S. C. Wong, and J. R. Ehleringer, Vegetation effects on the isotope composition of oxygen in atmospheric CO_2, *Nature*, *363*, 439–443, 1993.

Federer, C. A., Transpirational supply and demand: plant, soil, and atmospheric effects evaluated by simulation, *Water Resour. Res.*, *18*, 355–362, 1982.

Fischer, R. A., and N. C. Turner, Plant productivity in the arid and semiarid zones, *Ann. Rev. Plant Physiol.*, *29*, 277–317, 1978.

Förstel, H., A. Putral, G. Schleser, and H. Leith, The world pattern of oxygen–18 in rain water and its importance in understanding the biogeochemical oxygen cycle, in *Isotope Ratios as Pollutant Source and Behavier Indicators*, pp. 323–344, Int. At. Energy Agency, Vienna, 1975.

Francey, R. J., and H. S. Goodman, The DAR stable isotope reference scale for CO_2, in *Baseline Atmospheric Program (Australia) 1986*, edited by B. W. Forgan and P. J. Fraser, pp. 40–46, Department of Administrative Services, Bureau of Meteorology in cooperation with CSIRO Division of Atmospheric Research, 1988.

Francey, R. J., and P. P. Tans, Latitudinal variation in oxygen–18 of atmospheric CO_2, *Nature*, *327*, 495–497, 1987.

Fung, I., C. B. Field, J. A. Berry, M. V. Thompson, J. T. Randerson, C. M. Malmstroem, P. M. Vitousek, G. J. Collatz, P. J. Sellers, D. A. Randall, A. S. Denning, F. Badeck, and J. John, Carbon 13 exchanges between the atmosphere and biosphere, *Global Biogeoch. Cycl.*, *11*, 507–533, 1997.

Gamo, T., M. Tsutsumi, H. Sakai, T. Nakazawa, M. Tanaka, H. Honda, H. Kubo, and T. Itoh, Carbon and oxygen isotope ratios of carbon dioxide of a stratospheric profile over japan, *Tellus*, *41B*, 127–133, 1989.

Gemery, P. A., M. Trolier, and J. W. C. White, Oxygen isotopic exchange between carbon dioxide and water following atmospheric sampling using glass flasks, *J. Geophys. Res.*, *101*, 14 415–14 420, 1996.

Gillon, J., and D. Yakir, Internal conductance to CO_2 diffusion and $C^{18}OO$ discrimination in C_3 leaves, *Plant Physiology*, *123*, 201–213, 2000a.

Gillon, J., and D. Yakir, Naturally low carbonic anhydrase activity in C_4 and C_3 plants limits discrimination against $C^{18}OO$ during photosynthesis, *Plant, Cell and Environment*, *23*, 903–915, 2000b.

Gillon, J., and D. Yakir, Influence of carbonic anhydrase activity in terrestrial vegetation on the ^{18}O content of atmospheric CO_2, *Science*, *291*, 2 584–2 587, 2001.

GLOBALVIEW-CO_2, Cooperative atmospheric data integration project — carbon dioxide, CD–ROM, NOAA CMDL, Boulder, Colorado [Also available on Internet via anonymous FTP to ftp.cmdl.noaa.gov, Path: ccg/co2/GLOBALVIEW], 2002.

Goldstein, A. H., N. E. Hultman, J. M. Fracheboud, M. R. Bauer, J. A. Panek, M. Xu, Y. Qi, A. B. Guenther, and W. Baugh, Effects of climate variability on the carbon dioxide, water, and sensible heat fluxes above a ponderosa pine plantation in the sierra nevada (CA), *Agricultural and Forest Meteorology*, *101*, 113–129, 2000.

Granier, A., Sarrebourg, France, the Euroflux data set 2000, in *Carbon, Water and Energy exchanges of European forests*, edited by R. Valentini et al., Ecological Studies, Springer Verlag, Heidelberg, 2002, in press.

Grünwald, T., and C. Bernhofer, Data gap filling with regression modelling, in *Forest ecosystem modelling, upscaling and remote sensing*, edited by R. J. M. Ceulemans, F. Veroustrate, V. Gond, and J. B. H. F. Van Rensbergern, pp. 61–67, SPB Academic Publishing bv, The Haque, The Netherlands, 2000.

Gurney, K. R., R. M. Law, A. S. Denning, P. J. Rayner, D. Baker, P. Bousquet, L. Bruhwiler, Y. H. Chen, P. Ciais, S. Fan, I. Y. Fung, M. Gloor, M. Heimann, K. Higuchi, J. John, T. Maki, S. Maksyutov, K. Masarie, P. Peylin, M. Prather, B. C. Pak, J. Randerson, J. Sarmiento, S. Taguchi, T. Takahashi, and C. W. Yuen, Towards robust regional estimates of annual mean CO_2 sources and sinks, *Nature*, *415*, 626–630, 2002.

Hao, W. M., and M.-H. Liu, Spatial and temporal distribution of tropical biomass burning, *Global Biogeoch. Cycl.*, *8*, 495–503, 1994.

Heimann, M., The global atmospheric tracer model TM2, *Tech. Rep. 10*, Deutsches Klimarechenzentrum, Hamburg, 1995.

Heimann, M., and C. D. Keeling, A three–dimentional model of atmospheric CO_2 transport based on observed winds: 2. model description and simulated tracer experiments, in *Aspects of climate variability in the Pacific and the Western Americas, Geophysical monograph 55*, edited by P. D. H., pp. 237–275, AGU, 1989.

Hesshaimer, V., Tracing the global carbon cycle with bomb radiocarbon, Ph.D. thesis, Universiät Heidelberg, 1997.

Hoffmann, G., M. Werner, and M. Heimann, Water isotopes module of the ECHAM atmospheric general circulation model: A study on timescales from days to several years, *J. Geophys. Res.*, *103*, 16 871–16 896, 1998.

Hoffmann, G., V. Masson, and J. Jouzel, Stable water isotopes in atmospheric general circulation models, *Hydrological Processes*, *14*, 1 385–1 406, 2000.

Hollinger, D. Y., S. M. Goltz, E. A. Davidson, J. T. Lee, K. Tu, and H. T. Valentine, Seasonal patterns and environmental control of carbon dioxide and water vapour exchange in an ecotonal boreal forest, *Global Change Biology*, *5*, 891–902, 1999.

IAEA/WMO, Global network of isotopes in precipitation, The GNIP Database. Accessible at: http://isohis.iaea.org, 2001.

Janssens, I. A., A. S. Kowalski, and R. Ceulemans, Intercomparison of forest floor CO_2 efflux estimates by eddy correlation and a chamber–based empirical model, *Agricultural and Forest Meteorology*, *106*, 61–69, 2001.

Jones, H. G., *Plants and Microclimate*, Cambridge University Press, Cambridge, UK, 1983.

Jouzel, J., G. L. Russell, R. J. Suozzo, R. D. Koster, J. W. C. White, and W. S. Broecker, Simulations of the HDO and $H_2^{18}O$ atmospheric cycles using the NASA/GISS general circulation model: The seasonal cycle for present–day conditions, *J. Geophys. Res.*, *92*, 14 739–14 760, 1987.

Kaminski, T., M. Heimann, P. Peylin, P. Bousquet, and P. Ciais, Inverse modeling of atmospheric carbon dioxide fluxes, *Science*, *294*, 259, 2001.

Kaminski, T., W. Knorr, M. Heimann, and P. J. Rayner, Assimilating atmospheric data into a terrestrial biosphere model: A case study of the seasonal cycle, *J. Geophys. Res.*, p. submitted, 2002.

Keeling, C. D., The concentration and isotopic abundances of carbone dioxide in rural and marine air, *Geochim. Cosmochim. Acta*, pp. 277–298, 1961.

Keeling, C. D., R. B. Bacastow, A. F. Carter, S. C. Piper, T. P. Whorf, M. Heimann, W. G. Mook, and H. Roeloffzen, A three–dimensional model of atmospheric CO_2 transport based on observed winds, 1. Analysis on observational data, in *Aspects of Climate Variability in the Pacific and the Western Americas, Geophys. Monogr. Ser.*, edited by D. H. Peterson, vol. 55, pp. 165–236, AGU, Washington, D.C., 1989.

Keeling, R. F., and R. P. Najjar, What atmospheric oxygen measurements can tell us about the global carbon cycle, *Global Biogeoch. Cycl.*, *7*, 37–67, 1993.

Kicklighter, D. W., A. Bondeau, A. L. Schloss, J. Kaduk, A. D. McGuire, and T. P. of the Potsdam NPP Model Intercomparison, Comparing global models of terrestrial net primary productivity (npp): global pattern and differentiation by major biomes, *Global Change Biology*, *5 (Suppl. 1)*, 16–24, 1999.

Kjellström, E., J. Feichter, and G. Hoffmann, Transport of SF_6 and $^{14}CO_2$ in the atmospheric general circulation model ECHAM4, *Tellus*, *52B*, 1–18, 2000.

Kjellström, E., K. Holmén, K. Eneroth, and M. Engardt, Summertime siberian CO_2 simulations with the regional transport model MATCH: A feasibility study of carbon uptake calculations from EUROSIB data, *Tellus*, *54B*, 2002, in press.

Knorr, W., Satellite remote sensing and modelling of the global CO_2 exchange of land vegetation: a synthesis study, Ph.D. thesis, Max–Planck Institute for Meteorologie, Hamburg, 1997, in german.

Knorr, W., Annual and interannual CO_2 exchange of the terrestrial biosphere: process–based simulations and uncertainties, *Global Ecology and Biogeography*, *9*, 225–252, 2000.

Knorr, W., and M. Heimann, Impact of drought stress and other factors on seasonal land biosphere CO_2 exchange studied through an atmospheris tracer transport model, *Tellus*, *47B*, 471–489, 1995.

Knorr, W., and M. Heimann, Uncertainties in global terrestrial biosphere modeling: 1. a comprehensive sensitivity analysis with a new photosynthesis and energy balance scheme, *Global Biogeoch. Cycl.*, *1*, 207–225, 2001a.

Knorr, W., and M. Heimann, Uncertainties in global terrestrial biosphere modeling: Part ii: Global constraints for a process–based vegetation model, *Global Biogeoch. Cycl.*, *1*, 227–246, 2001b.

Lai, C. T., G. Katul, J. Butnor, D. Ellsworth, and R. Oren, Modelling night–time ecosystem respiration by a constrained source optimization method, *Global Change Biology*, *8*, 124–141, 2002.

Langendörfer, U., M. Cuntz, P. Ciais, P. Peylin, T. Bariac, I. Milyukova, O. Kolle, T. Naegler, and I. Levin, Modelling of biospheric CO_2 gross fluxes via oxygen isotopes in a spruce forest canopy: a ^{222}Rn calibrated box model approach, *Tellus*, *54B*, 2002, in press.

Law, B. E., P. Thornton, J. Irvine, S. Van Tuyl, and P. M. Anthoni, Carbon storage and fluxes in ponderosa pine forests at different developmental stages, *Global Change Biology*, *7*, 755–777, 2001.

Law, R. M., P. J. Rayner, A. S. Denning, D. Erickson, I. Y. Fung, M. Heimann, S. C. Piper, M. Ramonet, S. Taguchi, J. A. Taylor, C. M. Trudinger, and I. G. Watterson, Variations in modeled atmospheric transport of carbone dioxide and the consequences for CO_2 inversion, *Global Biogeoch. Cycl.*, *4*, 1996, 783–796.

Levin, I., J. Schuchard, B. Kromer, and K. O. Münnich, The continental European Suess effect, *Radiocarbon*, *31*, 431–440, 1989.

Levin, I., P. Ciais, R. Langenfelds, M. Schmidt, M. Ramonet, K. Sidorov, N. Tchebakova, M. Gloor, M. Heimann, E.-D. Schulze, N. N. Vygodskaya, O. Shibistova, and J. Lloyd, Three years of trace gas observations over the eurosiberian domain derived from aircraft sampling — a concerted action, *Tellus*, *54B*, 2002a, in press.

Levin, I., U. Langendörfer, M. Schmidt, C.Facklam, M. Ramonet, C. Bourg, V. Kazan, P. Ciais, R. L. Langenfelds, C. E. Allison, R. J. Francey, A. Jordan, W. A. Brand, R. E. M. Neubert, H. A. J. Meijer, and K. Holmén, Eurosiberian carbonflux — CO_2 intercomparison, in *Report of the eleventh WMO/IAEA meeting of experts on carbon dioxide concentration and related tracer measurement techniques, Tokyo, 25.–28. Sep. 2001*, edited by S. Toru, chap. 3.8, pp. 35–50, World Meteorological Organisation, 2002b, in press.

Lindroth, A., Flakaliden, Sweden, the Euroflux data set 2000, in *Carbon, Water and Energy exchanges of European forests*, edited by R. Valentini et al., Ecological Studies, Springer Verlag, Heidelberg, 2002, in press.

Lindroth, A., and S. Halldin, Numerical analysis of pine forest evaporation and surface resistance, *Agriculture and Forest Meteorology*, *38*, 59–79, 1986.

Lindroth, A., A. Grelle, and A. S. Moren, Long–term measurements of boreal forest carbon balance reveal large temperature sensitivity, *Global Change Biology*, *4*, 443–450, 1998.

Lloyd, J., and G. D. Farquhar, ^{13}C discrimination during CO_2 assimilation by the terrestrial biosphere, *Oecologia*, *99*, 201–215, 1994.

Lloyd, J., and J. A. Taylor, On the temperature dependance of soil respiration, *Functional Ecology*, *8*, 315–323, 1994.

Lloyd, J., R. L. Langenfelds, R. J. Francey, M. Gloor, N. M. Tschebakova, D. Zolotukhine, W. A. Brand, R. A. Werner, A. Jordan, C. A. Allison, V. Zrazhewske, O. Shibistova, and E.-D. Schulze, A trace gas climatology above Zotino, central Siberia, *Tellus*, *54B*, 2002a, in press.

Lloyd, J., O. Shibistova, D. Zolothukhine, O. Kolle, A. Arneth, J. Styles, N. M. Tchebakova, and E.-D. Schulze, Seasonal and annual variations in the photosynthetic productivity and carbon balance of a central Siberian pine forest, *Tellus*, *54B*, 2002b, in press.

Long, S. P., E. G. Moya, S. K. Imbamba, A. Kamnalrut, M. T. F. Piedade, J. M. O. Scurlock, Y. K. Shen, and D. O. Hall, Primary productivity of natural grass ecosystems of the tropics: a reappraisal, *Plant and Soil*, *115*, 155–166, 1989.

Luz, B., E. Barkan, M. L. Bender, M. H. Thiemens, and K. A. Boering, Triple–isotope composition of atmospheric oxygen as a tracer of biosphere productivity, *Nature*, *400*, 547–550, 1999.

Mahowald, N. M., P. J. Rasch, and R. G. Prinn, Cumulus parameterizations in chemical transport models, *J. Geophys. Res.*, *100*, 26 173–26 189, 1995.

Majoube, M., Fractionnement en oxygene–18 et en deuterium entre l'eau et sa vapeur, *Journal de Chimie et Physique*, *58*, 1 423–1 436, 1971.

Markkanen, T., Ü. Rannik, P. Keronen, T. Suni, and T. Vesala, Eddy covariance fluxes over a boreal scots pine forest, *Boreal Environment Research*, *6*, 65–78, 2001.

Marland, G., R. J. Andres, T. A. Boden, C. Johnston, and A. Brenkert, Global, regional and national CO_2 emission estimates from fossil fuel burning, cement production and gas flaring: 1751–1996 (revised March 1999), *Data Report ORNL NDP–030*, Carbon Dioxide Inf. Anal. Cent., Oak Ridge Natl. Lab., Oak Ridge, Tenn., 1998.

Masarie, K. A., R. L. Langenfelds, C. E. Allison, T. J. Conway, E. J. Dlugokencky, R. J. Francey, P. C. Novelli, L. P. Steele, P. P. Tans, B. Vaughn, and J. W. C. White, NOAA/CSIRO flask air intercomparison experiment: A strategy for directly assesing consistency among atmospheric measurements made by independent laboratories, *J. Geophys. Res.*, *106*, 20 445–20 464, 2001.

Mattson, K. G., CO_2 efflux from coniferous forest soils: comparison of measurement methods and effects of added nitrogen, in *Soils and Global Change*, edited by R. Lal, J. Kimble, E. Levine, and B. A. Stewart, pp. 329–342, CRC Press, Inc., Boca Raton, Florida, 1995.

Mauersberger, K., Measurements of heavy ozone in the stratosphere, *Geophysical Research Letters*, *8*, 935–937, 1981.

Meentemeyer, V., Macroclimate and lignin control of litter decomposition rates, *Ecology*, *59*, 465–472, 1978.

Melayah, A., L. Bruckler, and T. Bariac, Modeling the transport of water stable isotopes in unsaturated soils under natural conditions. 2. comparison with field experiments, *Water Resources Research*, *32*, 2 055–2 065, 1996.

Merlivat, L., and J. Jouzel, Global climatic interpretation of the deuterium–oxygen 18 relationship for precipitation, *Journal of Geophysical Research*, *84*, 5 029–5 033, 1979.

Meyers, T. P., A comparison of summertime water and CO_2 fluxes over rangeland for well watered and drought conditions, *Agricultural and Forest Meteorolog*, *106*, 205–214, 2001.

Miller, J. B., D. Yakir, J. W. C. White, and P. P. Tans, Measurement of $^{18}O/^{16}O$ in the soil–atmosphere CO_2 flux, *Global Biogeoch. Cycl.*, *13*, 761–774, 1999.

Miller, J. B., P. P. Tans, J. W. C. White, T. J. Conway, and B. W. Vaughn, The atmospheric signal of terrestrial carbon isotopic discrimination and its implication for partitioning carbon fluxes, *Tellus*, 2002, in press.

Mills, G. A., and H. C. Urey, The kinetics of isotopic exchange between carbon dioxide, bicarbonate ion, carbonate ion and water, *J. Am. Chem. Soc.*, *62*, 1 019–1 026, 1940.

Milyukova, I. M., O. E. Kolle, A. B. Varlagin, N. N. Vygodskaya, E.-D. Schulze, and J. Lloyd, Carbon balance of a southern taiga spruce stand in european russia, *Tellus*, *54B*, 2002, in press.

Miranda, A. C., H. S. Miranda, J. Lloyd, J. Grace, R. J. Francey, P. Riggan, and J. Brass, Fluxes of carbon dioxide and water vapour over cerrado vegetation in Central Brazil. An analysis using eddy correlation and stable isotope techniques, *Plant, Cell and Environment*, *20*, 315–328, 1996.

Modellbetreuungsgruppe, The ECHAM3 atmospheric general circulation model, *Tech. Rep. 6*, Deutsches Klimarechenzentrum, Hamburg, 1994.

Oechel, W. C., G. L. Vourlitis, S. J. Hastings, R. P. Ault, and P. Bryant, The effects of water table manipulation and elevated temperature on the net CO_2 flux of wet sedge tundra ecosystems, *Global Change Biology*, *4*, 77–90, 1998.

Olson, R. J., J. M. O. Scurlock, S. D. Prince, D. L. Zheng, and K. R. J. (eds.), NPP multi–biome: NPP and driver data for ecosystem model–data intercomparison, Available on–line [http://www.daac.ornl.gov/] from the Oak Ridge National Laboratory Distributed Active Archive Center, Oak Ridge, Tennessee, U.S.A., 2001.

Pataki, D. E., J. R. Ehleringer, L. B. Flanagan, D. Yakir, D. R. Bowling, C. Still, N. Buchmann, J. Kaplan, and J. A. Berry, The application and interpretation of keeling plots in terrestrial carbon cycle research, *Global Biogeoch. Cycl.*, 2002, in press.

Peylin, P., The composition of ^{18}O in atmospheric CO_2: A new tracer to estimate global photosynthesis, Ph.D. thesis, L'Université Paris VI, Paris, 1999, in french.

Peylin, P., P. Ciais, P. P. Tans, K. Six, J. A. Berry, and A. S. Denning, ^{18}O in atmospheric CO_2 simulated by a 3–D transport model: A sensitivity study to vegetation and soil fractionation factors, *Phys. and Chem. of the Earth*, *21*, 463–469, 1997.

Peylin, P., P. Ciais, A. S. Denning, P. P. Tans, J. A. Berry, and W. C. White, A three–dimensional study of $\delta^{18}O$ in atmospheric CO_2: contributin of different land ecosystems, *Tellus*, *51B*, 642–667, 1999.

Pilegaard, K., P. Hummelshoj, N. O. Jensen, and Z. Chen, Two years of continuous CO_2 eddy–flux measurements over a danish beech forest, *Agricultural and Forest Meteorology*, *107*, 29–41, 2001.

Prentice, I. C., G. D. Farquhar, M. J. R. Fasham, M. L. Goulden, M. Heimann, V. J. Jaramillo, H. S. Kheshgi, C. Le Quéré, R. J. Scholes, and D. W. R. Wallace, The carbon cycle and atmospheric CO_2, in *Third Assessment Report of Climate Change*, edited by J. T. Houghton and D. Yihui, Report of the International Panel on Climate Change, chap. 3, pp. 38–71, Cambridge University Press, New York, 2001.

Quay, P. D., B. Tilbrook, and C. S. Wong, Oceanic uptake of fossil fuel CO_2 : Carbon–13 evidence, *Science*, *256*, 74–79, 1992.

Raich, J. W., and C. S. Potter, Global patterns of carbon dioxide emissions from soils, *Global Biogeoch. Cycl.*, *9*, 23–36, 1995.

Raich, J. W., and W. H. Schlesinger, The global carbon dioxide flux in soil respiration and its relationship to vegetation and climate, *Tellus*, *44B*, 81–99, 1992.

Ramonet, M., and P. Monfray, CO_2 baseline concept in 3–D atmospheric transport models, *Tellus*, *48*, 502–520, 1996.

Ramonet, M., P. Ciais, I. Nepomniachii, K. Sidorov, J. Lloyd, R. Neubert, D. Picard, V. Kazan, S. Biraud, O. Kolle, and D. S. E, 3 years of aircraft CO_2 and isotope measurements over Fyodorovskoye in European Russia, *Tellus*, *54B*, 2002, in press.

Rasch, P. J., and D. L. Williamson, Computational aspects of moisture transport in global models of the atmosphere, *Q. J. R. Meteorol. Soc.*, *116*, 1 071–1 090, 1990.

Rayner, P. J., I. G. Enting, R. J. Francey, and R. Langenfelds, Reconstructing the recent carbon cycle from atmospheric CO_2, ^{13}C and O_2/N_2 observations, *Tellus*, *51B*, 213–232, 1999.

Riley, W. J., C. J. Still, M. S. Torn, and J. A. Berry, A mechanistic model of $H_2^{18}O$ and $C^{18}OO$ fluxes between ecosystems and the atmosphere: Model description and sensitivity analyses, *Global Biogeoch. Cycl.*, 2002, in press.

Roche, C., Interactions biosphere–atmosphere aux echelles locales et composition isotopique (^{13}C, ^{18}O) du CO_2 atmospherique : application a la foret landaise, Ph.D. thesis, Université Paris VI, Pierre et Marie Curie, 1999, in french.

Roden, J. S., and J. R. Ehleringer, Observations of hydrogen and oxygen isotopes in leaf water confirm the Craig–Gordon model under wide–ranging environmental conditions, *Plant Physiology*, *120*, 1 165–1 173, 1999.

Roeckner, E., K. Arpe, L. Bengtsson, S. Brinkop, L. Dümenil, M. Esch, E. Kirk, F. Lunkeit, M. Ponater, B. Rockel, R. Sausen, U. Schlese, S. Schubert, and M. Windelband, Simulation of the present–day climate with the ECHAM model: impact of model physics and resolution, *Tech. Rep. 93*, Max–Planck Institut für Meteorologie, Hamburg, 1992.

Roeckner, E., K. Arpe, L. Bengtsson, M. Christoph, M. Clausen, L. Dümenil, M. Esch, M. Giorgetta, U. Schlese, and U. Schulzweida, The atmospheric general circulation model ECHAM–4: Model description and simulation of present–day climate, *Tech. Rep. 218*, Max–Planck Institut für Meteorologie, Hamburg, 1996.

Running, S. W., D. D. Baldocchi, D. P. Turner, S. T. Gower, P. S. Bakwin, and K. A. Hibbard, A global terrestrial monitoring network intergrating tower fluxes, flask sampling, ecosystem modeling and EOS satellite data, *Remote Sensing of Environment*, *70*, 108–127, 1999, fLUXNET data available on–line [http://www.daac.ornl.gov/] from the Oak Ridge National Laboratory Distributed Active Archive Center, Oak Ridge, Tennessee, U.S.A.

Ryan, M. G., Effects of climate change on plant respiration, *Ecol. Appl.*, *1*, 157–167, 1991.

Schimel, D., D. Alves, I. Enting, M. Heimann, F. Joos, D. Raynaud, T. Wigley, M. Prather, R. Derwent, D. Ehhalt, P. Fraser, E. Sanhueza, X. Zhou, P. Jonas, R. Charlson, H. Rohde, S. Sadasivan, K. P. Shine, Y. Fouquart, V. Ramaswamy, S. Solomon, J. Srinivasan, D. Albritton, I. Isaken, M. Lal, and D. Wuebbles, 2. radiative forcing of climate change, in *Climate Change 95, The Science of Climate Change*, edited by J. Houghton, L. M. Filho, B. Callander, N. Harris, A. Kattenberg, and K. Maskell, pp. 65–131, Intergovt. Panel on Clim. Change, Cambridge, England, 1996.

Schmidt, M., R. Graul, H. Sartorius, and I. Levin, Carbon dioxide and methane in continental europe: a climatology, and ^{222}Radon-based emission estimates, *Tellus*, *48B*, 457–473, 1996.

Schmidt, M., R. Neubert, C. Facklam, R. Heinz, R.Weller, and I. Levin, Variability of CO_2 and its stable isotopes at Schauinsland (Germany) and Neumayer (Antarctica), in *Sixth International Carbon Dioxide Conference: extended abstracts*, pp. 116–119, Organizing Committee of the 6$^{\text{th}}$ Conference, Sendai, Japan, 2001.

Schulze, E.-D., Carbon dioxide and water exchange in response to drought in the atmosphere and in the soil, *Ann. Rev. Plant Physiol.*, *13*, 127–141, 1986.

Schulze, E.-D., N. C. Turner, T. Gollan, and K. A. Shakel, Stomatal response to air humidity and to soil drought, in *Stomatal Function*, edited by E. Zeiger, G. Farquhar, and I. Cowan, pp. 311–321, Stanford University Press, Stanford, USA, 1987.

Schulze, E.-D., F. M. Kelliher, C. Lloyd, and R. Leuning, Relationships among maximum stomatal conductance, ecosystem surface conductance, carbon assimilation rate, and plant nitrogen nutrition: a global ecology scaling exercise, *Ann. Rev. Ecol. Syst.*, *25*, 629–660, 1994.

Schulze, E.-D., N. N. Vygodskaya, N. Tschebakova, C. I. Czimczik, D. Kozlov, J. Lloyd, D. Mollicone, E. Myachkova, K. Sidorov, A. Varlagin, and C. Wirth, The eurosiberian transect: An introduction to the experimental region, *Tellus*, *54B*, 2002, in press.

Scurlock, J. M. O., K. Johnson, and R. J. Olson, Estimating net primary productivity from grassland biomass dynamics measurements, *Global Change Biology*, *8*, 736–753, 2002.

Sellers, P. J., Canopy reflectance, photosynthesis, and transpiration, *Int. J. Remote Sensing*, *6*, 1 335–1 372, 1985.

Sellers, P. J., S. O. Los, C. J. Tucker, C. O. Justice, D. A. Dazlich, G. J. Collatz, and D. A. Randall, A revised land surface parameterization (SiB2) for atmospheric GCM: Part II the generation of global fields of terrestrial biospherical parameters from satellite data, *J. Climate*, *9*, 706–737, 1996a.

Sellers, P. J., D. A. Randall, G. J. Collatz, J. A. Berry, C. B. Field, D. A. Dazlich, C. Zhang, and G. D. Collelo, A revised land surface parameterization (SiB2) for atmospheric GCM: Part I model formulation, *JOC*, *9*, 676–705, 1996b.

Shibistova, O., J. Lloyd, G. Zrazhewskaya, A. Arneth, O. Kolle, N. Astrakhantceva, I. Shijneva, A. Knohl, and J. Schmerler, Ecosystem respiration budget for a pinus sylvestris stand in central Siberia, *Tellus*, *54B*, 2002, in press.

Stephens, B. B., S. C. Wofsy, R. F. Keeling, P. P. Tans, and M. J. Potosnak, The CO_2 budget and rectification airborne study: Strategies for measuring rectifiers and regional fluxes, in *Inverse Methods in Global Biogeochemical Cycles*, edited by P. Kasibhatla et al., vol. 114 of *Geophysical Monograph Series*, pp. 311–324, American Geophysical Union, Washington D. C., 1999.

Stern, L. A., R. Amundson, and W. T. Baisden, Influence of soils on oxygen isotope ratio of atmospheric CO_2, *Global Biogeoch. Cycl.*, *15*, 753–760, 2001.

Stryer, L., *Biochemistry*, W. H. Freeman and Co, San Francisco, 1981.

Styles, J. M., J. Lloyd, D. Zolotukhin, K. A. Lawton, N. M. Tschebakova, R. J. Francey, A. A. Arneth, D. Salamakho, O. Kolle, and E.-D. Schulze, Estimates of regional surface CO_2 exchange and carbon and oxygen isotope discrimination during photosynthesis from concentration profiles in the atmospheric boundary layer, *Tellus*, *54B*, 2002a, in press.

Styles, J. M., M. R. Raupach, G. D. Farquhar, O. E. Kolle, K. A. Lawton, W. A. Brand, R. A. Werner, A. Jordan, E.-D. Schulze, O. Shibistova, and J. Lloyd, Soil and canopy CO_2, $^1 3CO_2$, H_2O and sensible heat flux partitions in a forest canopy inferred from concentration measurements, *Tellus*, *54B*, 2002b, in press.

Suits, N. S., A. S. Denning, J. A. Berry, C. J. Still, J. Kaduk, and J. Randerson, Seasonal and spatial variations in carbon isotopic ratios of plant biomass, terrestrial CO_2 fluxes and atmospheric CO_2, *Global Biogeoch. Cycl.*, 2002, in review.

Takahashi, T., R. H. Wanninkhof, R. A. Feely, R. F. Weiss, D. W. Chipman, N. Bates, J. Olafsson, C. Sabine, and S. C. Sutherland, Net sea–air CO_2 flux over the global oceans: An improved estimate based on the sea–air pCO_2 difference, in *2nd International Symposium, CO_2 in the Oceans, extended abstracts*, Center Global Env. Res., Tsukuba, Japan, 1999.

Tans, P. P., Oxygen isotopic equilibrium between carbon dioxide and water in soils, *Tellus*, *50B*, 163–178, 1998, with Erratum, *Tellus, 50B*, 400, 1998.

Tans, P. P., I. Y. Fung, and T. Takahashi, Observational constraints on the global atmospheric carbon dioxide budget, *Science*, *247*, 1 431–1 438, 1990.

Tans, P. P., J. A. Berry, and R. F. Keeling, Oceanic ^{13}C data: a new window on CO_2 uptake by the oceans, *Global Biogeoch. Cycl.*, *7*, 353–368, 1993.

Taylor, J. A., Atmospheric mixing and the CO_2 seasonal cycle, *Geophysical Research Letters*, *25*, 4 173–4 176, 1998.

Thiemens, M. H., Mass–independent isotope effects in planetary atmospheres and the early solar system, *Science*, *283*, 341–345, 1999.

Timmreck, C., H.-F. Graf, and J. Feichter, Simulation of Mt. Pinatubo volcanic aerosol with the Hamburg climate model ECHAM4, *Theor. Appl. Climatol.*, *62*, 85–108, 1999.

Trolier, M., J. W. C. White, P. P. Tans, K. A. Massarie, and P. A. Gemery, Monitoring the isotopic composition of atmospheric CO_2: Measurements from the NOAA global air sampling network, *J. Geophys. Res.*, *101*, 25 897–25 916, 1996.

Turner, N. C., Adaptation to water deficits: a changing perspective, *Aust. J. Plant Physiol.*, *13*, 338–342, 1986.

Vesala, T., Hyytiälä, Finland, the Euroflux data set 2000, in *Carbon, Water and Energy exchanges of European forests*, edited by R. Valentini et al., Ecological Studies, Springer Verlag, Heidelberg, 2002, in press.

Vogel, J. C., P. M. Grootes, and W. G. Mook, Isotopic fractionation between gaseous and dissolved carbon dioxide, *Z. Phys.*, *230*, 225–238, 1970.

Wanninkhof, R., Relationship between wind speed and gas exchange over the ocean, *J. Geophys. Res.*, *97*, 7 373–7 382, 1992.

Werner, M., Räumliche und zeitliche variabilität von wasserisotopen im polaren niederschlag, Ph.D. thesis, Universiät Hamburg, 2000, in german.

Werner, M., M. Heimann, and G. Hoffmann, Isotopic composition and origin of polar precipitation in present and glacial climate simulations, *Tellus*, *53B*, 53–71, 2001.

White, J. W. C., The climatic significance of D/H ratios in white pine in the Northeastern United States, Ph.D. thesis, Columbia University, New York, 1983.

Wilson, M. F., and A. Henderson-Sellers, A global archive of land cover and soils data for use in general circulation models, *J. Climate*, *5*, 119–143, 1985.

Yakir, D., Oxygen–18 of leaf water: a crossroad for plant–associated isotopic signals, in *Stable isotopes: integration of biological, ecological and geochemical processes*, edited by H. Griffiths, chap. 10, pp. 147–168, βIOS Scientific Publisher Limited, Oxford, UK, 1998.

Yakir, D., and L. S. L. Sternberg, The use of stable isotopes to study ecosystem gas exchange, *Oecologia*, *123*, 297–311, 2000.

Yakir, D., and X.-F. Wang, Fluxes of CO_2 and water between terrestrial vegetation and the atmosphere estimated from isotope measurements, *Nature*, *380*, 515–517, 1996.

Zahn, A., R. Neubert, M. Maiss, and U. Platt, Fate of long–lived trace species near the northern hemispheric tropopause: Carbon dioxide, methane, ozone, and sulfur hexafluoride, *J. Geophys. Res.*, *104*, 13 923–13 942, 1999.

Zahn, A., R. Neubert, and U. Platt, Fate of long–lived trace species near the northern hemispheric tropopause: 2. isotopic composition of carbon dioxide ($^{13}CO_2$, $^{14}CO_2$, and $C^{18}O^{16}O$), *J. Geophys. Res.*, *105*, 6 719–6 735, 2000.

Merci

Every little helps. So I would like to thank all little bits and pieces contributing, helping, and supporting one way or another this thesis.

MERCI to 'little big boss' **Philippe Ciais** for the never–ending energy and the joy for isotopes. *MERCI* to 'little boss' **Georg Hoffmann**, I would have cracked several times without you. *MERCI* to 'big boss' **Ingeborg Levin** being the very needed complementary pole to the 'French touch'.

Also a big *MERCI* to the 'Germans' at the institute who make you forget sometimes that you are far away from home: *Merci* **Susanne** for the coffees in our favourite Café; *Merci* **Martina** for the compassionate smile to all my stupid questions; *Merci* **Tobias** for the life at ease in the flat, most times; *Merci* **Norbert** for all the tattle, not only 'de la vallée'; *Merci* **Sandra**, speech and poster designer par excellence.

But what would be France without the Frenchmen: *Merci* **Titi**, 'dogs bollocks' is waiting for us; *Merci* **Anne**, I still want you back in my office; *Merci* **Gaëlle**, the joy of life is very becoming to you; *Merci* **Seb**, another Kilkenny?; *Merci* **Philippe**, say 'le Peylin', the fight will go on, I exercise; *Merci* **Philippe**, say 'le Bousquet', for the help with French bureaucracy; *Merci* **Roro** for the smilesmile; *Merci* **David**, solid as a rock in everyday life; *Merci* **Laurence** for the serendipity of Wednesday.

And what would be France without its bureaucracy: *Merci* to all the **LSCE** in general and the direction in particular for housing my humble person in your splendid lieu; *Merci* **Maryse** being the most efficient of all down there; *Merci* **François** for your dry comments; *Merci* **Laurent**, you are fighting against windmills.

Some people aside deserve a big *MERCI*: *Merci* **Martin Werner**, come back to isotopes, we need you; *Merci* **Martin Heimann**, you helped me out in the right moment; *Merci* **Uwe**, let's smoke a fag in the kitchen.

During my PhD, I got funded from the Deutsche Akademische Austauschdienst (**DAAD**) who enabled me first to come to Paris. I appreciate very much that you had confidence in me. I had also a travel grant of the Biosphere Atmosphere Stable Isotope Network (**BASIN**) which allowed me to visit three exceptional laboratories. *Merci* for the unbureaucratic funding. *Merci* to **Joe Berry**, **Jim Ehleringer**, and **Pieter Tans** for their uncomplicated attitude which facilitated me a pleasant journey.

I never thank enough all my friends who have not abandoned me in the distance. *Merci* for the 'good old days'. *Merci* **Thilo**, I don't know what's worse, France or Bavaria; *Merci* **Susanne**, I am looking forward to my first double somersault, one Sunday or another; *Merci* **Stephan**, there is always a reason going to Jena; *Merci* **Manfred** for your own way; *Merci* **Violaine** for the smooth start in a harsh environment; *Merci* **Doro** for housing me even in the worst situations.

The last *Merci* goes to my family, last but not least: *Merci* **Irene**, **Jürgen**, and **Sina** for taking a heavy burden from my shoulders; *Merci* **Mum**, ever beloved.